Diploma Thesis

Modelling of Mercury (Hg) Distribution in Natural Gas Mixtures

Christos Mentzelos

Supervisor: Dr. Epaminondas C. Voutsas

Table of contents

*Note: At the end of each chapter, its’ respective references are being presented

Περίληψη

Ο υδράργυρος (Hg) είναι ένα τοξικό χημικό στοιχείο που απαντάται ευρέως στην διεθνή βιβλιογραφία ως «quicksilver» ή «hydrargyrum». Ο υδράργυρος, ευρισκόμενος σε όλα τα μίγματα υδρογονανθράκων, έχει καταγραφεί η παρουσία του σε πεδία εξόρυξης τόσο φυσικού αερίου όσο και πετρελαίου σε πολλά μέρη ανά την υφήλιο. Σημαντικά υψηλές συγκεντρώσεις υδραργύρου μπορεί κανείς να βρεί σε μίγματα φυσικού αερίου που περιέχουν ελαφριούς υδρογονάνθρακες όπως το μεθάνιο και σε λιμνάζοντα με υγρασία περιβάλλοντα. Ο υδράργυρος μπορεί να προκαλέσει σημαντικά προβλήματα στις διεργασίες των βιομηχανιών φυσικού αερίου όπως για παράδειγμα αστοχίες σε εναλλάκτες θερμότητας από αλουμίνιο, μόλυνση των καταλυτών που χρησιμοποιούνται, επιμολυσμένα τελικά προϊόντα -product streams- φυσικού αερίου καθώς και διαρροές αυτού.

Δοθέντων των προβλημάτων που δύναται να δημιουργήσει ο Hg τόσο στην βιομηχανία, όσο και στην ανθρώπινη υγεία, όντας τοξικό μέταλλο, κρίνεται απαραίτητη η επιστημονική διερεύνηση του ζητήματος. Ο σκοπός της παρούσας διπλωματικής είναι η ανάπτυξη θερμοδυναμικών μοντέλων τα οποία θα είναι σε θέση να προβλέψουν την κατανομή του στοιχειακού Hg σε δυαδικά και πολυσυστατικά μίγματα φυσικού αερίου. Έτσι τα μοντέλα αυτά θα μπορούν να αξιολογηθούν και στο μέλλον να χρησιμοποιηθούν για την πρόβλεψη της κατανομής του Hg σε πραγματικές διεργασίες επεξεργασίας φυσικού αερίου. Αυτός είναι και ο πιο αποτελεσματικός τρόπος για να βρεθεί λύση στα προβλήματα που προκαλούνται από αυτό το χημικό στοιχείο.

Για τον σκοπό αυτό, η Peng-Robinson (PR) και η Soave-Redlich-Kwong (SRK) κυβικές καταστατικές εξισώσεις (EOS) εξετάστηκαν με τη χρήση διαφορετικών εκφράσεων της παραμέτρου τους «άλφα». Για αυτή την παράμετρο αναπτύχθηκαν παράμετροι καθαρών συστατικών για τον Hg, σύμφωνα με τις εκφράσεις των Mathias-Copeman (MC) και Twu-Coon (Twu) για την PR και την SRK EOS αντίστοιχα, μέσω της προσαρμογής αυτών σε πειραματικά δεδομένα τάσης ατμών του καθαρού Hg. Τα νέα μοντέλα που προκύπτουν με την χρήση των αντίστοιχων εκφράσεων της παραμέτρου «άλφα» συμβολίζονται ως PR-MC και SRK-Twu EOS. Εκτός από αυτές τις παραμέτρους υπολογίστηκαν επίσης παράμετροι αλληλεπίδρασης μεταξύ του Hg και διαφόρων υδρογονανθράκων (HC), με την προσαρμογή των παραμέτρων σε πειραματικά δεδομένα διαλυτότητας του Hg σε διαδυκά μίγματα με διάφορους HC, τα οποία αξιολογούνται επίσης.

Για όλα τα διαδικά μίγματα του Hg με άλλα συστατικά, πλήν του μίγματος του Hg με το νερό, υπολογίστηκαν σταθερές παράμετροι αλληλεπίδρασης. Ειδικά για το μίγμα του Hg με το νερό αναπτύχθηκαν θερμοκρασιακά εξαρτώμενες παράμετροι λόγω

της αδυναμίας των εν λόγω μοντέλων να περιγράψουν την επίδραση του δεσμού υδρογόνου του τελευταίου.

Επιπροσθέτως δημιουργήθηκαν και δύο γενικευμένες συσχετίσεις για την πρόβλεψη των συντελεστών αλληλεπίδρασης του Hg με HCs για τους οποίους δεν υπάρχουν διαθέσιμα πειραματικά δεδομένα στην βιβλιογραφία. Αυτές οι συσχετίσεις αφορούν τόσο στην PR-MC όσο και στην SRK-Twu EOS. Αυτές οι γενικευμένες συσχετίσεις έχουν ως βάση τους για τον υπολογισμό των παραμέτρων αλληλεπίδρασης τον αριθμό ατόμων άνθρακα (CN) των HCs καθώς επίσης και το σημείο βρασμού τους (T_b). Επίσης οι συσχετίσεις αυτές αξιολογήθηκαν κατ' αντιπαράθεση με πειραματικά δεδομένα που αφορούν στην κατανομή του Hg σε ένα διαδικό και ένα τριαδικό μίγμα.

Ακόμη ένα μοντέλο για το οποίο αναπτύχθηκαν παράμετροι, είναι το UMR-PRMC που προτάθηκε από τον Βουτσά και τους συνεργάτες του. Το μοντέλο αυτό χρησιμοποιεί ως βάση του την PR EOS με Mathias-Copeman παραμέτρους ωστόσο αντί για τους κλασσικούς κανόνες ανάμιξης χρησιμοποιεί τους 'universal mixing rules'. Οι συγκεκριμένοι κανόνες ανάμιξης βασίζονται σε παραμέτρους συνεισφοράς ομάδων Unifac αντί για τις κλασσικές παραμέτρους αλληλεπίδρασης.

Τέλος τα τρία μοντέλα που αναπτύχθηκαν καθώς και οι γενικευμένες συσχετίσεις αξιολογήθηκαν αντιπαραβάλλοντας τις προβλέψεις τους για την κατανομή του Hg με αντίστοιχα πειραματικά δεδομένα που αφορούν σε ένα πολυσυστατικό και ένα τριαδικό μίγμα, καθώς επίσης και με την πειραματική μεταβλητή «K», η οποία είναι το μολαρικό κλάσμα της συγκέντρωσης του Hg στην αέρια φάση στον αριθμητή, με το μολαρικό κλάσμα του Hg στην υγρή φάση στον παρονομαστή, όπου τα πειραματικά δεδομένα καθιστούσαν τον υπολογισμό της εν λόγω μεταβλητής εφικτή.

Οι παραπάνω αξιολογήσεις έχουν τριπλό στόχο. Ο πρώτος είναι να ελεγχθεί πώς τα ανεπτυγμένα μοντέλα ανταποκρίνονται με τις προβλέψεις τους σε πιο σύνθετα συστήματα από απλά δυαδικά μίγματα. Καθ΄αυτό τον τρόπο θα είναι πιο ασφαλές να συμπεράνει κανείς κατά πόσο τα μοντέλα μπορούν να χρησιμοποιηθούν στο μέλλον σε προσομοιώσεις πραγματικών διεργασιών φυσικού αερίου, παρέχοντας ασφαλείς προβλέψεις για την κατανομή του Hg σε αυτές, δεδομένου ότι δεν υπάρχουν πειραματικά δεδομένα που να αφορούν σε πραγματικές διεργασίες. Ο δεύτερος στόχος είναι να διερευνηθεί η ικανότητα των μοντέλων να προβλέψουν την μεταβλητή «K», η οποία είναι μείζονος σημασίας όταν πρόκειται να υπάρξει αξιολόγηση μοντέλων σε πραγματικές διεργασίες. Ο τρίτος στόχος είναι η ανάδειξη της καλύτερης γενικευμένης συσχέτισης η οποία θα δύναται να χρησιμοποιηθεί το μέλλον για προσομοιώσεις διεργασιών.

Τα αποτελέσματα της διπλωματικής μπορούν να συνοψισθούν ως εξής. Πρώτον όλα τα μοντέλα, ονομαστικά η PR-MC, η SRK-Twu EOS και το UMR-PRMC, δύνανται να συσχετίσουν τον στοιχειακό Hg με τους HCs και επίσης να προβλέψουν με ακρίβεια το μολαρικό κλάσμα του σε πολυσυστατικά μίγματα. Δεύτερον όλα τα μοντέλα μπορούν να προβλέψουν την μεταβλητή «K» στα αντίστοιχα διαδικά μίγματα με ικανοποιητική ακρίβεια. Τρίτον όσον αφορά στον καθορισμό του βέλτιστου τύπου γενικευμένης συσχέτισης, και οι δύο τύποι προκύπτει ότι παρέχουν παρόμοιες προβλέψεις σε κάθε περίπτωση που εξετάστηκε εκτός από τα μίγματα που περιέχουν το ισο-βουτάνιο. Σ' αυτές τις περιπτώσεις τα μοντέλα που χρησιμοποιούν τις γενικευμένες σχέσεις που βασίζονται στο CN παρουσιάζουν ένα συγκριτικό πλεονέκτημα έναντι των υπολοίπων. Επομένως εναπόκειται στον χρήστη να αποφασίσει ποιός τύπος γενικευμένης συσχέτισεις ενδείκνυται να χρησιμοποιηθεί κάθε φορά αναλόγως την περίσταση, δοθέντος του γεγονότος ότι και οι δύο τύποι συσχετίσεων παρέχουν αξιόπιστα αποτελέσματα. Τέλος μπορεί από τα παραπάνω να εξαχθεί το συμπέρασμα ότι όλα τα μοντέλα που αναπτύχθηκαν καθώς και οι αντίστοιχες γενικευμένες σχέσεις μπορούν να χρησιμοποιηθούν σε πραγματικές προσομοιώσεις διεργασιών φυσικού αερίου, έχοντας υπόψην ότι τα πειραματικά δεδομένα για τους διακλαδισμένους και αρωματικούς HCs από την IUPAC χαρακτηρίζονται ως «tentative», παρέχοντας αξιόπιστα αποτελέσματα.

Summary

Mercury (Hg) is a toxic chemical element, commonly known as quicksilver or hydrargyrum. Found in all hydrocarbon mixtures, mercury has been recorded in natural gas and oil fields all over the world. Significantly high levels of mercury concentration can be found in the natural gas with light hydrogen isotopes of methane and at lacustrine dispositional environment. Mercury can cause significant problems to processes of the gas industry such as aluminum heat exchanger failures, poisoned catalysts, contaminated product streams and gas leaks.

Given the problems that Hg can cause to the industry and the human health, an investigation on the matter is required. The scope of this thesis is the development of thermodynamic models which are able to predict the elemental Hg distribution in binary and multicomponent mixtures. This way the developed and evaluated models can be used later on, for the prediction of the Hg distribution in real processes. That will be the most efficient way of dealing with this component and the problems caused from it.

To this purpose, the Peng-Robinson (PR) and the Soave-Redlich-Kwong (SRK) cubic equations of state (EOS) were examined by employing different expressions for the alpha parameter of the EOS. For this parameter, Mathias-Copeman (MC) and Twu-Coon (Twu) pure components parameters were developed for Hg for PR and SRK EOS respectively by fitting them to vapor pressure data of elemental Hg. These models are symbolized as PR-MC and SRK-Twu EOS. Except for those parameters, binary interaction parameters for Hg and hydracarbons (HC) were developed as well by fitting them to experimental solubility data of Hg in binary mixtures with various HCs, which are also evaluated.

For all binary mixtures of Hg with other components, except the one containing Hg with water, constant binary interaction parameters have been developed. As far as the binary mixture of Hg with water is concerned, temperature dependent parameters have been developed due to the models' weakness regarding the description of the effect of the hydrogen bond.

Furthermore two predictive correlations have been developed, in order to estimate the binary interaction parameters for binary mixtures of Hg with HC for which no experimental data are available in the literature, for both the PR-MC and the SRK-Twu EOS. These correlations have been based on the carbon number (CN) and also the normal boiling temperature (T_b). In addition to that, the generalized correlations have been tested against experimental data regarding a ternary and a multicomponent mixture.

Another model developed is the UMR-PRMC proposed by Voutsas et al. This model uses as its' basis the Peng-Robinson EOS with the Mathias-Copeman parameters, but instead of the classical mixing rules, it introduces the universal mixing rules. These mixing rules use the Unifac contribution group parameters instead of binary interaction parameters.

Finally the three models developed as well as their corresponding generalized correlations have been evaluated against experimental data concerning two multicomponent mixtures, as well as the experimental 'K' variable, that is the division of the Hg mole fraction in the vapor phase with the Hg mole fraction in the liquid phase, where possible.

These evaluations have three objectives. The first one is to test how the developed models cope against more complex systems than just binary mixtures. That way it will be safer to conclude whether or not the models can be used in process simulations at a later stage and provide reliable results, given the fact that there are no experimental data regarding real processes. The second one is to explore the capability of the models to predict the 'K' variable, which is very important when it comes down to evaluating models in a process. The last one is to find the optimum type of the generalized correlations estimating the binary interaction parameters that should be used for process simulations in the future.

The results can be summarized as follows. First of all every model, namely the PR-MC, the SRK-Twu EOS and the UMR-PRMC are able to correlate elemental Hg in binary mixtures and also accurately predict its' mole fraction in multicomponent mixtures. Secondly all models are capable of predicting the 'K' variable of the corresponding mixtures satisfyingly enough. Thirdly as far as the optimum type of the generalized correlation is concerned, both types appear to provide very similar results in all cases, except for the mixtures containing iso-butane, where the correlations based on the CN seem to have the advantage. Therefore it is up to the user to decide which type is appropriate according to the occasion, since both types provide reliable results. Finally it can be concluded that all models and generalized correlations can be used in process simulations at a future stage with some caution regarding the branched alkanes and the aromatic HCs due to their tentative experimental data, providing reliable results.

Acknowledgments

This master thesis was accomplished at the Norwegian University of Science and Technology (NTNU) and the National Technical University of Athens (NTUA). My primary supervisors have been professors Even Solbraa and Epaminondas C. Voutsas, and my research advisors Mr. Efstathios Skouras and Ms. Andrea Carolina Machado Miguens from Statoil.

I would like to express my sincere thankfulness to my supervisors and all my research advisors for their helpfulness during my period of work at Statoil. To emphasize my gratefulness I dedicate to them the words of my Greek ancestor Alexander the Great:

'I am indebted to my father for living, but to my teachers for living well.'

I would also like to thank the Erasmus program and all people supporting it, for giving me the opportunity to go to the NTNU in order to do my master thesis and Statoil for helping me out during my stay at Trondheim and providing me with various resources for the completion of my master thesis.

Finally I would like to thank my family, my closest friends Mitrou Michalis, Dimopoulos Ilias, Kokkinos Dimitrios, Chatziloudis Charalampos, Petsagourakis Giannis and Thomas George for always supporting me in my work.

Chapter 1: Introduction

Mercury is the chemical element symbolized as Hg and has the atomic number 80 and molecular weight of 200.59 g/mole. It is commonly known as quicksilver or hydrargyrum. It is a heavy, silver colored, d-block element, and furthermore it is the only liquid metal at standard temperature and pressure (STP) conditions. It has a freezing point of -38.83 ^{o}C and boiling point 356.73 ^{o}C [1]. It is a poor conductor of heat but a fair conductor of electricity. It exists in two main oxidation states, I and II. The metal is relatively stable in dry air, but in moist air tarnishes slowly to form a gray oxide coating.

The corrosive properties of mercury in the natural gas industry were firstly reported at 1973, when an aluminum-heated transformer at a liquid natural gas plant of Algeria was totally destroyed. After investigation was conducted on the matter it was found out that corrosion caused by mercury in the natural gas, was the cause of the damage [2].

Found in all hydrocarbon mixtures, mercury has been recorded in natural gas and oil fields all over the world. Generally significantly high levels of mercury concentration are found in the natural gas with light hydrogen isotopes of methane and at lacustrine dispositional environment. Mercury can cause significant problems such as aluminum heat exchanger failures, poisoned catalysts, contaminated product streams, contaminated waste water and gas leaks [3].

Specifically about the equipment used in a natural gas process, mercury readily forms alloys - amalgams- with a variety of metals such as aluminum, brass, chromium, copper, zinc, iron, nickel, silver, gold and tin that are weaker than mercury-free metals, causing mechanical failures and gas leaks. Because it does not amalgamate with iron, mercury is often stored in containers made out of this material.

Liquid metal embrittlement (LME) is a complex metal fracture mechanism that starts without a warning in advance. Liquid mercury has a disastrous effect on aluminum. It can be traced in natural gas feed stock, usually at very low levels, none the less it can accumulate in quantities sufficient to cause failure of cryogenic aluminum heat exchanger. Mercury can degrade the aluminum cold box's materials -where the cryogenic distillation happens- by three different mechanisms.

1) Amalgamation

   This is the process by which mercury forms liquid solutions with various metals, mainly with Al, Au, Ag and Zn. If the metal is Al, its' concentration in

the amalgam is relatively low, therefore the depth of the corrosion is limited. Furthermore aluminum is generally prevented from coming in contact with mercury by the Al_2O_3 protective surface oxide -for the amalgam reaction to begin, mercury must wet the aluminum metallic surface first-. The oxide aluminum is not homogeneous and contains numerous defects, but in general mercury will not migrate through these microscopic cracks and defects to reach the underlying metal. However, if the extent or severity of such defects is increased by thermal or mechanical stresses, abrasion or chemical environments, the risk of mercury damage is increased.

2) Amalgam corrosion

This is the combined action of mercury and moisture producing a corrosion process that propagates with miniscule amounts of mercury. The reaction has two steps and is as follows:

$Hg + Al \rightarrow Hg(Al)$ amalgam (1)

$Hg(Al) + 6\ H_2O \rightarrow 2AlO3 \cdot 3H_2O + 3H_2 + Hg$ (2)

Small amounts of aluminum can be dissolved in liquid mercury, diffused to a mercury‑moist air interface, and then rapidly oxidized. Since, oxidation removes aluminum from the mercury, further aluminum can dissolve, and the process can continue until the aluminum is completely converted to oxide. Rapid oxidation requires the presence of moisture. Reaction rates are slow in its absence.

3) LME

LME is generally much more severe and therefore more important than other embrittling processes, such as hydrogen-embrittlement or stress-corrosion cracking. Once cracks have initiated, very rapid subcritical cracking can occur even at low stresses. Cracking occurs preferentially along grain boundaries for the Al:Hg couple (and for many other couples), but transgranular fractures can also occur. Liquid metals are drawn into growing cracks so that the crack tip is always in contact with embrittling metal atoms. The rate-controlling process for cracking is still being debated, but the rate of flow of liquid within cracks may control the rate of cracking in some circumstances.

Adsorption of embrittling atoms at crack tips weakens substrate interatomic bonds, and facilitates crack growth by enabling interatomic bonds to break or

shear more easily than in inert environments. Thin films of liquid metal are left behind the advancing crack tip and, hence, fracture surfaces are covered with a film of liquid metal. For the Al:Hg system, 'de-wetting' can occur so that small globules of mercury are present on fracture surfaces. The presence of mercury on fracture surfaces can also result in the growth of oxide whiskers after fracture, a phenomenon peculiar to aluminum and discussed in the preceding section.

For LME cracks to initiate there must be intimate contact between liquid and solid metals, with no intervening oxide films to prevent wetting and adsorption. Al alloys are covered by a thin, protective oxide film, and surfaces can be covered by liquid mercury indefinitely without any reaction until the oxide is damaged. Oxide films can be broken by mechanical processes, e.g. by scribing or abrasion, by chemical processes, e.g. corrosion, or by plastic deformation of the aluminum resulting in slip steps at the surface.

The aluminum amalgam in particular is extremely corrosive since it reacts with the moisture to form a metal oxide, releasing the mercury to perpetuate the corrosive process. This corrosion can lead to catastrophic failure of cryogenic heat exchanger and wellhead valve stems and gates. [4, 5]

It is obvious that Hg can pose a major problem for the natural gas industry due to its properties and its behavior. Therefore an investigation on the matter is required. This way the most efficient way of dealing with this component and the problems caused by it can be detected and solved.

The scope of this master thesis is the development of thermodynamic models that will be able to predict the elemental Hg solubility in multicomponent mixtures. To this purpose, the Peng-Robinson (PR) [6] and the Soave-Redlich-Kwong (SRK) [7] cubic equations of state (EOS) will be examined by employing different expressions for the 'alpha' parameter of the EOS. For this parameter, Mathias-Copeman [8] and Twu-Coon [9] pure components parameters will be developed for Hg for PR and SRK EOS respectively by fitting them to vapor pressure data of elemental Hg. Except for those parameters, binary interaction parameters for Hg and hydracarbons (HC) will be developed as well by fitting them to solubility data of Hg in binary mixtures with various HC. Furthermore the UMR-PRMC model proposed by Voutsas et al [10] will be examined as well. This model belongs to the EOS/G^E class of models and combines the PR EOS [6] with Mathias-Copeman [8] parameters, with an original Unifac-type G^E model that employs temperature dependent group interaction parameters which are estimated by fitting them to solubility data of Hg with HCs and other components.

Two different types for the binary interaction parameters will be developed. Constant ones for all binary mixtures except the one containing Hg with water. For this particular mixture temperature dependent parameters will be introduced. In addition there will also be presented two predictive correlations in order to estimate them for binary mixtures of Hg with HCs for which no experimental data are available in the literature. Finally the models will be tested with one binary, one ternary and two multicomponent mixtures.

References:

[1] http://www.chemicool.com/elements/mercury.html

[2]http://www.americanlaboratory.com/913-Technical-Articles/114246-Determination-of-Mercury-in-the-Environment-Petrochemical-Products-and-Fuels/

[3] Wilhelm M., Bloom N.(2000) , ''Mercury in petroleum'', Fuel Processing technology, vol. 63, i.1, p. 1-27

[4] Coade R., Coldham D. (2006), ''The interaction of mercury and aluminium in heat exchangers in a natural gas plants'' ,International Journal of Pressure Vessels and Piping, Vol. 83, I. 5, p. 336–342

[5] Wilhelm M. (2009), ''Risk Analysis for Operation of Aluminum Heat Exchangers Contaminated by Mercury'', Process Safety Progress, Vol. 28, Issue 3, p. 259–266

[6] Peng, D. Y., and Robinson, D. B. (1976). "A New Two-Constant Equation of State". Industrial and Engineering Chemistry: Fundamentals 15, p. 59–64

[7] Soave (1972), G. Equilibrium Constants from a Modified Redlich–Kwong Equation of State, Chem. Eng. Sci., 27, p. 1197-1203

[8] Otilio Hernández-Garduza, Fernando Garcia-Sánchez, David Ápam-Martınez, Richart Vázquez-Román (2002), Vapor pressures of pure compounds using the Peng-Robinson equation of state with three different attractive terms, Fluid Phase Equilibria, p. 195-228

[9] Twu C. et al (1995), ''A new generalized alpha function for a cubic equation of state Part 2. Redlich-Kwong equation'', Fluid Phase Equilibria 105, p. 61-69

[10] V. Louli et al. (2012), ''Measurement and prediction of dew point curves of natural gas mixtures '', Fluid Phase Equilibria 334, p. 2-4

Chapter 2: Theory

As far as the electron configuration of mercury is concerned, electrons fill up all the available 1s, 2s, 2p, 3s, 3p, 3d, 4s, 4p, 4d, 4f, 5s, 5p, 5d and 6s subshells. Since this configuration strongly resists removal of an electron, mercury behaves similarly to noble gas elements, which form weak bonds and become solids which melt easily at relatively low temperatures. The stability of the 6s shell is due to the presence of a filled 4f shell. An f shell poorly screens the nuclear charge that increases the attractive Coulomb interaction of the 6s shell and the nucleus. [1]

As far as the critical properties of mercury are concerned, meaning its' critical temperature and critical pressure, there has not been an agreement yet. The values of these properties vary in the literature and the experiments that have been conducted to determine them do not agree with each other. More details about these properties will be discussed in the 3rd chapter. The values which are widely used however are 1735.15 K and 1608 bar respectively.

2.1 Forms of mercury in natural gas

Mercury can be present in a natural gas mixture mainly in the elemental form (Hg^0) due to its volatility, oxidized (Hg^{+1}) and (Hg^{+2}) form, organic or inorganic ionic forms. Furthermore it is present at concentrations way below saturation. That fact indicates that there is no liquid phase mercury in most reservoirs. All these types of mercury bare unique species-dependent physical, physiological and chemical properties.

Mercury can form two kinds of compounds called:

1. Mercurous, when it uses two electrons in the bonding process
2. Mercuric, when it uses just one electron to bond with another element

Although mercury emissions from the natural gas sector have not been widely calculated or reported, information and data about natural gas processing certainly indicate that the natural gas sector could be a significant source of both global mercury supply and emissions.

Organic compounds contain mercury at the +2 oxidation state. They include organometallic compounds -with a Hg-C covalent bond-. Organic mercury forms consist of two main groups:

1. R-Hg-X compounds -partly alkylated species-
2. R-Hg-R compounds -fully alkylated species-,

Where R stands for organic species, of which methyl (-CH3) is prominent, and X stands for inorganic anions, such as chloride, nitrate or hydroxide. The R-Hg-X group includes mainly monomethylmercury compounds. The most prominent R-Hg-R compound is dimethylmercury (CH_3HgCH_3). Other examples of these categories are $C_2H_5HgC_2H_5$, $C_3H_7HgC_3H_7$ and $ClHgCH_3$.

As far as the inorganic forms of mercury are concerned, there are two categories. One contains the ionic mercury salts, which can be $Hg^{2+}X$ or $Hg^{2+}X_2$, where X symbolizes an inorganic ion for the first one and the other one contains mercury salts (mostly halides) like mercuric chloride, which are soluble in gas condensates, but they prefer to partition to the water phase in primary separations.

Gas processing can cause transformation of one chemical form of mercury to another. A characteristic example is the reaction of elemental mercury with sulfur compounds. The mixing of gas and/or condensate from sour and sweet wells allows reaction of elemental mercury with S_2 or ionic mercury with H_2S to form HgS that can settle out in tanks and deposit in equipment, or become attached to suspended particles with small particle size. [2, 3, 4, 5]

2.2 Mercury distribution on gas processing plants

Elemental mercury and organic compounds of mercury can be found in many gas fields. Table 1 shows some average concentrations of Hg in natural gas fields of several places over the globe.

Table 1: Regional Average Level of Mercury in Natural Gas

Location	Elemental Hg concentration [μg/m^3]
South America	69-119
East Asia	58-193
North Africa	0.3-130
North Europe	0.01-180
Middle East	1-9
Eastern US Pipeline	0.019-0.44
Midwest US Pipeline	0.001-0.1
North America	0.005-0.04

As already mentioned Hg^0 has a normal boiling point of 356.73 ^oC and it would therefore be expected to have a limited distribution in a gas processing plant. However due to its mobility and its ability to be readily bonded to most of the surfaces that it comes in contact with, this is not the case. Since mercury can be bonded to gas gathering pipelines it is possible that it may take some time until it arrives at the main plant. Therefore problems may be caused since it was not

expected and no precautionary measures were taken in advance. Table 2 shows the change in the concentration of Hg in feed gas with time for two different plants.

Table 2: Change in the concentration of Hg in feed gas with respect to time ($\mu g/m^3$)

	Start up	**Year 7**
Plant A	0.25 to 0.45	17 to 69
Plant B	0.01	0.253

Especially for Plant A the difference in the concentration of Hg is very significant. In case the scale of this difference was not known beforehand, there could have been some very serious damage to the pipelines and the equipment used.

This high mobility of Hg implies that, if not removed at source, it will distribute throughout the whole process streams and in plant effluents. The course of mercury in gas processing is easier to predict since the process is simpler than that of oil processsing. Therefore no transformation of the elemental mercury to the species that were mentioned above is caused. Gas processing does not include molecular transformations to come up with final products, it is in simple terms put, a treatment and separation process. The treatment part has to do with the removal of unwanted constituents like CO_2, H_2S and H_2O and contaminants -metals-. The separations are typically cryogenic utilizing selective condensation of fractions (C_2, C_3, C_4, C_4+) by removal of heat. It is a fact that some heavy condensate streams that are used in gas separation processes can contain amounts of suspended and oxidized forms of mercury as well as elemental mercury.

There have been a number of surveys by Johnson Matthey Catalysts on gas processing plants in several continents around the world [6]. Table 3 presents a typical example of the distribution of Hg on a 50 Million standard cubic feet per day (mmscfd) gas plant in the Far East as a steady-state flow.

Table 3: Distribution of Hg on a 50 mmscfd Gas Plant

Process Stream	**Mercury [kg/year]**
Raw Gas	220
Acid Gas Removal Vent	22
Dryer Vent	3
Condensate	45
Sales Gas	150

Measurements on the raw gas of all plants of the survey revealed that the concentration of Hg ranged from 10 up to 70000 ng/m^3. The researchers Peter J. H. Carnell and Paul J. Openshaw, Johnson Matthey Catalysts [6] mention that even in the case of the plant with the lowest concentration of Hg in the initial feed of the

process, a small portion of it was present in both the sales gas and the condensate. As far as the acid gas removal and sulphur recovery is concerned, Hg was found in the rich amine liquor, in the stripper gas and in the elemental sulphur.

Finally as far as the product streams on all plants, meaning the sales gas and the condensate streams, are concerned, all of them displayed Hg concentration. That means that Hg is able to distribute throughout the whole process plant and not only in the condensate streams. Naturally the highest concentrations of Hg were found on the plants with no mercury removal units. However even in the presence of these units a significant percentage of the total Hg reached the rest of the process [6].

The distribution of Hg on the gas processing plants that were examined on the survey is shown in figure 1.

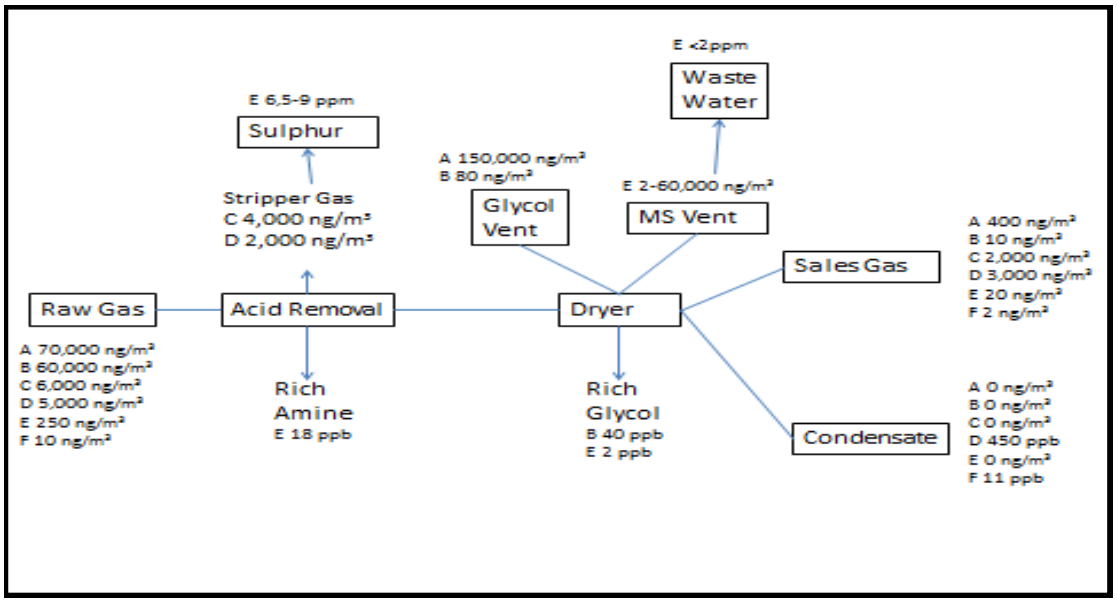

Figure 1: The distribution of Hg on the gas processing plants examined on the survey

References:

[1] Norrby, L.J. (1991). "Why is mercury liquid? Or, why do relativistic effects not get into chemistry textbooks?". Journal of Chemical Education 68 (2), p. 110

[2] Frech W. et al (1996), ''Determination and Speciation of Mercury in Natural Gases and Gas Condensates '', Analytical Communications, vol. 33 (7H-9H).

[3] Wilhelm M. (2000), Bloom N., ''Mercury in petroleum'', Fuel Processing technology, vol. 63, i.1, p. 1-27

[4] Wilhelm M. (2001), ''MERCURY IN PETROLEUM AND NATURAL GAS: ESTIMATION OF EMISSIONS FROM PRODUCTION, PROCESSING, AND COMBUSTION.'' U.S. Environmental Protection Agency, Washington, D.C., EPA/600/R-01/066

[5] http://www.frontiergs.com/files/Measuring-Mercury-in-Natural-Gas.pdf

[6] Carnell P. et al (2004),'' MERCURY DISTRIBUTION ON GAS PROCESSING PLANTS '', 83rd annual GPA convention proceedings, New Orleans.

Chapter 3: Evaluation of experimental data (critical properties, vapor pressure and solubility)

3.1 Available T_c, P_c, ω for Hg in literature

Throughout the literature search two different sets of critical temperature (T_c), critical pressure (P_c) and acentric factor (ω) for Hg have been encountered. One of them was proposed by DIPPR [1] and the other one by a report from NIST [2], whose purpose was to collect and evaluate all experimental data of P^s of Hg as well as create an equation capable of describing them. Table 4 presents the two sets.

Table 4: DIPPR's and NIST's sets of T_c, P_c and ω

	DIPPR's set	**NIST's set**
T_c [K]	1735.15	1764.15
P_c [bar]	1608	1670
ω	-0.1645	-0.1911

NIST's set of T_c and P_c was chosen from experimental data regarding those properties. In the report is stated that there has been a literature research on the matter and that the values considered the most reliable among the existing experimental data, were those of Kozhevnikov [3], who estimated that T_c = 1764 K and P_c = 1670 bar.

The ω was calculated afterwards using equation 1. The vapor pressure (P^s) of Hg at T_r = 0.7 was calculated using DIPPR's equation. T_r is defined as T divided by the T_c. The choice of this equation will be analyzed thoroughly later on.

Given the fact that there still is a debate about the value of these properties it was decided that these two sets should be checked, at least for the effect that they have on the calculation of the P^s while using the SRK and PR EOS.

$$\omega = \left(-logP_{\mathrm{rs}}\,|\mathrm{T_r}=0.7\right) - 1 \quad \text{(eq.1)}$$

3.2 Creation of P^s database and Solubility database

3.2.1 Evaluation of P^s experimental data

Any thermodynamic model should be able to predict the behavior of a given mixture if it is to be considered suitable for implementation in an industrial process. This means that it has to be able to predict the phases of the mixture as well as their

composition given the temperature (T), the pressure (P) and an initial composition. Therefore it is essential that the models can predict, on a first level, accurately the P^s of each component of the mixture in order to be able to predict correctly the phase equilibrium. For the models of this thesis it is of interest that they will be able to predict the P^s of Hg, which is the element in question.

The P^s of Hg is very important to the thermodynamic modeling that will be performed in this master thesis, because it will be used later on for the fitting of the Mathias-Copeman and the Twu-Coon parameters which are used in the 'alpha' parameter of the EOSs as will be explained in chapter 4.

There have been several attempts to measure the P^s of Hg for several temperatures over the previous centuries from many researchers like Ernsberger, Menzies, Ambrose and Douglas. All these researchers are mentioned in the report from NIST [2]. However taking into consideration the chronicle periods that these experiments were conducted it is obvious that the results alter depending on the means available. Therefore the uncertainty level of the measurements poses a crucial factor in deciding which data will be used for the creation of the database.

Most of the experimental data that are chosen to build a database for the P^s of Hg, deal with the temperature range of 285 K up to 900 K. For that temperature range these data have an uncertainty level of less than 1%.

It is noted that at lower temperatures the uncertainty level of the measurements is higher than that of the higher temperatures. This happens because the P^s of Hg is getting lower as the temperature declines. However since the purpose of this thesis is to predict the distribution of Hg throughout a process plant for the natural gas industry it is essential that the temperature range of the P^s also includes temperatures below 285 K, which is the lowest temperature for which the uncertainty level of the experimental data is less than 1%.

Therefore P^s experimental data for temperatures lower than 285 K and for temperatures higher than 900 K are added to the database. As far as the higher temperature region is concerned (1052 K – 1735 K) due to the lack of many experimental data, the data of Schonherr [2] are chosen. These data have a maximum uncertainty level of 3% for the highest temperature. As far as the lower temperature region is concerned (234 K – 275 K) the data of Douglas et al. [2] are chosen. These display a maximum uncertainty level of 1.5% at the lowest temperature.

Given these facts the database that was created has experimental P^s for the temperature range from the freezing temperature up to the critical temperature of Hg. The database is presented analytically at appendix A, at table A1.

3.2.2 Evaluation of DIPPR's equation for the prediction of P^S

As it can be seen at the database at table A1, the experimental data concerning the P^S of Hg are not evenly spread through the whole temperature range. Therefore it is extremely important to have a way -via an equation- to predict P^S almost equal to the available experimental data. Thus one will be able to use this equation in order to reliably estimate P^S for temperatures where no data are available. That way the P^S for the whole temperature range will be evenly described.

The equation from DIPPR (eq.2) for calculating the P^S of elemental Hg was tested for that purpose.

$$P^S = e^{(A+\frac{B}{T}+C*\ln(T)+D*T^E)} \quad \text{eq. (2)}$$

Where:

A = 30.951, B = -7717, C = -1.1296, D = 2.6938*10-7, E = 2

and P = [Pa] T = [K]

DIPPR equation's temperature range is mentioned to be from the triple point (234.31 K) up to the critical temperature of Hg (1735 K). At figure 2 it can be seen that the results from eq. 2 are in very good agreement with the experimental data. The name of each researcher as well as his/her experimental data are presented as points on the figure.

The greatest deviation noted was that for temperature 1051 K and was equal to 3.69%. One must keep in mind however that for these high temperatures the uncertainty level of the experimental data is around 3%, therefore the results of eq. 2 for the whole temperature range can be characterized as acceptable. In general the deviations that the equation displays towards the experimental data are less than 1% except for the temperatures above 1000 K. Table 5 presents some characteristic results of DIPPR's equation and their deviation from the experimental P^S. More details concerning the deviations of eq. 2 and the experimental data can be found at the appendix A at table A1, where the full version of table 5 is located.

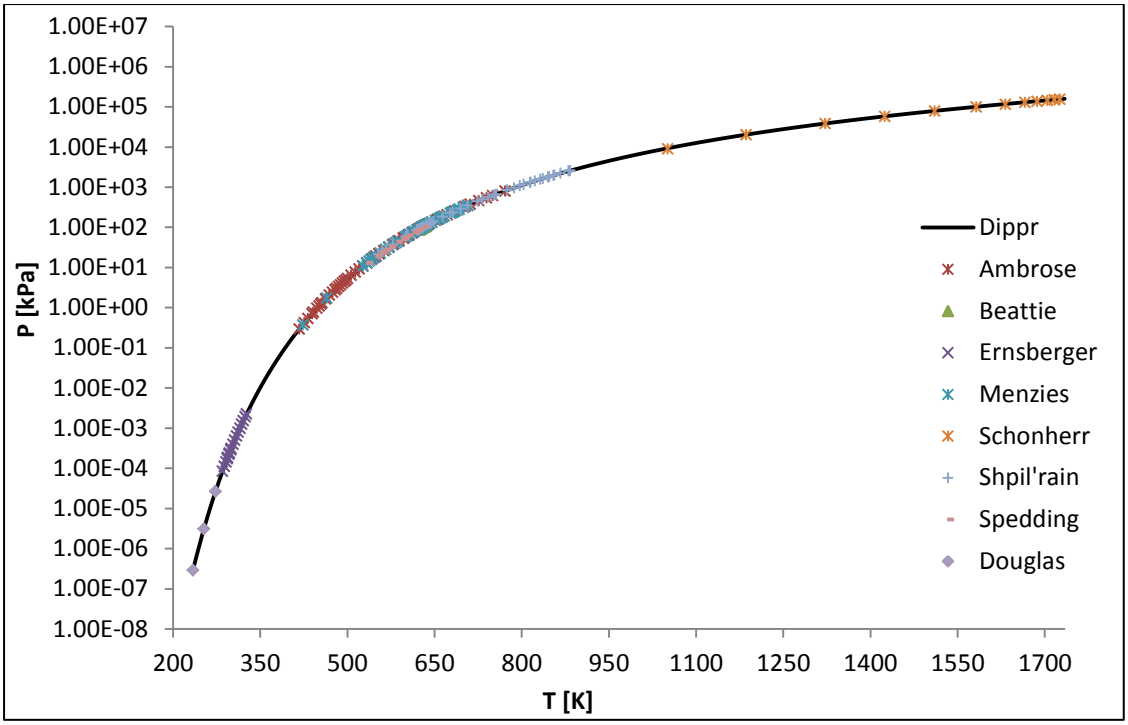

Figure 2: DIPPR's P^s compared to experimental P^s

Given figure 2, as well as the results from table 5 and table A1, it can be concluded that eq. 2 can provide reliable estimations for the P^s of Hg for the whole temperature range examined. Thus hereafter the term 'experimental P^s' will be referring to the values of eq.2 for the given temperature range.

Table 5: Comparison of DIPPR's estimated P^s with experimental P^s for some characteristic temperatures

	Exp. P^s	DIPPR's P^s	% Deviation
Temperature [K]	Pressure [kPa]	Pressure [kPa]	$((P^s_{exp}-P^s_{DIPPR})/P^s_{exp})*100$
285.22	8.45E-05	8.464E-05	-0.13%
294.11	0.000185	0.0001855	-0.15%
300.25	0.000312	0.0003102	0.45%
309.29	0.000636	0.0006368	-0.15%
321.15	0.001539	0.0015366	0.16%
417.095	0.293	0.293	-0.07%
447.681	0.964	0.965	-0.10%
462.634	1.627	1.629	-0.13%
497.53	4.882	4.879	0.07%
513.69	7.708	7.699	0.11%
546.934	18.080	18.045	0.19%
587.994	45.215	45.103	0.25%
624.85	92.662	92.429	0.25%
666.82	190.120	189.604	0.27%

Continuation of table 5			
683.43	246.290	245.784	0.21%
702.724	327.808	327.089	0.22%
749.788	617.883	616.913	0.16%
796.86	1079.800	1078.732	0.10%
814.46	1305.700	1307.372	-0.13%
854.54	1967.280	1966.343	0.05%
882.13	2553.520	2548.829	0.18%
1051.44	9006.415	9338.783	-3.69%
1510.37	78204.030	79191.073	-1.26%
1735.51	157499.800	159904.817	-1.53%

3.2.3 Development of database for binary Vapor-Liquid-Equilibrium (VLE) and Liquid-Liquid-Equilibrium (LLE) data of Hg with HC

As already mentioned in chapter 1 at the scope of this master thesis, solubility data for binary mixtures of Hg with various hydrocarbons (HCs) -as solvents- are necessary for the calculation of binary interaction parameters -k_{ij}- for all the models that are being developed.

Unfortunately only a few papers with such data are available in the literature [4, 5, 7, 8] and other than that the only available source is the IUPAC's book concerning the solubility of Hg in liquids and compressed gases [6]. Furthermore only [7] and [8] contained data concerning the solubility of Hg in light HC like methane and ethane, as well as solubility of Hg in other gases like CO_2 and N_2. The last four components mentioned are of great importance to the natural gas industry and this is the reason why they are specifically pointed out.

The available solubility data of Hg with HC have to do with the mole fraction of Hg in each binary system. Table 6 displays some information regarding all the binary mixtures found in literature as well as their source. All the data are presented analytically on tables C1-C7 at the appendix C from each reference respectively. All the data presented at table 6 concern liquid-liquid equilibrium (LLE) data of Hg with HCs except for the data concerning Hg in methane and N_2 that are vapor phased data and also Hg in ethane, propane, iso-butane and CO_2, which are vapor-liquid-equilibrium (VLE) data. The data of IUPAC[6] concerning Hg in propane and n.butane were excluded from the database due to the fact that they were at very high temperatures, thus making it impossible to compare with the rest available data, and therefore in a way unsafe to use.

The binary systems found at papers [4] and [5] concern Hg in n.C_6, cy-C_6, toluene, benzene and n.C_8 and toluene respectively. Except for the data concerning the binary mixtures of Hg in n.C_6, cy-C_6, toluene and benzene, the other data cannot be compared to the data from the IUPAC because they are at different temperatures.

Table 6: Basic informations about binary mixtures of Hg with various HCs, water, CO_2 and N_2

	HC	T range[K]	P [atm]	Number of data	Type of data
Robert R. Kuntz and Gilbert J. Mains [4]	n.C_6	298.15-336.15	1	3	LLE
	cy-C_6	298.15	1	1	LLE
	toluene	298.15	1	1	LLE
	benzene	298.15	1	1	LLE
M. M. MIEDANER, A. A. MIGDISOV, and A. E. WILLIAMS-JONES [5]	n.C_8	383.15-473.15	1	3	LLE
	toluene	393.15-473.15	1	4	LLE
IUPAC [6]	n.C_5	278.15-313.15	1	8	LLE
	n.C_6	273.15-338.15	1	14	LLE
	n.C_7	273.15-313.15	1	9	LLE
	n.C_8	273.15-313.15	1	9	LLE
	n.C_{10}	273.15-318.15	1	10	LLE
	2.2-dm-C_4	273.15-308.15	1	6	LLE
	cy-C_6	288.15-313.15	1	6	LLE
	water	273.15-393.15	1	22	LLE
	benzene	288.15-308.15	1	6	LLE
	o-xylene	273.15-308.15	1	5	LLE
	toluene	273.15-308.15	1	6	LLE
	2.2.4-tm-C_5	273.15-308.15	1	7	LLE
	m-cy-C_6	273.15-308.15	1	6	LLE
	cis-1.2-dm-cy-C_6	289.15-308.15	1	5	LLE
	cis-1.4-dm-cy-C_6	288.15-308.15	1	5	LLE
	trans-1.2-dm-cy-C_6	288.15-308.15	1	5	LLE
	trans-1.4-dm-cy-C_6	288.15-308.15	1	5	LLE
Confidential	i-C_4	263.15-278.15	1.09-1.875	4	VLE
Confidential	CH_4	248.15-293.15	27.58-68.95	19	VE
	C_2H_6	273.15-293.15	23.92-37.65	5	VLE
	C_3	273.15-293.15	4.76-8.34	5	VLE
	CO_2	273.15-293.15	34.82-57.30	5	VLE
	N_2	273.15	6.85-69.29	6	VE

The experimental data from references [4, 5, 6] will now be evaluated since they are all at the same temperatures, pressures, and also in the liquid phase. The rest of the data will be analytically evaluated later on because of their ranging in pressure. At tables C1 and C3 at appendix C, it can be seen that the data concerning benzene, toluene and n.C_6 from IUPAC and Robert et al. [4], are close to each other, except for the mole fraction of Hg in n.C_6 at 336.15 K. At that temperature the mole fraction is significantly bigger than the one of IUPAC for T = 338.15 K. This is not possible however because as figures later on show as well, the solubility of Hg in the solvent is increased monotonically as the temperature rises.

As far as cy-C_6 is concerned the common experimental point at 298.15 K is somewhat different. IUPAC state that the mole fraction of Hg in cy-C_6 is equal to 1.32E-06 whereas paper [4] states that it equal to 1.2E-06. Both values will be added to the database however because the mole fraction is too small and a difference of such magnitude could be well attributed to experimental errors.

The pressure of the binary systems found in IUPAC's book is considered to be equal to 1 atm because there is no evidence to suggest otherwise. Finally in IUPAC's book [6] all the binary systems that have as solvent any HC after benzene -as they are shown at table 6- are classed as tentative. However since there is no way to decide their validity, they will also be added to the solubility database as experimental data, keeping however that fact in mind.

After the solubility data have been collected, they are evaluated. The evaluation concerns the solubility of Hg in HCs and consists of a comparison between these data based on several criteria. The observations that are made from those comparisons are of great interest because they can be considered as a first indication of how Hg is expected to be distributed throughout the plant. This evaluation does not contain the solubility of Hg in propane and n.butane because these experimental data are at different temperatures and pressures compared to the rest of the data therefore there can be no comparison between them. However some indirect conclusions can be reached, with every precaution, about them as well.

Figures 3, 4 and 5 show the effect of the carbon number on the solubility of Hg in all types of HC. That means that the HC can be either n.alkane, cyclo-alkane, branched-alkane or aromatic HC.

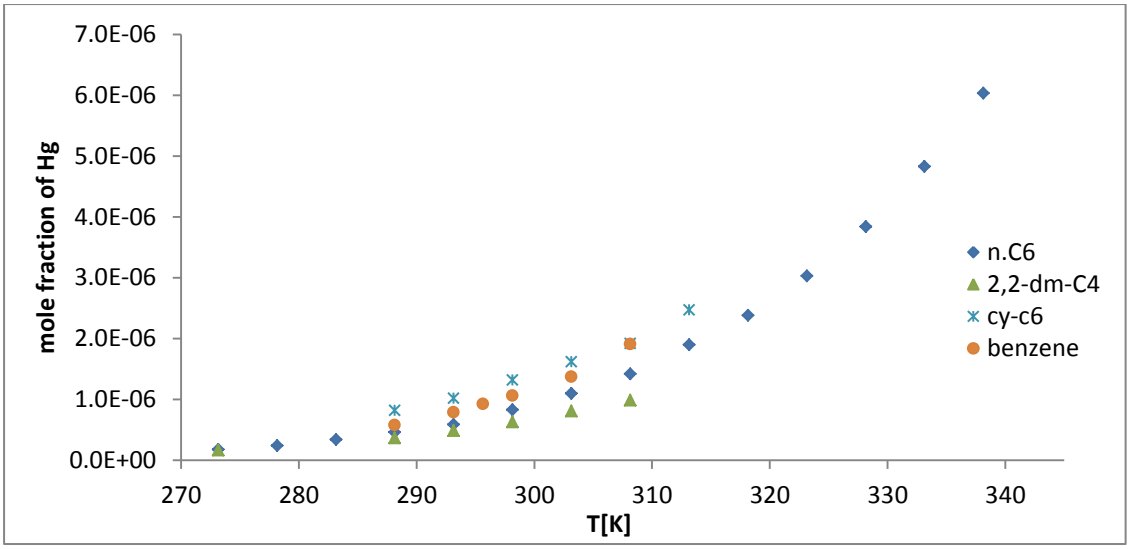

Figure 3: Solubility of Hg in liquid HC with carbon number 6

As far as the HC with 6 carbon atoms are concerned it is clear that Hg dissolves the least in branched alkanes, more in n. alkanes, even more in aromatic HC and the most in cyclo-alkanes.

At 273 K the branched alkanes dissolve almost the same amount of Hg as n.C_6 does. As the temperature rises however the solubility of Hg in n.C_6 is greater than that of Hg in all other branched alkanes.

As far as the solubility of Hg in benzene is concerned it is greater than that of Hg in n.C_6. It is however less than the solubility of Hg in cy-C_6 except for the highest temperature, where it is almost the same in both HCs. It is possible that in higher temperatures Hg 'prefers' -dissolves more, in terms of quantity- more benzene than cy-C_6.

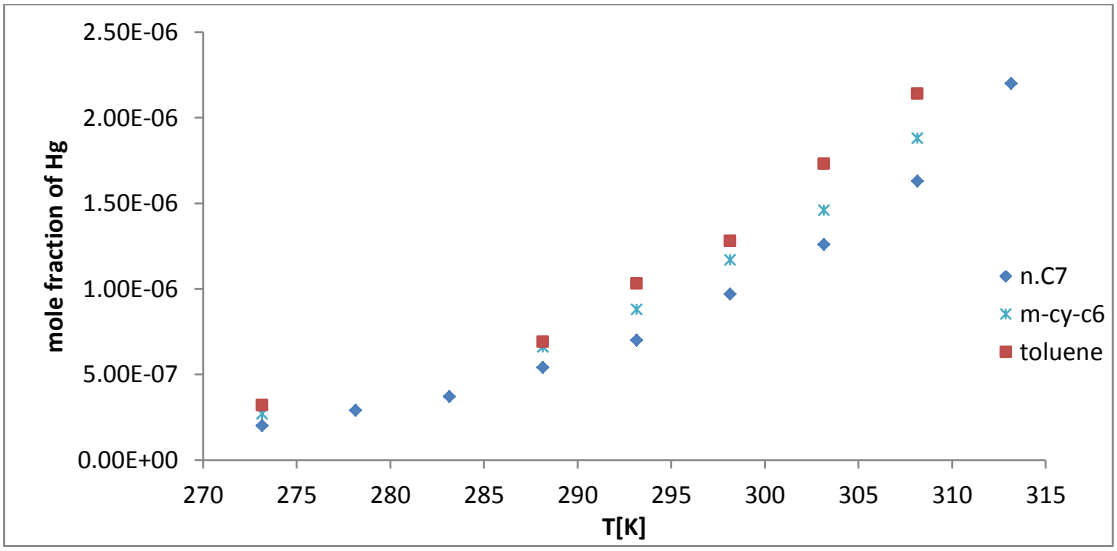

Figure 4: Solubility of Hg in liquid HC with carbon number 7

As far as the HC with 7 carbon atoms are concerned it is clear that Hg dissolves the least in n.C_7, even more in m-cy-C_6 and the most in toluene.

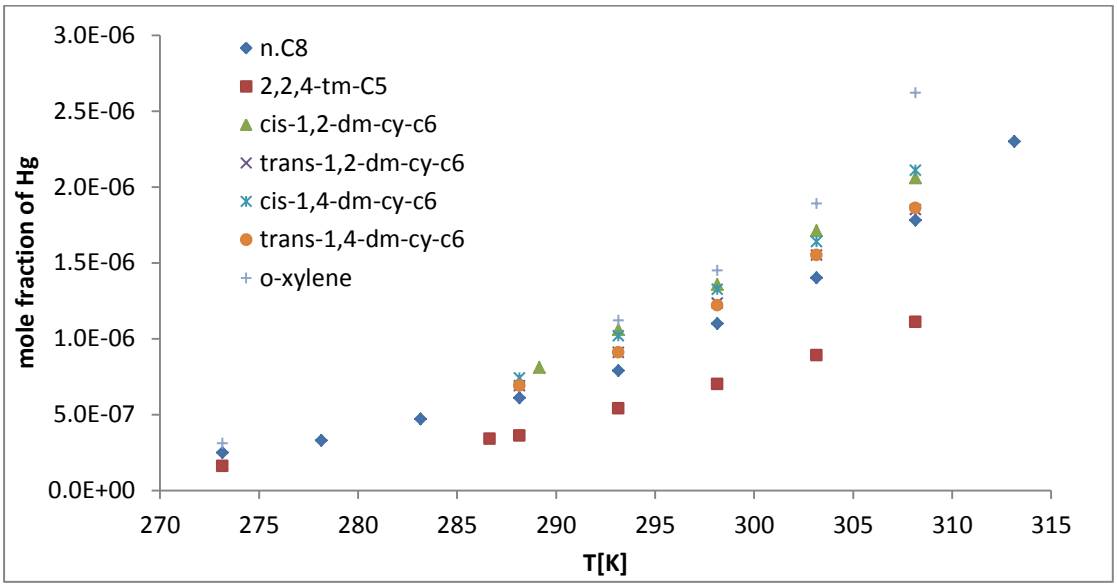

Figure 5: Solubility of Hg in liquid HC with carbon number 8

Finally as far as the HC with 8 carbon atoms are concerned, Hg 'prefers' the least the 2.2.4-tm-C_5, more than that it 'prefers' n.C_8, more than that the cyclo-alkanes and it is solubilized the most in the aromatic HC o-xylene.

One observation that can be made is that almost the same order of preference that applies to the solubility of Hg in HC with carbon number 6 applies to the HC with carbon number 7 and 8. The only difference can be located at the order of the cyclo-alkanes and the aromatic HC. The data of aromatic HC and cyclo-alkanes for 7 and 8 atoms of carbon number respectively suggest that Hg is more soluble in aromatic HC than in cyclo-alkanes.

Figure 6 shows the effect of the carbon number for straight-chained HC on the solubility of Hg in n.$C_{5\text{-}10}$ except for n.C_9 because there are no experimental data available for it.

Figure 6 shows that at the lower temperatures where solubility data are available, that all n.alkanes dissolve almost the same amount of Hg except for n.C_{10} that solubilizes a bigger amount. As the temperature rises figure 5 shows that the greater the number of C atoms of the n.alkane is, the more soluble Hg is in it. This observation is valid for the liquid data of propane as well because the mole fractions of Hg in it fluctuate from 10^{-8} to 10^{-7} magnitude of order as it will be seen at the next chapter [8].

Therefore a conclusion to which one can arrive from this figure is that the 'heavier' the n.alkane is, the more amount of Hg it dissolves. This trend may with every

precaution be valid for n.butane as well, meaning that n.alkanes with carbon number less than 5 may indeed solubilize less amount of Hg than what the rest of the n.alkanes do in the liquid phase. This is an important observation because after further analyzing it one may suggest that in a process plant the biggest part of the total Hg in the feed stream is expected to be found in the streams with the 'heavier' HC and in the liquid phase.

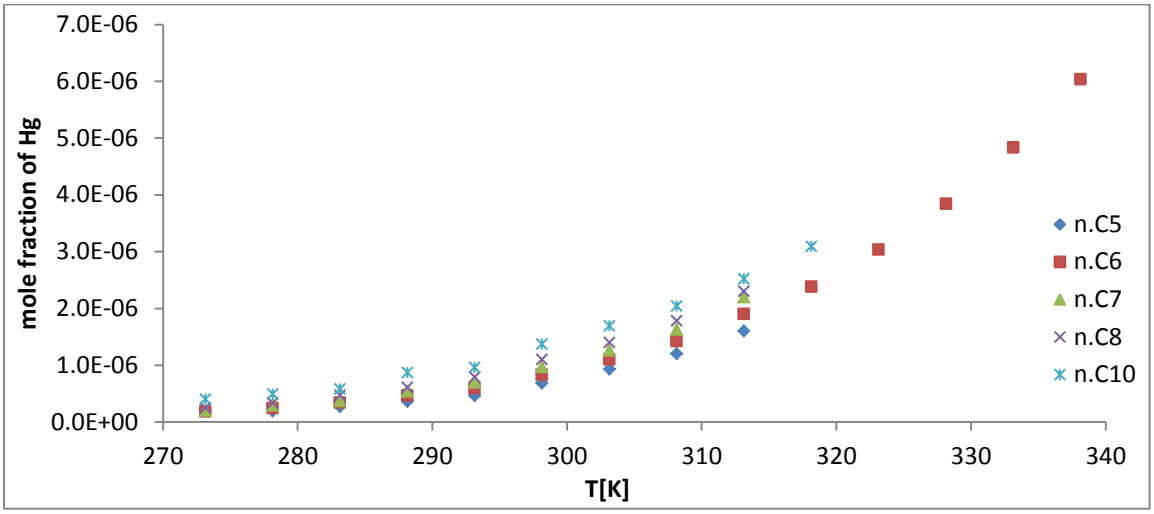

Figure 6: Solubility of Hg in liquid n. alkanes

The next case examines the effect of the branches that a HC may have on regardless of their carbon number. Figure 7 shows the solubility of Hg in all branched alkanes for which there are available experimental data.

As far as 2.2-dm-C_4 and 2.2.4-tm-C_5 are concerned, the data suggest that at temperatures lower than 288.15 K, they dissolve the same amount of Hg, and for higher temperatures, the heavier one can dissolve more Hg. This is in agreement with the conclusion deducted from the n.alkanes that Hg 'prefers' the heavier HC.

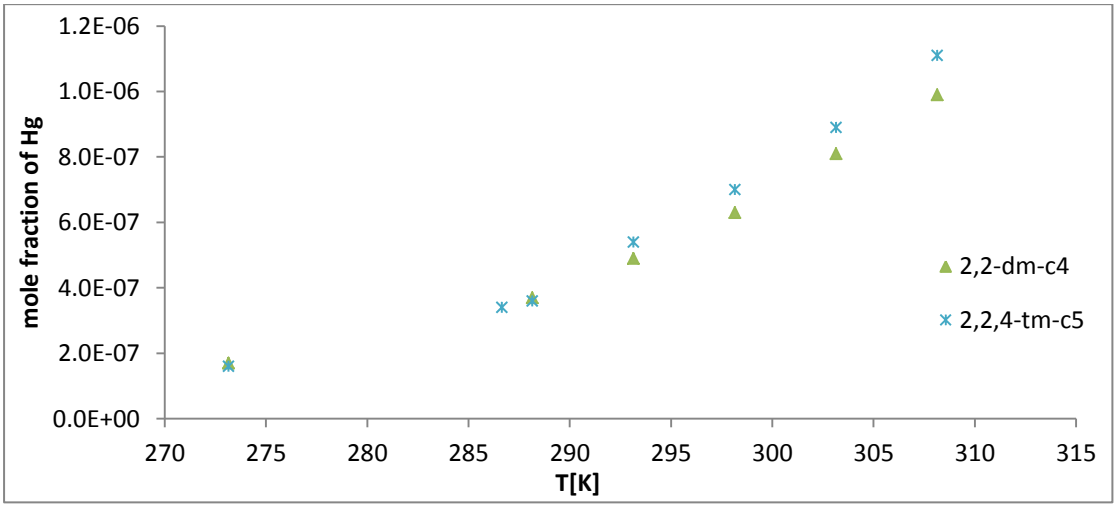

Figure 7: Solubility of Hg in liquid branched alkanes

The next figure presents the effect of the aromacity on the solubility of Hg in HC regardless of the number of C atoms of the HC. Figure 8 shows the solubility of Hg in all aromatic HC for which there are available experimental data. It is reminded that toluene's and o-xylene's data are classed as tentative.

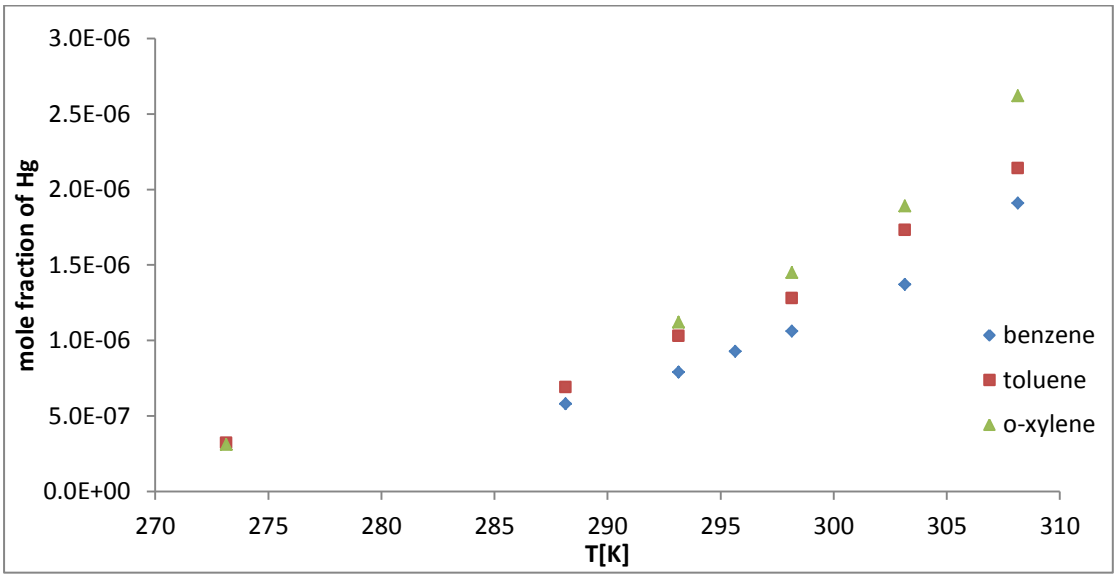

Figure 8: Solubility of Hg in liquid aromatic HC

At 273.15 K o-xylene and toluene dissolve almost the same amount of Hg. As the temperature rises however, it is made clear that Hg is more soluble in o-xylene than in toluene and more soluble in toluene than in benzene. In addition as the temperature rises figure 8 suggest that the difference among the solubility of Hg in 'heavier' and 'lighter' aromatic HC is constantly increasing. That means that for temperatures higher than 308.15 K one may well anticipate that this difference will keep increasing judging from figure 8.

Therefore it is observed that the aromatic HC with (n+1) C atoms can dissolve more Hg than the aromatic HC with (n) C atoms. The same thing is valid for n.alkanes as well. So one may suggest that there is a general 'rule' for the solubility of Hg in HC, that it is always more soluble in the HC with higher molecular weight when it comes to the same type of HC.

The next case examines the solubility of Hg in all cyclo-alkanes. Figure 9 shows the solubility of Hg in every cyclo-alkane for which there are experimental data available. It has to be reminded beforehand again that all the experimental data, except for those concerning the cy-C_6, are classed as tentative in the IUPAC's book [6].

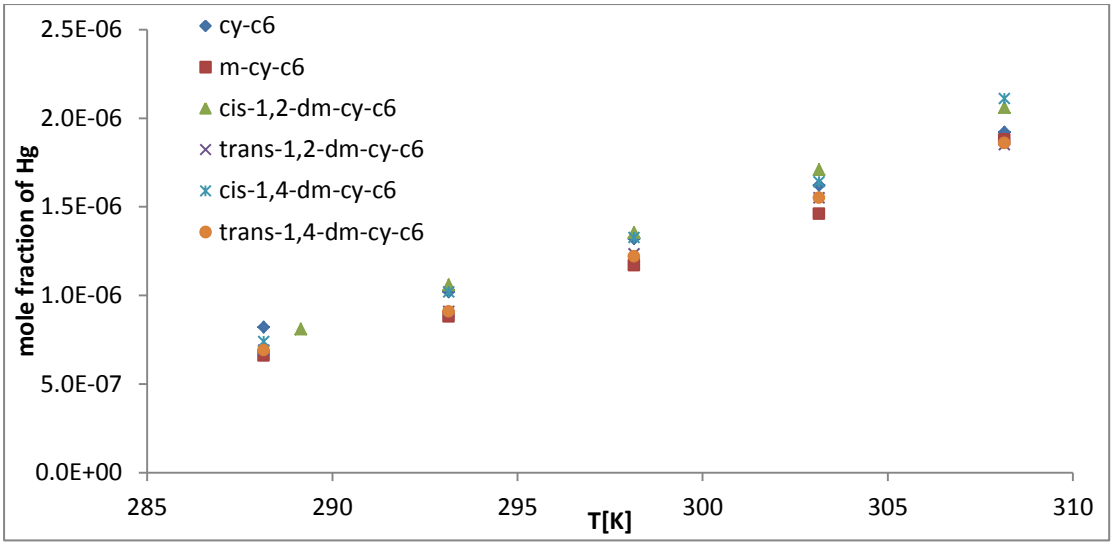

Figure 9: Solubility of Hg in liquid cyclo-alkanes

At 288.15 K cy-C_6 is the component that dissolves the biggest amount of Hg, cis-1.4-dm-cy-C_6 is the next best solvent and all the other solvents dissolve almost the same amount of Hg.

Figure 9 also suggest that m-cy-C_6 is the solvent that solubilizes the least amount of Hg. That doesn't apply for the temperature of 308.15 K where it can dissolve almost the same amount of Hg as all the other solvents except for cis-1.2-dm-cy-C_6 and cis-1.4-dm-cy-C_6.

Cy-C_6 is the best solvent at 288.15 K and among the bests up to 298.15 K. Above that temperature Hg 'prefers' the cis-1.2-dm-cy-C_6, and cis-1.4-dm-cy-C_6. Trans-1.2 and 1.4-dm-cy-C_6 present almost the same solubility ability regardless of the temperature. Although these components have the same number of C atoms as their respective cis structures, Hg is more soluble in the cis ones. This suggests that the trans structure is prohibiting Hg from dissolving in these solvents as much as it does in the cis structure.

As far as the cis-1.2 and 1.4-dm-cy-C_6 are concerned, they appear to be among the best solvents along with cy-C6. Above 300 K they dissolve a bigger amount of Hg than cy-C_6 does. An interesting fact is that at 303.15 K cis-1.2-dm-cy-C_6 is better solvent than the 1.4 respective one, but at 308.15 K the experimental data suggest the exact opposite. This fact can probably be attributed to the position of their second methyl-group.

A further analysis of these data can be found at the appendix C at figures C1-10 where 4 more cases are being investigated. After this analysis there are four general conclusions can be summed up as shown below:

1) Hg is more soluble in heavier HC compared to the lighter ones of the same type, meaning n.alkanes, cyclo-alkanes, aromatic HC, and branched alkanes

2) The branched alkanes dissolve the least amount of Hg

3) For all HC the order of their ability to dissolve Hg is as follows: branched alkanes < normal alkanes < cyclo-alkanes < aromatic HC. For the HCs with 6 C atoms there is a difference at the order of the aromatic HC and the cyclo-alkanes

4) At some cases the aromatic HC can dissolve more Hg than n.alkanes even if the n.alkanes have more C atoms than the aromatic HC. The same conclusion applies for the cyclo-alkanes as well.

Generally these conclusions present a good indication of how Hg is expected to distribute in a real process. One last comment about these data is that Hg is not very soluble in HCs and the deviations between its' solubility in various types of HCs are not very big. Therefore at a real process one may anticipate that the bigger part of Hg will end up in the streams with the 'heavier' HC and with the bigger concentration in aromatic HC and cyclo-alkanes, however this does not necessarily mean that almost no Hg will end up in other streams as well. This is said because of the results from Carnell's P. et al survey [9], which indicated that Hg distributes throughout entire gas processing plants. Thus it is not possible to provide a safe estimation beforehand about its' exact distribution throughout a process.

3.2.4 Experimental errors of the data assembled

It is of great importance for one to know the error margins of the experimental data at hand. Unfortunately all data available for the solubility of Hg in other components of interest to the natural gas industry do not include their experimental errors. It is obvious that for the data assembled from IUPAC [6], one cannot even estimate that error since the solubility of Hg is in the liquid phase. As far as the data assembled from [8] goes however, it is possible to have an estimation of it and thus get a feeling about the accuracy for the models that will be developed.

[8] has solubility data of Hg both in the liquid and in the vapor phase for some components as seen in section 3.2.3, at table 6. The vapor phased data can be used in order to get a feeling of the experimental error for this report's data.

It is known [10] that for "low pressures", which are within the margin of 1 to 20 bar, the following formulas are valid:

1) $dG = R\,T\,d(lnf)$ (eq. 3) if T, x constant

2) $dG = V\,dp$ (eq. 4) if T, x constant

3) By combining eq. 3, 4 it occurs: $R\,T\,d(lnf) = V\,dp$ (eq. 5)

4) $\varphi = \frac{f}{p}$ (eq.6)

5) From eq. 6 it occurs : $d(lnf) = d(ln\varphi) + \frac{dp}{p}$ (eq. 7)

6) By putting eq. 7 to eq. 5 and if $Z = \frac{p\,V}{n\,R\,T}$ it is: $ln\varphi = \int_0^p (Z-1)\,\frac{dp}{p}$ (eq. 8)

7) $f_i^v = f_i^l \Rightarrow y_i\,\hat{\varphi}_i\,p = x_i\,\gamma_i\,p_i^s \exp[\int_0^{p_i^s}(Z-1)\,\frac{dp}{p} + \frac{1}{R\,T}\int_{p_i^s}^{p}(V_i)\,dp]$ (eq. 9)

8) Assumptions:

   i) V_i is the liquid molar volume, independent of p and equal to V_i^s

   ii) V_i is negligible, therefore $V_i \to 0 \Leftrightarrow p = p_i^s \Rightarrow \frac{1}{R\,T}\int_{p_i^s}^{p}(V_i)\,dp = 0$

   iii) The gas phase is considered to be an ideal one, thus: $\hat{\varphi}_i = \varphi_i$

   iv) For ideal gasses it is considered that: $\varphi_i = \varphi = 1$ and also $Z = 1$

   v) Therefore $\int_0^{p_i^s}(Z-1)\,\frac{dp}{p} = 0$

   vi) The liquid phase is considered to be an ideal solution and also pure Hg. Thus it is deducted that $\gamma_i = 1$ and $x_i = 1$

9) By using the assumptions mentioned and eq. 9 one can conclude that: $y_i = \frac{p_i^s}{p}$ (eq. 10)

Where:

   a) dG is the derivative of the Gibbs energy

   b) R is the global constant of gasses

   c) f is the fugacity

d) V is the liquid grammomolar volume

e) φ is the fugacity coefficient

f) γ is the activity coefficient

g) $\hat{\varphi}_i$ is the fugacity coefficient of a gas "i" in a mixture consisted of many gasses

h) T is the absolute temperature [K]

i) p is the pressure

j) f_i^v is the fugacity of component "i" in the vapor phase

k) f_i^l is the fugacity of component "i" in the liquid phase

l) x_i is the liquid mole fraction of component "i"

m) y_i is the vapor mole fraction of component "i"

n) The superscript "s" indicates saturated property

By using the DIPPR's equation it is possible to estimate very accurately the p^s of Hg at the temperatures of the experimental data that fit within the "low" pressure margin. Tables 7 and 8 present the y_{ideal} of Hg estimated as $\frac{p_{Hg^s}}{p}$, the experimental y_i of Hg and their deviations for the binary systems of Hg with propane and N_2 respectively.

Table 7: Deviations between the experimental y_i and the y_{ideal} for Hg in propane

T [K]	Dy%
273.15	16.54
278.15	18.10
283.15	16.39
288.15	15.75
293.15	16.09
Overall dev.	16.57

Table 8: Deviations between the experimental y_i and the y_{ideal} for Hg in N_2

T [K]	Dy%
273.15	3.96
273.15	3.59
273.15	8.21
Overall dev.	5.26

Table 9: Deviations of the models from $y_{\text{ideal}} = \frac{p_{\text{Hg}}^{s}}{p}$ for the binary mixture of Hg with C_3

T [K]	PR-MC dev. %	SRK-Twu dev. %	UMR-PRMC dev.%
273.15	4.54	4.36	2.35
278.15	4.98	3.24	2.54
283.15	5.23	3.61	2.53
288.15	6.19	4.67	3.15
293.15	6.63	5.21	3.22
Overall dev. for each model %	5.51	4.22	2.76
Total overall dev. for all models %	4.16		

Table 10: Deviations of the models from $y_{\text{ideal}} = \frac{p_{\text{Hg}}^{s}}{p}$ for the binary mixture of Hg with N_2

T [K]	PR-MC dev. %	SRK-Twu dev. %	UMR-PRMC dev.%
273.15	2.70	1.44	2.64
273.15	2.76	1.50	2.69
273.15	7.77	6.77	7.64
Overall dev. for each model %	4.41	3.24	4.32
Total overall dev. for all models %	3.99		

The analytical results of tables 9 and 10 will be presented at their corresponding subchapters explicitly. The deviations of these tables imply that as the pressure rises, so does the deviation between the models and the y_{ideal}. This is expected since the raise of pressure means also the movement away from the area where the vapor mole fractions of Hg behave as an ideal gas.

It can be seen that the overall average experimental error is 16.57% for Hg in propane and 5.26% for the system of Hg with N_2 compared to the y_{ideal}. These percentages set an "ideal" experimental error area. However no system in nature can be considered as totally ideal, therefore there will always be a deviation from that ideal consideration. The three models that will be developed in the following chapter can provide an estimation of this deviation from the ideal state without of course being totally accurate. For that reason if the results from tables 7-10 are combined, it can be concluded that the approximate deviation of the experimental error of these data in the vapor phase compared to the more realistic non-ideal systems, is higher than 10% -around 13%- regarding the mole fractions of Hg in propane, and around 1.3% regarding the mole fractions of Hg in N_2. These experimental errors are extremely good, given the fact that the Hg solubility is

measured in ppb. Furthermore this area set by these percentages will be called for the rest of the master thesis as “non-ideal” experimental error area.

Given the experimental error for Hg in propane, this can be generalized to include all the vapor phased data in the database concerning Hg in HCs from [8], for which the respective parameters of each model will be estimated. This is important to know because that way one has an indication about whether the results of the models need to be further improved in order for them to be more accurate or not, depending on whether their results are within both experimental error areas and especially the “non-ideal” one.

References:

[1] T.E. Daubert et al.(1994), “Physical and Thermodynamic Properties of Pure Chemicals, Data Compilation”, Hemisphere, New York

[2] Marcia L. Huber et al.(2006), “The vapor pressure of mercury”, NIST

[3] Kozhevnikov et al.(1996), “S. Phase transitions and critical phenomena in mercury fluid probed by sound”, Fluid Phase Equilib., 125: 149-157

[4] Robert R. Kuntz et al.(1963), “The Solubility of Mercury in Hydrocarbons”, The Journal of Physical Chemistry

[5] M. M. Miedaner et al. (2005), “Solubility of metallic mercury in octane, dodecane and toluene at temperatures between 100 ^{o}C and 200 ^{o}C”

[6] IUPAC, “Solubility Data Series, Mercury in liquids, compressed gases molten salts and other elements”, Volume 29, p. 101-160

[7] **Confidential reference**

[8] **Confidential reference**

[9] Carnell P. et al (2004),''MERCURY DISTRIBUTION ON GAS PROCESSING PLANTS '', 83rd annual GPA convention proceedings, New Orleans

[10] Michael M.Abbott, Hendrick C. Van Ness (1983), ''Θερμοδυναμική'', Translated by Konstantinos N. Pattas, Nikolaos A. Kiriakis, Schaum outline series, Mc Graw-Hill, New York, p. 238-239, 262-263

Chapter 4: Thermodynamic modeling

4.1 SRK and PR EOS

In this thesis parameters for three models will be developed. These models are based on the SRK [1] and the PR EOS [2]. The reason why these two EOS are chosen is because they are widely used for process simulations at the industrial sector. There are of course other models, more advanced as well, that differ from these EOS. One example is the UMR-MCPRU model developed by Voutsas et.al[3] that uses more advanced mixing rules than the Van der Waals one fluid [4] used by classical EOS SRK and PR. One other example is the PC-SAFT equation [5] that is not a cubic equation of state. Such models could very well be examined as a future work in order to compare their results with the ones from the models that will be developed in this master thesis. It is mentioned that the "b" parameter is estimated for each model as described at [4] and is not analyzed in this master thesis since no adjusting for it has occurred.

The SRK EOS is presented as equation 11:

$$P = \frac{RT}{V_m - b} - \frac{a}{V_m(V_m + b)} \quad \text{(eq. 11), where}$$

$$a = \sum_i \sum_j x_i x_j (a_i a_j)^{0.5} (1 - k_{ij}) \quad \text{(eq. 12) and}$$

$$a_i = \alpha_i 0.42747 \frac{R^2 T_{ci}^2}{P_{ci}}, \alpha_i = alpha \quad \text{(eq. 13)}$$

The PR EOS is presented as equation 14:

$$P = \frac{RT}{V_m - b} - \frac{a}{V_m(V_m + b) + b(V_m - b)} \quad \text{(eq. 14), where}$$

$$a = \sum_i \sum_j x_i x_j (a_i a_j)^{0.5} (1 - k_{ij}) \quad \text{(eq. 15) and}$$

$$a_i = \alpha_i 0.45724 \frac{R^2 T_{ci}^2}{P_{ci}}, \alpha_i = alpha \quad \text{(eq. 16)}$$

4.2 Evaluation of SRK and PR EOS with two different sets of T_c, P_c, ω

The Neqsim tool [6] was used for the calculation of the P^s of Hg with SRK and PR EOS. It has to be mentioned that Neqsim was able to provide P^s from 238.15 K up to almost 1728 K (depending on the set of T_c, P_c, ω that was examined and on the EOS that was used). This temperature is close to the critical one and perhaps this is the reason why it was not able to provide P^s for any higher temperatures.

Figure 10 illustrates the deviations of the P^s acquired from Neqsim tool using the SRK with both sets of T_c, P_c and ω for temperatures from 238.15 K up to 640.15 K. It can be seen that the deviations are quite big and that SRK under-predicts the P^s of Hg at those temperatures.

NIST's set of T_c, P_c, ω predicts better the P^s than DIPPR's set does for these temperatures. The maximum deviation for DIPPR's set was observed at the lowest temperature and was 87.5%. The maximum deviation for NIST's set was also observed at the lowest temperature and was 66.7%.

For temperatures higher than 640 K, as figure 10 implies as well, the deviations become significantly smaller. Table A2 at the appendix A presents the deviations of the P^s calculated by the Neqsim tool using the SRK EOS and eq. 2 analytically.

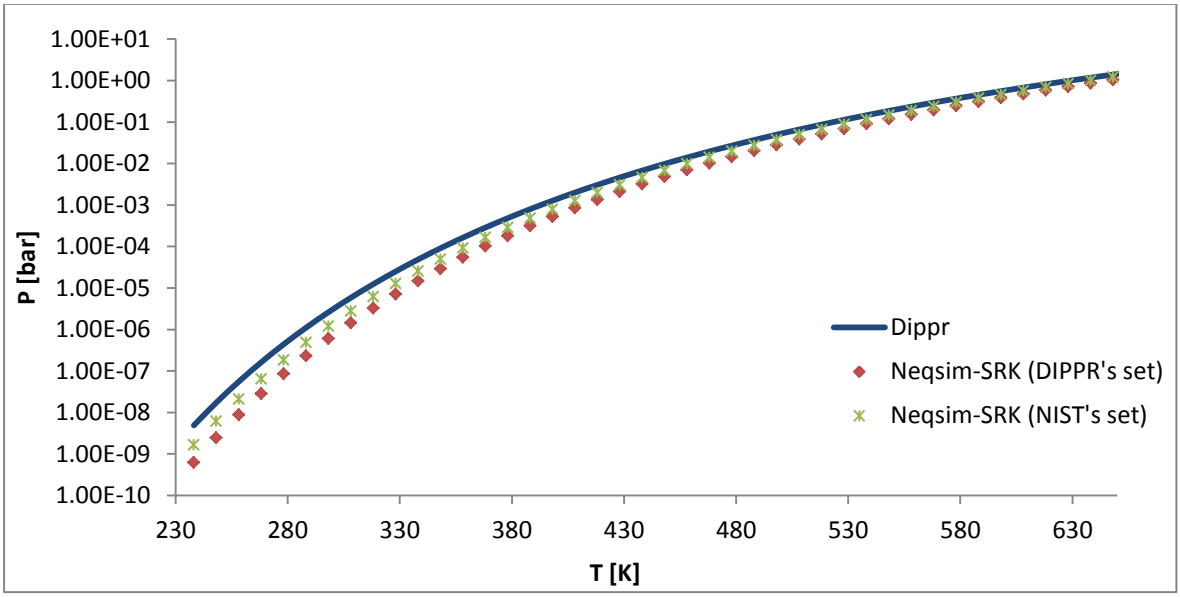

Figure 10: Comparison of results from DIPPR's eq. and Neqsim tool using the SRK EOS for both set of T_c, P_c and ω

Table 11: Absolute average deviation of each case examined

	SRK (DIPPR's set)	SRK (NIST's set)
Absolute average deviation %	18.53	12.02

Table 11 indicates that the set of T_c, P_c, ω from NIST's report improves the prediction of the P^s compared to the set proposed by DIPPR for the whole temperature range examined. However the absolute average deviation is considerably smaller -about 6.5%- than the deviations at the temperatures shown at figure 10, because as the temperature rises the deviations are getting significantly smaller. Thus the absolute average deviation is significantly reduced.

Table 12 presents some indicative P^s estimated from the SRK EOS and their respective deviations from the experimental P^s of eq.17. It can be seen that as the temperature rises the deviations of the estimated and the experimental P^s are declining and above 1500 K are rising again. Still the deviations are not that high -less than 2%-. Furthermore the SRK EOS using DIPPR's set is providing less accurate estimations of the P^s than the one using NIST's set for the whole temperature range.

$$\Delta P^s\ \% = \frac{(Pexp - Pcalc)*100}{Pexp} \quad \text{(eq. 17)}$$

Set 1 = DIPPR's set of T_c, P_c, ω

Set 2 = NIST's set of T_c, P_c, ω

Table 12: Indicative P^s estimated from Neqsim tool using SRK EOS and their respective deviations from the experimental P^s estimated by eq.17

T [K]	DIPPR P^s [bar]	Neqsim-SRK (set 1)	ΔP^s %	Neqsim-SRK(set 2)	ΔP^s %
238.15	4.90E-09	6.13E-10	87.49	1.63E-09	66.65
368.14	2.85E-04	1.01E-04	64.65	1.64E-04	42.53
478.14	0.027	1.44E-02	46.71	0.0194	28.27
588.14	0.452	3.06E-01	32.43	0.369	18.37
678.14	2.266	1.734	23.47	1.978	12.71
798.14	10.942	9.334	14.70	10.113	7.58
878.14	24.574	22.024	10.38	23.291	5.22
938.14	41.200	38.007	7.75	39.617	3.84
1058.14	97.501	93.908	3.69	95.712	1.83
1188.14	205.531	204.177	0.66	204.471	0.52
1298.14	347.101	350.607	-1.01	347.152	-0.01
1308.14	362.641	366.719	-1.12	362.776	-0.04
1428.14	588.989	601.037	-2.05	588.825	0.03
1538.14	870.370	889.198	-2.16	864.756	0.64
1648.14	1236.647	1256.377	-1.60	1214.210	1.81

Figure 11 shows the deviations of the P^s acquired from Neqsim tool while using the PR EOS this time for both sets of T_c, P_c and ω at temperatures from 238.15 K up to 640.15 K. It can be seen that the deviations are bigger than those for the SRK EOS.

Also PR seems to under-predict the P^s of elemental Hg at those temperatures while using the DIPPR's set, whereas it over-predicts it while using the NIST's set.

The use of DIPPR's set of T_c, P_c, ω seems to lead to better results P^s than NIST's set does at low temperatures. The maximum absolute deviation noted was 89.5% for NIST's set, whereas DIPPR's set had a maximum deviation of 32.7%.

For higher temperatures, as figure 11 implies as well, the deviations become significantly smaller. Table A2 at the appendix A presents the deviations of the P^s calculated by Neqsim tool using the PR EOS and analytically.

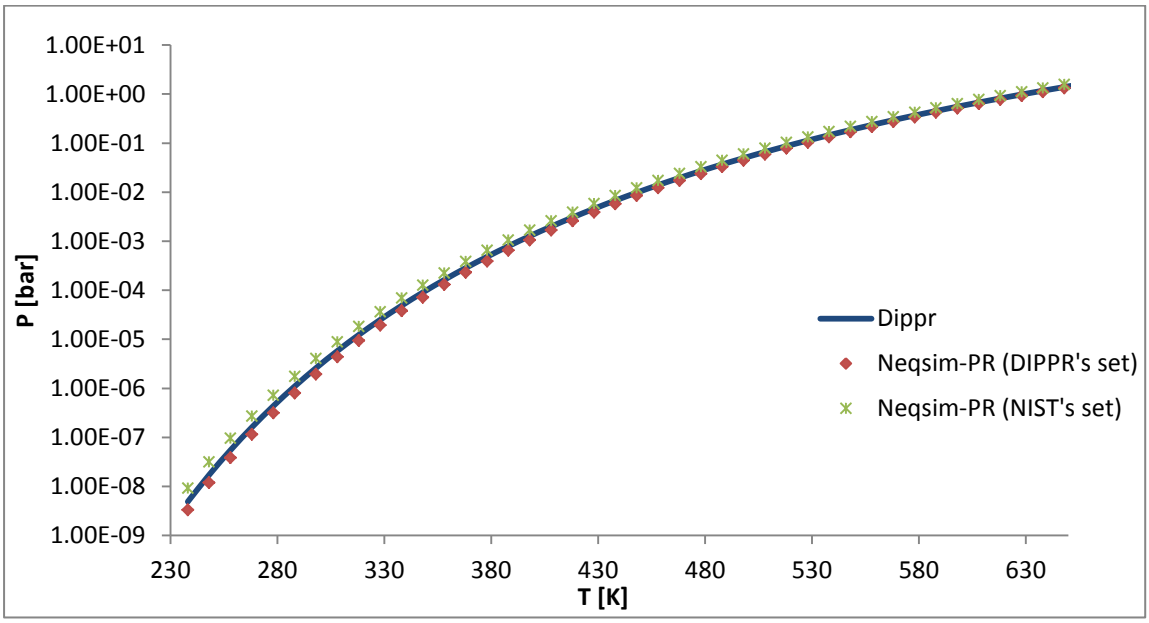

Figure 11: Comparison of results from DIPPR's eq. and Neqsim tool using the PR EOS for both set of T_c, P_c and ω

Table 13 presents some indicative P^s estimated from the PR EOS and their respective deviations from the experimental P^s of eq. 2. Like the SRK EOS and the PR EOS show, as the temperature rises, the deviations of the estimated and the experimental P^s are declining and above 1500 K are rising again. In addition the PR EOS using NIST's set is providing less accurate estimations of the P^s than the one using DIPPR's set for the whole temperature range.

$$\Delta P^s\,\% = \frac{(Pexp - Pcalc)*100}{Pexp} \quad \text{(eq. 18)}$$

Set 1 = DIPPR's set of T_c, P_c, ω

Set 2 = NIST's set of T_c, P_c, ω

Table 13: Indicative P^s estimated from Neqsim tool using PR EOS and their respective deviations from the experimental P^s of eq.18

T [K]	DIPPR P^s [bar]	Neqsim-PR(set 1)	ΔP^s %	Neqsim-PR(set 2)	ΔP^s %
238.15	4.90E-09	3.30E-09	32.70	9.29E-09	-89.50
368.14	2.85E-04	2.298E-04	19.47	0.00039	-35.84
478.14	0.027	0.0238	11.95	0.033	-21.89
588.14	0.452	0.4216	6.81	0.521	-15.07
678.14	2.266	2.177	3.95	2.528	-11.58
798.14	10.942	10.785	1.43	11.857	-8.36
878.14	24.574	24.504	0.28	26.242	-6.79
938.14	41.200	41.364	-0.40	43.602	-5.83
1058.14	97.501	98.913	-1.45	101.721	-4.33
1188.14	205.531	210.101	-2.22	211.860	-3.08
1298.14	347.101	356.113	-2.60	354.502	-2.13
1308.14	362.641	372.128	-2.62	370.0579	-2.05
1428.14	588.989	604.594	-2.65	594.509	-0.94
1538.14	870.370	890.477	-2.31	868.048	0.27
1648.14	1236.647	1256.077	-1.57	1215.157	1.74

Table 14: Absolute average deviation of each case examined for the whole temperature range

	PR (DIPPR's set)	PR (NIST's set)
Absolute average deviation %	3.76	11.83

To sum up, table 14 indicates that the set of T_c, P_c, ω from DIPPR improves the prediction of the P^s compared to the set proposed by NIST for the whole temperature range examined when used by the PR EOS. This is the exact opposite conclusion compared to the one from the SRK EOS. Furthermore the PR EOS seems to be able to predict more accurately the P^s of Hg than the SRK EOS does. Thus there is no clear advantage for NIST's set over the one from DIPPR.

DIPPR's set in addition has the advantage that is used in official software like Hysys, PROII and PVT-Sim. Therefore it has been decided that this set will be used for the calculations and the fitting of all the parameters necessary for the thermodynamic models that will be developed for this master thesis.

4.3 Calculation of the Mathias-Copeman parameters for Hg for the PR EOS

The parameters of Mathias-Copeman (MC) [7] will be introduced in the PR EOS. These parameters are fitted to experimental P^s data of pure components and provide a better description of the P^s than the correlation of Soave for the 'alpha' parameter. The MC parameters are associated with the calculation of the 'alpha' parameter for the EOS. The equation with these parameters is equation 19 and the alpha parameter of Soave is equation 20. The objective function that is used for the calculation of the MC parameters is equation 21.

$$\alpha(Tr) = [1 + c_1\left(1 - \sqrt{Tr}\right) + c_2\left(1 - \sqrt{Tr}\right)^2 + c_3\left(1 - \sqrt{Tr}\right)^3]^2 \quad \text{(eq.19)}$$

$$\alpha(Tr) = [1 + c_1\left(1 - \sqrt{Tr}\right)]^2 \quad \text{(eq.20)}$$

$$F = \sum_i \left(\frac{100*(P^s_{icalc} - P^s_{iexp})}{P^s_{iexp}}\right)^2 \quad \text{(eq.21)}$$

The results from eq. 2 at table A1 were used as experimental data for the fitting of the MC parameters because they cover Hg's temperature range from the freezing point up to the critical point. Table 15 presents the parameters calculated for DIPPR's set of T_c, P_c and ω as well as the temperature range of the fitting in terms of T_r.

Table 15: The estimated MC parameters

MC Parameters	T_r ε [0.137, 0.875]
MC1	0.1491
MC2	-0.1652
MC3	0.1447

As table 15 illustrates, the temperature fitting range is from T_r = 0.137 (that means T = 238.15 K) up to T_r = 0.875 (which means T = 1518.15 K). Given the fact that the freezing point of Hg is at 234.15 K, the lower limit of the T_r range can be characterized as satisfying.

After the MC parameters were determined, the PR EOS was employed while calculating the new alpha parameter as it stands at eq.19, for the prediction of the P^s anew (hereafter this EOS shall be referred as PR-MC). Figure 12 presents the deviation between the results from PR and PR-MC EOS with the results from eq. 2 respectively, for T_r = 0.137 up to T_r = 0.97.

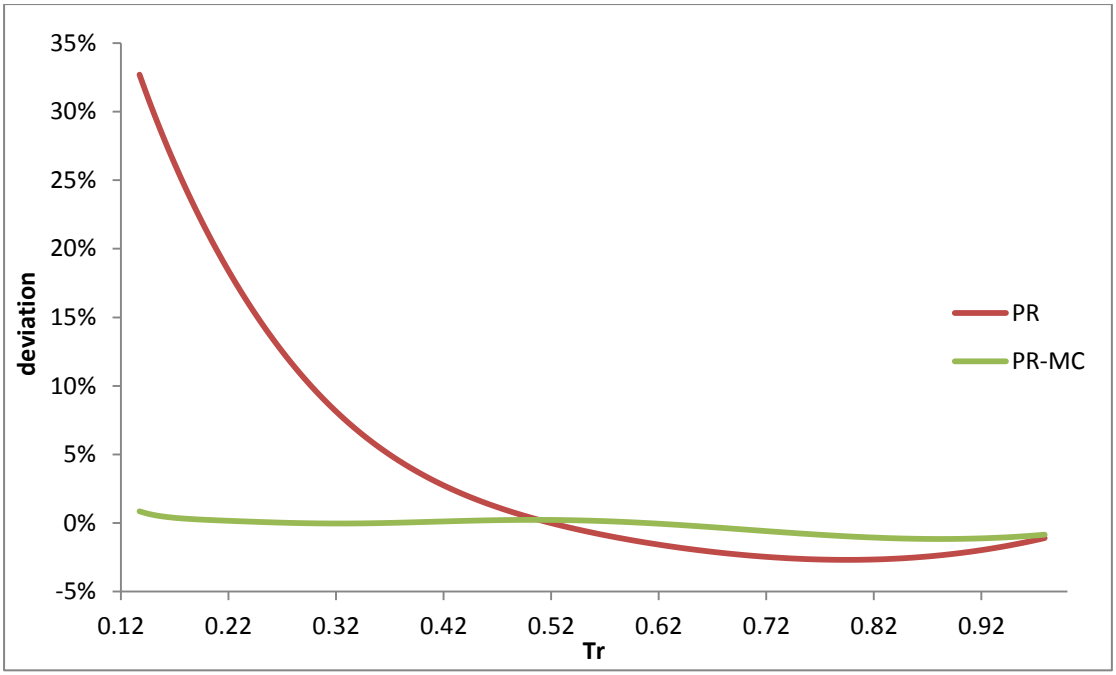

Figure 12: Deviation of P^s estimated from eq.2 and Neqsim tool using the PR and PR-MC EOS

As figure 12 indicates the results from PR-MC are much closer to those from eq.2 compared to those from PR EOS. This fact can be attributed to the effect of the MC parameters, something that also reveals the importance of these parameters to the model under development.

It can also be observed that for T_r = 0.88 and above that the deviation becomes significantly larger compared to what it was below that reference temperature. This could be explained up to a point by the fact that the temperature range that was used for the fitting was up to T_r = 0.875. However these deviations are still less than 1.2% and furthermore they will have no effect on the testing of the models because the processes in the natural gas industry take place at much lower temperatures.

At the appendix B at table B1 analytical P^s for all temperatures and their respective deviations can be found for PR-MC.

Table 16: Absolute average deviation of PR and PR-MC EOS from the experimental P^s for temperatures from 238.15 K up to 608.15 K

	PR	**PR-MC**
Absolute average deviation %	16.75	0.19

As an overall comment as table 16 shows, the P^s calculated from PR-MC present small deviation to the P^s calculated from eq.2 from 238.15 K up to 608.15 K. This is

extremely important because this temperature range also includes the temperatures where the processes of natural gas take place.

4.4 Calculation of Twu parameters for Hg for the SRK EOS

The L, M, N parameters introduced by Twu [8] also apply to the calculation of the alpha parameter for the SRK-Twu EOS. Like the MC parameters, these are also fitted to experimental P^S data of pure components and assist in a better description of the P^S for pure Hg. The equation with these parameters is eq.22. The objective function for the calculation of these parameters is again equation 21.

$$\alpha(Tr) = Tr^{N(M-1)} \exp[L(1 - Tr^{MN})] \quad \text{(eq.22)}$$

The temperature range at which the author did the fitting of the L, M, N parameters was that of 238.15 K up to 1508.15 K. As mentioned for the MC parameters as well, given the fact that the freezing point of Hg is at 234.15 K, the lower limit of the T_r range can be characterized as satisfying. Table 17 presents the parameters estimated for the SRK EOS.

Table 17: Estimated L, M, N parameters

Twu-Coon Parameters	**T_r ε [0.137, 0.875]**
L	0.09245
M	0.9784
N	2.244

After the determination of the L, M, N parameters, SRK EOS was used while taking into consideration the parameters for the calculation of the new 'alpha', for the prediction of the P^S of pure Hg. The SRK EOS when combined with these parameters will be hereafter referred as SRK-Twu EOS. Analytical results and deviations of SRK-Twu with the experimental P^S can be found at the appendix B at table B2.

Figure 13 shows the deviation between the experimental P^S and the results from SRK and SRK-Twu EOS respectively for T_r = 0.137 up to T_r = 0.978. As figure 13 indicates the P^S acquired from the SRK-Twu EOS are much closer to the experimental data than the ones acquired from the SRK EOS. This fact can be attributed to the effect of the estimated parameters.

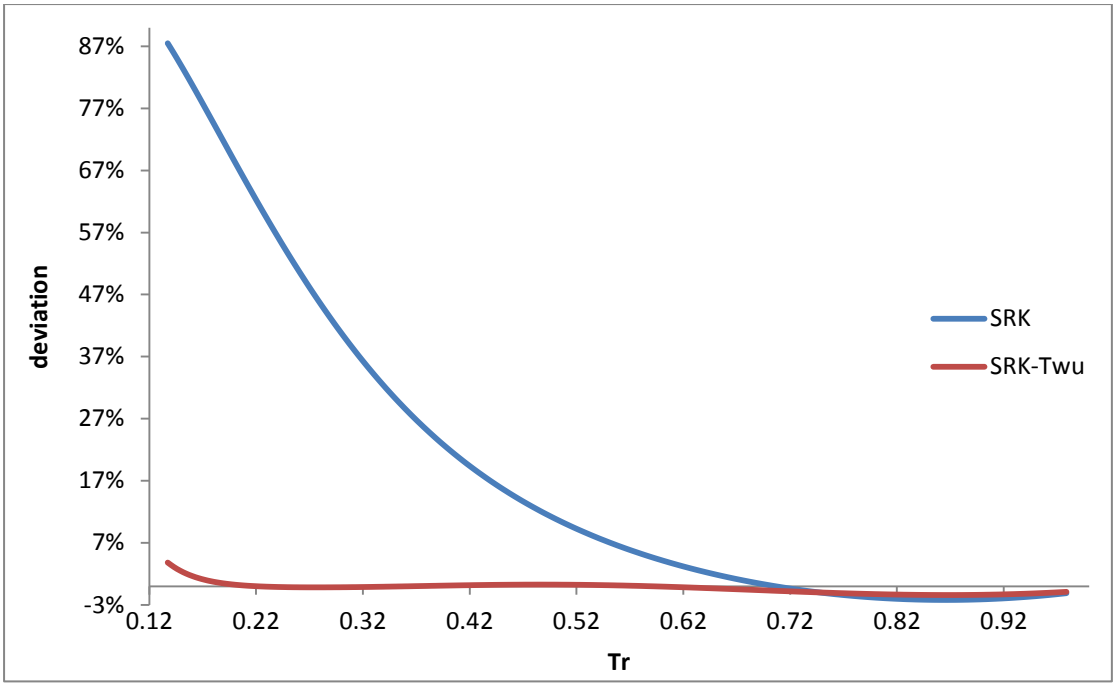

Figure 13: Deviation of P^s estimated from eq.2 and Neqsim tool using the SRK and SRK-Twu EOS

One more comment that can be made concerning those parameters and the MC parameters respectively is the fact that PR-MC EOS at the temperature range of 238.15 K up to 348.15 K seems to give a better prediction for the P^s of Hg compared to SRK-Twu EOS. The maximum deviation of the PR-MC at that temperature range is 0.86% whereas the respective deviation of the SRK-Twu using the author's L, M, N parameters is 3.82% as table 18 presents.

This fact is mentioned because this is the temperature range of major interest to the gas industry. Therefore it is a critical observation for the evaluation of the results that the models will provide once tested for a real process.

Table 18: P^s calculated using SRK-Twu and PR-MC and their deviations from the P^s of eq.2 for the temperature range of 238.15 K up to 378.15 K.

	DIPPR's eq.	**PR-MC**		**SRK-Twu**	
T [K]	**P^s [bar]**	**P^s [bar]**	**ΔP^s %**	**P^s [bar]**	**ΔP^s %**
238.15	4.90E-09	4.86E-09	0.86	4.71E-09	3.82
248.15	1.73E-08	1.72E-08	0.72	1.67E-08	3.11
258.15	5.52E-08	5.49E-08	0.62	5.38E-08	2.53
268.15	1.62E-07	1.61E-07	0.53	1.58E-07	2.05
278.15	4.37E-07	4.35E-07	0.47	4.30E-07	1.65
288.15	1.10E-06	1.10E-06	0.41	1.09E-06	1.32
298.15	2.61E-06	2.60E-06	0.37	2.58E-06	1.05
308.15	5.82E-06	5.81E-06	0.33	5.78E-06	0.82
318.15	1.24E-05	1.23E-05	0.30	1.23E-05	0.63

Continuation of table 18					
328.15	2.51E-05	2.50E-05	0.28	2.49E-05	0.48
338.15	4.86E-05	4.85E-05	0.25	4.85E-05	0.35
348.15	9.08E-05	9.06E-05	0.23	9.06E-05	0.25
358.15	1.64E-04	1.63E-04	0.21	1.63E-04	0.16
368.15	2.85E-04	2.85E-04	0.19	2.85E-04	0.09
378.15	4.83E-04	4.82E-04	0.17	4.83E-04	0.03

4.5 Estimation of the binary interaction parameters (k_{ij}) for binary systems of Hg with hydrocarbons

4.5.1 Calculation of the k_{ij} parameters

The k_{ij} parameter [9] is an important parameter that needs to be estimated for the thermodynamic models under development. The k_{ij} parameter is an empirical factor introduced to increase the accuracy of the cubic equations of states through a better representation of different pair interactions. Its implementation will help the model give a better estimation for the phase equilibrium of systems containing Hg with HCs and other components as well.

This parameter is calculated by fitting experimental solubility data of binary mixtures consisting of Hg and other hydrocarbons or other components. All the experimental data of the binary mixtures used for the fitting of the k_{ij} parameters that will be presented are in the liquid phase, except for the parameters concerning Hg in methane and N_2, which were fitted to vapor phased data.

The Neqsim-tool was used for the fitting. The objective function that the program has to minimize can be seen at equation 23.

$$F = \sum_i \left(\frac{100\ (x_{\text{icalc}} - x_{\text{iexp}})}{x_{\text{iexp}}}\right)^2 \quad \text{(eq.23)},$$

Where x represents the mole fraction of Hg.

As mentioned before, this parameter is calculated by fitting solubility data of binary mixtures of Hg with other hydrocarbons. The corresponding database has been presented in Chapter 3. For this thesis k_{ij} parameters for two different models are calculated.

The first one is the PR EOS which takes into consideration the Mathias Copeman parameters for the calculation of the 'alpha' parameter and the second one is the SRK-Twu EOS which uses the L, M, N parameters of all components for the calculation of the same parameter. The L, M, N parameters for all components were

taken from the official program PROII and the MC parameters from Neqsim's database. At the appendix D at tables D1 and D2 one can find the L, M, N and MC1, MC2, MC3 parameters of each component respectively.

Table 19 presents the k_{ij} parameters that were calculated for each binary system and each EOS respectively.

Table 19: k_{ij} parameters calculated for each binary system

System	**k_{ij}**	
	SRK-Twu	**PR-MC**
Hg-CH_4	**Confidential data**	
Hg-C_2H_6		
Hg-C_3		
Hg-n.C_5		
Hg-n.C_6		
Hg-n.C_7		
Hg-n.C_8		
Hg-n.C_{10}		
Hg-2.2-dm-C_4		
Hg-2.2.4-tm-C_5		
Hg-cy-C_6		
Hg-toluene		
Hg-m-cy-C_6		
Hg-benzene		
Hg-o-xylene		
Hg-cis-1.2-dm-cy-C_6		
Hg-cis-1.4-dm-cy-C_6		
Hg-trans-1.4-dm-cy-C_6		
Hg-trans-1.2-dm-cy-C_6		
Hg-CO_2		
Hg-N_2		
Hg-water	-	-

It is interesting to note that as table 19 shows, the k_{ij} parameters for both models when it comes to the same binary mixture are very similar to one another. In addition to that although for n.alkanes with CN equal to or greater than 3 the k_{ij} parameters are constantly declining, the respective parameters of methane and ethane do not exactly fit in this pattern. Therefore given the fact that their respective parameters have been safely derived from experimental data, these components will not be taken into consideration later on when generalized correlations for these parameters will be developed.

It is important to mention that for the binary mixtures of Hg in ethane, propane and CO_2, there are experimental data available both in the liquid phase, as well as in the vapor phase. For the fitting of the parameters required for each model, the data of the liquid phase have been used as already mentioned. Afterwards these parameters were used with each model respectively in order to predict the experimental data in the vapor phase.

The Neqsim-tool was used for the fitting of the k_{ij} parameters, as well as the prediction of the mole fractions of Hg in the vapor phase for these mixtures as well. For the prediction of the mole fractions of Hg in the vapor phase the Neqsim-tool was employed once again, doing a Bubble Point Pressure (B.P.P) calculation this time. The data given to the tool were the liquid mole fraction estimated from the fitting of the k_{ij} parameters, the k_{ij} parameters, and the pressures. This happened in order for the results of the B.P.P calculations to be in agreement, in terms of consistency, with the fitted data. This method was adopted for the B.P.P calculations of all models.

Finally a component that should be treated with extra caution is water. As table 16 indicates the binary mixture of Hg with water [13] has no constant k_{ij} parameters. For the k_{ij} parameters it was observed and concluded that they are strongly dependent on the temperature. Therefore temperature dependent parameters were developed. In order to do that the parameters were first fitted to the experimental data at 293.15 K and 363.15 K respectively and exclusively. This temperature range was decided upon the fact that at that particular area, the experimental data presented a somewhat linear behavior. After that the two parameters resulted from the fitting were combined into a linear equation.

It is stated beforehand however that due to the hydrogen bond of H_2O, the last two models are not the best option for conducting simulations of processes, since they fail to take these bonds into account.

Table 20 presents the equations of the k_{ij} parameters for the PR-MC and the SRK-Twu models, as well as the overall absolute deviations of their predictions from the experimental data. The analytical results can be found at appendix E at tables E21 and E42.

Table 20: Equations of temperature dependent k_{ij} parameters for Hg and H_2O

Model	**k_{ij} = a T[K] + b**	**Abs. Deviation (%)**
SRK-Twu	k_{ij} = 0.00254 T – 0.11382	12.86
PR-MC	k_{ij} = 0.00246 T – 0.09719	13.06

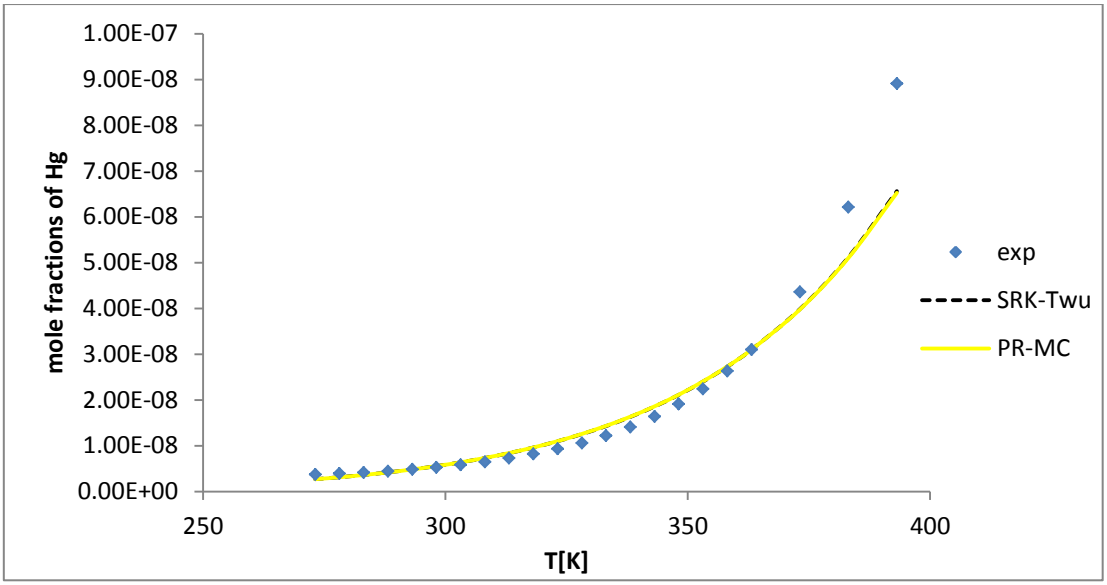

Figure 14: Experimental and predicted mole fractions of Hg in H_2O with PR-MC and SRK-Twu models

As figure 14 displays the PR-MC and SRK-Twu models fail to provide accurate predictions of the mole fraction of Hg at temperatures higher than 373.15 K. It is important however that up to that temperature the maximum deviation of both models is around 28% at 273.15 K and less than 20% for all other temperatures. Furthermore the results of both models are extremely close to one another as figure 14 illustrates and table 20 suggests as well.

Table 21 presents the absolute average deviation of the mole fraction of Hg for all systems and each EOS examined. It is noted that water was excluded from this calculation since it is considered to be a "special" component as mentioned. The 'k_{ij}=con.' means that the k_{ij} parameter is constant with temperature and different than zero. The absolute average deviation is estimated as eq. 24 shows.

In principle one may say that once the k_{ij} is calculated for each binary mixture respectively and then taken into account for the calculations of the mole fraction of Hg, as table 21 indicates as well, the accuracy of the results is improving significantly for most of the mixtures.

$$\Delta x\% = \frac{\sum_i^n (|x_{\text{icalc}} - x_{\text{iexp}}|)\ 100/x_{\text{iexp}}}{n} \quad \text{(eq.24)},$$

where x stands for the mole fraction of Hg

Table 21: The overall absolute average deviation (%) of the mole fraction of Hg in the liquid phase for each EOS

	Absolute average deviation of mole fraction of Hg for each EOS(%)	
	SRK-Twu	PR-MC
k_{ij} = 0	32.83	29.18
k_{ij} = con.	4.55	4.57

Tables 22 and 23 present the absolute overall deviation of each model -with the k_{ij} parameters- regarding the mole fractions of Hg from the experimental data of the liquid and the vapor phase respectively. Table 23 also presents the total average deviation of the models compared to the experimental data for the vapor phase.

Table 22: Absolute overall deviation (%) of the mole fractions of Hg in each binary mixture for each model concerning the liquid phase

Model	**SRK-Twu**	**PR-MC**
System	**Absolute Overall Deviation %**	
Hg-C_2H_6	5.82	5.66
Hg-C_3	0.40	0.42
Hg-n.C_5	3.33	3.62
Hg-n.C_6	2.29	1.71
Hg-n.C_7	2.04	2.21
Hg-n.C_8	3.71	3.07
Hg-n.C_{10}	12.60	12.27
Hg-2.2-dm-C_4	9.19	8.71
Hg-2.2.4-tm-C_5	5.88	5.86
Hg-cy-C_6	7.39	7.15
Hg-toluene	4.01	3.83
Hg-m-cy-C_6	3.31	2.94
Hg-benzene	1.99	2.11
Hg-o-xylene	2.91	3.52
Hg-cis-1.2-dm-cy-C_6	4.59	4.47
Hg-cis-1.4-dm-cy-C_6	3.44	3.71
Hg-trans-1.4-dm-cy-C_6	3.97	4.09
Hg-trans-1.2-dm-cy-C_6	4.35	4.05
Hg-CO_2	5.24	7.49

Table 23: Absolute overall deviation (%) of the mole fractions of Hg in each binary mixture for each model concerning the vapor phase

Model	**SRK-Twu**	**PR-MC**
System	**Absolute Overall Deviation %**	
Hg-CH_4	2.35	2.22
Hg-C_2H_6	16.33	15.37
Hg-C_3	13.04	11.96
Hg-CO_2	2.28	12.36
Hg-N_2	1.34	0.90
Total deviation %	**7.07**	**8.56**

The overall deviations illustrated at table 22 reveal that both the SRK-Twu and the PR-MC models are able to predict accurately enough Hg's mole fractions in the liquid phase. The biggest deviations from the experimental data are presented in the binary mixtures of Hg with n.C_{10} and 2.2-dm-C_4, namely around 12% and 9% for both models.

It is also notable that the overall deviations of both models for each binary mixture are very similar, as verified from table 19 as well since their k_{ij} parameters are also very close to each other. The only binary mixture that presents a difference of about 2% regarding these deviations is that of Hg in CO_2. Given however the fact that these deviations are less than 10% for all binary mixtures except for the one of Hg with n.C_{10} which is around 12.4%, which is also a very small percentage given the magnitude of order of the experimental data, it can be concluded that the models are reliable.

The overall deviations illustrated at table 23 reveal that the SRK-Twu and the PR-MC models are able to predict Hg's mole fractions in the vapor phase satisfyingly enough as well. It is very important that both models are able to predict extremely accurately the vapor phase of Hg in methane, since this is the main component of interest when it comes to natural gas processes.

The biggest deviations from the experimental data are presented in the binary mixtures of Hg with ethane and propane, namely around 15% and 12% respectively. These deviations are on the verge of the "non-ideal" experimental error area and within the "ideal" experimental error area, as defined at subchapter 3.2.4. However since they are so close to the "non-ideal" area and the solubility of Hg is measured in ppb, therefore there is also always the case of a computation error by the algorithm due to the extremely small magnitude of order, the results of the models are acceptable for both cases.

The binary mixture that once again stands out is that of Hg in CO_2. This is the first time that the PR-MC and the SRK-Twu models display such a difference in their predictions either regarding the liquid or the vapor phase. Tables 24 - 25 and figure 15 illustrate the mole fractions of Hg in the vapor phase, as estimated from the models.

Table 24: Mole fractions of Hg in CO_2 with the PR-MC model in the vapor phase

T[K]	P_{exp}[bar]	y_{exp}	y_{calc}	Δy%
273.15				12.27
278.15				10.30
283.15				12.19
288.15				11.90
293.15	**Confidential data**			15.15
Overall dev%				**12.36**

Table 25: Mole fractions of Hg in CO_2 with the SRK-Twu model in the vapor phase

T[K]	P_{exp}[bar]	y_{exp}	y_{calc}	Δy%
273.15				3.34
278.15				3.36
283.15				1.40
288.15				2.07
293.15	**Confidential data**			1.21
Overall dev%				**2.28**

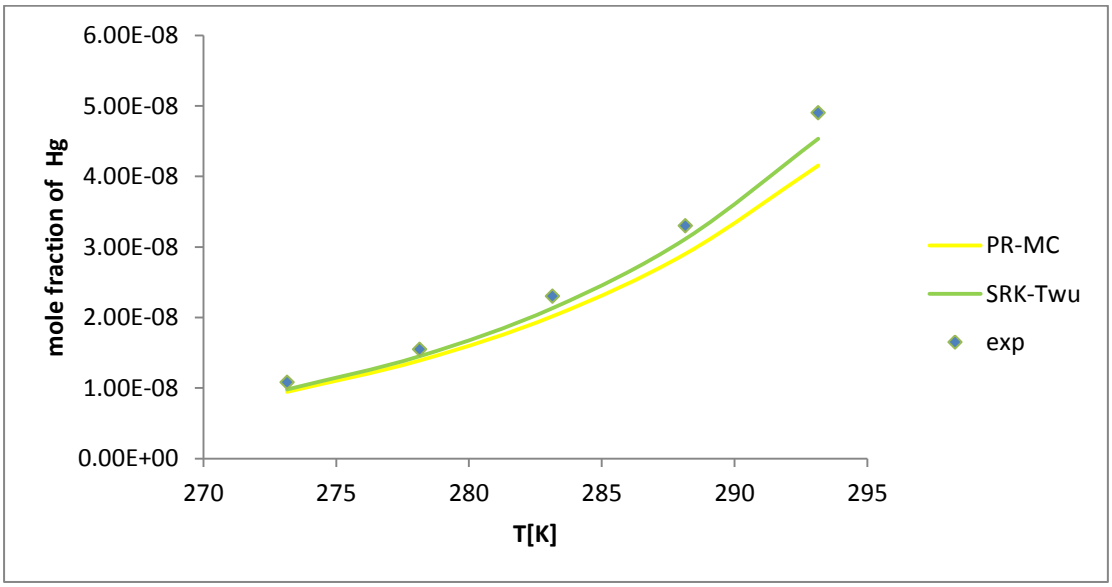

Figure 15: Experimental and estimated mole fractions of Hg in CO_2 in the vapor phase from the SRK-Twu and the PR-MC model

As tables 24 and 25 show, the mole fractions of Hg in the vapor phase, as estimated from PR-MC vary from the experimental data by 10.30% up to 15.15%, whereas the ones predicted by SRK-Twu vary by 1.21% up to 3.36%. The 15.15% appears only at the experimental point with the highest temperature and pressure and is very close to the "non-ideal" experimental error margin, therefore it can be accepted. Apparently the SRK-Twu model can describe better the experimental data, none the less both models' predictions have to be considered valid ones.

The analytical results for all binary mixtures in both the liquid and the vapor phase - where available- and both models can be found at appendices E and G, at tables E1-42 and G1-9. Figures E1-42 and G1-3 at the same appendices illustrate these results graphically.

Conclusively both the PR-MC and the SRK-Twu models are able to provide satisfactory predictions regarding the mole fractions of Hg in both the vapor and the liquid phase. There are of course some deviations in certain binary mixtures, however by still being within or very close to the acceptable limits, set by the "non-ideal" experimental error margin and within the "ideal" experimental error area, concerning the vapor phase, the models' estimations for all mixtures are considered to be credible and can be used for process simulations at a later stage.

4.6 The UMR-PRMC model

The next task of this master thesis is to estimate the Unifac group interaction parameters for the UMR-PRMC model. This is a predictive model belonging to the category of the EOS/G^E models. It is based on the PR-MC model and instead of the classical mixing rules with the k_{ij} parameters, it combines the PR-MC with a Unifac-type G^E model via the universal mixing rules developed by Voutsas et al [3]. Equations 25 to 35 describe the corresponding mixing rules.

$$\frac{\alpha}{bRT} = \frac{1}{A}\frac{G_{AC}^{E,SG}+G_{AC}^{E,res}}{RT} + \sum_i x_i \frac{\alpha_i}{b_i RT} \quad \text{(eq.25)}$$

$$b = \sum_i \sum_j x_i x_j b_{ij} \quad \text{(eq.26)}$$

$$b_{ij} = \left(\frac{b_i^{1/2}+ b_j^{1/2}}{2}\right)^2 \quad \text{(eq.27)}$$

$$\frac{G_{AC}^{E,SG}}{RT} = 5 \sum_i \left(x_i\ q_i\ ln\frac{\theta_i}{\varphi_i}\right) \quad \text{(eq.28)}$$

$$\frac{G_{AC}^{E,res}}{RT} = \sum_i \left(x_i\ \nu^i_k\ ln\frac{\Gamma_k}{\Gamma^i_k}\right) \quad \text{(eq.29)}$$

$$\ln \Gamma_k = Q_k [\, 1 - \ln(\sum_m \theta_m \Psi_{mk}) - \sum_m \frac{\theta_m \Psi_{mk}}{\sum_n \theta_n \Psi_{nm}} \quad \text{(eq.30)}$$

For component "i"

$$\varphi_i = \frac{x_i r_i}{\sum_j x_j r_j} \quad \text{(eq.31)}$$

$$\theta_i = \frac{x_i q_i}{\sum_j x_j q_j} \quad \text{(eq.32)}$$

For Unifac group "m"

$$\theta_m = \frac{Q_m X_m}{\sum_n Q_n X_n} \quad \text{(eq.33)}$$

$$X_m = \frac{\sum_j \nu_m^{(j)} x_j}{\sum_j \sum_n \nu_n^{(j)} x_j} \quad \text{(eq.34)}$$

$$\Psi_{nm} = \exp[\, - \frac{A_{nm} + B_{nm}\,(T-298.15) + C_{nm}\,(T-298.15)^2}{T}] \quad \text{(eq.35)}$$

Where:

a) A_{nm}, B_{nm}, C_{nm} are the Unifac interaction parameters between groups n and m
b) b is the co-volume parameter of an EOS
c) v is the molar volume
d) r_i is the relative Van der Waals volume of compound "i"
e) q_i is the relative Van der Waals surface area of compound "i"
f) Q_k is the relative Van der Waals surface area of sub-group "k"
g) x is the mole fraction
h) X_m is the group mole fraction of group "m"
i) Ψ is the Unifac parameter
j) $G_{AC}^{E,SG}$ is the Staverman-Guggenheim term of the combinatorial part of the excess Gibbs energy
k) $G_{AC}^{E,res}$ is the Staverman-Guggenheim term of the residual part of the excess Gibbs energy
l) R is the global constant for gasses
m) Γ_k is the residual activity coefficient of group "k" in a solution
n) θ_i is the surface area fraction of component "i"
o) φ_i is the segment fraction of component "i"
p) T is the absolute temperature [K]
q) The parameter "A" (eq.25) is equal to -0.53

The advantage of this model compared to the previous ones is the fact that it considers that all components are comprised of the unifac groups and describes them as a combination of these groups. This allows the model to use the

corresponding unifac parameters for components where no experimental solubility data are available and provide a better approximation of the composition of any mixture that has two different phases in equilibrium.

A good example to underline this importance is n.dodecane. For the binary mixture of this component with Hg there are no experimental data regarding the solubility of Hg in it. The PR-MC and SRK-Twu models using the classical mixing rules, if not for the generalized correlations -that will be developed later on-, would be in no position to estimate a k_{ij} parameter, thus providing questionable results. The UMR-PRMC model however is able to construct n.dodecane as a combination of its respective unifac groups and use the groups' respective parameters in the universal mixing rules, thus resulting in more credible results. It is exactly for this reason that the UMR-PRMC model can be characterized as a "predictive" model.

To this purpose, Hg is considered to be a separate Unifac group and based on its solubility data with other HC, the parameters in question are estimated using the Neqsim-tool.

The objective function used by Neqsim for the fitting is:

$F = \sum_i (\frac{100*(x_{\text{icalc}} - x_{\text{iexp}})}{x_{\text{iexp}}})^2$ (eq.36), where x symbolizes the mole fraction of Hg.

For the usage of the UMR-PRMC model except for the group interaction parameters, two more parameters for Hg are essential. One of them is the relative Van der Waals volume parameter (r), which is equal to 10.598 and the other one is the relative Van der Waals surface area parameter (q), which is equal to 8.739 [14].

4.6.1 Main groups ACH and $ACCH_3$

As it can be seen at table 26, the experimental data of the aromatic HCs are divided into two main groups. Table 26 also presents the structure of each HC. This structure is used for the fitting of the UMR-PRMC parameters. Thus the interaction parameters between main groups of Hg, ACH and $ACCH_3$ can be estimated given the available data from the solubility database.

Table 26: Unifac's group structure of each aromatic HC at the solubility database

Unifac group	ACH	$ACCH_3$
Components		
benzene	6	-
toluene	5	1
o-xylene	4	2

First of all for the parameters of Hg with groups ACH and $ACCH_3$ two approaches were adopted. As table 26 shows only benzene [13], toluene [13] and o-xylene [13] are composed out of unifac main groups ACH and $ACCH_3$. Therefore there is lack of many experimental solubility data which is the reason leading to the two approaches.

The first approach is to simultaneously fit the experimental data of all three HCs into two sets of A_{ij} and B_{ij} parameters. Thus A_{ij} and B_{ij} sets of parameters will be calculated simultaneously for interactions between groups Hg-ACH and Hg-$ACCH_3$. The ij index stands for interaction between groups i and j. The second one is to fit the A_{ij} and B_{ij} parameters first to benzene and then while keeping these as constants for group interaction Hg-ACH, to fit the set A_{ij} and B_{ij} parameters (the interaction of groups Hg-$ACCH_3$) for toluene and o-xylene.

Table 27: Estimated unifac group interaction parameters between ACH, $ACCH_3$ and Hg estimated with both approaches for the UMR-PRMC model

i	**j**	**A_{ij} [K]**	**B_{ij} [-]**	**C_{ij} [K^{-1}]**	**A_{ji} [K]**	**B_{ji} [-]**	**C_{ji} [K^{-1}]**	**Type of fitting**
ACH	Hg	**Confidential data**						Simultaneous fit
$ACCH_3$	Hg							
ACH	Hg	**Confidential data**						Separate fit
$ACCH_3$	Hg							

As table 27 presents the parameters estimated for both cases are similar to each other. In addition to that, as tables F17-19 and F20-22 at appendix F show, the results of the UMR-PRMC model using the estimated parameters are close to the experimental data for both cases. It is mentioned that only parameters A_{ACH-Hg}, B_{ACH-Hg}, $A_{ACCH3-Hg}$ and $B_{ACCH3-Hg}$ parameters estimated so far. The parameters A_{Hg-ACH}, B_{Hg-ACH}, $A_{Hg-ACCH3}$ and $B_{Hg-ACCH3}$ had no effect on the results and were thus set equal to 2000 each A_{ji} and 0 each B_{ji} respectively.

Figures 16-18 graphically present the experimental data and the results of the UMR-PRMC model using the group interaction parameters for each aromatic HC. The ‘sep’ means that these are the results from UMR-PRMC using the parameters estimated from the separate fitting and the ‘sim’ from the simultaneous fitting.

Table 28 shows that for the separate fitting the absolute average deviations of toluene and o-xylene are slightly worse than those of the simultaneous fitting, however there is a notable difference when it comes to benzene. As expected the absolute average deviation of the separate fitting for benzene is better compared to that of the simultaneous fit because the interaction parameter of Hg and ACH are

estimated based solely on experimental data concerning these groups. From these results it can be concluded that the parameters from the simultaneous fitting should be used because the data used for this fitting are used all together and not separately, like the other case, thus making the parameters estimated more reliable.

Table 28: Absolute average deviation of the mole fraction of Hg for each approach in the liquid phase

Simultaneous fit			
HC	toluene	o-xylene	benzene
Abs.av.dev. %	4.67	2.81	2.41
Separate fit			
HC	toluene	o-xylene	benzene
Abs.av.dev. %	4.27	2.49	1.59

Finally table 29 presents the overall absolute deviations for each binay mixture with the SRK-Twu and the PR-MC models. It can be seen that all three models have a similar absolute average deviation for these mixtures. This is very promising for the UMR-PRMC model given the fact that the fitting of the unifac group parameters has been performed simultaneously for all three binary mixtures.

Table 29: Overall absolute deviations of SRK-Twu and PR-MC models for Hg with benzene, toluene and o-xylene respectively in the liquid phase

Model	**SRK-Twu**	**PR-MC**
System	**Overall Abs. Deviation (%)**	
Hg-benzene	1.99	2.11
Hg-toluene	4.01	3.83
Hg-o-xylene	2.91	3.52

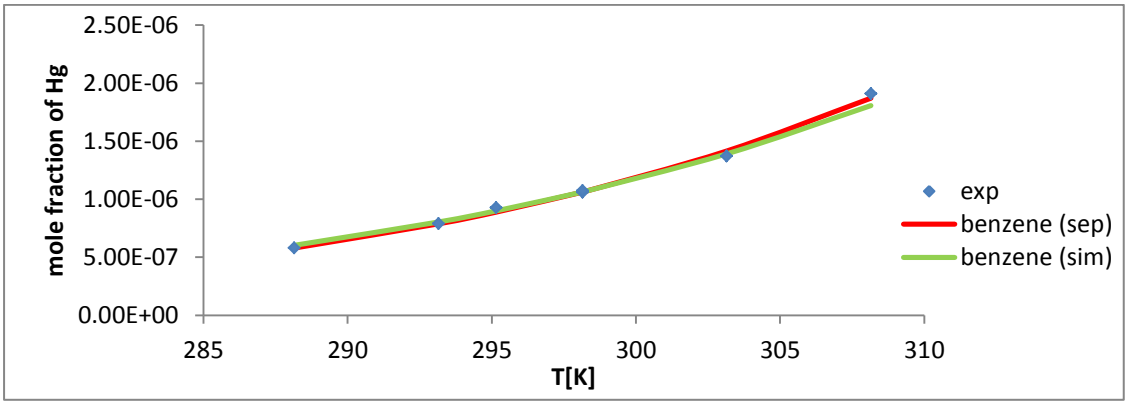

Figure 16: Experimental and calculated mole fractions of Hg estimated with the UMR-PRMC model for benzene in the liquid phase

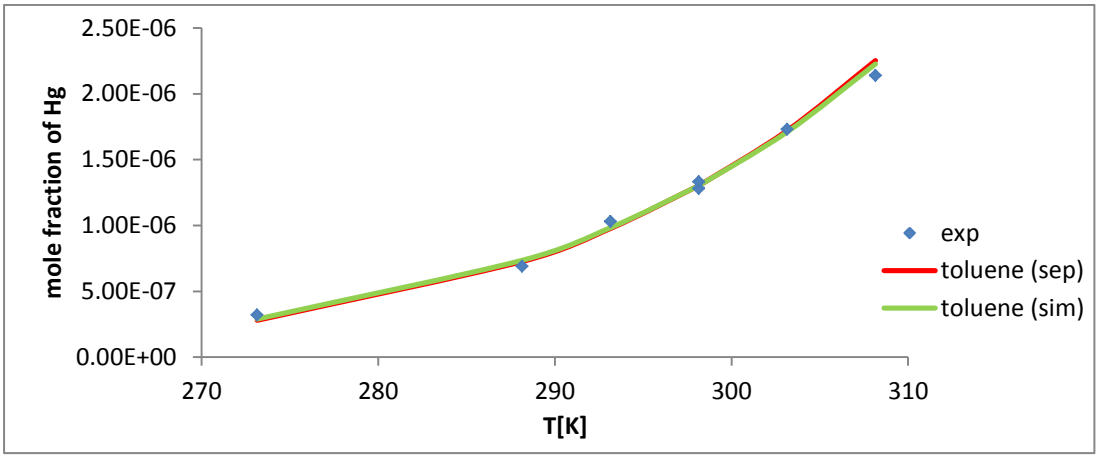

Figure 17: Experimental and calculated mole fractions of Hg estimated with the UMR-PRMC model for toluene in the liquid phase

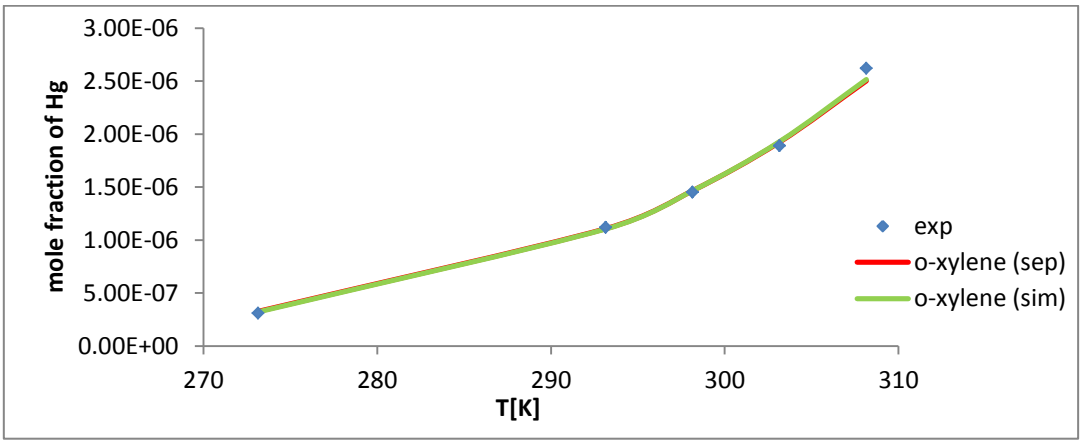

Figure 18: Experimental and calculated mole fractions of Hg estimated with the UMR-PRMC model for o-xylene in the liquid phase

4.6.2 Main group CH_2

The next Unifac parameters estimated are the ones for main groups of Hg and CH_2. Group CH_2 contains all the normal and branched alkanes [11, 13] of the solubility database in the liquid phase as it can be seen ta table 30. There are also other components in the database which are also normal alkanes like methane [11] or ethane [11] for instance, but these are considered to be individual groups, therefore will be presented at a following subchapter separately.

Table 30: Unifac's group structure of each normal and branched alkane in the solubility database

Unifac group	CH_2			
Unifac subgroup	CH_3	CH_2	CH	C
Components				
n.C_3	2	1	-	-
n.C_5	2	3	-	-
n.C_6	2	4	-	-
n.C_7	2	5	-	-
n.C_8	2	6	-	-
n.C_{10}	2	8	-	-
2.2-dm-C_4	4	1	-	1
2.2.4-tm-C_5	5	1	1	1

For the cyclo-alkanes, a new group will also be introduced later on because it was observed that by fitting them with main group CH_2, they could not be predicted well enough. The interaction parameters between main groups of Hg and CH_2 can be estimated given the available data from the solubility database. Table 31 presents the estimated parameters and some information about the results and table 32 the absolute average deviation of the mole fraction of Hg estimated by the UMR-PRMC model for each HC respectively, while using the A_{ij} and B_{ij} parameters for the corresponding groups. It is mentioned that only parameters $A_{CH2\text{-}Hg}$ and $B_{CH2\text{-}Hg}$ were estimated. The parameters $A_{Hg\text{-}CH2}$, $B_{Hg\text{-}CH2}$ had no effect on the results and were thus set equal to 2000 each A_{ji} and 0 each B_{ji} respectively.

Table 31: Estimated unifac group interaction parameters between CH_2 and Hg for the UMR-PRMC model

i	**j**	**A_{ij} [K]**	**B_{ij} [-]**	**C_{ij} [K^{-1}]**	**A_{ji} [K]**	**B_{ji} [-]**	**C_{ji} [K^{-1}]**
CH_2	Hg	**Confidential data**					
Number Of Data Points		79					
Abs.dev (%)		11.54					

Table 32: Absolute average deviation for the mole fraction of Hg in each HC, as estimated by the UMR-PRMC model in the liquid phase

Hydrocarbons	**Absolute deviation%**
n.C_3	11.35
n.C_5	5.99
n.C_6	5.57
n.C_7	7.93

Continuation of table 32	
$n.C_8$	12.28
$n.C_{10}$	19.96
2.2-dm-C_4	13.55
2.2.4-tm-C_5	35.24

As table 32 suggests the results of the UMR-PRMC model with the fitted parameters are not as good as the ones with the PR-MC and the SRK-Twu models. Tables F3-10 and figures F3-10 at appendix F present the results of the UMR-PRMC model compared to the experimental data for each HC individually.

Furthermore as table 32 shows, only $n.C_5$, $n.C_6$ and $n.C_7$ have an overall absolute deviation of less than 10%. However all overall deviations of all binary mixtures except for 2.2.4-tm-C_5 and $n.C_{10}$ are less than 14%, thus making the results very accurate. These deviations none the less can be completely justified if one takes into account the fact that the UMR-PRMC is a model based on the unifac groups as mentioned, thus has no exclusive parameters for each binary mixture as it occurs for the SRK-Twu and the PR-MC models, which present generally slightly better overall deviations as table 22 shows.

As far as propane is concerned the UMR-PRMC model predicts its experimental data accurately enough as figure 19 illustrates. As far as the other normal alkanes are concerned the UMR-PRMC model does not predict the experimental data with the same accuracy. It can be seen that except for $n.C_{10}$, for all other alkanes the model can predict the mole fraction of Hg at low temperatures, however as the temperature rises, the accuracy of the model declines and under-predicts the experimental data.

For the branched alkanes the UMR-PRMC model seems to constantly over-predict the mole fraction of Hg in them. The same thing happened even if the corresponding group was fitted exclusively to these two alkanes. This means that the UMR-PRMC model appears to fail to accurately describe this type of HCs. That fact could pose a problem for the model, however due to the overall deviations of these particular HCs, where one is quite acceptable and one is not, it is not safe to assume anything further than that one has to be cautious when using it with this type of HCs.

Finally figures 20-23 show the solubility of Hg for the HC, which are grouped according to their carbon number. One thing that can be said about these figures is that the calculated by the UMR-PRMC model values of the mole fraction of Hg in $n.C_8$ and 2.2.4-tm-C_5 and respectively in $n.C_6$ and 2.2-dm-C_4 are very close to each other.

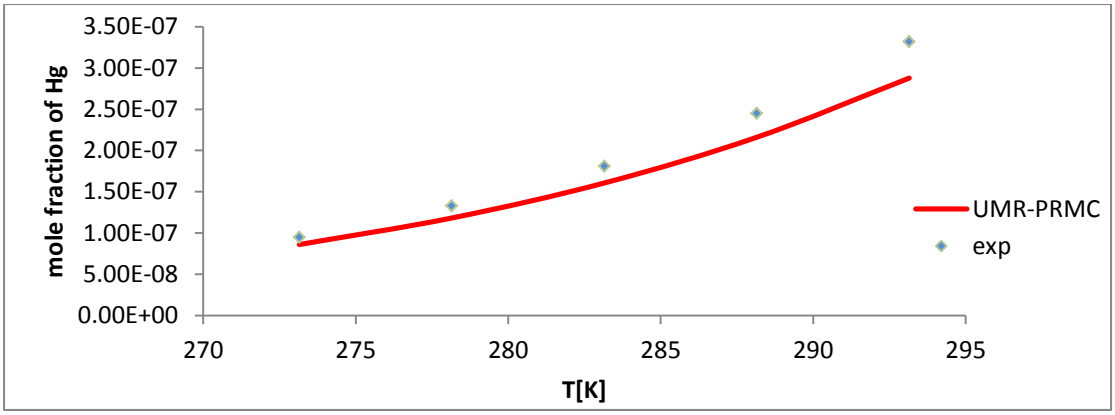

Figure 19: Mole fractions of Hg in propane in the liquid phase estimated with the UMR-PRMC model

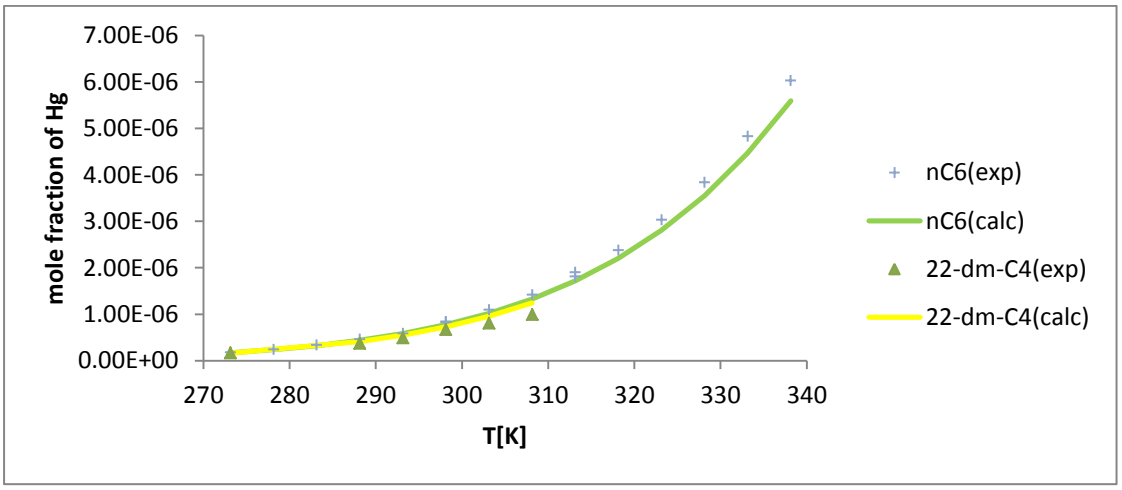

Figure 20: Mole fractions of Hg in HCs with CN=6 in the liquid phase, estimated with the UMR-PRMC model

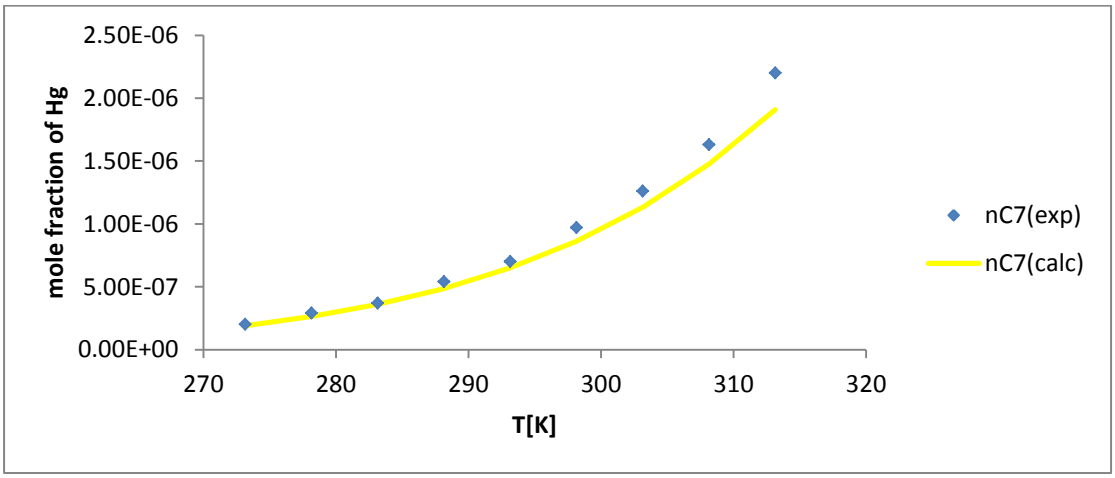

Figure 21: Mole fractions of Hg in n.C_7 in the liquid phase, estimated with the UMR-PRMC model

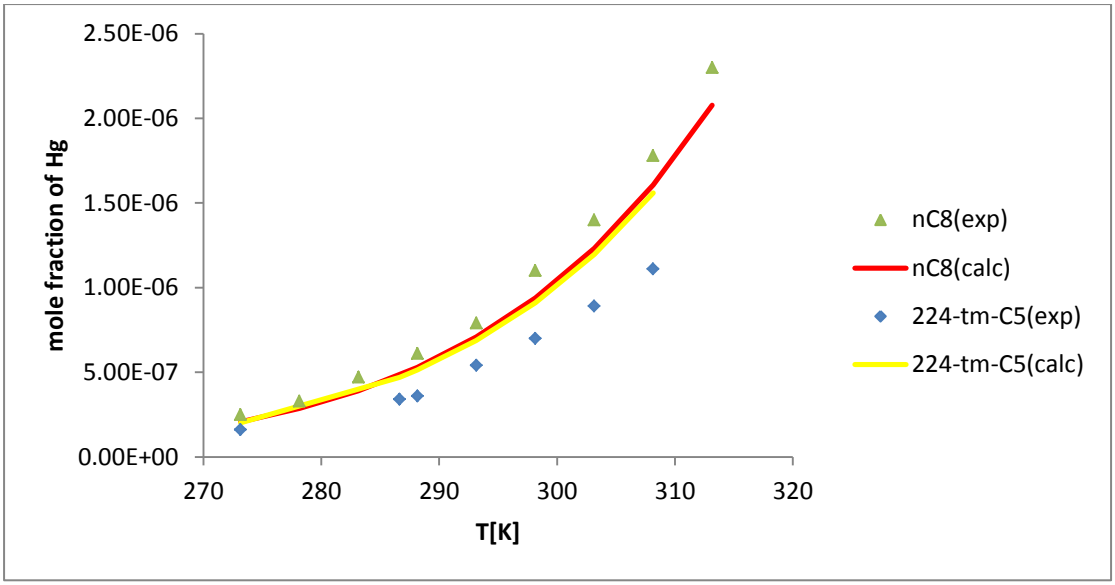

Figure 22: Mole fractions of Hg in HCs with CN=8 in the liquid phase, estimated with the UMR-PRMC model

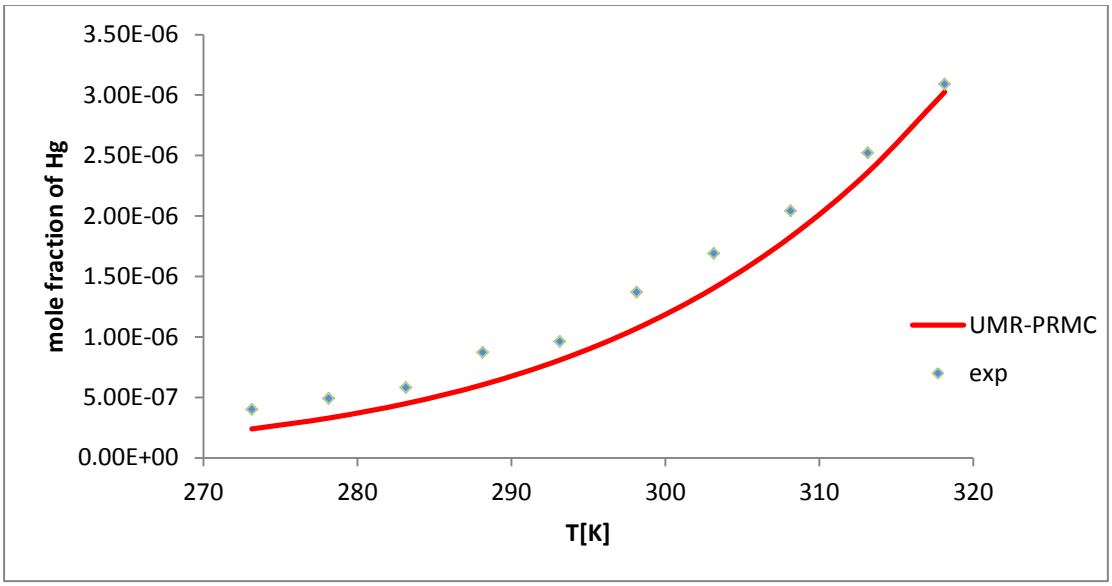

Figure 23: Mole fractions of Hg in HCs with n.C_{10} in the liquid phase, estimated with the UMR-PRMC model

One last thing that has to be examined is the data available for propane regarding its vapor phase. These data were predicted with B.P.P calculations, the same way as it was done for the PR-MC and SRK-Twu model. Table 33 and figure 24 present the predictions from UMR-PRMC. Figure 24 also displays the results of the other two models, since it is interesting to see how UMR-PRMC copes against them, given the fact that it didn't have as accurate predictions in the liquid phase as the other two models.

Table 33: Experimental and estimated mole fractions of Hg with C_3 in the vapor phase from the UMR-PRMC model

T[K]	P[bar]	y_{exp}	y_{calc}	Abs. Deviation%
273.15				14.58
278.15				16.02
283.15				14.28
288.15				13.10
293.15	**Confidential data**			13.38
Overall deviation %				**14.27**

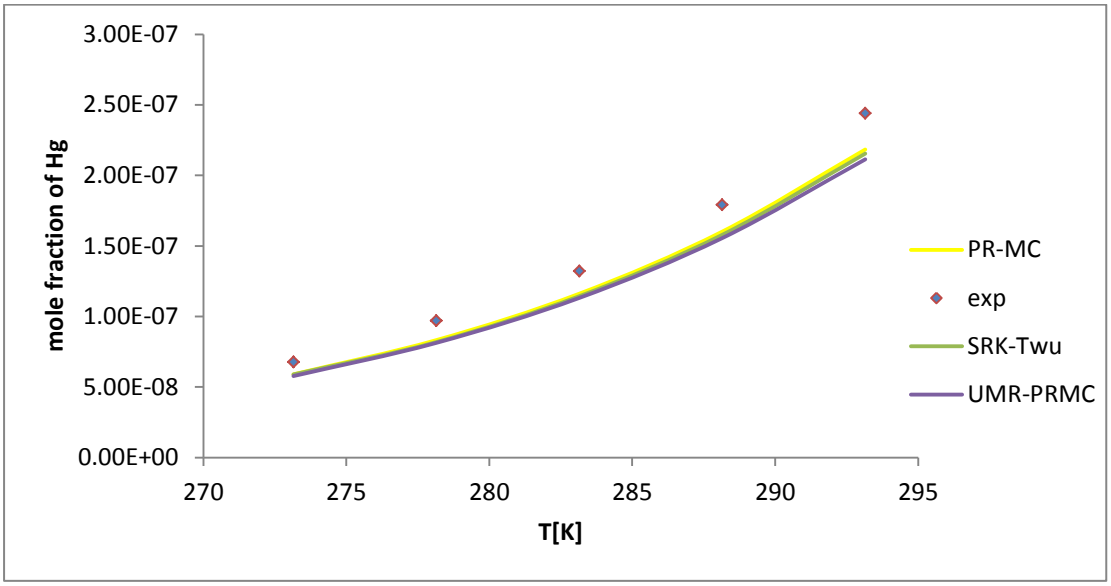

Figure 24: Experimental and estimated mole fractions of Hg in propane in the vapor phase from all models

As figure 24 illustrates all three models provide almost the same predictions at low temperatures, and only as the temperature rises, one can see a slight distinction among them. This is of course very encouraging for UMR-PRMC since C_3 is a very important component in natural gas mixtures.

4.6.3 Main group cy-CH_2

As already mentioned, for the better prediction of the cyclo-alkanes [13], the new main group 'cy-CH_2' is going to be introduced. Furthermore the Neqsim-tool [6] was modified in order to include this new main group and do the fitting of the parameters. For the interaction parameters between the unifac groups of Hg and CH_2 the values presented at table 31 were used. Once again, as expected, the

parameters $A_{Hg\text{-}cyCH2}$, $B_{Hg\text{-}cyCH2}$ had no effect on the results and were thus set equal to 2000 and 0 respectively. Finally the unifac group interaction parameters between the groups of CH_2 and cy-CH_2 are considered to be equal to zero.

Table 34 presents the unifac group structure of all components comprising of the 'cy-CH_2' group. Tables 35 and 36 show the estimated parameters for this group and the overall absolute deviation, as well as the absolute average deviation for the mole fraction of Hg in each HC as estimated by the UMR-PRMC model, respectively.

Table 34: Unifac's group structure of each cyclo-alkane in the solubility database

Unifac group	CH_2	cy-CH_2	
Unifac subgroup	CH_3	cy-CH_2	cy-CH
Components			
cy-C_6	-	6	-
m-cy-C_6	1	5	1
cis-1.2-dm-cy-C_6	2	4	2
cis-1.4-dm-cy-C_6	2	4	2
trans-1.2-dm-cy-C_6	2	4	2
trans-1.4-dm-cy-C_6	2	4	2

Table 35: Estimated unifac group interaction parameters between cy-CH_2 and Hg for the UMR-PRMC model

i	**j**	**A_{ij} [K]**	**B_{ij} [-]**	**C_{ij} [K^{-1}]**	**A_{ji} [K]**	**B_{ji} [-]**	**C_{ji} [K^{-1}]**
cy-CH_2	Hg	**Confidential data**					
Number Of Data Points		33					
Abs.ov.dev (%)		4.97					

Table 36: Absolute average deviation for the mole fraction of Hg in each HC, as estimated by the UMR-PRMC model in the liquid phase

Hydrocarbons	**Absolute deviation%**
cy-C_6	5.90
m-cy-C_6	5.69
cis-1.2-dm-cy-C_6	5.42
cis-1.4-dm-cy-C_6	2.98
trans-1.2-dm-cy-C_6	3.57
trans-1.4-dm-cy-C_6	5.77

The analytical results of table 36 can be found at appendix F, at tables F11-16. Figures 25 and 26 illustrate the results of the UMR-PRMC model compared to the

experimental data for cy-C_6 and m-cy-C_6 respectively as indicative ones, since these are more usual components met in a natural gas mixture. The rest graphical illustrations of the results are also to be found at appendix F, at figures F11-16.

As a comment one can say that the fitting and in extension the predictions of the UMR-PRMC model for the components of this group are very satisfactory since they are in addition to that very close to the predictions of the SRK-Twu and PR-MC models as well, as table 22 presents. To confirmation of that, the highest overall deviation met for the UMR-PRMC model is that of Hg with cy-C_6, which ammounts 5.90%.

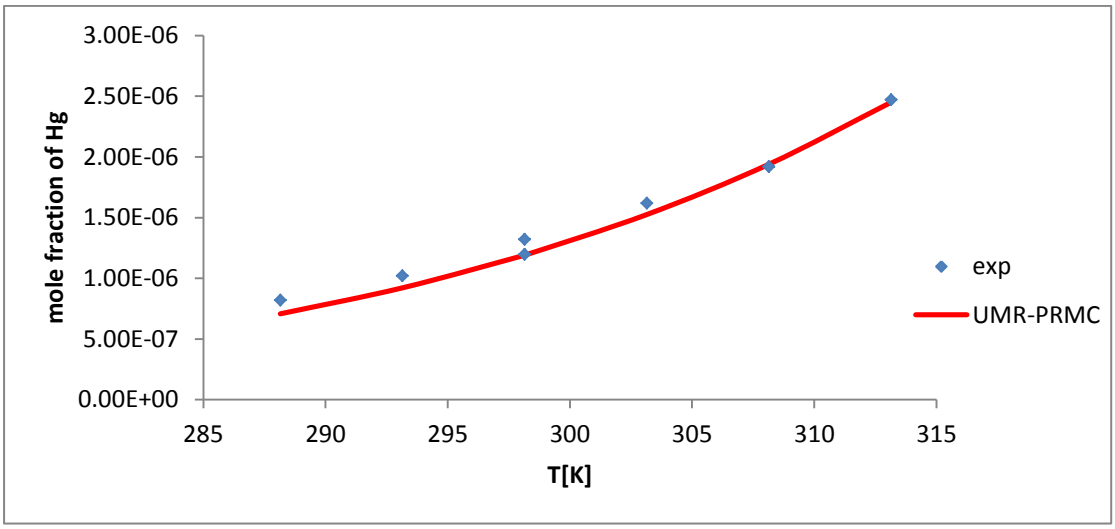

Figure 25: Experimental and calculated mole fractions of Hg estimated with the UMR-PRMC model for binary mixture with cy-C_6 in the liquid phase

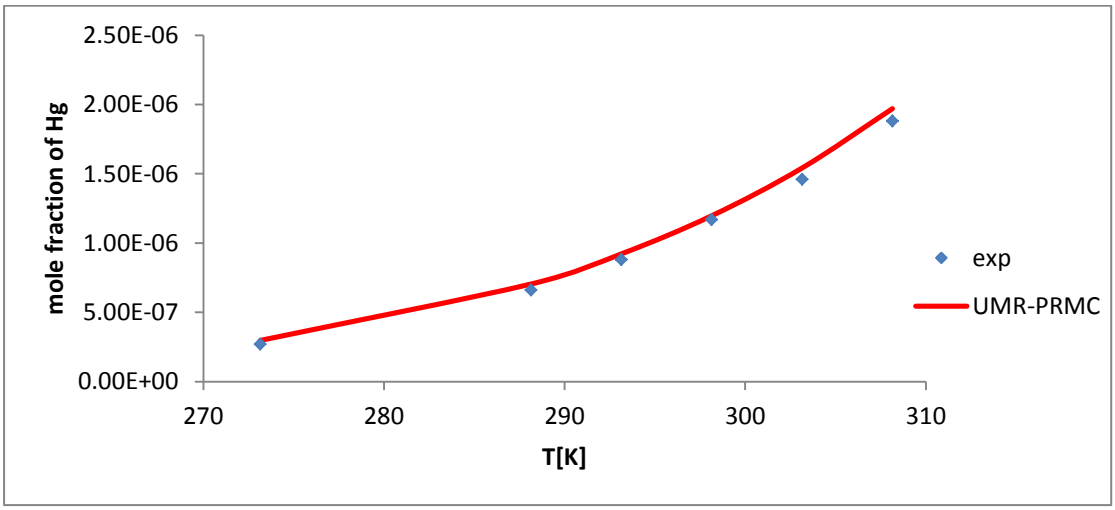

Figure 26: Experimental and calculated mole fractions of Hg estimated with the UMR-PRMC model for binary mixture with m-cy-C_6 in the liquid phase

4.6.4 Main group CH_4

For the binary mixture of Hg in methane [11] the Neqsim-tool [6] was used for the fitting of the unifac-group parameters of the UMR-PRMC model, as well as for the prediction of the mole fractions of Hg in the vapor phase, in which the experimental data are available. Table 37 presents the unifac parameters estimated for the main groups of Hg and CH_4.

Table 37: Estimated unifac group interaction parameters between CH_4 and Hg for the UMR-PRMC model

i	j	A_{ij} [K]	B_{ij} [-]	C_{ij} [K^{-1}]	A_{ji} [K]	B_{ji} [-]	C_{ji} [K^{-1}]
CH_4	Hg	**Confidential data**					
Number Of Data Points		33					
Abs.ov.dev (%)		2.26					

As table 37 presents the parameters have been fitted very satisfyingly to the experimental data since the overall absolute deviation of the model is just 2.26%. Figure 27 also confirms the good performance of the UMR-PRMC model given the fact that its predictions match the experimental data almost precisely. The analytical results can be found at Appendix F, at table F1.

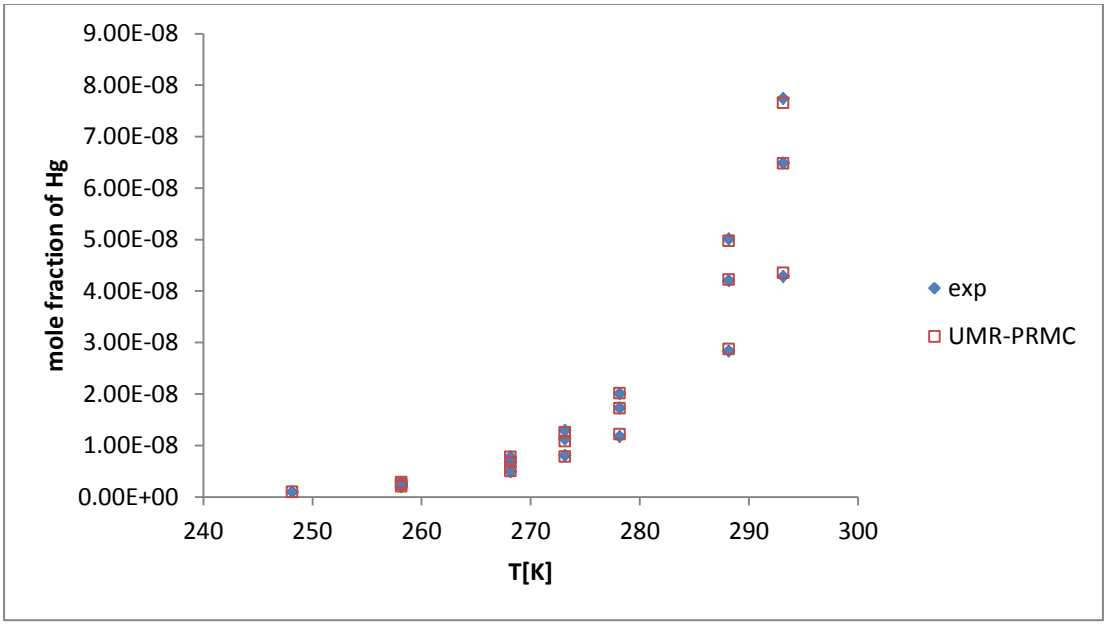

Figure 27: Experimental and predicted mole fractions of Hg in CH_4 with the UMR-PRMC model in the vapor phase

Figures 28 and 29 present predictions of the PR-MC and the SRK-Twu models regarding the mole fractions of Hg in CH_4. Table 38 re-presents the absolute overall deviations of these models for this mixture. As table 38 shows, the deviations are almost the same as the one of the UMR-PRMC model.

Table 38: Overall absolute deviations of SRK-Twu and PR-MC models for Hg and CH_4 in the vapor phase

Model	k_{ij} parameter	Abs. Deviation (%)
SRK-Twu	**Confidential data**	2.35
PR-MC		2.22

Like the UMR-PRMC's model, these models' predictions match almost perfectly the experimental mole fractions of Hg in the vapor phase as shown at table 23 and figures 28 and 29. This is very important to know because the primary component of every natural gas mixture is methane. Therefore it is utterly important that the models are able to accurately predict the composition of Hg in the vapor phase in this binary mixture, thus making the prediction of the final composition of Hg in the sales gas of a natural gas processing plant more reliable. The analytical results of the SRK-Twu and PR-MC models are presented at Appendix E and tables E1 and E22.

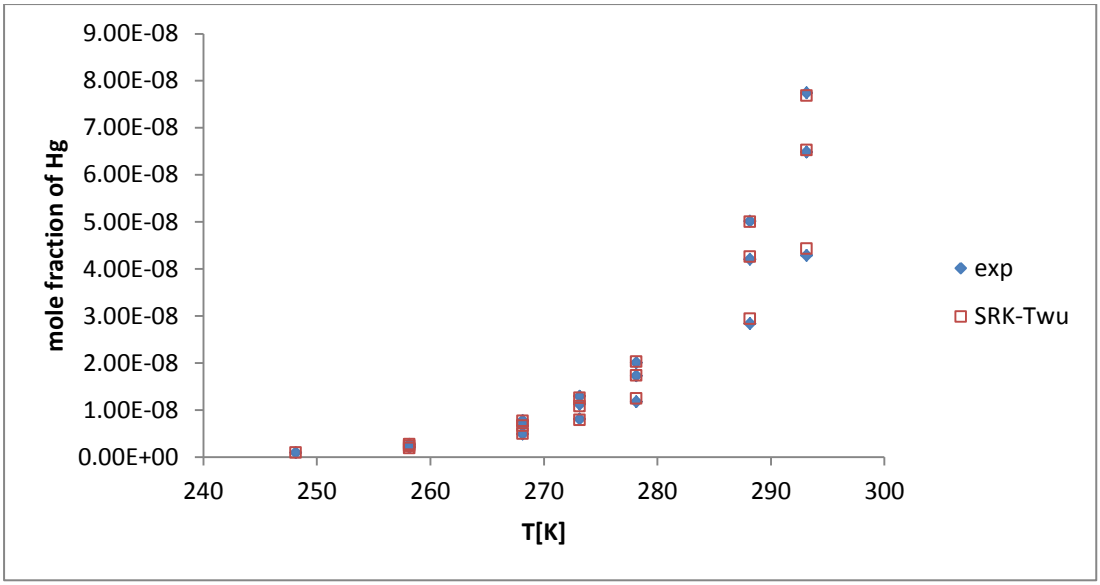

Figure 28: Experimental and predicted mole fractions of Hg in CH_4 with the SRK-Twu model

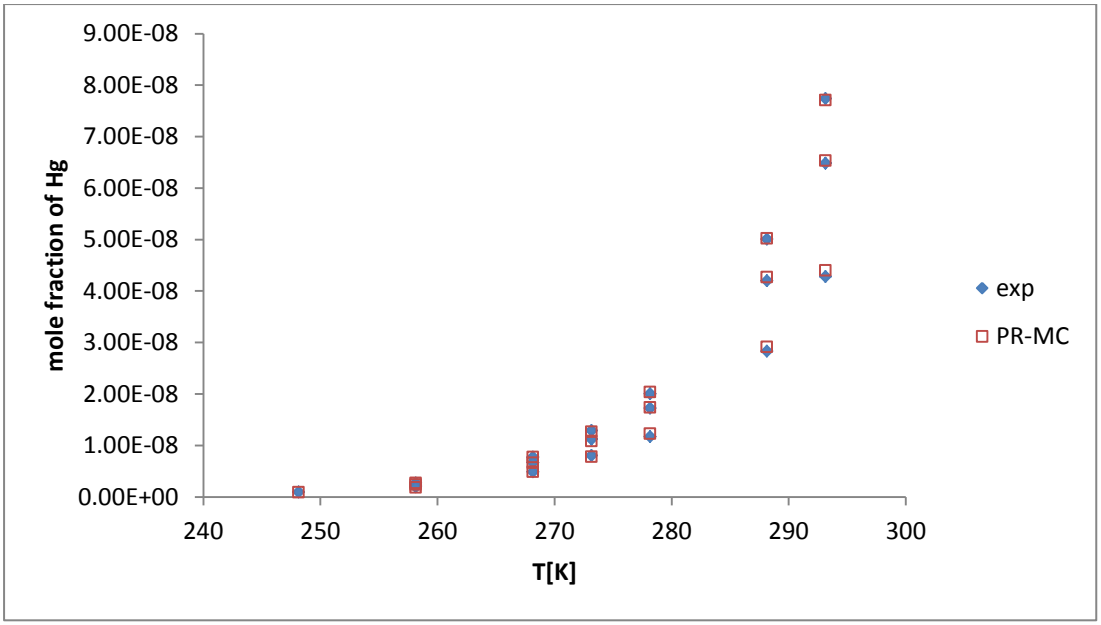

Figure 29: Experimental and predicted mole fractions of Hg in CH_4 with the PR-MC model

4.6.5 Main group C_2H_6

For the binary mixture of Hg in ethane [11] there are, as mentioned, experimental data available in the liquid phase, as well as in the vapor phase. For the fitting of the parameters required for the UMR-PRMC model, the data of the liquid phase have been used. Afterwards these parameters were used with in order to predict the experimental data in the vapor phase. For the parameter fitting and the prediction of the mole fractions of Hg in the vapor phase, the Neqsim-tool [6] was employed once again, doing B.P.P in the same fashion as described for previous binary mixtures as well.

If assumed that 'i' represents the C_2H_6 group and 'j' the Hg group, the unifac parameters estimated from the liquid phase data are the ones presented at table 39.

Table 39: Estimated unifac group interaction parameters between C_2H_6 and Hg for the UMR-PRMC model

i	j	A_{ij} [K]	B_{ij} [-]	C_{ij} [K^{-1}]	A_{ji} [K]	B_{ji} [-]	C_{ji} [K^{-1}]
C_2H_6	Hg	**Confidential data**					
Number Of Data Points		5					
Abs.ov.dev (%)		0.27					

The analytical results from the fitting can be located at appendices F, at table F2. It is worth mentioning that the UMR-PRMC model clearly has an advantage when it comes to the description of the liquid phase of Hg in ethane compared to the other two models because their overall absolute deviation was about 5.7% as table 40 illustrates.

Table 40: Overall absolute deviations of SRK-Twu and PR-MC models for Hg and C_2H_6 in the liquid phase

Model	**k_{ij} parameter**	**Abs. Deviation (%)**
SRK-Twu	**Confidential data**	5.82
PR-MC		5.66

Table 41 and figure 30 present the predictions of UMR regarding the vapor solubility of Hg in ethane. It is interesting to also compare the predictions of the other two models with the ones from UMR-PRMC as they appear at figure 30, because for propane even though there were deviations regarding the liquid solubility of Hg, in the vapor phase all three models provided similar results.

Table 41: B.P.P calculations with the UMR-PRMC model for Hg with ethane in the vapor phase

T[K]	**P[bar]**	**y_{exp}**	**y_{calc}**	**Abs. Deviation%**
273.15	**Confidential data**			8.26
278.15				8.79
283.15				6.19
288.15				2.95
293.15				3.52
Overall deviation %				**5.94**

As figure 30 shows the UMR-PRMC model predicts more accurately the mole fraction of Hg in the vapor phase compared to the other two models. The PR-MC and SRK-Twu models provide almost identical results with an overall average deviation between 15% and 16%. Still the predictions of all three models are acceptable since once again they are very close the “non-ideal” experimental error margin and within the “ideal” experimental error margin as already explained.

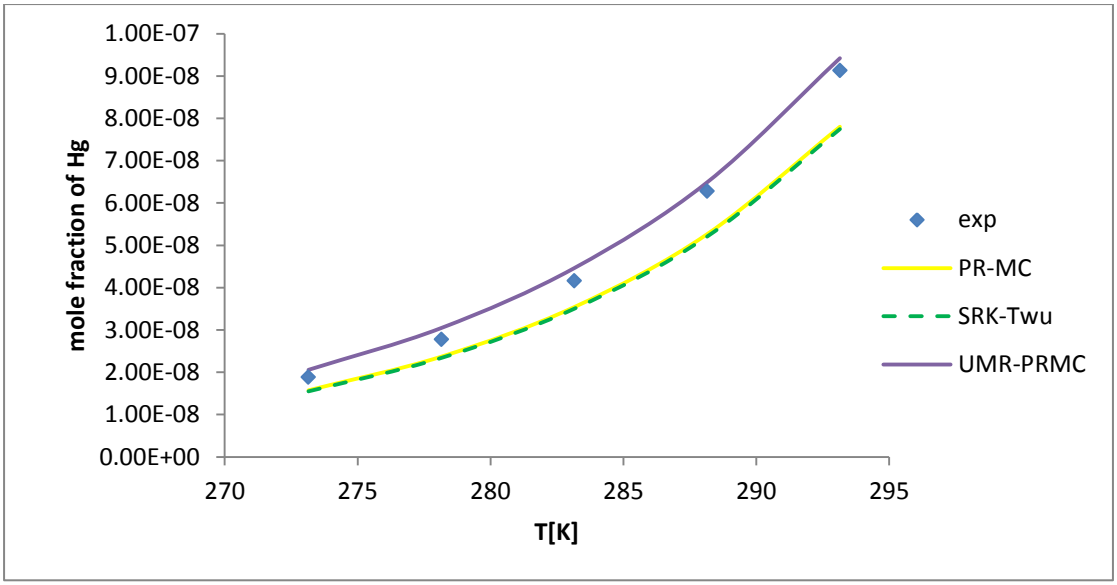

Figure 30: Experimental and estimated mole fractions of Hg in C_2H_6 in the vapor phase from all three models

4.6.6 Main group CO_2

For the binary mixture of Hg in CO_2 [11] there are also experimental data available in the liquid phase, as well as in the vapor phase. For the fitting of the Unifac parameters, the data of the liquid phase have been used. Afterwards these parameters were used with in order to predict the experimental data in the vapor phase by conducting B.P.P calculations with the same methodology as before with Neqsim-tool [6]. At Appendices F and G, the results of the fitting and the B.P.P calculations with the UMR-PRMC model are presented at tables F19 and G7 respectively. Figures F25 and G3 present them graphically as well.

Table 42: Overall absolute deviations of SRK-Twu and PR-MC models for Hg and CO_2 in the liquid phase

Model	k_{ij} parameter	Abs. Deviation (%)
SRK-Twu	**Confidential data**	5.24
PR-MC		7.49

If assumed that i represents the CO_2 group and j the Hg group, the unifac parameters estimated from the liquid phase data are the ones presented at table 43.

Table 43: Estimated unifac group interaction parameters between CO_2 and Hg for the UMR-PRMC model in the liquid phase

i	j	A_{ij} [K]	B_{ij} [-]	C_{ij} [K^{-1}]	A_{ji} [K]	B_{ji} [-]	C_{ji} [K^{-1}]
CO_2	Hg	**Confidential data**					
Number Of Data Points		5					
Abs.ov.dev (%)		0.55					

Table 44 and figure 31 present the predictions of UMR-PRMC regarding the vapor solubility of Hg in CO_2. It is also interesting to compare the predictions of the other two models with the ones from UMR-PRMC as they appear at figure 31, to see if they have the same behavior as they did for the binary mixture of Hg with ethane or the one with propane.

Table 44: B.P.P calculations with the UMR-PRMC model for Hg in CO_2 in the vapor phase

T[K]	P[bar]	y_{exp}	y_{calc}	Abs. Deviation%
273.15	**Confidential data**			7.57
278.15				5.78
283.15				5.19
288.15				3.77
293.15				2.73
Overall deviation %				**5.01**

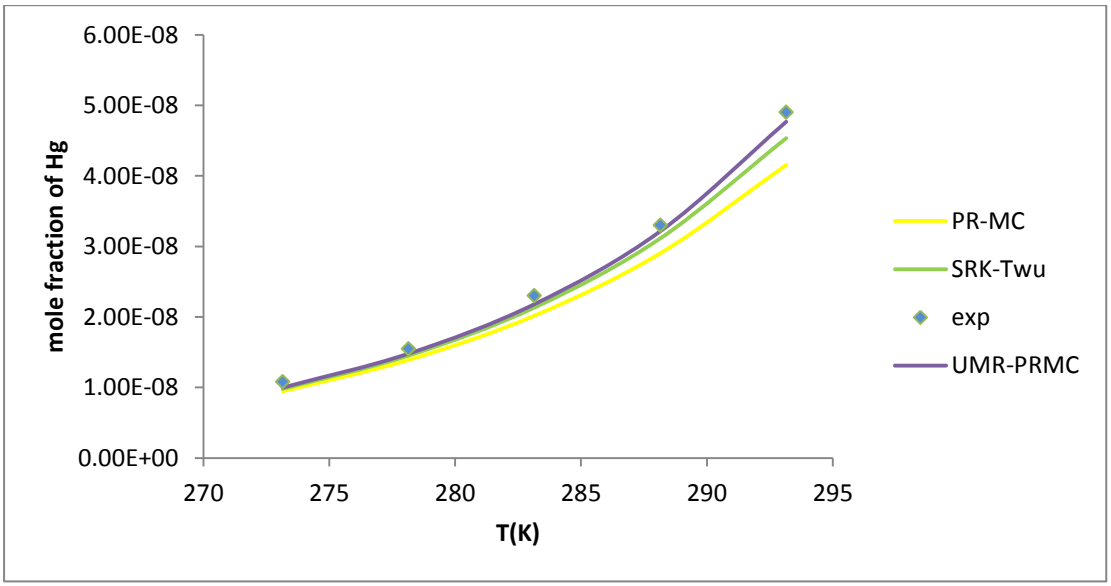

Figure 31: Experimental and estimated mole fractions of Hg in CO_2 in the vapor phase from the all three model

From figure 31 it can be concluded that this mixture follows a similar behavior to the one of Hg with ethane regarding the results of Hg in vapor phase. As figure 31 shows the UMR-PRMC model provides the most accurate estimations for the solubility of Hg in the vapor phase in comparison with the other two models. The PR-MC model provides the least accurate ones. However all models' predictions are within both the "ideal" and "non-ideal" experimental error margin. It is reminded that the average deviation of the PR-MC and the SRK-Twu models is 12.36% and 2.28% respectively for the vapor phase. This is the reason why at low temperatures the SRK-Twu model has similar results to the ones from the UMR-PRMC model.

4.6.7 Main group N_2

For this binary mixture experimental data are available only in the vapor phase [11], like it happens for methane. The Neqsim-tool [6] was used for the fitting of the unifac-group parameters as well as for the prediction of the mole fractions of Hg in the vapor phase.

Like the previous groups, if 'i' represents the N_2 group and 'j' the Hg group, the Unifac parameters estimated are the following ones:

Table 45: Estimated unifac group interaction parameters between N_2 and Hg for the UMR-PRMC model in the vapor phase

i	j	A_{ij} [K]	B_{ij} [-]	C_{ij} [K^{-1}]	A_{ji} [K]	B_{ji} [-]	C_{ji} [K^{-1}]
N_2	Hg	**Confidential data**					
Number Of Data Points		6					
Abs.ov.dev (%)		0.89					

In this particular binary mixture all the experimental data have a constant temperature of 273.15 K. Thus the B parameters, which pose the temperature dependency of the unifac parameters cannot be estimated.

As figure 32 and table 38 present, the model's predictions of the mole fractions of Hg agree very well with the experimental data. The analytical results and the experimental data are presented at Appendix F at table F23. Also figure F17 presents a visual view of the results.

Like the other two models', UMR-PRMC's predictions match almost perfectly the experimental mole fractions of Hg in the vapor phase as shown at figure 32, exactly like it happened for the binary mixture of Hg with CH_4. It is reminded that the

absolute deviations of PR-MC and SRK-Twu are 0.9% and 1.34% as presented at table 46, meaning almost identical to the 0.89% of the UMR-PRMC model.

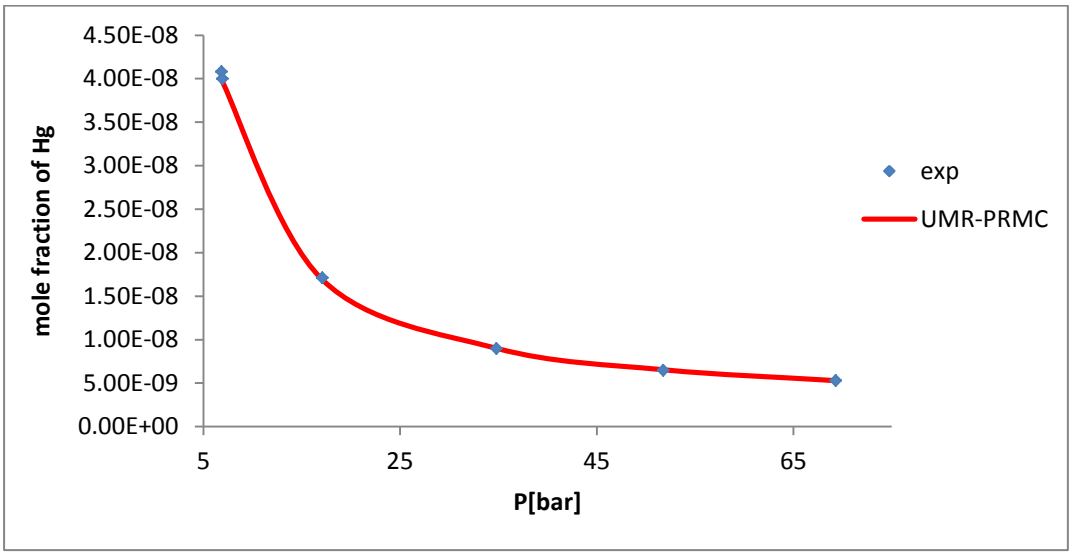

Figure 32: Experimental and predicted mole fractions of Hg in N_2 with the UMR-PRMC model in the vapor phase

Table 46: Overall absolute deviations of SRK-Twu and PR-MC models for Hg and N_2

Model	k_{ij} parameter	Abs. Deviation (%)
SRK-Twu	**Confidential data**	1.34
PR-MC		0.90

Thus it is concluded that all models' predictions are very accurate and acceptable since they also can be located within both the "ideal" and the "non-ideal" experimental error margin regarding this particular binary mixture.

4.6.8 Main group H_2O

For the binary mixture of Hg with water as already established the only source of experimental data is IUPAC [13]. The Neqsim-tool [6] was used for the fitting of the unifac-group parameters as well as for the prediction of the mole fractions of Hg.

Like the previous groups, if 'i' represents the H_2O group and 'j' the Hg group, the unifac parameters estimated are the following ones:

Table 47: Estimated unifac group interaction parameters between H_2O and Hg for the UMR-PRMC model

i	j	A_{ij} [K]	B_{ij} [-]	C_{ij} [K^{-1}]	A_{ji} [K]	B_{ji} [-]	C_{ji} [K^{-1}]
H_2O	Hg	**Confidential data**					
Number Of Data Points		22					
Abs.ov.dev (%)		0.09					

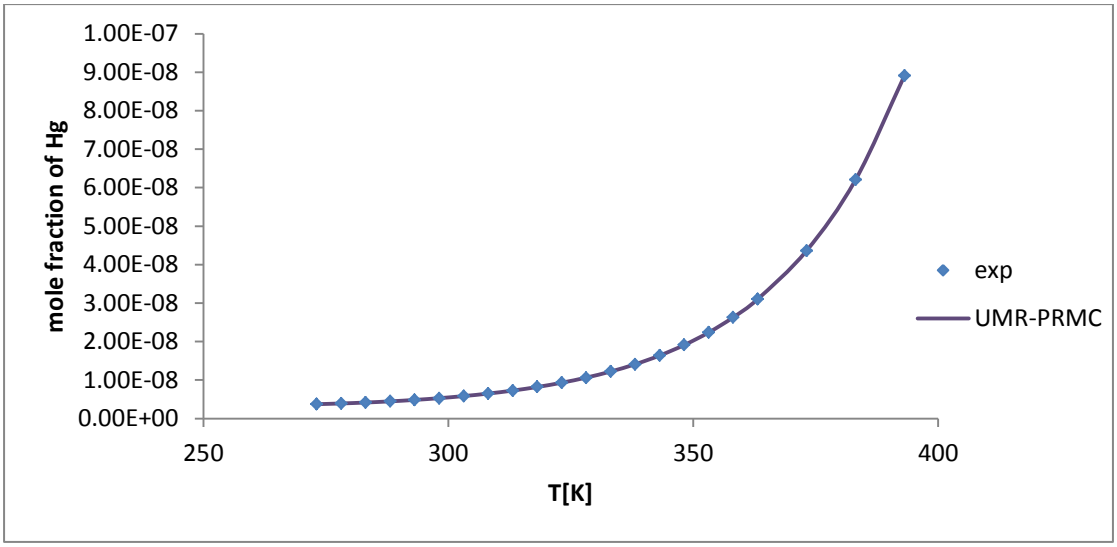

Figure 33: Experimental and predicted mole fractions of Hg in H_2O with the UMR-PRMC model

As figure 33 and table 39 present, the model's predictions of the mole fractions of Hg agree very well with the experimental data. This is very important and encouraging because it means that the UMR-PRMC model is at an advantageous position since it is implied by the fitting that it can be used in process simulations containing water as well, thus closer to a realistic mixture that can be met in the natural gas industry. The analytical results and the experimental data are presented at appendix F at table F24.

In contrast to the other two models', UMR-PRMC's predictions match almost perfectly the experimental mole fractions of Hg, as shown at figure 33 and table 47. This is proof that the universal mixing rules are not bounded by the limitations of the classical mixing rules regarding the hydrogen bond. It is reminded that the absolute deviations of PR-MC and SRK-Twu are 13.06% and 12.86% as presented at table 20 with a maximum deviation around 27.5% shown by both models at the lowest and highest temperatures respectively as shown at appendix E at tables E21 and E42 explicitly.

4.7 Generalized correlations for the binary interaction parameters based on the T_b and the CN of the HC

As already mentioned there are not many available data in the literature concerning binary mixtures consisting of Hg with HCs. There are many HCs not included in the database like iso-hexane, p-xylene, and of course other branched HCs and HCs with a CN higher than 10. These data are of great importance for the models under development given the fact that the feed stream of a natural gas process plant consists from all those components as well. Therefore it is important that the models -namely SRK-Twu and PR-MC- will have k_{ij} parameters for all components so that they will be able more accurately predict the amount of Hg that ends up in the product stream. It is noted that no correlations are needed for the UMR-PRMC model, since it's a "predictive" model by itself.

One way to deal with this lack of data concerning these and other components as well, is to use the existing data to create generalized correlations based on a property of the HCs, which will provide an estimation of the value of the k_{ij} parameters. The two properties that have been chosen are the normal boiling point (T_b) of the HC and the carbon number (CN).

This choice was based on the fact that in contrast with other properties like the molecular weight (Mr) or the acentric factor (ω) each HC has a unique T_b, therefore the correlations will be able to provide more accurate results for each HC. The T_b values of each HC were found at Hysys software[14]. The choice of the CN property was also made, as this is the easiest and fastest way for an engineer to produce these parameters.

From scientific point of view looking at this subject however, it is clearly stated that the generalized correlations based on the T_b property are the correct ones. This can be easily justified through an example. If one has to estimate k_{ij} parameters for n.C_4 and iso-butane for instance, it is obvious that both HCs cannot share the same parameter. Thus their T_b property can guarantee that their parameters will be different, something that does not happen with their CNs property.

In order to create these correlations, all mixtures are divided into three categories. The first one includes all mixtures that contain Hg with paraffinic HC, the second one includes all mixtures that contain Hg with naphthenic HC and the third one includes all mixtures that contain Hg with aromatic HC. Tables 48-50 present all three categories of HC along with their respective T_b values.

Table 48: First category

Binary mixtures of paraffinic HC with Hg	
Name	**T_b [^{o}C]**

Continuation of table 48	
n.C_5	36.05
n.C_6	68.75
n.C_7	98.45
n.C_8	125.65
n.C_{10}	174.15

Table 49: Second category

Binary mixtures of naphthenic HC with Hg	
Name	**T_b [^{o}C]**
trans-1.2-dm-cy-C_6	123.4
m-cy-C_6	100.9
cy-C_6	80.75

Table 50: Third category

Binary mixtures of aromatic HC with Hg	
Name	**T_b [^{o}C]**
benzene	80.15
toluene	110.65
o-xylene	139.15

Table 51: Generalized correlations of the k_{ij} parameters based on the CN for each category and model along with the R^2 of each correlation

Models	Paraffinic HC	R^2	Naphthenic HC	R^2	Aromatic HC	R^2
SRK-Twu(all)	**Confidential data**	0.993	**Confidential data**	0.979	**Confidential data**	0.910
PR-MC		0.994		0.999		0.910

Table 52: Generalized correlations of the k_{ij} parameters based on the T_b [^{o}C] for each category and model along with the R^2 of each correlation

Models	Paraffinic HC	R^2	Naphthenic HC	R^2	Aromatic HC	R^2
SRK-Twu(all)	**Confidential data**	1	**Confidential data**	0.988	**Confidential data**	0.921
PR-MC		1		0.997		0.921

As it can be seen at tables 51 and 52 all generalized correlations for the HC are linear ones. This is happening because the second order equations' curve, due to their order, present a minimum at n.C_{10} and afterwards rise again monotonically. This means that after a certain T_b the k_{ij} parameters provided from these correlations will

start rising instead of further decreasing as expected. Moreover the linear correlations have a very decent R^2, therefore their results will be reliable for usage.

At appendix H and figures H1-12 one can see the graphs of the generalized correlations based both on the CN and the T_b along with the fitted k_{ij} parameters for all models and HC categories. It shall finally be recommended that as far as the correlation for the paraffinic HC goes, it can be used safely for HC from $n.C_4$ up to $n.C_{10}$. For HC with a CN less than 4 the fitted parameters are recommended to be used.

Table 53 presents the fitted k_{ij} parameter values as well as the k_{ij} values that are estimated by both types of generalized correlations. In total the generalized correlations, as expected, are predicting satisfyingly enough the k_{ij} parameters. It can be observed that as the carbon number of the HCs is declining the value of the k_{ij} parameter is rising for all models when it comes to the paraffinic and iso-paraffinic HC. The same applies for the aromatic and the naphthenic HC as well.

The greatest deviations between the k_{ij} values are as expected those that concern the binary mixtures of Hg with trans-1.2-dm-cy-C_6, trans-1.4-dm-cy-C_6 and cis-1.2-dm-cy-C_6 [13]. It is also important to emphasize the fact that these correlations predict particularly well the k_{ij} values of all paraffinic HC for all models because these are the main HC that compose a natural gas mixture once it is extracted.

Table 53: Values of fitted and estimated from generalized correlations k_{ij} parameters for all models

Binary mixtures of Hg with HC	**SRK-Twu**			**PR-MC**		
	Fitted k_{ij}	**Generalized k_{ij} (CN)**	**Generalized k_{ij} (T_b)**	**Fitted k_{ij}**	**Generalized k_{ij} (CN)**	**Generalized k_{ij} (T_b)**
i-C_4	**Confidential data**			**Confidential data**		
n.C_4						
n.C_5						
n.C_6						
n.C_7						
n.C_8						
n.C_{10}						
2.2-dm-C_4						
2.2.4-tm-C_5						
cy-C_6						
m-cy-C_6						
cis-1.2-dm-cy-C_6						
cis-1.4-dm-cy-C_6						
trans-1.4-dm-cy-C_6						
trans-1.2-dm-cy-C_6						

Continuation of table 53		
benzene	**Confidential data**	**Confidential data**
toluene		
o-xylene		

4.7.1 Evaluation of the generalized correlations for the binary interaction parameters based on the T_b and the CN of the HC

After the development of the generalized correlations it is essential that they are put to the test in order to check their credibility. For this purpose two mixtures, one ternary and one multicomponent, from the literature have been selected [10, 11], in order to check the Hg solubility in them. Tables 54 and 55 present the composition of these mixtures. It is noted that for the first mixture, the fitted parameters of C_3 were used for the testing.

Table 54: Composition of the first mixture

Component
C_3
i-C_4

Table 55: Composition of the second mixture

Component
n.C_4
n.C_5
n.C_6

Figures 34 and 35 present the Hg solubility in these mixtures predicted from all three models. In parenthesis next to the SRK-Twu and the PR-MC model, the type of the generalized correlation used for the estimation of the k_{ij} parameters is stated.

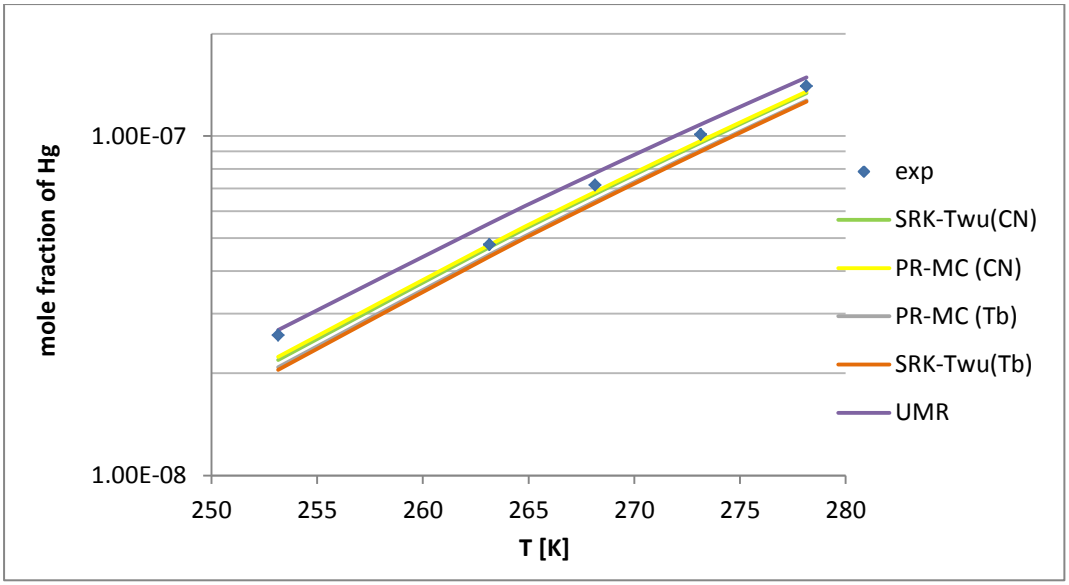

Figure 34: Hg mole fraction in liquid iso-butane + C_3 mixture at 69 bar

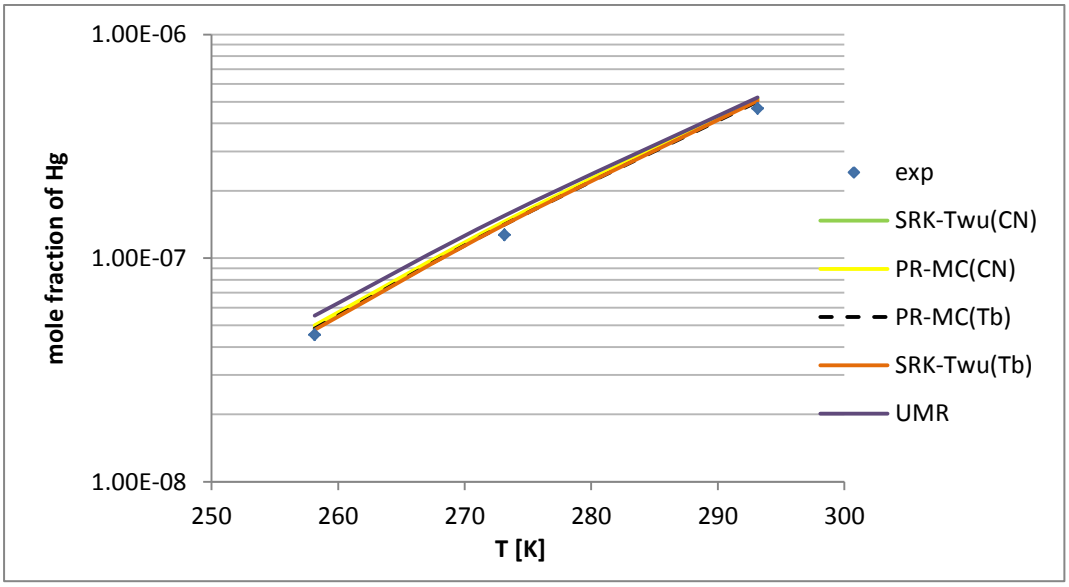

Figure 35: Hg mole fraction in liquid n.C_4 + n.C_5 + n.C_6 mixture at approximately 21 bar

At appendix J one can find the analytical results concerning figures 34 and 35 at tables J1-J10**.** As far as the first mixture is concerned as figure 34 shows, all models provide satisfyingly enough results. The UMR-PRMC model is the only one over-predicting the experimental data. All the other models are under-predicting them. It also appears that the models using the k_{ij} parameters based on the CN provide better results than the ones using the T_b based correlations. This however is to be expected because as it will be seen in the next chapter, the models using the CN correlations are able to predict much more accurately the mole fractions of Hg in iso-butane. The average deviations of the UMR-PRMC, the PR-MC(T_b), the PR-MC (CN), the SRK-

Twu(T_b) and the SRK-Twu (CN) models are 8.14%, 11.17%, 5.26%, 12.18% and 6.63% respectively.

As far as the second multicomponent mixture is concerned, once again as figure 35 displays all models seem to over-predict the experimental data. Still the results are very satisfactory. The UMR-PRMC model is the one that shows the biggest deviations compared to the other ones. Furthermore in this case the models using the T_b based generalized correlations appear to have a slight advantage over the other models in contrast to the previous mixture. The average deviations of the UMR-PRMC, the PR-MC(T_b), the PR-MC (CN), the SRK-Twu(T_b) and the SRK-Twu (CN) models are 18.55%, 8.33%, 11.72%, 8.18% and 9.87% respectively.

Conclusively one can say that the generalized correlations seem to produce very good results for the mixtures tested. It is up to the user to decide which type of generalized correlations will be used depending on the work at hand and the field of interest.

References:

[1] Peng, D. Y., and Robinson, D. B. (1976). "A New Two-Constant Equation of State". Industrial and Engineering Chemistry: Fundamentals 15, p. 59–64

[2] Soave (1972), G. Equilibrium Constants from a Modified Redlich–Kwong Equation of State, Chem. Eng. Sci., 27, p. 1197-1203

[3] Voutsas et al.(2005), “Thermodynamic property calculations with the universal mixing rule for EOS/G^E models: Results with the Peng-Robinson EOS and a UNIFAC model”

[4] E.H.Benmekki et al.(1987), “Van der Waals Mixing Rules for Cubic Equations of State”, ACS Symposium Series, Vol. 329, American Chemical Society

[5] Gross J., Sadowski G (2002), “Application of the perturbed chain SAFT equation of state to associating systems”, Industrial and Engineering Chemistry Research, vol. 41, issue 22, p. 5510-5515

[6] Solbraa Even (2002), ''Measurement and Modelling of Absorption of Carbon Dioxide into Methyldiethanolamine Solutions at High Pressures'', Norwegian University of Science and Technology Department of Refrigeration and Air Conditioning

[7] Mathias, P.M., Copeman, T.W. (1983), “Extension of the Peng-Robinson equation of state to complex mixtures”, Fluid Phase Equilibria 13, p. 91-108

[8] Twu C. et al (1995),'' A new generalized alpha function for a cubic equation of state Part 2. Redlich-Kwong equation'', Fluid Phase Equilibria 105, p. 61-69

[9] Prausnitz (1986), John M. et al., “MOLECULAR THERMODYNAMICS OF FLUID-PHASE EQUILIBRIA”, Prentice Hall Inc.

[10] **Confidential reference**

[11] **Confidential reference**

[12] V. Louli et al (2012), ''Measurement and prediction of dew point curves of natural gas mixtures '', Fluid Phase Equilibria 334, p. 2-4

[13] IUPAC, “Solubility Data Series, Mercury in liquids, compressed gases molten salts and other elements”, Volume 29, p. 101-160

[14] Hysys simulation program’s database, v.7.2

Chapter 5: Testing of PR-MC, SRK-Twu and UMR-PRMC model in binary and multicomponent mixtures

5.1 Iso-butane

For research purposes, once a database is complete, it is useful to separate it into two sections. One that will be used for the fitting of the required parameters and one that will be used for predictions with the models developed. Thus one can have a first evaluation of the models developed. In this master thesis the second part is consisted of two multicomponent mixtures of Hg and experimental data on the solubility of Hg in iso-butane [1]. Only iso-butane was chosen as binary mixture with Hg for evaluation of the models, due to the lack of many experimental data on the matter as explained at the 3rd chapter.

For the binary mixture of Hg in iso-butane [1] there are experimental data available in the liquid phase, as well as in the vapor phase. However this time for the SRK-Twu and the PR-MC models the parameters are not fitted to the data as explained. This time the parameters are estimated from the generalized correlations of these models, both with the ones based on the T_b of the components and the ones based on the CN of the components.

These parameters are used with each model respectively in order to predict the experimental data in the liquid phase at first with flash calculations using the Neqsim-tool. Afterwards by using the liquid mole fractions of Hg estimated, the Neqsim-tool performs B.P.P calculations in order to predict the vapor mole fraction of Hg. The same procedure is followed for the UMR-PRMC model as well. However since it is a "predictive" model, no new parameters are required for it.

At appendix I and tables I1-I5 one can see the analytical results of these calculations. Table 56 shows the parameters estimated from the generalized correlations for each model as well as their deviations from the experimental data. In parenthesis the type of the correlation is stated. The UMR-PRMC model has no k_{ij} parameters, therefore the corresponding Unifac parameters estimated in chapter 4 are used. Figures 36 and 37 present them graphically.

Table 56: Parameters and deviations all models for Hg and i-C_4

Model	k_{ij} parameter	Abs. Deviation in liquid phase (%)	Abs. Deviation in vapor phase (%)
SRK-Twu (T_b)	**Confidential data**	26.68	15.18
PR-MC (T_b)		25.11	12.73
SRK-Twu (CN)		16.57	15.12
PR-MC (CN)		14.18	12.61
UMR-PRMC	-	9.66	13.23

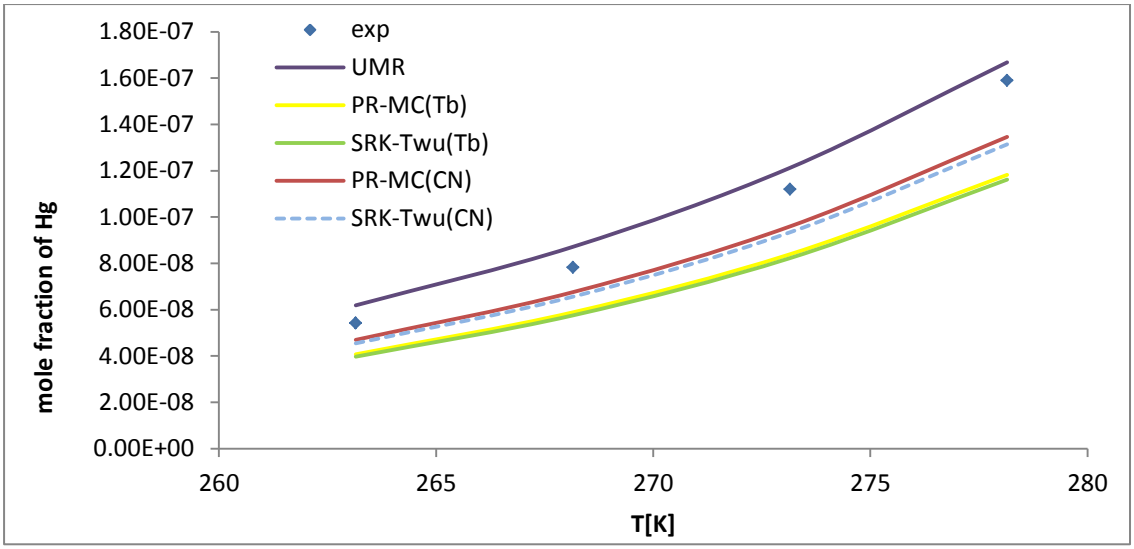

Figure 36: Experimental and estimated mole fractions of Hg in i-C_4 in the liquid phase from all models and both generalized correlations

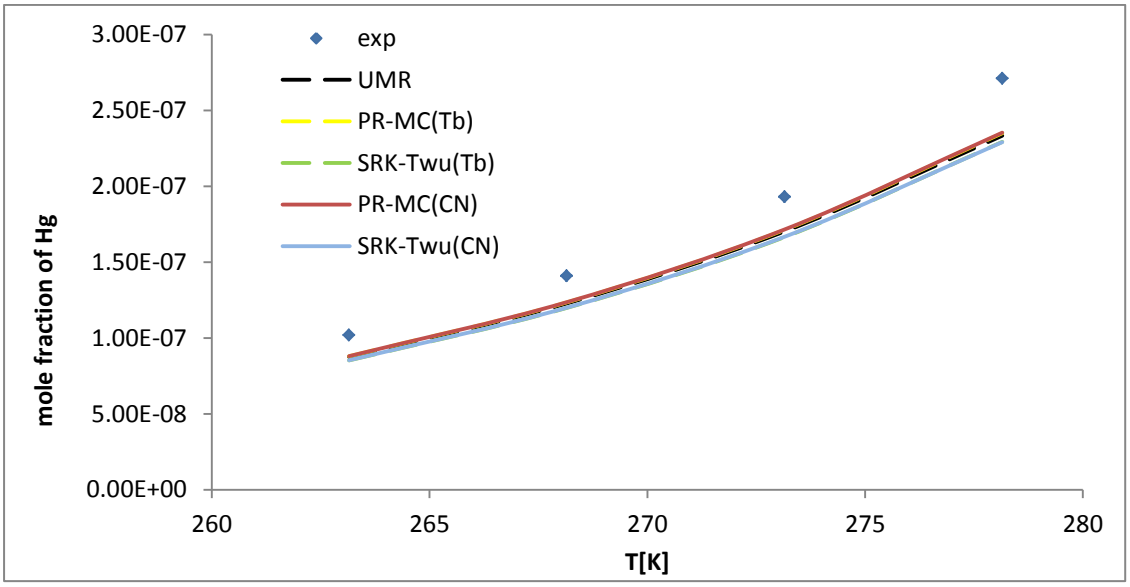

Figure 37: Experimental and estimated mole fractions of Hg in i-C_4 in the vapor phase from all models and both generalized correlations

As far as the mole fractions of Hg in the liquid phase are concerned figure 36 clearly shows that the UMR-PRMC model can predict them better than the other two models regardless of the generalized correlation used for the estimation of the k_{ij} parameters. It is also obvious that the SRK-Twu and PR-MC models using the generalized correlations based on the CN can estimate better the mole fraction of Hg in the liquid phase than the ones using the correlations based on the T_b.

As far as the mole fractions of Hg in the vapor phase are concerned figure 37 shows that all models provide almost the same results, which is expected as table 56 indicates at their absolute overall deviations from the experimental data. That's the

reason why UMR-PRMC, SRK-Twu(T_b) and PR-MC(T_b) "cover" one another at figure 37. Generally the PR-MC model seems to have a slight advantage over the other ones as tables I1-I5 at appendix I show and also as figure 37 implies. It should also be mentioned the SRK-Twu and PR-MC models make almost identical predictions of the mole fraction of Hg regardless of the generalized correlation used for the k_{ij} parameter.

5.2 'K' variable

After the completion of the estimation of the k_{ij} parameters for the SRK-Twu and the PR-MC models and the unifac parameters for the UMR-PRMC model and the comparison of the models' results with the experimental data, it is also important to investigate one more aspect for them. This is none other than the 'K' variable. The K variable is practically the division of the mole fraction of Hg in the vapor phase, with the mole fraction of Hg in the liquid phase [3].

$K_i = \frac{y_i}{x_i}$ (eq. 37)

This variable can provide yet another indication of the accuracy of the models. Obviously for 'K' to be estimated, data in both the vapor and the liquid phase for Hg are required. It is reminded that the components for which such data are available are ethane, propane, iso-butane and CO_2 [1, 2].

5.2.1 'K' variable for ethane

The first component's 'K' variable presented is the one for ethane. Table 57 presents the estimated 'K' for ethane of all models as well as their deviations from the experimental ones for each temperature and pressure and figure 38 illustrates them graphically.

Table 57: Experimental and estimated 'K' variables from each model for ethane and their respective deviations

Model			**PR-MC**		**SRK-Twu**		**UMR-PRMC**	
T [K]	**P [bar]**	**Kexp**	**Kcalc**	**ΔK%**	**Kcalc**	**ΔK%**	**Kcalc**	**ΔK%**
273.15	**Confidential data**		**Confidential data**	22.81	**Confidential data**	24.13	**Confidential data**	9.60
278.15				17.54		18.63		9.18
283.15				13.40		14.30		7.15
288.15				10.64		11.43		3.79
293.15				6.52		6.90		2.91

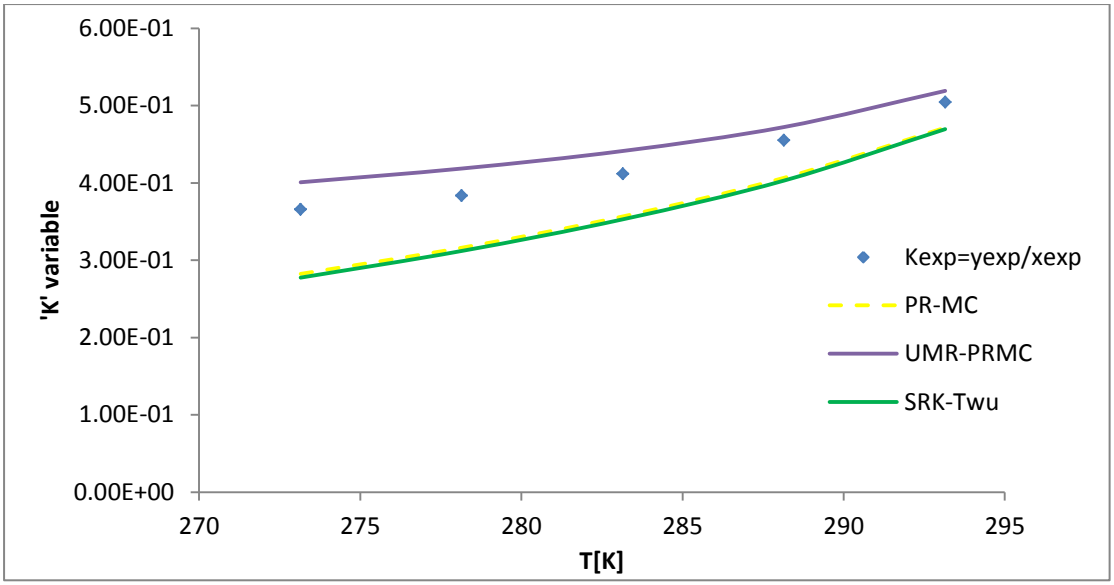

Figure 38: Experimental and estimated 'K' variables from each model for Hg in ethane

As figure 38 shows the UMR-PRMC model describes the 'K' variable better than the other two models. These show almost the same behavior, meaning that they begin with a deviation around 23%, which as the temperature rises, declines for both models to around 6.7%. Furthermore these models estimate almost the same 'K' variable with the PR-MC model to be slightly more accurate. It is also interesting to note the fact that the 'K' variable is rising along with the temperature.

The results of all models can be justified by the deviations they present -as shown at tables 22, 23, 39, 41 and figure 30- in the estimation of the mole fraction of Hg in the vapor phase, as well as in the liquid phase, although the k_{ij} parameters were fitted to the experimental data of the liquid phase. In addition to that, these deviations regarding the 'K' variable are quite acceptable given the deviations the models presented in the prediction of the mole fractions of Hg in both the liquid and the vapor phase.

5.2.2 'K' variable for propane

The next component's 'K' variable presented is the one for propane. Table 58 presents its' estimated 'K' for all models as well as their deviations from the experimental data for each temperature and pressure. Figure 39 illustrates the results graphically.

Table 58: Experimental and estimated 'K' variables from each model for propane and their respective deviations

Model			PR-MC		SRK-Twu		UMR-PRMC	
T [K]	P [bar]	Kexp	Kcalc	ΔK%	Kcalc	ΔK%	Kcalc	ΔK%
273.15	Confidential data		Confidential data	13.09	Confidential data	14.53	Confidential data	5.85
278.15				13.50		14.90		5.55
283.15				12.19		13.57		3.43
288.15				10.93		12.27		1.46
293.15				10.11		11.40		0.06

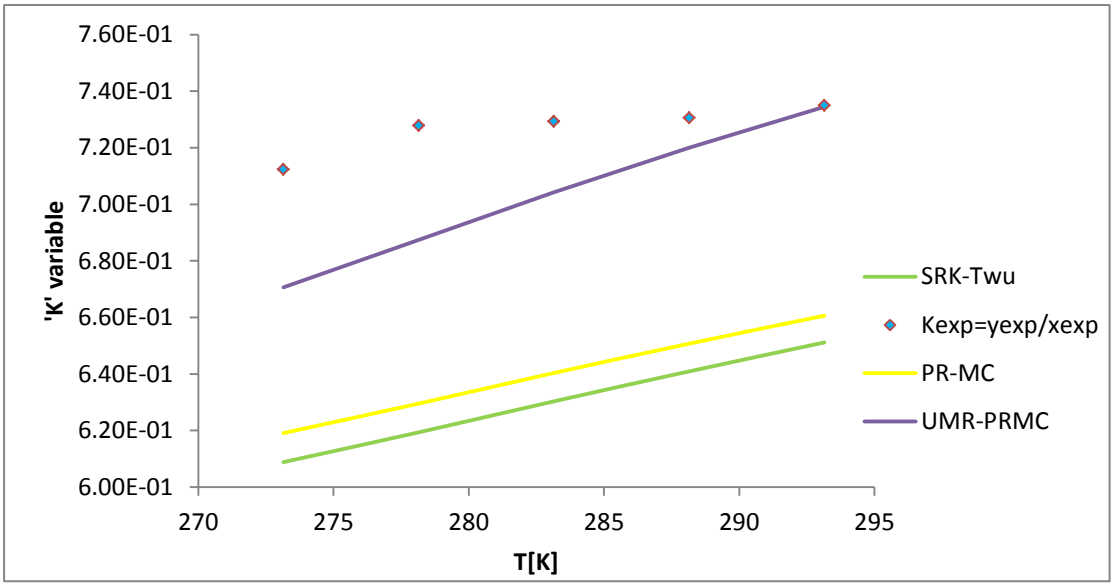

Figure 39: Experimental and estimated 'K' variables from each model for Hg in propane

As figure 39 shows the UMR-PRMC model once again is able to describe the 'K' variable better than the other two models. For propane the PR-MC and SRK-Twu models present once more almost the same behavior, meaning that they begin with a deviation around 13% and 14% respectively, which as the temperature rises, declines - slower compared to the corresponding rate presented for Hg in ethane - for both models to around 10% and 11% respectively. It is also noted that for this binary mixture the 'K' variable rises along with the temperature for the first 10 K but after that remains relatively the same.

The results of these models can be explained by the deviations they present -as shown at tables 23, 33 and figure 24- in the estimation of the mole fraction of Hg in the vapor phase of the binary mixture, since the k_{ij} parameters were fitted very well to the experimental data of the liquid phase, whereas the unifac parameters had a deviation of 11.35%.

5.2.3 'K' variable for CO_2

The penultimate component providing the 'K' variable is CO_2. Table 59 presents its estimated 'K' for all models as well as their deviations from the experimental data for each temperature and pressure. Figure 40 illustrates the results graphically.

Table 59: Experimental and estimated 'K' variables from each model for CO_2 and their respective deviations

Model			PR-MC		SRK-Twu		UMR-PRMC	
T [K]	P [bar]	Kexp	Kcalc	ΔK%	Kcalc	ΔK%	Kcalc	ΔK%
34.92	Confidential data		Confidential data	19.93	Confidential data	15.00	Confidential data	7.16
39.74				16.13		11.60		6.79
45.12				10.75		6.30		4.69
50.98				5.96		1.73		3.37
57.40				2.30		1.38		3.03

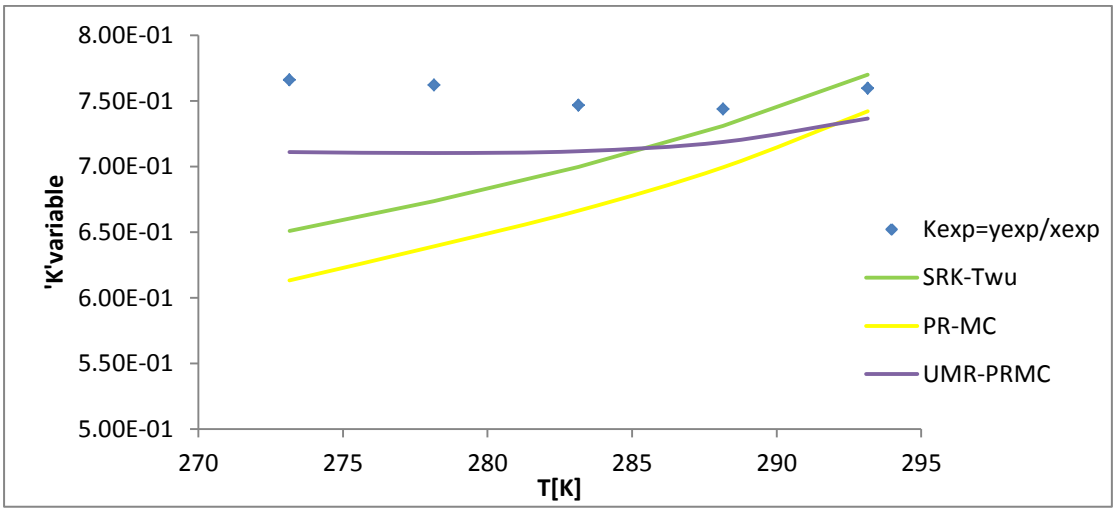

Figure 40: Experimental and estimated 'K' variables from each model for Hg in CO_2

As figure 40 shows the model that least accurately describes the 'K' variable is PR-MC. It presents a maximum deviation of 19.93% at 273.15 K, however as the temperature rises this deviation is declining and at 293.15 K it is just 2.30%. Therefore given the deviations this model has in the prediction of the mole fraction of Hg in the vapor and the liquid phase -as shown at tables 22, 23 and figure 31- , the results of the estimation of the 'K' variable are considered to be expected and acceptable.

The SRK-Twu model is the one estimating the variable better than the other two models for temperatures equal or higher than around 285 K. It is also the first time that a model appears to over-predict this variable at the temperature of 293.15 K by 1.38%. Both the SRK-Twu and the PR-MC model however appear to have a

constantly rising prediction for the 'K' variable in contrast with the UMR-PRMC model. Of course the results of this model are also expected and acceptable for the same reasons mentioned for the PR-MC model.

The UMR-PRMC model appears to be the most reliable one compared to the other two models. This is said not only because it is able to more accurately predict the mole fraction of Hg in both the vapor and the liquid phase, but also because it systematically under-predicts the 'K' variable by about 3% - 7%. That means that its' estimations are consistent and there appears to be no danger to over-estimate the variable, as the temperature rises, by a big deviation. The trend-lines of the other models imply that when the temperature rises higher than the data available, they will over-predict the variable by a significant deviation, given the fact that from figure 40, 'K', constantly appears to be around 0.745 and 0.770.

5.2.4 'K' variable for iso-butane

The last component examined for the 'K' variable is iso-butane. This component is special compared to the other ones presented so far. This is because its' data were immediately predicted from the models and were not included in the database used for the fitting of the respective parameter for each model.

Tables 60 and 61 present its' estimated 'K' for all models as well as their deviations from the experimental data for each temperature and pressure. Figure 41 illustrates the results graphically. In parenthesis is stated the type of the generalized correlation used for the estimation of the k_{ij} parameters for the SRK-Twu and the PR-MC models.

Table 60: Experimental and estimated 'K' variables from UMR-PRMC for iso-butane and their respective deviations

Model			**UMR-PRMC**	
T [K]	**P [bar]**	**Kexp**	**Kcalc**	**ΔK%**
263.15	**Confidential data**		**Confidential data**	24.86
268.15				21.78
273.15				18.57
278.15				17.96
263.15				24.86

Table 61: Experimental and estimated 'K' variables from each EOS for iso-butane and their respective deviations

Model			PR-MC (CN)		PR-MC (T_b)		SRK-Twu (CN)		SRK-Twu (T_b)	
T [K]	P [bar]	Kexp	Kcalc	ΔK%	Kcalc	ΔK%	Kcalc	ΔK%	Kcalc	ΔK%
263.15	Confidential data		Conf. data	0.44	Conf. data	14.71	Conf. data	0.35	Conf. data	14.00
268.15				1.55		16.47		1.51		15.61
273.15				3.68		18.38		3.51		17.39
278.15				2.54		16.57		2.25		15.74
263.15				0.44		14.71		0.35		14.00

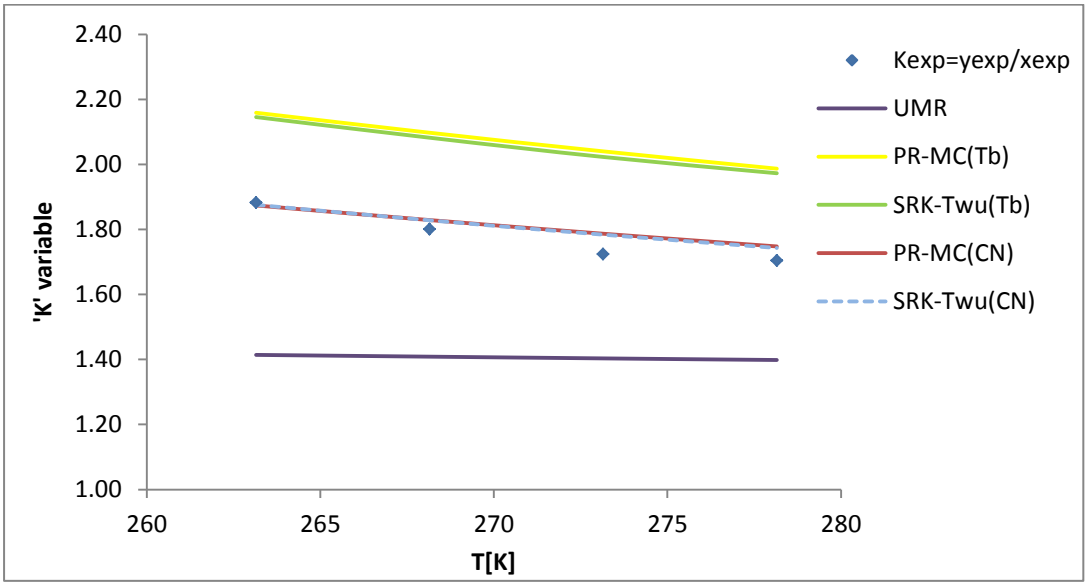

Figure 41: Experimental and estimated 'K' variables from each model for Hg in iso-butane

First of all the UMR-PRMC model is the only model under-predicting the 'K' variable in contrast with the other models. The deviations are between 18% and 25%. These deviations are to be expected in a way, given the fact that the unifac groups describing this component have been fitted to a large amount of experimental data and therefore naturally present deviations at the estimation of the mole fraction of Hg in the vapor, as well as in the liquid phase. Worth-noting is also the fact that the 'K' estimated from this model is almost constant and around 1.40 and 1.41.

The PR-MC and SRK-Twu models using the CN based generalized correlations provide 'K' variables almost in complete agreement to the experimental ones. This is expected of course since as figure 41 shows, these correlations describe with almost the same deviations the experimental mole fractions of Hg in both liquid and vapor phase.

The PR-MC and SRK-Twu models using the T_b based generalized correlations in contrast to the previous ones over-predict the experimental 'K's. This is expected because as figure 36 implies as well, these models under-predict the liquid mole fraction of Hg. However since their deviations are between 18.4% and 14%, their respective results are also considered to be acceptable.

In conclusion the 'K' variables of four different binary mixtures have been estimated and compared to their respective experimental data. The results of all models examined can be justified by the analysis of chapter 4 for all binary mixtures. Thus all models -and generalized correlations- appear to be in position to provide reliable results concerning the distribution of Hg in a natural gas process. Finally based on the analysis done, the UMR-PRMC model appears to be the most consistent one in terms of accuracy -over or under-estimation of the experimental 'K' variables- and deviations compared to the other models.

5.3 Multi-component mixtures

After the completion of the estimation of all necessary parameters for the models depending on binary mixtures and vapor pressure data for Hg, it is important to see how they cope against experimental data regarding more complex than binary symstems containing Hg. That way one can be more certain that the results produced by them regarding the Hg distribution within a process will be more reliable. This is the final and most important test for the models, since there are no experimental data from any process that can confirm the results for it.

For this testing two different mixtures will be examined. Tables 62 to 63 present their components and their respective composition. It is mentioned that the experimental data of the first mixture are available at two different pressures, namely at 27.58 bar and at 69 bar. The second mixture has data available at approximately 21 bar. Also at appendix D at table D3 one can find the unifac group parameters between all other groups, except for Hg, used for the prediction of the two mixtures with the UMR-PRMC model.

Table 62: Composition of the first mixture

Component
CH_4
C_2H_6
C_3
N_2
CO_2
Sum

Table 63: Composition of the second mixture

Component
$n.C_4$
$n.C_5$
$n.C_6$
Sum

Tables 64 and 65 as well as figures 42 and 43 illustrate the results concerning the first multicomponent mixture. It can be seen that all three models are able to predict very accurately the experimental data. Also as table 64 indicates, at low temperatures the models under-predict the experimental data at 69 bar and at 20 ^{o}C they over-predict them. However at 27.58 bar they constantly under-predict the data. In total all models present very close results with one another. This is also the reason why at figures 42 and 43 the line presenting the results from the PR-MC practically "covers" the one from the SRK-Twu model. This can be made even clearer by comparing the results displayed at tables 64 and 65 for each model against the other two.

Finally as figures 42 and 43 illustrate all models fail to accurately predict the experimental data at 10 ^{o}C at both pressures. Still the figures imply that the data follow a linear trend-line. Thus one may assume that at this particular temperature there has been some sort of experimental error.

Table 64: Experimental data, conditions and results of the first mixture with all three models

Conditions		**Model**	**SRK-Twu**	**PR-MC**	**UMR-PRMC**
P [bar]	T [^{o}C]	Exp. Mole fraction of Hg	Calc. Mole fraction of Hg		
Confidential data		**Confidential data**	**Confidential data**		

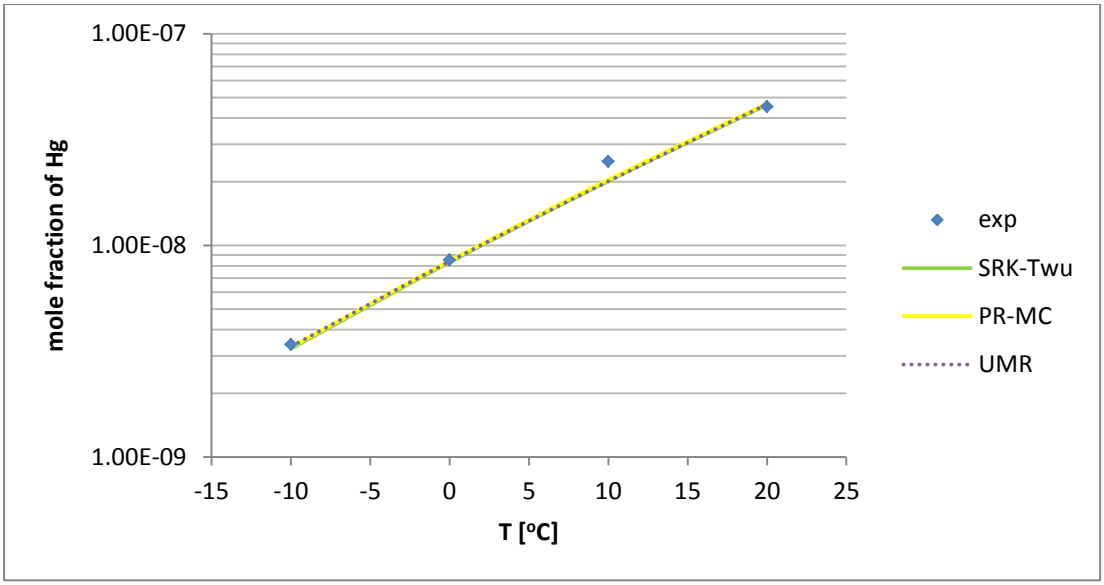

Figure 42: Experimental and predicted mole fractions of Hg in the first multicomponent mixture with the all three models at 69 bar

Table 65: Experimental data, conditions and results of the first mixture with all three models

Conditions		**Model**	**SRK-Twu**	**PR-MC**	**UMR-PRMC**
P [bar]	T [°C]	Exp. Mole fraction of Hg	Calc. Mole fraction of Hg		
Confidential data		**Confidential data**	**Confidential data**		

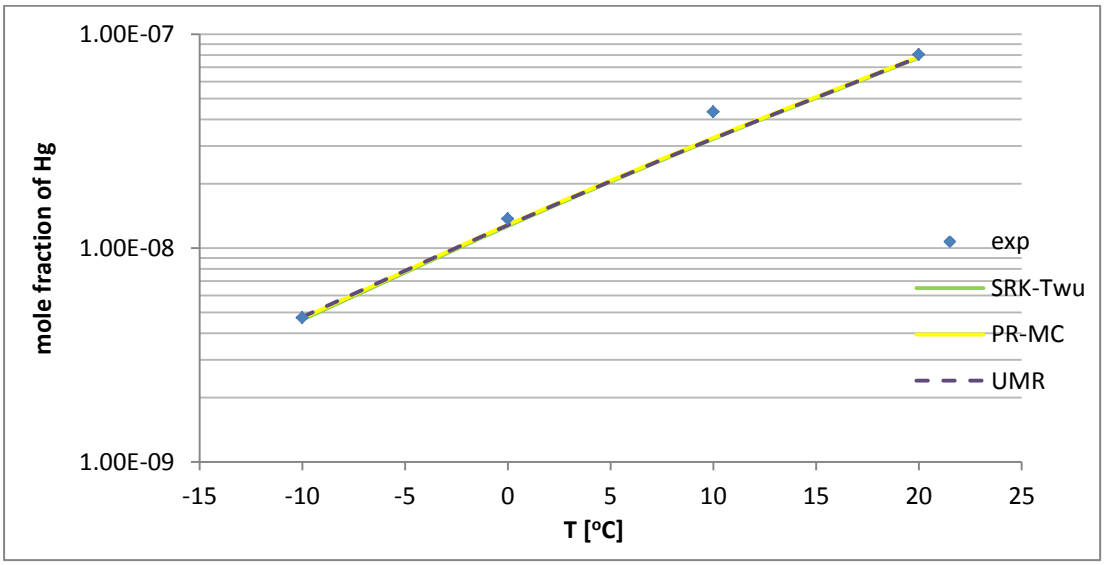

Figure 43: Experimental and predicted mole fractions of Hg in the first multicomponent mixture with the all three models at 27.58 bar

Tables 66 and 67 and figure 44 present the experimental data and the results of the second multicomponent mixture. It is mentioned that for this mixture the k_{ij} parameters for n.C_4 have been estimated by both types of generalized correlations, which are shown in parenthesis next to the models. The rest k_{ij} parameters taken into employment from the models are the fitted ones.

Table 66: Experimental data, conditions and results of the second mixture with the UMR-PRMC model

Conditions		**Model**	**UMR-PRMC**
P [bar]	T [^{o}C]	Exp. data	Calc. Mole fraction of Hg
Confidential data		**Confidential data**	**Confidential data**

Table 67: Experimental data, conditions and results of the second mixture with the PR-MC and SRK-Twu models using the generalized correlations for the k_{ij} of n.C_4

Conditions		**Model**	**SRK-Twu (CN)**	**SRK-Twu (T_b)**	**PR-MC (CN)**	**PR-MC (T_b)**
P [bar]	T [^{o}C]	Exp. data	Calc. Mole fraction of Hg			
Confidential data		**Confidential data**	**Confidential data**			

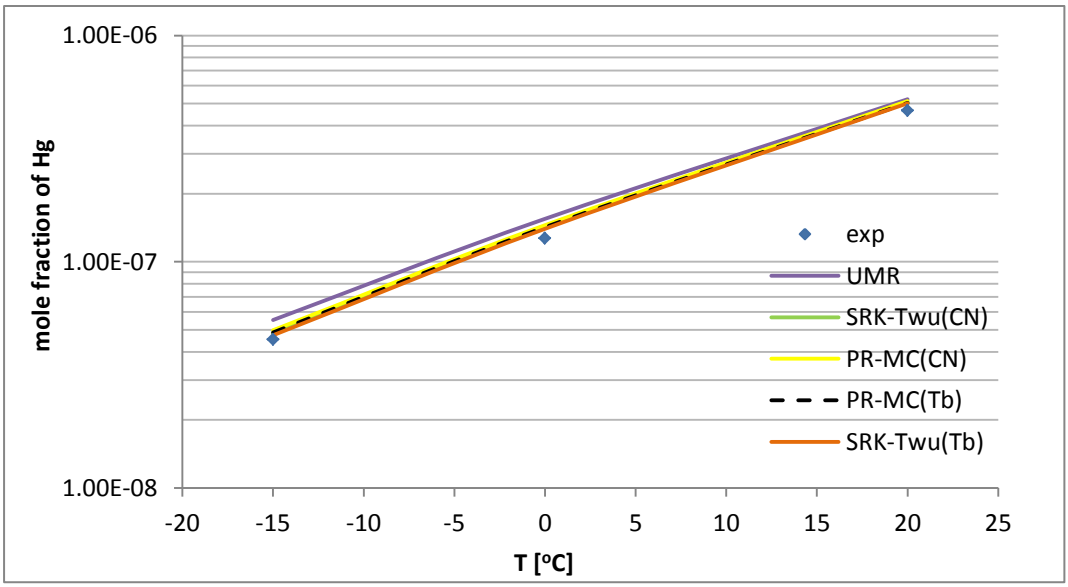

Figure 44: Experimental and predicted mole fractions of Hg in the second multicomponent mixture with the all models at approximately 21 bar

It can be seen that all three models are able to predict very well the experimental data. Also table 67 indicates the differences between the models using the CN based and the T_b based generalized correlations are practically negligible. This can be attributed to the fact that for the paraffinic HCs, both had a R^2 around 0.99. In addition to that as table 53 illustrates, both correlations estimate very similar parameters for n.C_4.

Conclusively it appears that all three models can be characterized as trustworthy for the prediction of the Hg distribution in multicomponent mixtures as well as in binary mixtures. It is also underlined that this happens despite the fact that all models were not able to accurately estimate the 'K' variable of propane and the PR-MC and SRK-Twu the one for ethane. In addition it is also important to specially emphasize the fact that the multicomponent mixture of table 62 basically resembles a typical feed stream of any natural gas industry. Therefore the fact that the models' predictions match very well the experimental data is also an indication that the models can be used later on for process simulations. Furthermore the results of this particular mixture are within the range of the study presented by Carnell P. et al, at table 2, fact which adds credibility to the study, the experimental data and the models as well.

References:

[1] **Confidential reference**

[2] **Confidential reference**

[3] Tassios et al (2001), ''Applied Thermodynamics of Chemical Engineering'', NTUA, p. 521

[4] Michael M.Abbott, Hendrick C. Van Ness (1983), ''Θερμοδυναμική'', Translated by Konstantinos N. Pattas, Nikolaos A. Kiriakis, Schaum outline series, Mc Graw-Hill, New York, p. 238-239, 262-263

[5] Carnell P. et al (2004),'' MERCURY DISTRIBUTION ON GAS PROCESSING PLANTS '', 83rd annual GPA convention proceedings, New Orleans.

Chapter 6: Conclusions

In this master thesis three thermodynamic models have been developed, using the PR and the SRK EOSs as their basis, in order to predict the elemental Hg distribution throughout a natural gas processing plant.

The first step was the evaluation of two different sets of critical properties about Hg that are suggested in literature. One of them was proposed by a report from NIST and the other one was proposed by DIPPR. Since the set of NIST has no real advantage over the other set and in addition the set from DIPPR is used by official softwares like Hysys and PROII it was decided that this set will be used for the rest of the thesis.

The second step was the compilation of the data regarding the P^S of Hg. These data were used afterwards in order to estimate the Mathias-Copeman parameters for the PR EOS and the Twu-Coon parameters for the SRK EOS for a temperature range from the triple point of Hg, up to its' critical point. These parameters were incorporated via the 'alpha' parameter in the EOSs and with them the ability of the models to accurately predict the P^S of elemental Hg improved significantly.

The third step was the creation of a database concerning the solubility of Hg in HCs and other components. This database contains LLE data for all binary mixtures except for those concerning Hg in propane CO_2, ethane and iso-butane, which are VLE data. Furthermore there are data regarding the solubility of Hg only in the vapor phase, namely those of Hg in methane and N_2. These data have been evaluated and then used in order to estimate the binary interaction parameters between Hg and each HC as constants for each model respectively. These parameters assist the models to provide a better estimation for the phase equilibriums of systems containing elemental Hg with HCs and other components.

The fourth step was the creation of temperature dependent binary interaction parameters for Hg and water. This was found to be necessary because with the respective constant parameters all models failed to accurately predict the phase equilibriums of this particular binary system. This can be attributed to the hydrogen bond of water that the classical EOSs like PR-MC and SRK-Twu fail to take into consideration successfully.

The fifth step was the estimation of the Unifac group contribution parameters for the UMR-PRMC model for all groups of which the experimental data consist of, by using the data of the assembled database. Given the fact that this model is based on the PR-MC model, no further action was needed for its' completion.

Due to the lack of experimental data regarding the solubility of Hg in many HCs, the sixth step was the creation of generalized correlations for each model respectively. These correlations are able to provide estimation about the binary interaction parameters that cannot be calculated otherwise. The properties of the HCs chosen to create these correlations were their normal boiling point and their respective carbon number. In addition to that, the generalized correlations have been tested against experimental data regarding a ternary and a multicomponent mixture.

The final part of this thesis was the evaluation of the three models developed as well as their corresponding generalized correlations, against experimental data concerning multicomponent mixtures and also against the experimental 'K' variable, which is the division of the Hg mole fraction in the vapor phase with the Hg mole fraction in the liquid phase, where possible.

These evaluations had three objectives. The first one was to test how the developed models cope against more complex systems than just binary mixtures. That way it would be safer to conclude whether or not the models can be used in process simulations at a later stage while providing reliable results, given the fact that there are no experimental data regarding processes. The second one was to explore the capability of the models to predict the 'K' variable, which is very important when it comes down to evaluating models in a process. The last one was to find the optimum type of binary interaction parameters that should be used for process simulations in the future.

The conclusions can be summarized as follows:

1. All models, namely the PR-MC, the SRK-Twu EOS and the UMR-PRMC are able to accurately predict the mole fraction of elemental Hg both in binary and multicomponent mixtures.

2. All models are capable of predicting the 'K' variable of the corresponding mixtures very accurately.

3. As far as the optimum type of the generalized correlation is concerned, both types appear to provide very similar results in all cases, except for the mixtures containing iso-butane, where the correlations based on the CN seem to have the advantage. Therefore it is concluded that it is up to the user to decide which type is appropriate according to the occasion, since both types provide reliable results.

4. All models and generalized correlations can be used in process simulations at a future stage with some caution regarding the branched alkanes and the

aromatic HCs due to their tentative experimental data, providing reliable results.

Chapter 7: Future work

The models created are able to predict the distribution of Hg in binary, ternary and multicomponent mixtures. However there are several steps necessary to be made, in order to improve their predictive abilities and also assist in a further evaluation for them. Some options include:

1. The usage of the models at a real process of a natural gas plant where the distribution of elemental Hg throughout the plant will be evaluated.

2. The veryfication of the results of the models via experimental data from the process.

3. The extension of the database concerning the solubility of Hg in HC for binary mixtures of Hg with components 'heavier' than n.C_{10}, so that binary interaction parameters can be fitted for these components as well.

4. The extension of the same database for the solubility of Hg in other components like H_2S and He, which are of interest to the natural gas industry.

5. The veryfication of tha data included in the database of this master thesis that are characterized as tentative ones.

6. It has been mentioned that although Hg is mainly found in its' elemental form in the natural gas, this is not its' only form that is contained there. Therefore the chemistry of Hg, meaning its' chemical reactions and various forms can be included in the models as well.

7. There can also be a further extension of the models tested for the prediction of the distribution of Hg. Except for PR and SRK EOS there are other mode advanced models. One of them is the PC-SAFT model, which can also make predictions about the phase equilibrium of water. This is important enviromentaly speaking because that way the industrial world will be able to know the composition of their waste in Hg and thus proceed to take any measures if necessary.

Appendix A

Table A1: Experimental data and comparison with results from DIPPR's equation for P^s

		Exp. Data	Dippr's eq.	Deviation %
Researcher (uncert. level %)	**T [K]**	**P [Kpa]**	**P [Kpa]**	**$((P_{exp}-P_{calc})/P_{exp})$%**
Ambrose (<0.03)	417.10	0.293	0.293	-0.07
	426.20	0.424	0.426	-0.42
	432.28	0.538	0.541	-0.61
	439.29	0.706	0.708	-0.27
	441.72	0.774	0.775	-0.16
	447.68	0.964	0.965	-0.10
	451.38	1.101	1.102	-0.10
	454.12	1.213	1.214	-0.11
	456.32	1.309	1.312	-0.19
	462.63	1.627	1.629	-0.13
	469.18	2.024	2.027	-0.15
	474.57	2.414	2.415	-0.04
	479.04	2.784	2.785	-0.02
	485.15	3.369	3.368	0.04
	491.86	4.128	4.126	0.04
	497.53	4.882	4.879	0.07
	549.47	19.193	19.175	0.09
	554.72	21.742	21.700	0.19
	562.76	26.162	26.106	0.21
	579.98	38.203	38.112	0.24
	589.082	46.244	46.130	0.25
	597.32	54.686	54.547	0.25
	605.65	64.484	64.316	0.26
	611.99	72.866	72.686	0.25
	621.15	86.564	86.340	0.26
	627.81	97.795	97.543	0.26
	628.88	99.711	99.458	0.25
	629.95	101.643	101.388	0.25
	638.37	118.032	117.728	0.26
	639.86	121.141	120.845	0.24
	645.49	133.558	133.189	0.28
	654.71	155.987	155.590	0.25
	663.19	179.295	178.846	0.25
	671.78	205.659	205.159	0.24
	681.17	237.992	237.429	0.24
	685.43	253.933	253.351	0.23
	702.72	327.808	327.089	0.22
	711.62	371.975	371.197	0.21

	Continuation of table A1			
Ambrose (<0.03)	726.55	456.609	455.737	0.19
	739.69	543.039	542.119	0.17
	749.79	617.883	616.913	0.16
	771.24	802.526	802.659	-0.02
	481.65	3.023	3.022	0.03
	488.13	3.689	3.688	0.02
	494.93	4.522	4.520	0.05
	500.62	5.339	5.336	0.06
	506.66	6.342	6.336	0.10
	513.69	7.708	7.699	0.11
	520.26	9.205	9.191	0.15
	526.17	10.753	10.739	0.13
	533.78	13.074	13.052	0.17
	541.59	15.879	15.850	0.18
	546.93	18.080	18.045	0.19
	555.22	21.998	21.953	0.20
	572.032	32.173	32.099	0.23
	587.99	45.215	45.103	0.25
	596.47	53.760	53.625	0.25
	605.05	63.675	63.568	0.17
	612.93	74.144	73.999	0.20
	621.86	87.728	87.491	0.27
	630.16	102.037	101.766	0.27
	624.85	92.667	92.429	0.26
	627.96	98.061	97.812	0.25
	632.34	106.099	105.827	0.26
	623.25	89.986	89.755	0.26
	624.85	92.662	92.429	0.25
	626.41	95.342	95.098	0.26
	633.75	108.792	108.519	0.25
	636.49	114.202	113.914	0.25
	629.47	100.764	100.510	0.25
	633.75	108.794	108.519	0.25
	635.13	111.489	111.207	0.25
	630.92	103.440	103.177	-1.83
Beattie (0.03)	629.76	101.325	101.049	0.27
	622.96	89.523	89.280	0.27
	624.56	92.188	91.936	0.27
	626.055	94.739	94.484	0.27
	627.69	97.591	97.327	0.27
	629.077	100.075	99.806	0.27
	630.58	102.819	102.545	0.27
	632.0069	105.472	105.199	0.26

	Continuation of table A1			
Beattie (0.03)	633.43	108.168	107.903	0.25
	634.71	110.655	110.388	0.24
	635.65	112.492	112.230	0.23
	634.15	109.565	109.294	0.25
	632.80	106.976	106.702	0.26
	631.40	104.344	104.071	0.26
	629.96	101.688	101.414	0.27
	628.42	98.897	98.634	0.27
	626.85	96.126	95.867	0.27
	625.39	93.605	93.352	0.27
	623.29	90.0733	89.827	0.27
	624.99	92.914	92.664	0.27
	626.76	95.967	95.710	0.27
	631.19	103.940	103.669	0.26
	632.63	106.646	106.372	0.26
	633.94	109.160	108.891	0.25
	634.92	111.047	110.785	0.24
	632.26	105.943	105.672	0.26
	627.62	97.470	97.204	0.27
Ernsberger (1)	285.22	8.45E-05	8.46E-05	-0.13
	288.15	0.000111	0.000110	0.97
	291.10	0.000145	0.000143	1.25
	294.11	0.000185	0.000185	-0.15
	297.22	0.000241	0.000241	-0.05
	300.25	0.000312	0.000310	0.45
	303.18	0.000393	0.000394	-0.03
	306.17	0.000501	0.000499	0.25
	309.29	0.000636	0.000637	-0.15
	312.11	0.000793	0.000790	0.36
	315.15	0.000995	0.000992	0.25
	318.17	0.00124	0.00124	0.22
	321.15	0.00154	0.00154	0.16
	324.12	0.00190	0.00190	0.20
	326.63	0.00226	0.002258	0.08
	293.24	0.000174	0.000172	0.78
	296.22	0.000223	0.000222	0.32
	299.20	0.000287	0.000285	0.69
Menzies (0.5)	423.10	0.374	0.376	-0.56
	464.58	1.736	1.740	-0.21
	526.92	10.943	10.949	-0.06
	533.29	12.911	12.890	0.16
	537.10	14.201	14.185	0.11
	540.92	15.604	15.592	0.08

	Continuation of table A1			
Menzies (0.5)	544.75	17.141	17.119	0.13
	548.61	18.805	18.785	0.11
	556.53	22.641	22.632	0.04
	565.97	28.103	28.065	0.14
	571.23	31.592	31.539	0.17
	577.63	36.429	36.245	0.50
	583.62	41.294	41.167	0.31
	587.20	44.652	44.367	0.64
	599.51	57.186	56.988	0.35
	602.72	60.942	60.728	0.35
	607.01	66.396	66.041	0.53
	611.05	71.667	71.390	0.39
	615.66	78.228	77.926	0.39
	619.97	84.660	84.475	0.22
	620.57	85.622	85.421	0.23
	624.95	93.023	92.598	0.46
	625.06	93.022	92.785	0.25
	627.66	97.609	97.282	0.33
	628.79	99.700	99.292	0.41
	630.13	102.050	101.718	0.32
	630.54	102.560	102.471	0.09
	633.86	108.920	108.731	0.17
	635.24	111.510	111.424	0.08
	638.43	118.090	117.858	0.20
	641.34	124.340	123.989	0.28
	645.54	133.660	133.294	0.27
	651.46	147.810	147.370	0.30
	656.74	161.400	160.923	0.30
	659.45	168.730	168.262	0.28
	662.35	176.800	176.414	0.22
	666.82	190.120	189.604	0.27
	677.05	223.350	222.807	0.24
	679.94	232.550	232.990	-0.19
	683.43	246.290	245.784	0.21
	689.93	271.59	271.116	0.17
	692.87	283.42	283.241	0.06
	699.29	311.21	311.233	-0.01
	706.78	346.53	346.641	-0.03
	707.47	349.88	350.058	-0.05
Schonherr (3)	1051.44	9006.415	9338.783	-3.69
	1186.24	19992.89	20352.414	-1.80
	1322.14	38198.32	38520.392	-0.84
	1424.66	57101.07	58131.280	-1.80

	Continuation of table A1			
Schonherr (3)	1510.37	78204.03	79191.073	-1.26
	1581.99	99103.96	100534.610	-1.44
	1632.52	115498.60	117887.026	-2.07
	1665.97	127496.70	130509.868	-2.36
	1686.68	134500.80	138805.413	-3.20
	1704.76	142996.60	146360.096	-2.35
	1716.40	148999.00	151382.444	-1.60
	1726.05	153498.70	155642.459	-1.40
	1735.51	157499.80	159904.817	-1.53
Shpil'rain (0.6 - 0.8)	554.11	21.52	21.392	0.59
	560.61	25.05	24.860	0.76
	567.11	28.93	28.789	0.49
	578.91	37.40	37.254	0.39
	600.61	58.54	58.247	0.50
	604.11	62.61	62.409	0.32
	621.11	86.35	86.280	0.08
	622.21	88.11	88.053	0.06
	623.71	90.38	90.518	-0.15
	626.81	95.47	95.793	-0.34
	629.41	100.20	100.408	-0.21
	635.21	111.70	111.365	0.30
	643.31	127.90	128.285	-0.30
	619.71	84.19	84.067	0.15
	628.11	98.15	98.078	0.07
	628.31	98.89	98.434	0.46
	630.91	103.40	103.153	0.24
	635.61	112.30	112.155	0.13
	639.81	121.00	120.733	0.22
	642.11	125.70	125.654	0.04
	643.81	129.30	129.394	-0.07
	664.30	182.54	182.074	0.26
	707.29	349.21	349.164	0.01
	742.78	561.47	564.202	-0.49
	755.98	663.72	666.639	-0.44
	774.67	839.05	836.017	0.36
	648.01	138.62	139.027	-0.29
	677.30	225.31	223.674	0.73
	681.50	237.79	238.641	-0.36
	694.70	290.70	291.006	-0.11
	724.09	441.07	440.824	0.06
	732.39	491.11	492.654	-0.31
	752.68	638.37	639.761	-0.22
	774.57	834.49	835.030	-0.06

	Continuation of table A1			
Shpil'rain (0.6 - 0.8)	786.77	962.52	962.405	0.01
	796.86	1079.80	1078.732	0.10
	814.46	1305.70	1307.372	-0.13
	836.25	1635.51	1640.125	-0.28
	803.66	1161.17	1163.067	-0.16
	815.46	1319.73	1321.399	-0.13
	822.45	1423.02	1422.710	0.02
	831.85	1569.96	1568.223	0.11
	845.39	1795.51	1797.513	-0.11
	847.24	1825.05	1830.722	-0.31
	854.54	1967.28	1966.343	0.05
	856.44	1999.68	2002.861	-0.16
	866.64	2211.86	2207.780	0.18
	880.43	2514.78	2509.577	0.21
	882.13	2553.52	2548.829	0.18
	883.23	2572.95	2574.472	-0.06
Spedding (0.03)	533.83	13.06	13.066	-0.04
	549.81	19.337	19.330	0.04
	558.95	23.954	23.932	0.09
	564.72	27.351	27.289	0.23
	565.74	27.964	27.922	0.15
	573.61	33.293	33.226	0.20
	586.013	43.39	43.284	0.25
	594.74	51.918	51.785	0.26
	597.25	54.588	54.474	0.21
	604.29	62.792	62.627	0.26
	613.87	75.568	75.355	0.28
	620.25	85.144	84.922	0.26
	630.24	102.22	101.927	0.29
Douglas et al (<1.5)	234.30	2.921E-07	2.93276E-07	-0.40
	253.17	0.00000311	3.13695E-06	-0.74
	273.15	0.00002661	2.68401E-05	-0.86

Table A2 : Analytical results from Neqsim tool using SRK and PR EoS and deviations from the results of DIPPR's equation.

$$\Delta P^s\ \% = \frac{(Pexp - Pcalc) * 100}{Pexp} \quad \text{(eq. A1)}$$

Set 1 = DIPPR's set of T_c, P_c, ω

Set 2 = NIST's set of T_c, P_c, ω

T [K]	DIPPR P^s [bar]	Neqsim-SRK (set 1)	ΔP^s %	Neqsim-SRK(set 2)	ΔP^s %	Neqsim-PR(set 1)	ΔP^s %	Neqsim-PR(set 2)	ΔP^s %
238.15	4.90E-09	6.13E-10	87.49	1.63E-09	66.65	3.30E-09	32.70	9.29E-09	-89.50
248.15	1.73E-08	2.44E-09	85.87	6.14E-09	64.49	1.19E-08	31.45	3.14E-08	-81.66
258.15	5.52E-08	8.72E-09	84.21	2.08E-08	62.39	3.85E-08	30.25	9.66E-08	-74.86
268.15	1.62E-07	2.83E-08	82.50	6.41E-08	60.33	1.15E-07	29.09	2.73E-07	-68.92
278.15	4.37E-07	8.41E-08	80.76	1.82E-07	58.32	3.15E-07	27.97	7.15E-07	-63.70
288.15	1.10E-06	2.31E-07	78.99	4.81E-07	56.36	8.05E-07	26.89	1.75E-06	-59.09
298.15	2.61E-06	5.94E-07	77.21	1.19E-06	54.45	1.93E-06	25.85	4.04E-06	-54.99
308.15	5.82E-06	1.43E-06	75.41	2.76E-06	52.60	4.38E-06	24.85	8.81E-06	-51.33
318.15	1.24E-05	3.26E-06	73.61	6.08E-06	50.80	9.41E-06	23.88	1.83E-05	-48.05
328.15	2.51E-05	7.06E-06	71.80	1.28E-05	49.05	1.93E-05	22.94	3.64E-05	-45.11
338.15	4.86E-05	1.46E-05	70.00	2.56E-05	47.34	3.79E-05	22.03	6.93E-05	-42.44
348.15	9.08E-05	2.89E-05	68.21	4.93E-05	45.69	7.16E-05	21.15	1.27E-04	-40.03
358.15	1.64E-04	5.49E-05	66.42	9.15E-05	44.09	1.30E-04	20.29	2.26E-04	-37.84
368.14	2.85E-04	1.01E-04	64.65	1.64E-04	42.53	2.30E-04	19.47	3.88E-04	-35.84
378.14	4.83E-04	1.79E-04	62.90	2.85E-04	41.02	3.93E-04	18.67	6.47E-04	-34.00
388.14	7.95E-04	3.09E-04	61.17	4.80E-04	39.56	6.53E-04	17.89	1.05E-04	-32.33
398.14	1.28E-03	5.17E-04	59.45	7.89E-04	38.14	0.00106	17.14	0.00167	-30.78
408.14	2.00E-03	8.44E-04	57.77	0.00126	36.76	0.00167	16.42	0.00258	-29.36
418.14	3.06E-03	1.34E-03	56.10	0.00198	35.43	0.00258	15.71	0.00392	-28.05
428.14	4.60E-03	2.09E-03	54.47	0.00303	34.14	0.00390	15.03	0.00583	-26.83
438.14	6.78E-03	3.20E-03	52.86	0.00455	32.89	0.00580	14.37	0.00852	-25.70
448.14	0.0098	4.78E-03	51.28	0.00670	31.68	0.00846	13.74	0.0122	-24.65
458.14	0.0140	7.02E-03	49.72	0.00971	30.51	0.0121	13.12	0.0173	-23.66
468.14	0.0196	1.01E-02	48.20	0.0138	29.37	0.0171	12.53	0.0240	-22.75
478.14	0.0271	1.44E-02	46.71	0.0194	28.27	0.0238	11.95	0.0330	-21.89
488.14	0.0369	2.02E-02	45.26	0.0269	27.21	0.0327	11.39	0.0447	-21.08
498.14	0.0497	2.79E-02	43.83	0.0367	26.18	0.0443	10.86	0.0598	-20.32
508.14	0.0660	3.80E-02	42.43	0.0494	25.19	0.0592	10.34	0.0790	-19.61
518.14	0.0869	5.12E-02	41.07	0.0658	24.23	0.0783	9.84	0.103	-18.93
528.14	0.1130	6.81E-02	39.74	0.0867	23.30	0.102	9.35	0.134	-18.29
538.14	0.1456	8.96E-02	38.44	0.113	22.41	0.133	8.89	0.171	-17.69
548.14	0.1857	1.17E-01	37.18	0.146	21.54	0.170	8.44	0.218	-17.11
558.14	0.2349	1.50E-01	35.94	0.186	20.71	0.216	8.01	0.274	-16.57
568.14	0.2946	1.92E-01	34.74	0.236	19.90	0.272	7.59	0.342	-16.04

Continuation of table A2									
578.14	0.3664	2.43E-01	33.57	0.296	19.12	0.340	7.19	0.423	-15.55
588.14	0.452	3.06E-01	32.43	0.369	18.37	0.422	6.81	0.521	-15.07
598.14	0.555	3.81E-01	31.32	0.457	17.65	0.519	6.44	0.636	-14.62
608.14	0.675	4.71E-01	30.23	0.561	16.95	0.634	6.08	0.771	-14.19
618.14	0.816	5.78E-01	29.18	0.684	16.27	0.770	5.74	0.929	-13.77
628.14	0.981	7.05E-01	28.16	0.828	15.62	0.928	5.41	1.113	-13.37
638.14	1.173	8.54E-01	27.17	0.997	15.00	1.113	5.10	1.325	-12.98
648.14	1.393	1.028	26.21	1.193	14.39	1.327	4.79	1.569	-12.61
658.14	1.647	1.231	25.27	1.419	13.81	1.573	4.50	1.849	-12.26
668.14	1.937	1.465	24.36	1.680	13.25	1.855	4.22	2.167	-11.91
678.14	2.266	1.734	23.47	1.978	12.71	2.177	3.95	2.528	-11.58
688.14	2.639	2.043	22.62	2.318	12.19	2.542	3.69	2.937	-11.26
698.14	3.0606	2.394	21.78	2.703	11.69	2.955	3.44	3.396	-10.95
708.14	3.534	2.793	20.98	3.138	11.21	3.421	3.21	3.911	-10.65
718.14	4.0641	3.243	20.19	3.627	10.74	3.943	2.98	4.485	-10.36
728.14	4.6555	3.751	19.43	4.176	10.29	4.527	2.76	5.125	-10.08
738.14	5.313	4.320	18.69	4.789	9.86	5.178	2.54	5.834	-9.81
748.14	6.0418	4.956	17.97	5.471	9.45	5.900	2.34	6.619	-9.55
758.14	6.847	5.664	17.28	6.228	9.04	6.700	2.15	7.484	-9.30
768.14	7.734	6.450	16.60	7.0645	8.66	7.583	1.96	8.434	-9.05
778.14	8.709	7.320	15.95	7.987	8.29	8.554	1.78	9.476	-8.81
788.14	9.776	8.279	15.31	9.001	7.93	9.619	1.60	10.615	-8.58
798.14	10.942	9.334	14.70	10.113	7.58	10.785	1.43	11.857	-8.36
808.14	12.214	10.491	14.10	11.384	7.25	12.058	1.27	13.208	-8.14
818.14	13.596	11.758	13.52	12.654	6.92	13.444	1.12	14.674	-7.93
828.14	15.0949	13.139	12.96	14.097	6.61	14.949	0.96	16.261	-7.72
838.14	16.718	14.643	12.41	15.662	6.32	16.581	0.82	17.976	-7.53
848.14	18.471	16.276	11.88	17.357	6.03	18.345	0.68	19.825	-7.33
858.14	20.360	18.046	11.36	19.189	5.75	20.249	0.54	21.815	-7.15
868.14	22.392	19.959	10.86	21.165	5.48	22.300	0.41	23.951	-6.96
878.14	24.574	22.0236	10.38	23.291	5.22	24.504	0.28	26.242	-6.79
888.14	26.913	24.247	9.91	25.576	4.97	26.870	0.16	28.694	-6.62
898.14	29.416	26.636	9.45	28.025	4.73	29.403	0.04	31.313	-6.45
908.14	32.0883	29.198	9.01	30.646	4.50	32.112	-0.07	34.106	-6.29
918.14	34.939	31.943	8.58	33.447	4.27	35.003	-0.18	37.081	-6.13
928.14	37.974	34.876	8.16	36.435	4.05	38.085	-0.29	40.244	-5.98
938.14	41.200	38.007	7.75	39.617	3.84	41.364	-0.40	43.602	-5.83
948.14	44.625	41.344	7.35	43.001	3.64	44.848	-0.50	47.163	-5.69
958.14	48.257	44.893	6.97	46.594	3.45	48.546	-0.60	50.933	-5.55
968.14	52.101	48.664	6.60	50.404	3.26	52.463	-0.70	54.920	-5.41
978.14	56.166	52.664	6.23	54.439	3.07	56.609	-0.79	59.130	-5.28
988.14	60.459	56.902	5.88	58.706	2.90	60.990	-0.88	63.571	-5.15
998.14	64.986	61.386	5.54	63.212	2.73	65.615	-0.97	68.250	-5.02

Continuation of table A2									
1008.14	69.756	66.123	5.21	67.966	2.57	70.492	-1.05	73.174	-4.90
1018.14	74.776	71.123	4.89	72.975	2.41	75.627	-1.14	78.350	-4.78
1028.14	80.0533	76.3923	4.57	78.246	2.26	81.0288	-1.22	83.786	-4.66
1038.14	85.595	81.942	4.27	83.788	2.11	86.705	-1.30	89.488	-4.55
1048.14	91.408	87.777	3.97	89.607	1.97	92.664	-1.37	95.464	-4.44
1058.14	97.501	93.908	3.69	95.712	1.83	98.913	-1.45	101.721	-4.33
1068.14	103.881	100.342	3.41	102.110	1.70	105.460	-1.52	108.266	-4.22
1078.14	110.555	107.087	3.14	108.808	1.58	112.313	-1.59	115.107	-4.12
1088.14	117.530	114.152	2.87	115.816	1.46	119.480	-1.66	122.249	-4.02
1098.14	124.815	121.545	2.62	123.138	1.34	126.967	-1.72	129.702	-3.91
1108.14	132.417	129.275	2.37	130.784	1.23	134.784	-1.79	137.470	-3.82
1118.14	140.342	137.348	2.13	138.760	1.13	142.938	-1.85	145.563	-3.72
1128.14	148.600	145.774	1.90	147.074	1.03	151.437	-1.91	153.985	-3.62
1138.14	157.196	154.560	1.68	155.734	0.93	160.288	-1.97	162.746	-3.53
1148.14	166.139	163.714	1.46	164.747	0.84	169.499	-2.02	171.852	-3.44
1158.14	175.437	173.245	1.25	174.119	0.75	179.0785	-2.08	181.309	-3.35
1168.14	185.0960	183.161	1.05	183.860	0.67	189.0334	-2.13	191.125	-3.26
1178.14	195.125	193.468	0.85	193.975	0.59	199.372	-2.18	201.306	-3.17
1188.14	205.531	204.177	0.66	204.471	0.52	210.101	-2.22	211.860	-3.08
1198.14	216.321	215.293	0.48	215.357	0.45	221.229	-2.27	222.794	-2.99
1208.14	227.505	226.825	0.30	226.639	0.38	232.764	-2.31	234.114	-2.91
1218.14	239.0879	238.782	0.13	238.324	0.32	244.712	-2.35	245.827	-2.82
1228.14	251.0791	251.169	-0.04	250.420	0.26	257.0821	-2.39	257.940	-2.73
1238.14	263.486	263.996	-0.19	262.932	0.21	269.881	-2.43	270.460	-2.65
1248.14	276.317	277.270	-0.35	275.869	0.16	283.117	-2.46	283.394	-2.56
1258.14	289.579	290.999	-0.49	289.237	0.12	296.798	-2.49	296.748	-2.48
1268.14	303.280	305.189	-0.63	303.042	0.08	310.930	-2.52	310.529	-2.39
1278.14	317.429	319.849	-0.76	317.292	0.04	325.522	-2.55	324.744	-2.30
1288.14	332.033	334.986	-0.89	331.993	0.01	340.580	-2.57	339.399	-2.22
1298.14	347.101	350.607	-1.01	347.152	-0.01	356.113	-2.60	354.502	-2.13
1308.14	362.641	366.720	-1.12	362.776	-0.04	372.128	-2.62	370.058	-2.05
1318.14	378.660	383.332	-1.23	378.871	-0.06	388.633	-2.63	386.074	-1.96
1328.14	395.168	400.450	-1.34	395.443	-0.07	405.634	-2.65	402.558	-1.87
1338.14	412.172	418.081	-1.43	412.499	-0.08	423.139	-2.66	419.515	-1.78
1348.14	429.681	436.234	-1.52	430.046	-0.08	441.156	-2.67	436.952	-1.69
1358.14	447.704	454.914	-1.61	448.089	-0.09	459.692	-2.68	454.876	-1.60
1368.14	466.250	474.129	-1.69	466.636	-0.08	478.754	-2.68	473.292	-1.51
1378.14	485.326	493.885	-1.76	485.691	-0.08	498.350	-2.68	492.209	-1.42
1388.14	504.943	514.191	-1.83	505.263	-0.06	518.487	-2.68	511.631	-1.32
1398.14	525.108	535.052	-1.89	525.356	-0.05	539.173	-2.68	531.566	-1.23
1408.14	545.831	556.475	-1.95	545.976	-0.03	560.414	-2.67	552.019	-1.13
1418.14	567.122	578.468	-2.00	567.131	0.00	582.219	-2.66	572.998	-1.04
1428.14	588.989	601.037	-2.05	588.825	0.03	604.594	-2.65	594.509	-0.94

Continuation of table A2									
1438.14	611.441	624.189	-2.08	611.065	0.06	627.548	-2.63	616.558	-0.84
1448.14	634.489	647.930	-2.12	633.857	0.10	651.086	-2.62	639.152	-0.73
1458.14	658.143	672.267	-2.15	657.206	0.14	675.217	-2.59	662.296	-0.63
1468.14	682.411	697.207	-2.17	681.119	0.19	699.948	-2.57	685.998	-0.53
1478.14	707.305	722.755	-2.18	705.601	0.24	725.286	-2.54	710.264	-0.42
1488.14	732.833	748.920	-2.20	730.657	0.30	751.239	-2.51	735.099	-0.31
1498.14	759.007	775.706	-2.20	756.294	0.36	777.813	-2.48	760.511	-0.20
1508.14	785.837	803.121	-2.20	782.516	0.42	805.017	-2.44	786.505	-0.09
1518.14	813.334	831.170	-2.19	809.331	0.49	832.858	-2.40	813.089	0.03
1528.14	841.508	859.861	-2.18	836.742	0.57	861.342	-2.36	840.267	0.15
1538.14	870.370	889.198	-2.16	864.756	0.64	890.477	-2.31	868.048	0.27
1548.14	899.932	919.189	-2.14	893.379	0.73	920.272	-2.26	896.436	0.39
1558.14	930.206	949.840	-2.11	922.615	0.82	950.732	-2.21	925.439	0.51
1568.14	961.201	981.157	-2.08	952.469	0.91	981.866	-2.15	955.063	0.64
1578.14	992.932	1013.145	-2.04	982.947	1.01	1013.681	-2.09	985.313	0.77
1588.14	1025.408	1045.811	-1.99	1014.055	1.11	1046.184	-2.03	1016.197	0.90
1598.14	1058.644	1079.161	-1.94	1045.798	1.21	1079.383	-1.96	1047.721	1.03
1608.14	1092.651	1113.201	-1.88	1078.180	1.32	1113.285	-1.89	1079.890	1.17
1618.14	1127.441	1147.937	-1.82	1111.207	1.44	1147.898	-1.81	1112.712	1.31
1628.14	1163.029	1183.374	-1.75	1144.885	1.56	1183.229	-1.74	1146.193	1.45
1638.14	1199.4262	1219.519	-1.68	1179.217	1.68	1219.287	-1.66	1180.340	1.59
1648.14	1236.647	1256.377	-1.60	1214.210	1.81	1256.077	-1.57	1215.157	1.74
1658.14	1274.701	1293.954	-1.51	1249.868	1.95	1293.609	-1.48	1250.653	1.89
1668.14	1313.615	1332.256	-1.42	1286.196	2.09	1331.890	-1.39	1286.833	2.04
1678.14	1353.390	1371.288	-1.32	1323.199	2.23	1370.926	-1.30	1323.705	2.19
1688.14	1394.0452	1411.057	-1.22	1360.883	2.38	1410.727	-1.20	1361.274	2.35
1698.14	1435.595	1451.568	-1.11	1399.251	2.53	1451.300	-1.09	1399.546	2.51
1708.14	1478.055	-	-	1438.308	2.69	-	-	1438.529	2.67
1718.14	1521.440	-	-	1478.061	2.85	-	-	1478.229	2.84
1728.14	1565.767	-	-	-	-	-	-	-	-
1734.14	1592.822	-	-	-		-	-	-	-

Appendix B

Table B1: Vapor pressures calculated using PR-MC from Neqsim tool and their deviations from the vapor pressures of DIPPR's equation

$$\Delta P^s\ \% = \frac{(Pexp - Pcalc) * 100}{Pexp} \quad \text{(eq. B1)}$$

As experimental values are considered the P^s calculated from DIPPR's equation

	DIPPR's eq.	PR-MC	
T [K]	**P^s [bar]**	**P^s [bar]**	**ΔP^s %**
238.15	4.90E-09	4.86E-09	0.86
248.15	1.73E-08	1.72E-08	0.72
258.15	5.52E-08	5.49E-08	0.62
268.15	1.62E-07	1.61E-07	0.53
278.15	4.37E-07	4.35E-07	0.47
288.15	1.10E-06	1.10E-06	0.41
298.15	2.61E-06	2.60E-06	0.37
308.15	5.82E-06	5.81E-06	0.33
318.15	1.24E-05	1.23E-05	0.30
328.15	2.51E-05	2.50E-05	0.28
338.15	4.86E-05	4.85E-05	0.25
348.15	9.08E-05	9.06E-05	0.23
358.15	1.64E-04	1.63E-04	0.21
368.15	2.85E-04	2.85E-04	0.19
378.15	4.83E-04	4.82E-04	0.17
388.15	7.95E-04	7.94E-04	0.15
398.15	1.28E-03	0.00127	0.14
408.15	2.00E-03	0.00199	0.12
418.15	3.06E-03	0.00306	0.10
428.15	4.60E-03	0.00459	0.09
438.15	6.78E-03	0.00677	0.07
448.15	0.0098	0.0098	0.06
458.15	0.014	0.014	0.04
468.15	0.019	0.019	0.03
478.15	0.027	0.027	0.02
488.15	0.036	0.036	0.01
498.15	0.0497	0.0497	0.00
508.15	0.066	0.066	-0.01
518.15	0.087	0.087	-0.02
528.15	0.113	0.113	-0.02
538.15	0.146	0.146	-0.03
548.15	0.186	0.186	-0.03
558.15	0.235	0.235	-0.03
568.15	0.295	0.295	-0.03
578.15	0.366	0.366	-0.03

Continuation of table B1			
588.15	0.452	0.452	-0.03
598.15	0.555	0.555	-0.02
608.15	0.675	0.675	-0.02
618.15	0.816	0.816	-0.01
628.15	0.981	0.981	0.00
638.15	1.173	1.173	0.01
648.15	1.393	1.393	0.02
658.15	1.647	1.646	0.03
668.15	1.936	1.936	0.04
678.15	2.266	2.265	0.05
688.15	2.639	2.638	0.07
698.15	3.061	3.058	0.08
708.15	3.534	3.531	0.09
718.15	4.064	4.060	0.11
728.15	4.655	4.650	0.12
738.15	5.313	5.306	0.13
748.15	6.041	6.033	0.14
758.15	6.847	6.836	0.16
768.15	7.734	7.721	0.17
778.15	8.709	8.693	0.18
788.15	9.776	9.758	0.19
798.15	10.942	10.921	0.20
808.15	12.214	12.188	0.21
818.15	13.595	13.567	0.21
828.15	15.094	15.062	0.22
838.15	16.717	16.680	0.22
848.15	18.470	18.428	0.23
858.15	20.359	20.313	0.23
868.15	22.392	22.340	0.23
878.15	24.574	24.517	0.23
888.15	26.913	26.851	0.23
898.15	29.415	29.348	0.23
908.15	32.088	32.016	0.22
918.15	34.938	34.862	0.22
928.15	37.973	37.893	0.21
938.15	41.199	41.116	0.20
948.15	44.625	44.539	0.19
958.15	48.256	48.168	0.18
968.15	52.101	52.013	0.17
978.15	56.165	56.078	0.16
988.15	60.458	60.374	0.14
998.15	64.986	64.906	0.12
1008.15	69.756	69.683	0.11
1018.15	74.776	74.712	0.09
1028.15	80.053	80.001	0.07

Continuation of table B1			
1038.15	85.595	85.557	0.04
1048.15	91.408	91.389	0.02
1058.15	97.501	97.504	0.00
1068.15	103.880	103.910	-0.03
1078.15	110.554	110.614	-0.05
1088.15	117.530	117.625	-0.08
1098.15	124.815	124.950	-0.11
1108.15	132.416	132.598	-0.14
1118.15	140.342	140.575	-0.17
1128.15	148.599	148.891	-0.20
1138.15	157.195	157.552	-0.23
1148.15	166.139	166.567	-0.26
1158.15	175.436	175.944	-0.29
1168.15	185.095	185.690	-0.32
1178.15	195.124	195.814	-0.35
1188.15	205.530	206.324	-0.39
1198.15	216.321	217.228	-0.42
1208.15	227.504	228.533	-0.45
1218.15	239.087	240.247	-0.48
1228.15	251.079	252.379	-0.52
1238.15	263.486	264.938	-0.55
1248.15	276.316	277.929	-0.58
1258.15	289.578	291.363	-0.62
1268.15	303.280	305.247	-0.65
1278.15	317.429	319.588	-0.68
1288.15	332.033	334.396	-0.71
1298.15	347.101	349.679	-0.74
1308.15	362.640	365.444	-0.77
1318.15	378.659	381.699	-0.80
1328.15	395.167	398.454	-0.83
1338.15	412.171	415.716	-0.86
1348.15	429.681	433.493	-0.89
1358.15	447.704	451.795	-0.91
1368.15	466.249	470.628	-0.94
1378.15	485.326	490.002	-0.96
1388.15	504.942	509.925	-0.99
1398.15	525.107	530.405	-1.01
1408.15	545.831	551.451	-1.03
1418.15	567.121	573.071	-1.05
1428.15	588.988	595.274	-1.07
1438.15	611.441	618.068	-1.08
1448.15	634.489	641.463	-1.10
1458.15	658.143	665.466	-1.11
1468.15	682.411	690.087	-1.12
1478.15	707.305	715.334	-1.14

Continuation of table B1			
1488.15	732.833	741.216	-1.14
1498.15	759.007	767.742	-1.15
1508.15	785.837	794.921	-1.16
1518.15	813.334	822.761	-1.16
1528.15	841.508	851.281	-1.16
1538.15	870.370	880.472	-1.16
1548.15	899.932	910.352	-1.16
1558.15	930.206	940.931	-1.15
1568.15	961.201	972.218	-1.15
1578.15	992.932	1004.221	-1.14
1588.15	1025.408	1036.952	-1.13
1598.15	1058.644	1070.418	-1.11
1608.15	1092.651	1104.630	-1.10
1618.15	1127.441	1139.598	-1.08
1628.15	1163.029	1175.331	-1.06
1638.15	1199.426	1211.839	-1.03
1648.15	1236.647	1249.132	-1.01
1658.15	1274.706	1287.220	-0.98
1668.15	1313.615	1326.114	-0.95
1678.15	1353.390	1365.824	-0.92
1688.15	1394.045	1406.360	-0.88
1698.15	1435.595	1447.732	-0.85
1708.15	1478.055	-	-
1718.15	1478.055	-	-

Table B2: Vapor pressures calculated using SRK-Twu from Neqsim tool and their deviations from the vapor pressures of DIPPR's equation

$$\Delta P^s\ \% = \frac{(Pexp - Pcalc)*100}{Pexp} \quad \text{(eq. B2)}$$

As experimental values are considered the P^s calculated from DIPPR's equation

	DIPPR's eq.	**SRK-Twu**	
T [K]	**P^s [bar]**	**P^s [bar]**	**ΔP^s %**
238.15	4.90E-09	4.71E-09	3.82%
248.15	1.73E-08	1.67E-08	3.11%
258.15	5.52E-08	5.38E-08	2.53%
268.15	1.62E-07	1.58E-07	2.05%
278.15	4.37E-07	4.30E-07	1.65%
288.15	1.10E-06	1.09E-06	1.32%
298.15	2.61E-06	2.58E-06	1.05%
308.15	5.82E-06	5.78E-06	0.82%
318.15	1.24E-05	1.23E-05	0.63%
328.15	2.51E-05	2.49E-05	0.48%

Continuation of table B2			
338.15	4.86E-05	4.85E-05	0.35%
348.15	9.08E-05	9.06E-05	0.25%
358.15	1.64E-04	1.63E-04	0.16%
368.15	2.85E-04	2.85E-04	0.09%
378.15	4.83E-04	4.83E-04	0.03%
388.15	7.95E-04	7.95E-04	0.02%
398.15	1.28E-03	1.28E-03	0.06%
408.15	2.00E-03	2.00E-03	0.09%
418.15	3.06E-03	3.07E-03	0.11%
428.15	4.60E-03	4.61E-03	0.13%
438.15	6.78E-03	6.79E-03	0.15%
448.15	0.0098	9.83E-03	0.16%
458.15	0.014	1.40E-02	0.17%
468.15	0.019	1.96E-02	0.17%
478.15	0.027	2.71E-02	0.17%
488.15	0.036	3.70E-02	0.17%
498.15	0.0497	4.97E-02	0.17%
508.15	0.066	6.62E-02	0.16%
518.15	0.087	8.70E-02	0.16%
528.15	0.113	0.113	0.15%
538.15	0.146	0.146	0.14%
548.15	0.186	0.186	0.13%
558.15	0.235	0.235	0.11%
568.15	0.295	0.295	0.10%
578.15	0.366	0.367	0.08%
588.15	0.452	0.453	0.07%
598.15	0.555	0.555	0.05%
608.15	0.675	0.675	0.04%
618.15	0.816	0.817	0.02%
628.15	0.981	0.981	0.00%
638.15	1.173	1.172	0.02%
648.15	1.393	1.393	0.04%
658.15	1.647	1.646	0.05%
668.15	1.936	1.935	0.07%
678.15	2.266	2.264	0.09%
688.15	2.639	2.637	0.11%
698.15	3.061	3.057	0.13%
708.15	3.534	3.529	0.14%
718.15	4.064	4.058	0.16%
728.15	4.655	4.647	0.18%
738.15	5.313	5.303	0.19%
748.15	6.041	6.030	0.20%
758.15	6.847	6.832	0.22%
768.15	7.734	7.717	0.23%
778.15	8.709	8.688	0.24%

Continuation of table B2			
788.15	9.776	9.752	0.25%
798.15	10.942	10.914	0.26%
808.15	12.214	12.182	0.26%
818.15	13.595	13.559	0.27%
828.15	15.094	15.054	0.27%
838.15	16.717	16.672	0.27%
848.15	18.470	18.420	0.27%
858.15	20.359	20.305	0.27%
868.15	22.392	22.332	0.27%
878.15	24.574	24.510	0.26%
888.15	26.913	26.845	0.25%
898.15	29.415	29.343	0.25%
908.15	32.088	32.013	0.24%
918.15	34.938	34.860	0.22%
928.15	37.973	37.893	0.21%
938.15	41.199	41.119	0.20%
948.15	44.625	44.545	0.18%
958.15	48.256	48.179	0.16%
968.15	52.101	52.027	0.14%
978.15	56.165	56.098	0.12%
988.15	60.458	60.400	0.10%
998.15	64.986	64.939	0.07%
1008.15	69.756	69.723	0.05%
1018.15	74.776	74.761	0.02%
1028.15	80.053	80.059	0.01%
1038.15	85.595	85.627	0.04%
1048.15	91.408	91.470	0.07%
1058.15	97.501	97.598	0.10%
1068.15	103.880	104.018	0.13%
1078.15	110.554	110.738	0.17%
1088.15	117.530	117.766	0.20%
1098.15	124.815	125.110	0.24%
1108.15	132.416	132.777	0.27%
1118.15	140.342	140.776	0.31%
1128.15	148.599	149.114	0.35%
1138.15	157.195	157.800	0.38%
1148.15	166.139	166.841	0.42%
1158.15	175.436	176.246	0.46%
1168.15	185.095	186.022	0.50%
1178.15	195.124	196.177	0.54%
1188.15	205.530	206.720	0.58%
1198.15	216.321	217.658	0.62%
1208.15	227.504	229.000	0.66%
1218.15	239.087	240.753	0.70%
1228.15	251.079	252.925	0.74%

Continuation of table B2			
1238.15	263.486	265.525	0.77%
1248.15	276.316	278.561	0.81%
1258.15	289.578	292.040	0.85%
1268.15	303.280	305.970	0.89%
1278.15	317.429	320.361	0.92%
1288.15	332.033	335.219	0.96%
1298.15	347.101	350.553	0.99%
1308.15	362.640	366.370	1.03%
1318.15	378.659	382.680	1.06%
1328.15	395.167	399.490	1.09%
1338.15	412.171	416.808	1.12%
1348.15	429.681	434.642	1.15%
1358.15	447.704	453.001	1.18%
1368.15	466.249	471.893	1.21%
1378.15	485.326	491.325	1.24%
1388.15	504.942	511.306	1.26%
1398.15	525.107	531.844	1.28%
1408.15	545.831	552.948	1.30%
1418.15	567.121	574.625	1.32%
1428.15	588.988	596.884	1.34%
1438.15	611.441	619.732	1.36%
1448.15	634.489	643.180	1.37%
1458.15	658.143	667.233	1.38%
1468.15	682.411	691.902	1.39%
1478.15	707.305	717.193	1.40%
1488.15	732.833	743.117	1.40%
1498.15	759.007	769.680	1.41%
1508.15	785.837	796.891	1.41%
1518.15	813.334	824.767	1.41%
1528.15	841.508	853.301	1.40%
1538.15	870.370	882.508	1.39%
1548.15	899.932	912.397	1.39%
1558.15	930.206	942.976	1.37%
1568.15	961.201	974.255	1.36%
1578.15	992.932	1006.242	1.34%
1588.15	1025.408	1038.945	1.32%
1598.15	1058.644	1072.373	1.30%
1608.15	1092.651	1106.535	1.27%
1618.15	1127.441	1141.440	1.24%
1628.15	1163.029	1177.096	1.21%
1638.15	1199.426	1213.512	1.17%
1648.15	1236.647	1250.697	1.14%
1658.15	1274.706	1288.659	1.09%
1668.15	1313.615	1327.409	1.05%
1678.15	1353.390	1366.954	1.00%

Continuation of table B2			
1688.15	1394.045	1407.304	0.95%
1698.15	1435.595	1448.467	0.90%
1708.15	1478.055	-	-
1718.15	1478.055	-	-

Appendix C

Table C1: Available solubility data of Hg in HC from IUPAC's book

Solvent	T [K]	Mole fraction of Hg (exp)
$n.C_5$	278.15	1.90E-07
	283.15	2.70E-07
	288.15	3.60E-07
	293.15	4.60E-07
	298.15	6.80E-07
	303.15	9.30E-07
	308.15	1.20E-06
$n.C_6$	313.15	1.60E-06
	273.15	1.80E-07
	278.15	2.40E-07
	283.15	3.40E-07
	288.15	4.60E-07
	293.15	5.90E-07
	298.15	8.30E-07
	303.15	1.10E-06
	308.15	1.42E-06
	313.15	1.90E-06
	318.15	2.38E-06
	323.15	3.03E-06
	328.15	3.84E-06
	333.15	4.83E-06
	338.15	6.03E-06
$n.C_7$	273.15	2.00E-07
	278.15	2.90E-07
	283.15	3.70E-07
	288.15	5.40E-07
	293.15	7.00E-07
	298.15	9.70E-07
	303.15	1.26E-06
	308.15	1.63E-06
	313.15	2.20E-06
$n.C_8$	273.15	2.50E-07
	278.15	3.30E-07
	283.15	4.70E-07
	288.15	6.10E-07
	293.15	7.90E-07
	298.15	1.10E-06
	303.15	1.40E-06

Continuation of table C1		
n.C_8	308.15	1.78E-06
	313.15	2.30E-06
n.C_{10}	273.15	4.00E-07
	278.15	4.90E-07
	283.15	5.80E-07
	288.15	8.70E-07
	293.15	9.60E-07
	298.15	1.37E-06
	303.15	1.69E-06
	308.15	1.90E-06
	313.15	2.52E-06
	318.15	2.66E-06
2.2-dm-C_4	273.15	1.70E-07
	288.15	3.70E-07
	293.15	4.90E-07
	298.15	6.70E-07
	303.15	8.10E-07
	308.15	9.90E-07
2.2.4-tm-C_5	273.15	1.60E-07
	286.65	3.40E-07
	288.15	3.60E-07
	293.15	5.40E-07
	298.15	7.00E-07
	303.15	8.90E-07
	308.15	1.11E-06
cy-C_6	288.15	8.20E-07
	293.15	1.02E-06
	298.15	1.32E-06
	303.15	1.62E-06
	308.15	1.92E-06
	313.15	2.47E-06
m-cy-C_6	273.15	2.70E-07
	288.15	6.60E-07
	293.15	8.80E-07
	298.15	1.17E-06
	303.15	1.46E-06
	308.15	1.88E-06

Continuation of table C1		
cis-1.2-dm-cy-C_6	289.15	8.10E-07
	293.15	1.06E-06
	298.15	1.36E-06
	303.15	1.71E-06
	308.15	2.06E-06
trans-1.2-dm-cy-C_6	288.15	6.90E-07
	293.15	9.10E-07
	298.15	1.23E-06
	303.15	1.55E-06
	308.15	1.85E-06
cis-1.4-dm-cy-C_6	288.15	7.40E-07
	293.15	1.02E-06
	298.15	1.33E-06
	303.15	1.64E-06
	308.15	2.11E-06
trans-1.4-dm-cy-C_6	288.15	6.90E-07
	293.15	9.10E-07
	298.15	1.22E-06
	303.15	1.55E-06
	308.15	1.86E-06
benzene	288.15	5.80E-07
	293.15	7.90E-07
	295.65	9.27E-07
	298.15	1.06E-06
	303.15	1.37E-06
	308.15	1.91E-06
toluene	273.15	3.20E-07
	288.15	6.90E-07
	293.15	1.03E-06
	298.15	1.28E-06
	303.15	1.73E-06
	308.15	2.14E-06
o-xylene	273.15	3.10E-07
	293.15	1.12E-06
	298.15	1.45E-06
	303.15	1.89E-06
	308.15	2.62E-06

Table C2: Available solubility data of Hg in n.propane and n.butane from IUPAC's book that were not used in the master thesis

	T[K]	P[atm]	Mole fraction of Hg (exp)
C_3	457.15	9.8	0.00140
	457.15	18.9	0.000747
	491.15	10.6	0.00384
	491.15	20.6	0.00204
	491.15	29.4	0.00143
	529.15	11.6	0.0100
	529.15	22.5	0.00527
	529.15	32.5	0.00369
$n.C_4$	457.15	9.6	0.00143
	457.15	17.8	0.000778
	457.15	24.1	0.000571
	491.15	10.5	0.00391
	491.15	19.6	0.00211
	491.15	27.2	0.00153
	529.15	11.5	0.0103
	529.15	21.9	0.00549
	529.15	30.6	0.00390

Table C3: Raw data for $n.C_8$, $cy\text{-}C_6$, benzene and toluene

	HC	T[K]	µmole/L (raw data)	Mole fraction of Hg (exp)
Robert R. Kuntz and Gilbert J. Mains	$n.C_6$	298.15	6.4	8.41E-07
		313.15	13.5	1.81E-06
		336.15	50.8	7.06E-06
	$cy\text{-}C_6$	298.15	11	1.20E-06
	toluene	298.15	12.5	1.33E-06
	benzene	298.15	12	1.074E-06

Table C4: Raw data for $n.C_8$ and toluene

	HC	T[K]	ppm (1000µg/kg) (raw data)	Mole fraction of Hg (exp)
M. M. MIEDANER, A. A. MIGDISOV, and A. E. WILLIAMS-JONES	$n.C_8$	383.15	54.2	3.09E-05
		423.15	184	1.10E-04
		473.15	821	4.70E-04

M. M. MIEDANER, A. A. MIGDISOV, and A. E. WILLIAMS-JONES	Continuation of table C4			
	toluene	393.15	14	6.43E-06
		423.15	75	3.45E-05
		443.15	111	5.10E-05
		473.15	280	1.30E-04

Table C5: Available solubility data of Hg in various HCs, CO_2 and N_2

Confidential data

Table C6: Available solubility data of Hg in iso-butane

Confidential data

Table C7: Available solubility data of Hg in H_2O from IUPAC's book

T [K]	P [bar]	Mole fraction of Hg (exp)
273.15	1	3.73E-09
278.15	1	3.91E-09
283.15	1	4.15E-09
288.15	1	4.46E-09
293.15	1	4.83E-09
298.15	1	5.28E-09
303.15	1	5.83E-09
308.15	1	6.48E-09
313.15	1	7.27E-09
318.15	1	8.20E-09
323.15	1	9.31E-09
328.15	1	1.06E-08
333.15	1	1.22E-08
338.15	1	1.41E-08
343.15	1	1.64E-08
348.15	1	1.91E-08
353.15	1	2.24E-08
358.15	1	2.63E-08
363.15	1	3.10E-08
373.15	1	4.36E-08
383.15	1	6.21E-08
393.15	1	8.91E-08

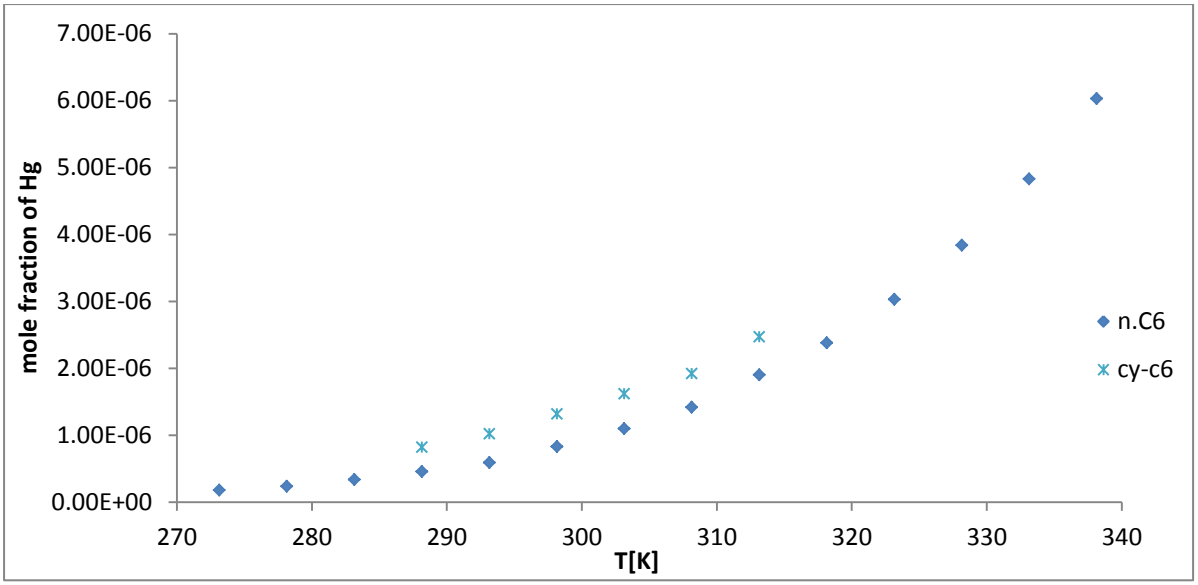

Figure C1: Solubility of Hg in cyclo and n.alkanes with carbon number 6

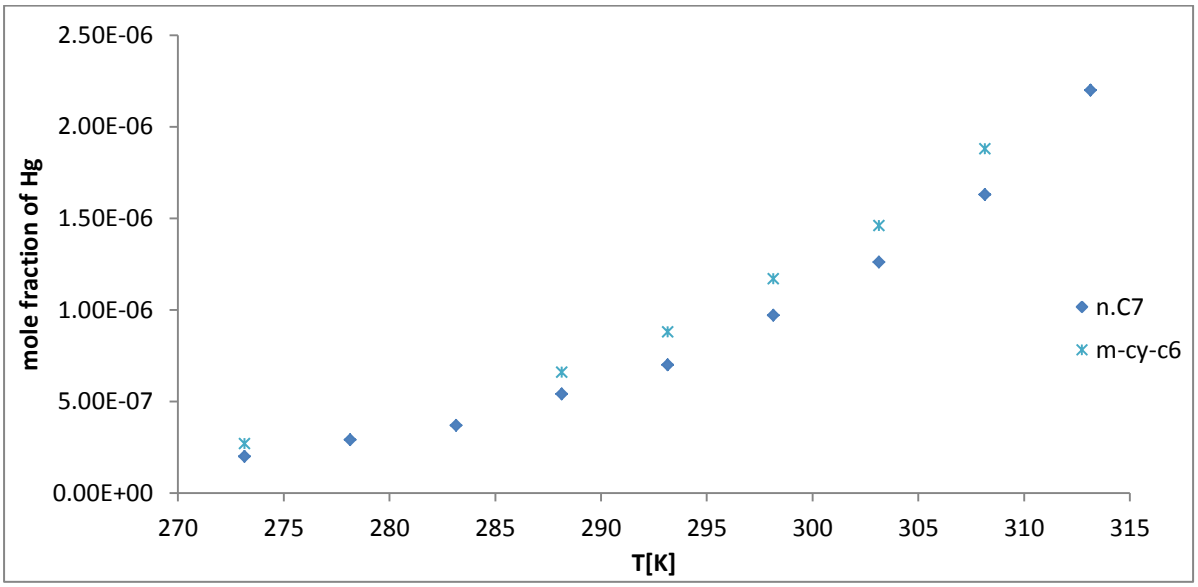

Figure C2: Solubility of Hg in cyclo and n.alkanes with carbon number 7

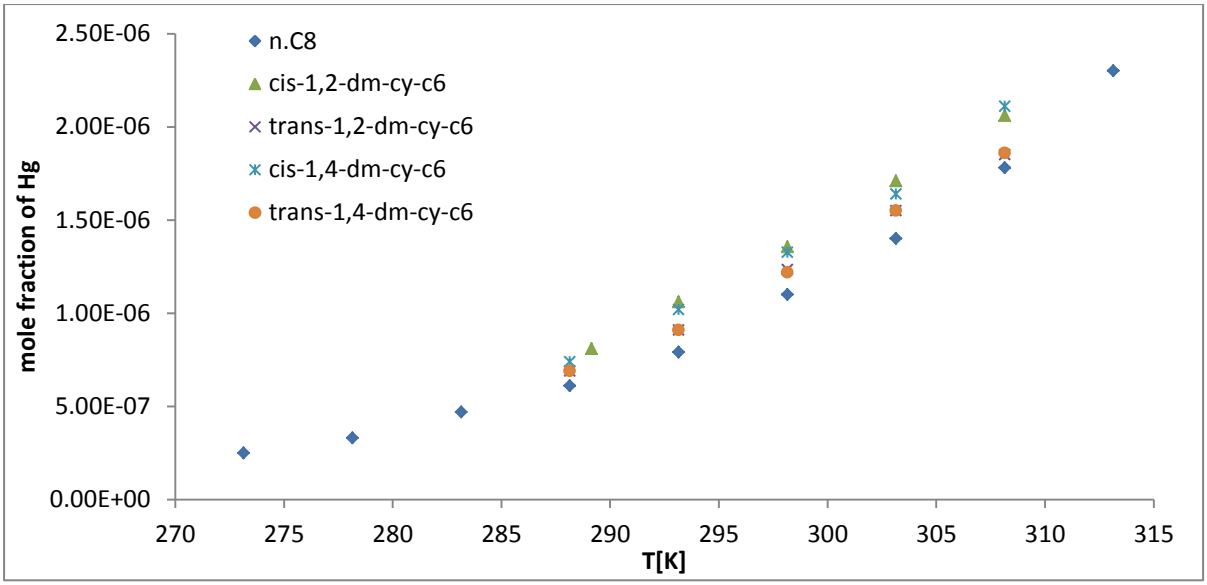

Figure C3: Solubility of Hg in cyclo and n.alkanes with carbon number 8

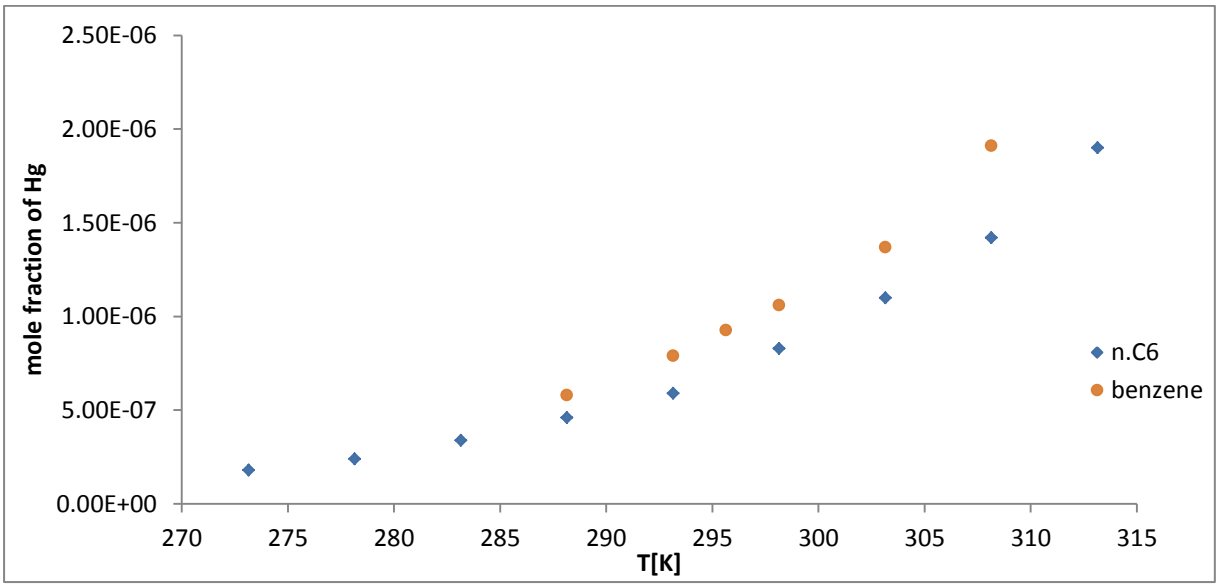

Figure C4: Solubility of Hg in aromatic HC and n.alkanes with carbon number 6

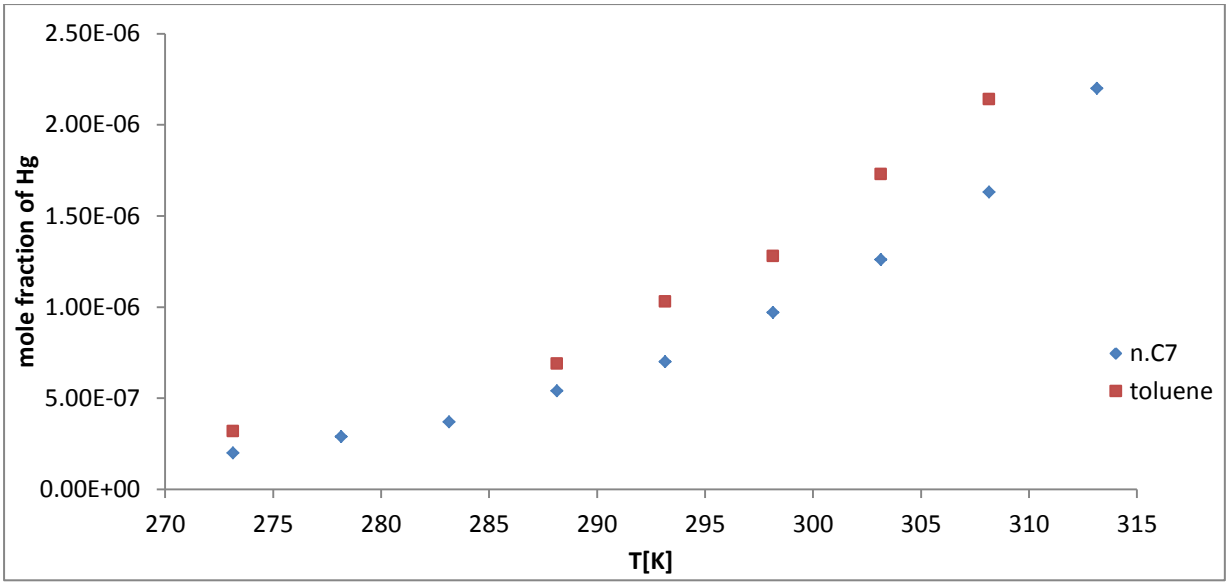

Figure C5: Solubility of Hg in aromatic HC and n.alkanes with carbon number 7

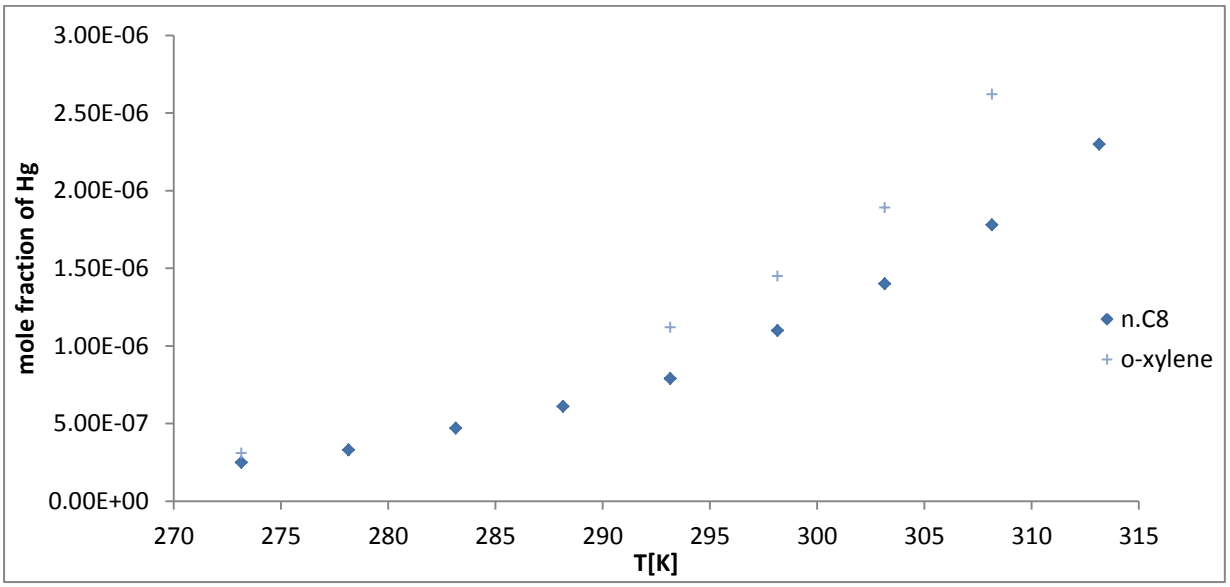

Figure C6: Solubility of Hg in aromatic HC and n.alkanes with carbon number 8

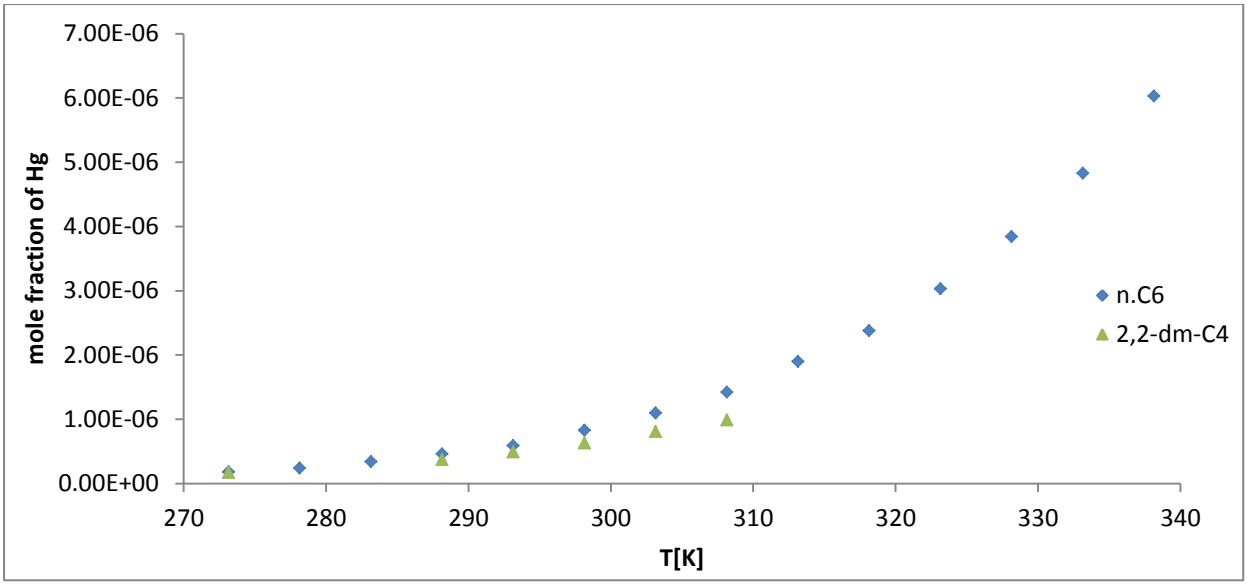

Figure C7: Solubility of Hg in branched and n.alkanes with carbon number 6

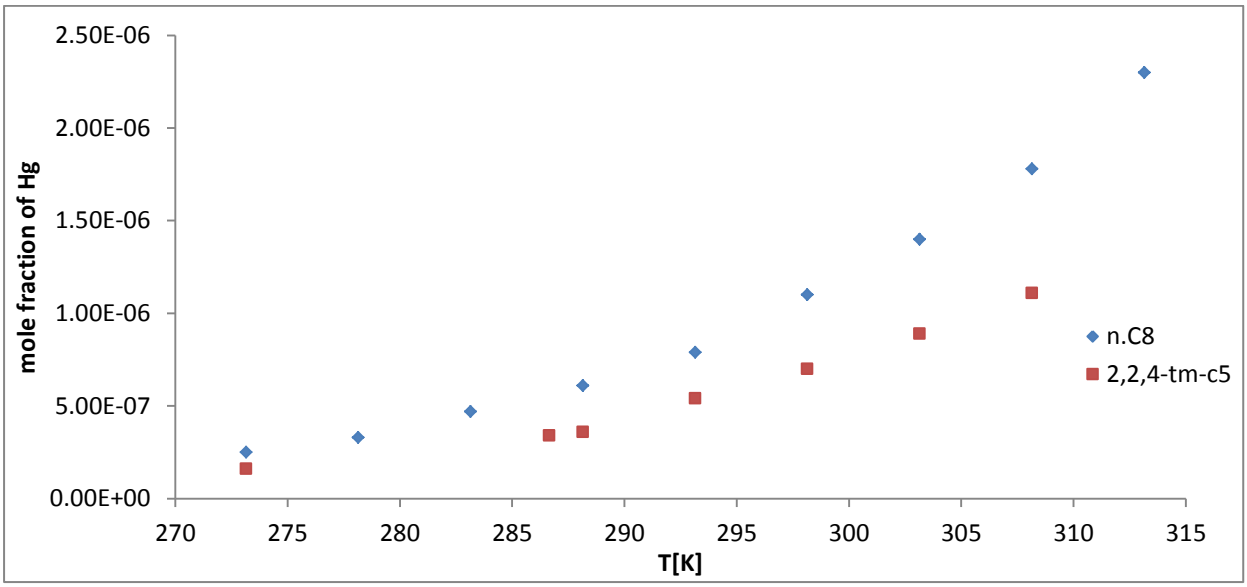

Figure C8: Solubility of Hg in branched and n.alkanes with carbon number 8

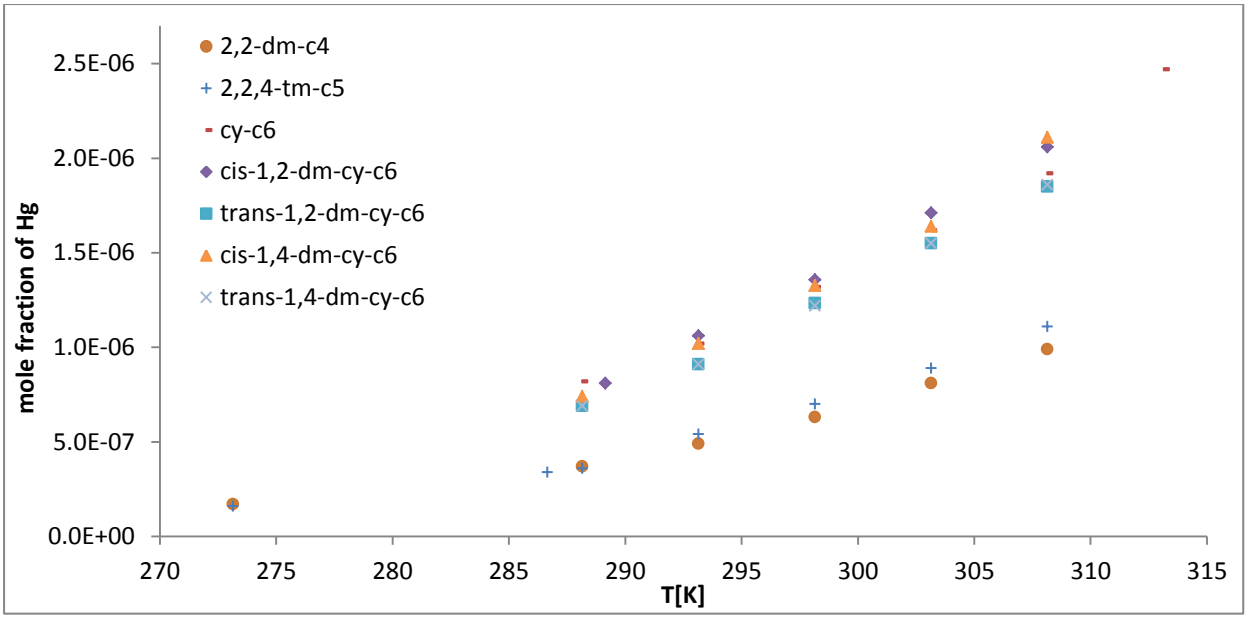

Figure C9: Solubility of Hg in branched and cyclo-alkanes

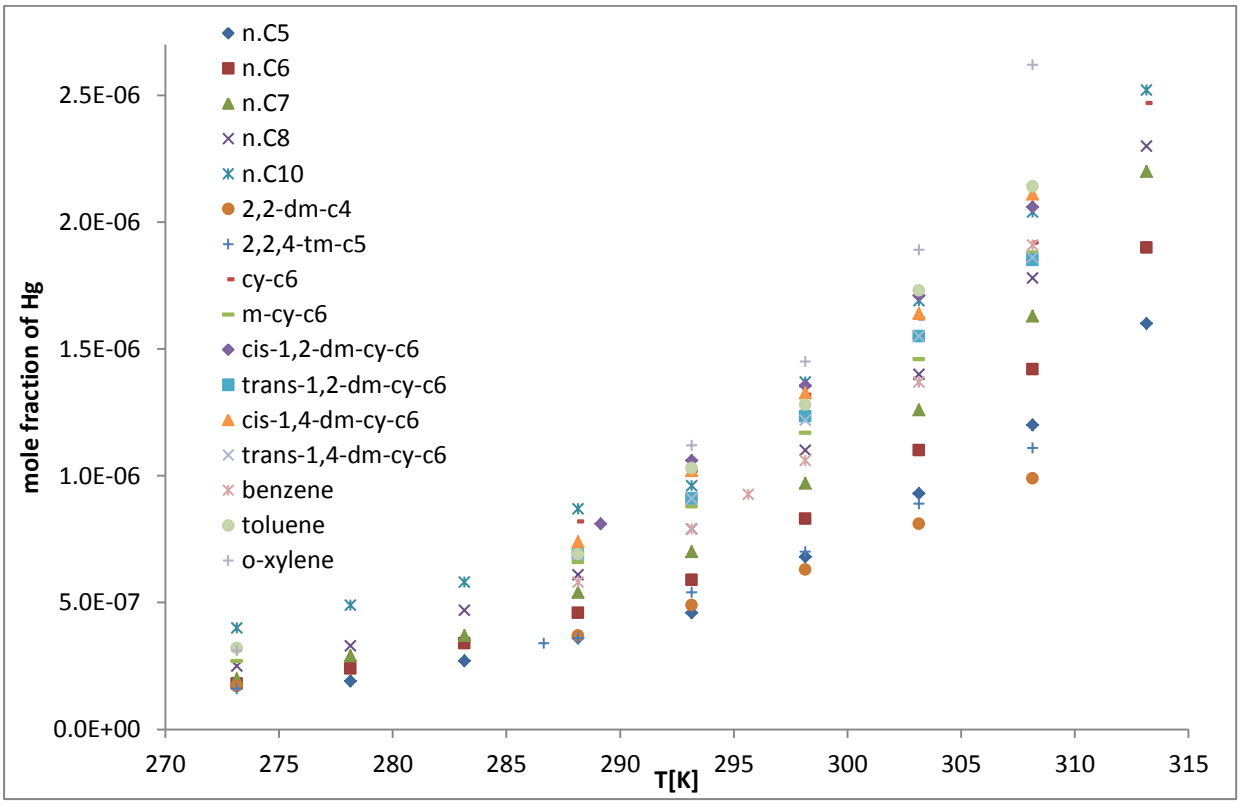

Figure C10: Solubility of Hg in all HC

Appendix D

Table D1: Twu-Coon parameters for all components

NAME	L	M	N
Hg	0.09245	0.9784	2.244
CH_4	0.5144	0.9903	1
C_2H_6	0.2424	0.88	1.9845
C_3	0.2349	0.8662	2.2076
i-C_4	0.2179	0.8489	2.2840
n.C_5	0.5316	0.87	1.481
n.C_6	0.1581	0.8728	3.8442
n.C_7	0.1648	0.8697	4.0451
n.C_8	0.23	0.8433	3.243
n.C_{10}	0.2028	0.8418	3.8472
benzene	0.103	0.8886	4.2837
toluene	0.3319	0.8432	2.0677
o-xylene	0.2561	0.8532	2.762
cy-C_6	0.0796	0.9161	6.0039
m-cy-C_6	0.1416	0.8755	3.6415
cis-1.2-dm-cy-C_6	0.0853	0.8909	4.9261
cis-1.4-dm-cy-C_6	0.0691	0.9052	5.9034
trans-1.2-dm-cy-C_6	0.106	0.8821	4.3185
trans-1.4-dm-cy-C_6	0.0977	0.8868	4.583
2.2-dim-C_4	0.3067	0.8562	2.1437
2.2.4-tm-C_5	0.2828	0.8453	2.4878
CO_2	1.4136	-0.6060	1.1018
N_2	0.1523	0.8945	2.3404
water	0.3533	0.8741	2.4996

Table D2: Mathias-Copeman parameters for all components

NAME	MC1	MC2	MC3
Hg	0.1491	-0.1652	0.1447
CH_4	0.3923	0	0
C_2H_6	0.5201	0.0043	0.1029
C_3	0.6184	-0.1607	0.4879
i-C_4	0.6562	-0.1387	0.5039
n.C_5	0.7506	-0.1073	0.3871
n.C_6	0.8347	-0.3180	1.0209
n.C_7	0.8648	0.0716	0.0669
n.C_8	0.9633	-0.2563	0.8864
n.C_{10}	1.0682	-0.0724	0.4364
benzene	0.6831	-0.1052	0.6671

Continuation of table D2			
toluene	0.7646	-0.0974	0.4257
o-xylene	0.8445	-0.2051	0.6115
cy-C_6	0.6805	-0.0690	0.5765
m-cy-C_6	0.7162	-0.0204	0.3396
cis-1.2-dm-cy-C_6	0.6288	0.7011	-0.7844
cis-1.4-dm-cy-C_6	0	0	0
trans-1.2-dm-cy-C_6	0	0	0
trans-1.4-dm-cy-C_6	0	0	0
2.2-dim-C_4	0.6989	0.1119	-0.0635
2.2.4-tm-C_5	0	0	0
CO_2	0.7137	-0.4476	2.4375
N_2	0.4363	0	0
water	0.9237	-0.3794	0.4424

Table D3: Unifac group parameters of all components included in the mixtures used for the predictions of the mole fraction of Hg

i	**j**	**A_{ij} [K]**	**B_{ij} [-]**	**C_{ij} [K^{-1}]**	**A_{ji} [K]**	**B_{ji} [-]**	**C_{ji} [K^{-1}]**
CH_4	C_2H_6	96.49	0.5073	0	-71.15	-0.4012	0
CH_4	CO_2	-83.73	-2.2570	0	301.98	1.6951	0
N_2	CH_4	-119.61	-0.7538	0	194.04	0.8318	0
CO_2	C_2H_6	90.86	-0.4893	0	117.63	-0.3263	0
N_2	C_2H_6	-154.52	-0.9021	0	303.92	0.9467	0
N_2	CO_2	-137.90	-1.6936	0	382.68	1.5736	0
CH_4	CH_2	328.80	1.8031	-0.011159	-214.41	-1.2202	0.004627
C_2H_6	CH_2	154.49	-0.2815	0.011039	-140.19	-0.1858	-0.005389
CO_2	CH_2	70.06	-0.7276	0.002452	84.68	-0.6989	0.002966
N_2	CH_2	112.52	-1.4903	0.000607	-4.26	0.6264	0.002043

Appendix E

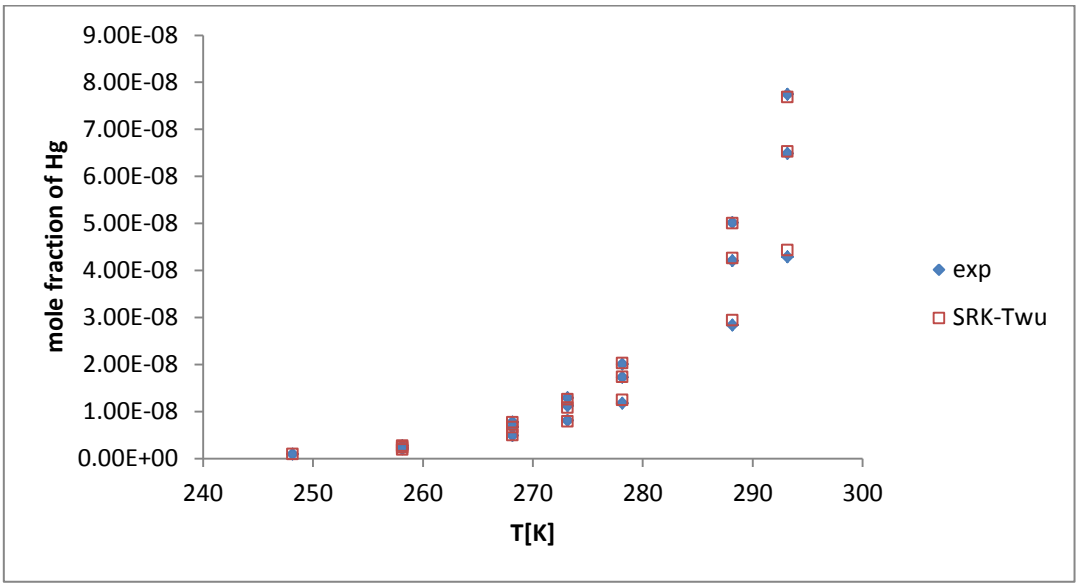

Figure E1: Mole fraction of Hg in methane calculated with SRK-Twu EOS with k_{ij} parameters in the vapor phase

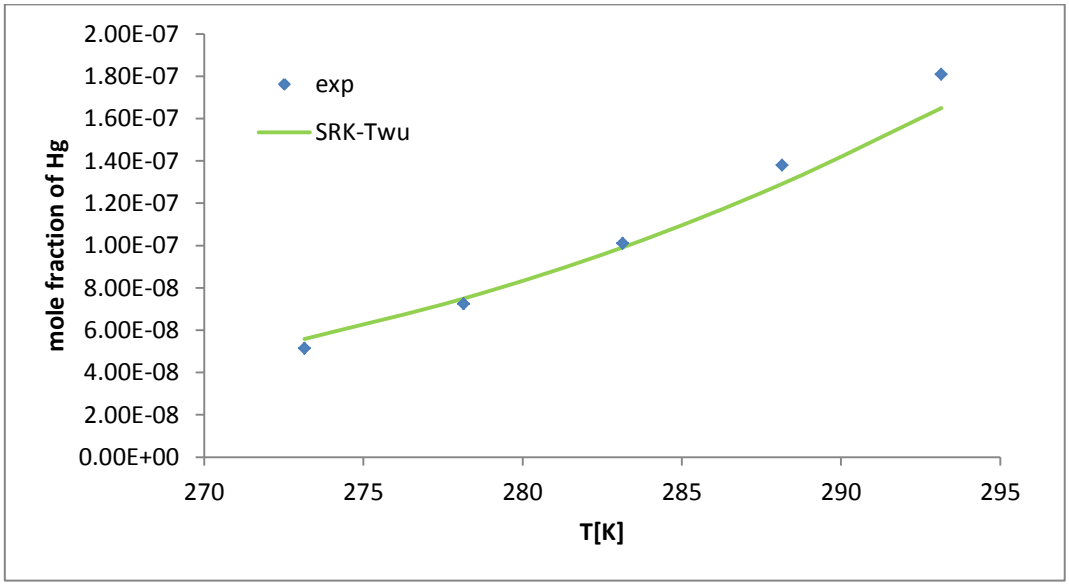

Figure E2: Mole fraction of Hg in ethane calculated with SRK-Twu EOS with k_{ij} parameters in the liquid phase

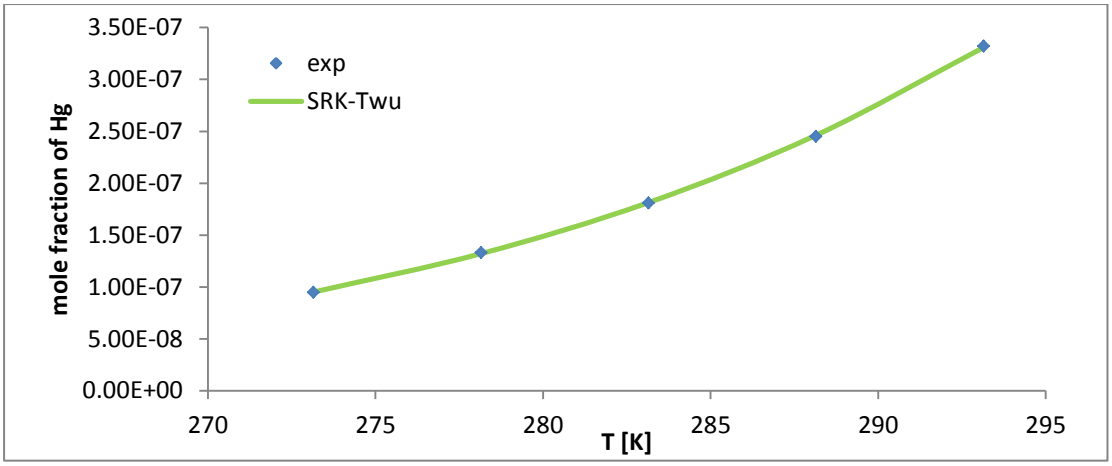

Figure E3: Mole fraction of Hg in propane calculated with SRK-Twu EOS with k_{ij} parameters in the liquid phase

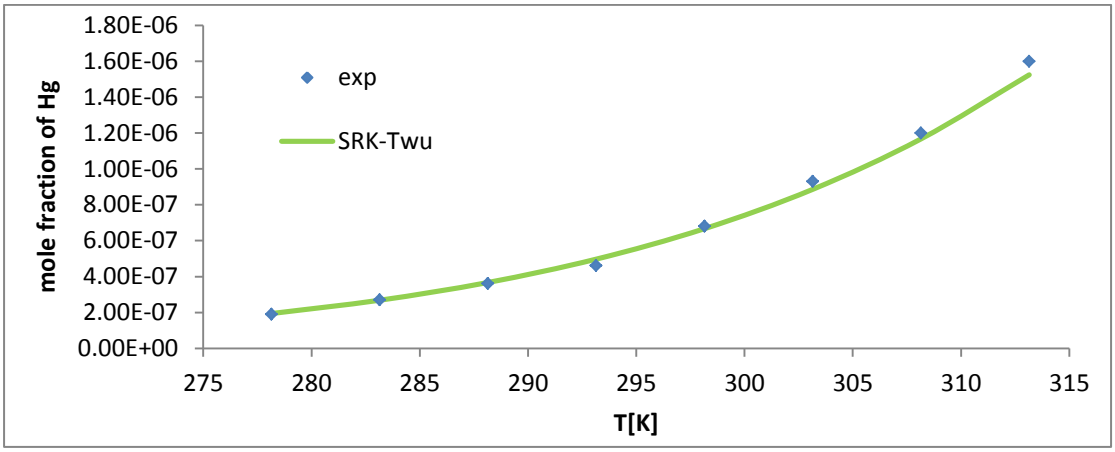

Figure E4: Mole fraction of Hg in n.C_5 calculated with SRK-Twu EOS with k_{ij} parameters in the liquid phase

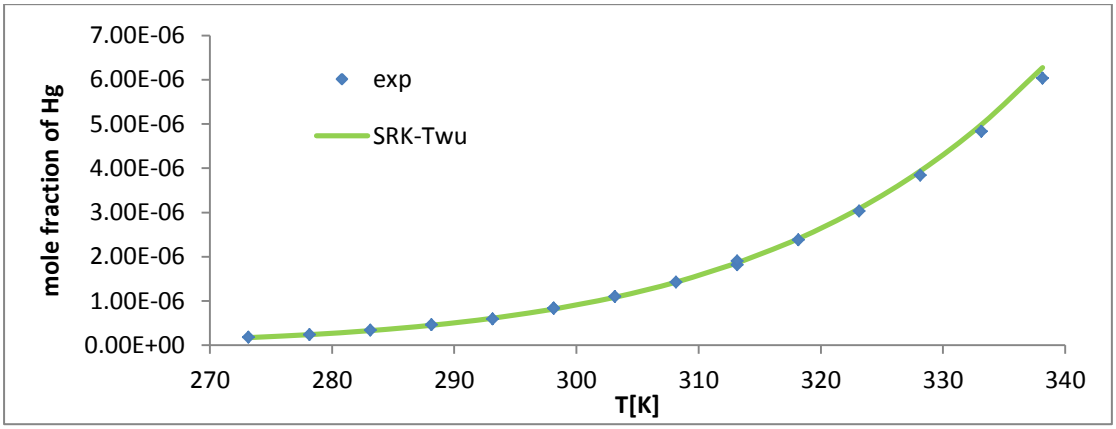

Figure E5: Mole fraction of Hg in n.C_6 calculated with SRK-Twu EOS with k_{ij} parameters in the liquid phase

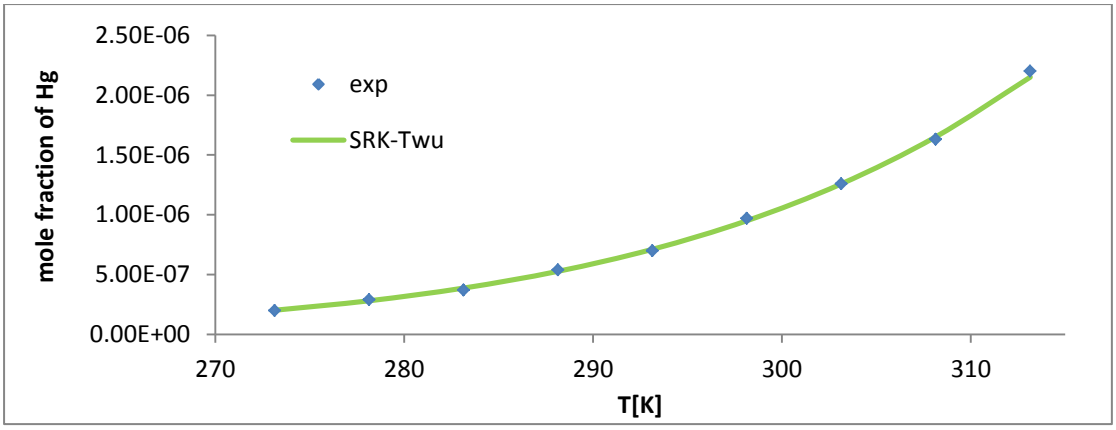

Figure E6: Mole fraction of Hg in n.C_7 calculated with SRK-Twu EOS with k_{ij} parameters in the liquid phase

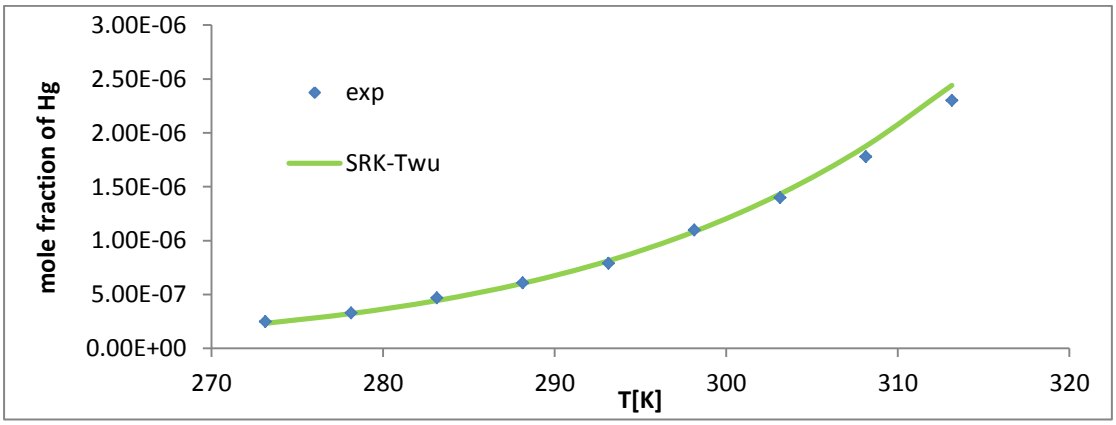

Figure E7: Mole fraction of Hg in n.C_8 calculated with SRK-Twu EOS with k_{ij} parameters in the liquid phase

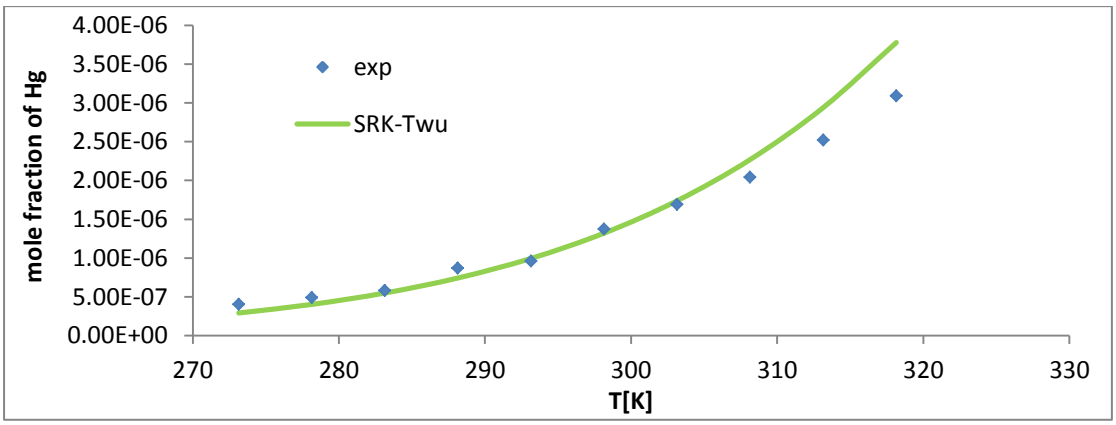

Figure E8: Mole fraction of Hg in n.C_{10} calculated with SRK-Twu EOS with k_{ij} parameters in the liquid phase

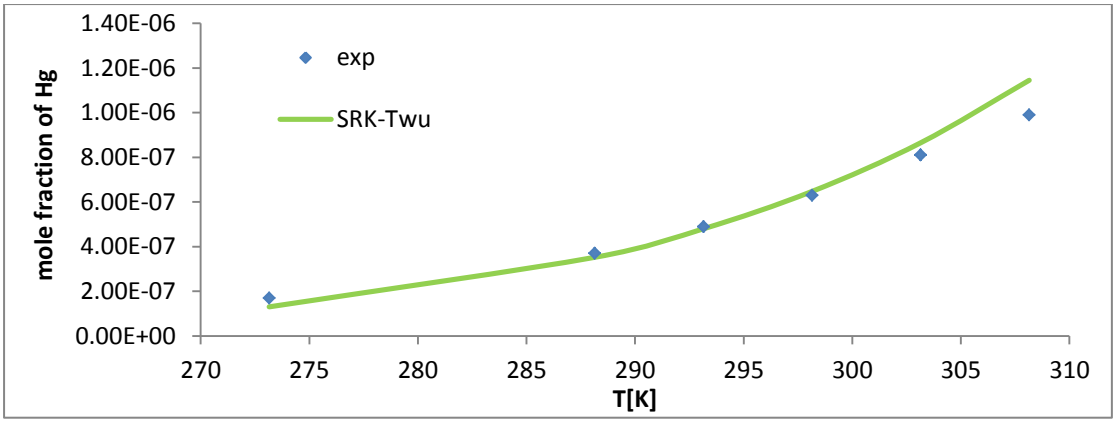

Figure E9: Mole fraction of Hg in 2.2-dm-C_4 calculated with SRK-Twu EOS with k_{ij} parameters in the liquid phase

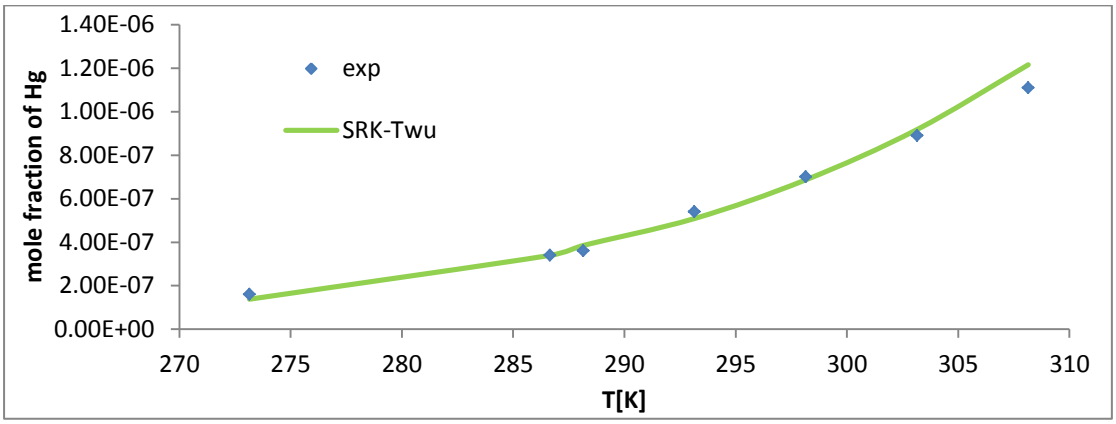

Figure E10: Mole fraction of Hg in 2.2.4-tm-C_5 calculated with SRK-Twu EOS with k_{ij} parameters in the liquid phase

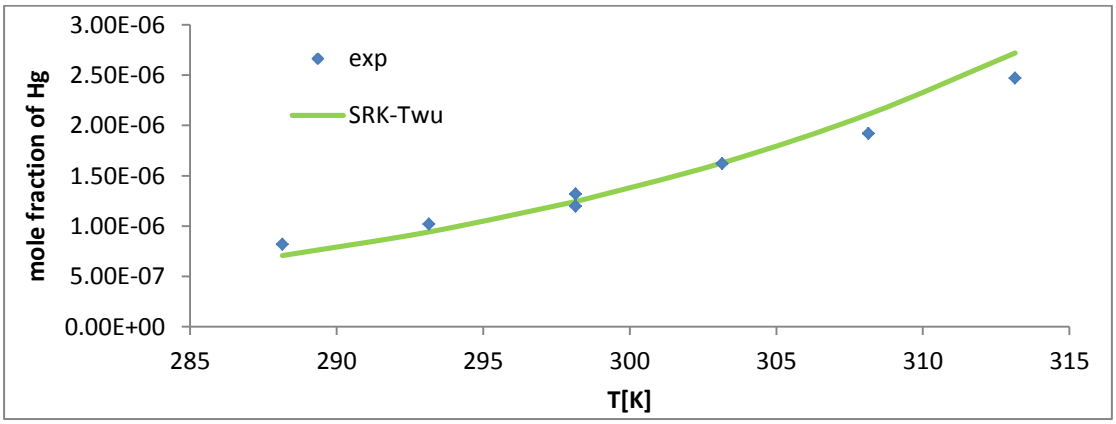

Figure E11: Mole fraction of Hg in cy-C_6 calculated with SRK-Twu EOS with k_{ij} parameters in the liquid phase

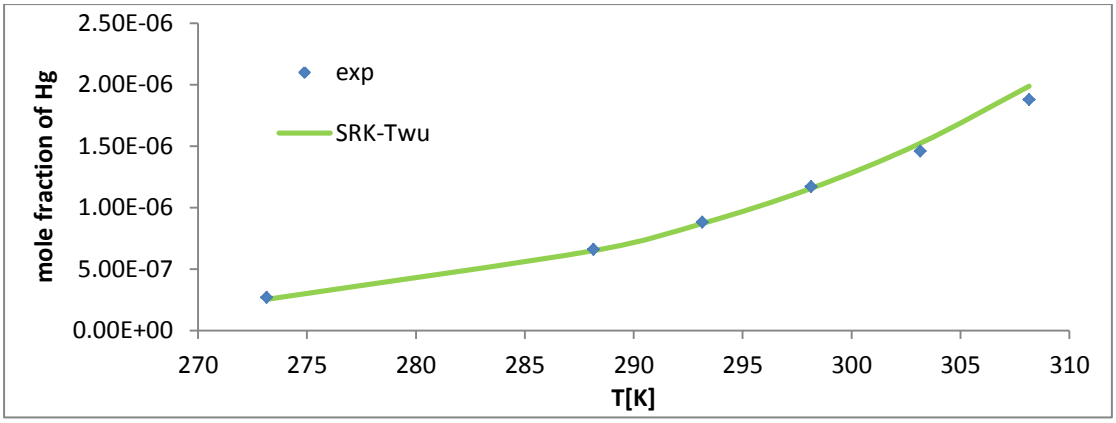

Figure E12: Mole fraction of Hg in m-cy-C_6 calculated with SRK-Twu EOS with k_{ij} parameters in the liquid phase

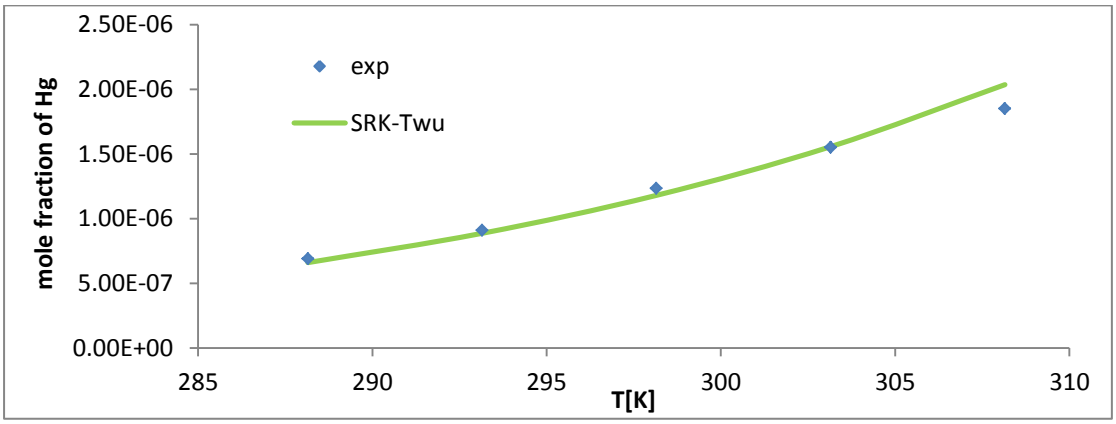

Figure E13: Mole fraction of Hg in trans-1.2-dm-cy-C_6 calculated with SRK-Twu EOS with k_{ij} parameters in the liquid phase

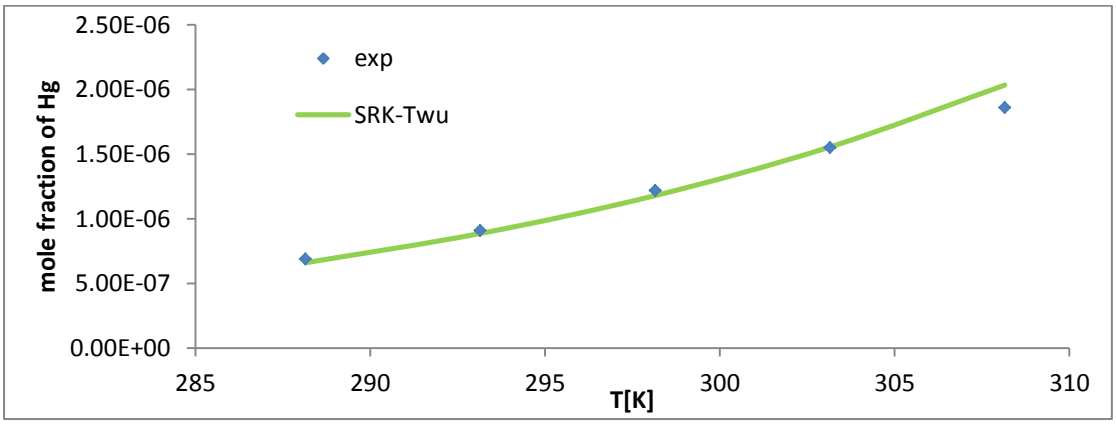

Figure E14: Mole fraction of Hg in trans-1.4-dm-cy-C_6 calculated with SRK-Twu EOS with k_{ij} parameters in the liquid phase

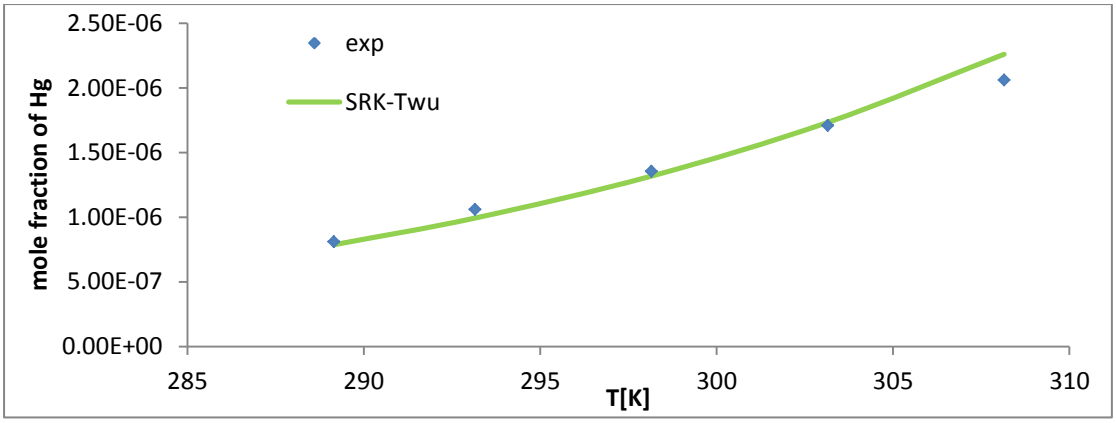

Figure E15: Mole fraction of Hg in cis-1.2-dm-cy-C_6 calculated with SRK-Twu EOS with k_{ij} parameters in the liquid phase

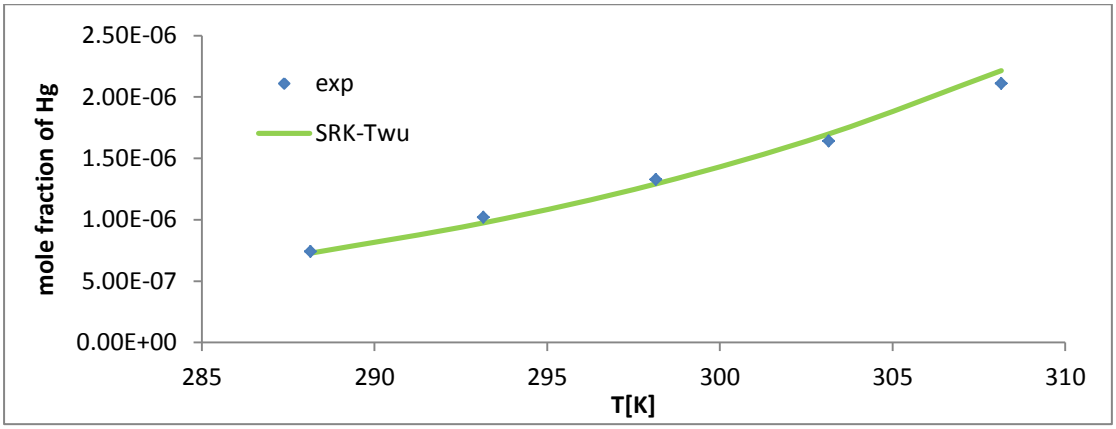

Figure E16: Mole fraction of Hg in cis-1.4-dm-cy-C_6 calculated with SRK-Twu EOS with k_{ij} parameters in the liquid phase

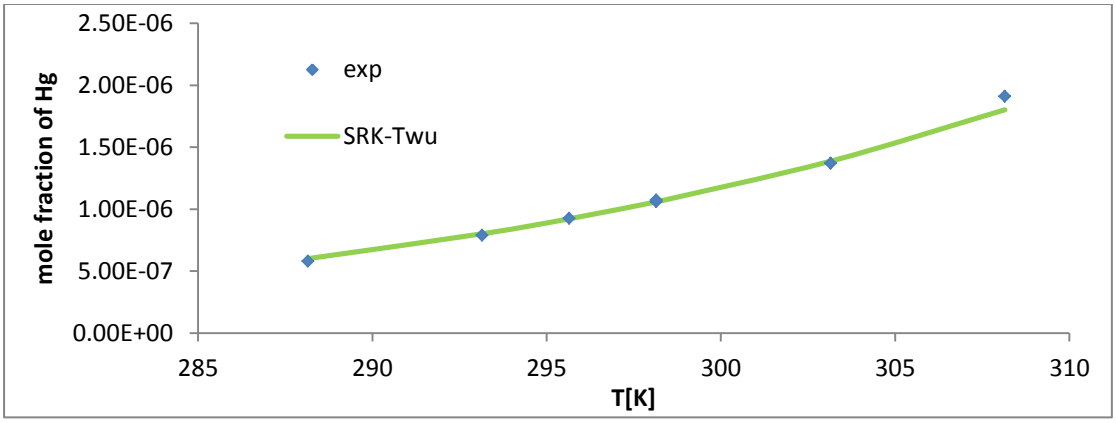

Figure E17: Mole fraction of Hg in benzene calculated with SRK-Twu EOS with k_{ij} parameters in the liquid phase

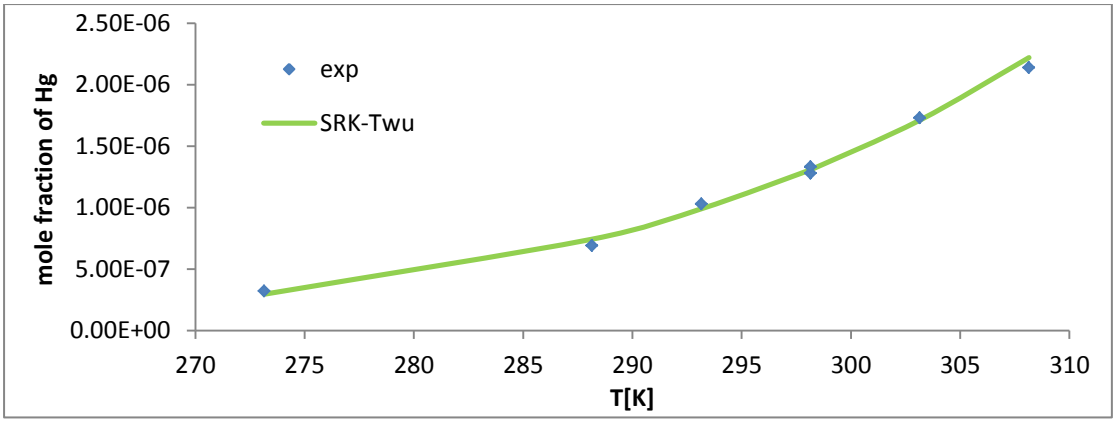

Figure E18: Mole fraction of Hg in toluene calculated with SRK-Twu EOS with k_{ij} parameters in the liquid phase

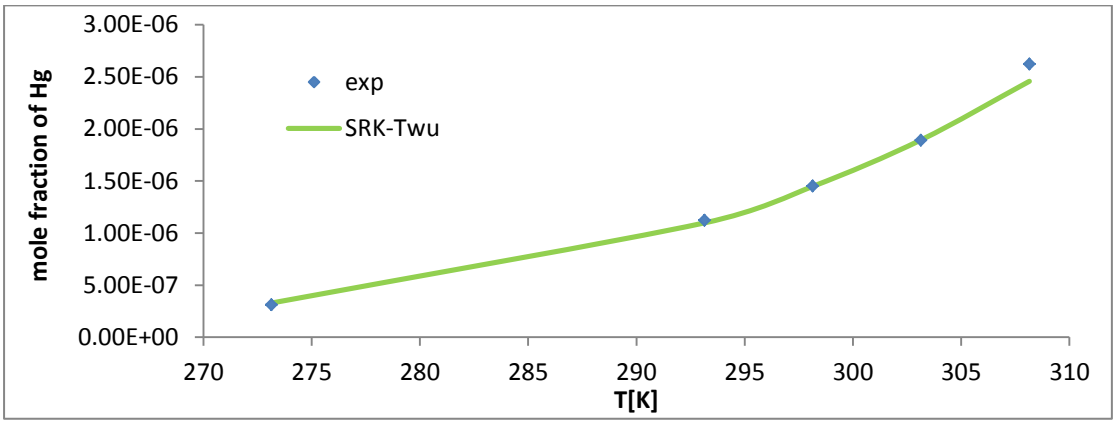

Figure E19: Mole fraction of Hg in o-xylene calculated with SRK-Twu EOS with k_{ij} parameters in the liquid phase

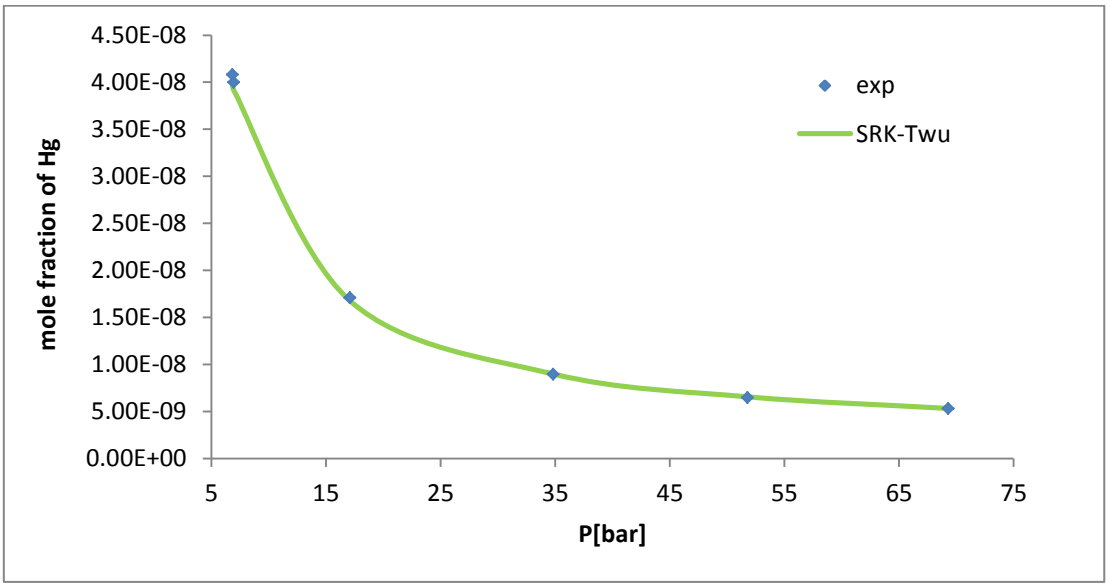

Figure E20: Mole fraction of Hg in N_2 calculated with SRK-Twu EOS with k_{ij} parameters in the vapor phase

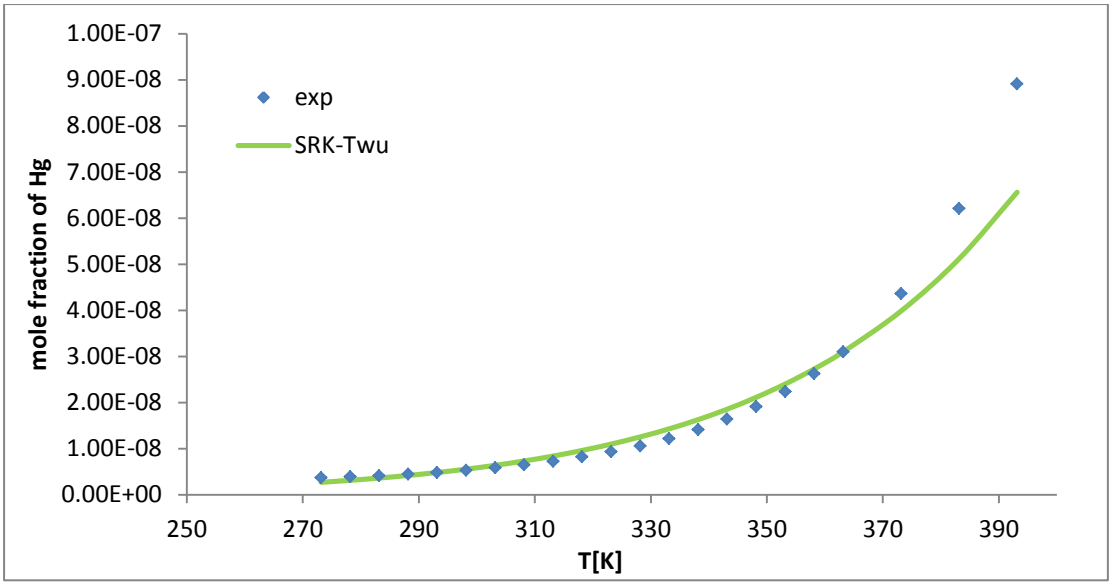

Figure E22: Mole fraction of Hg in water calculated with SRK-Twu EOS with k_{ij} parameters

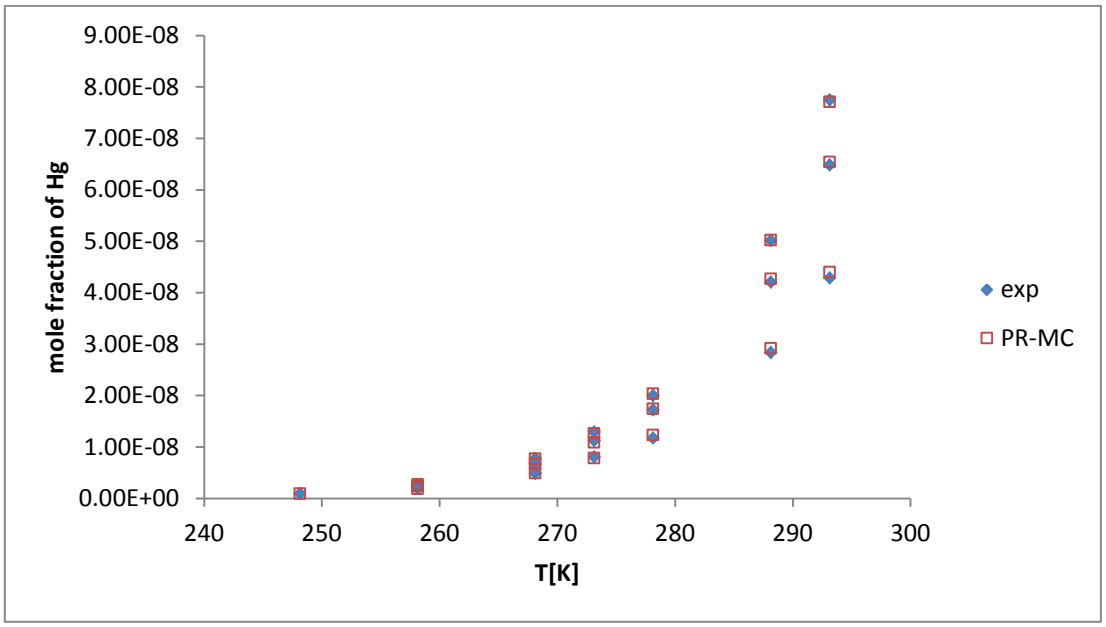

Figure E22: Mole fraction of Hg in methane calculated with PR-MC EOS with k_{ij} parameters in the vapor phase

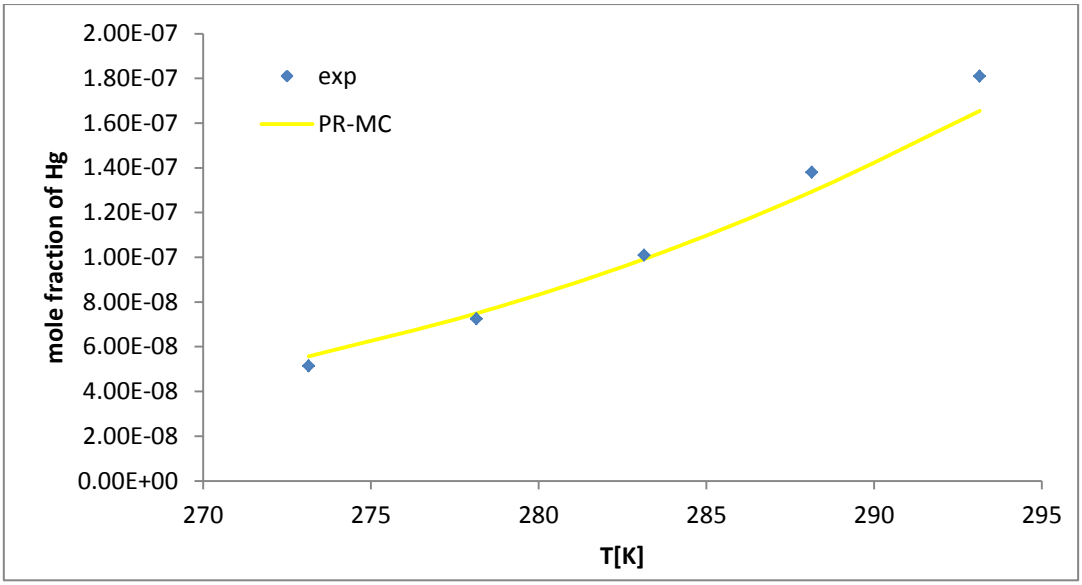

Figure E23: Mole fraction of Hg in ethane calculated with PR-MC EOS with k_{ij} parameters in the liquid phase

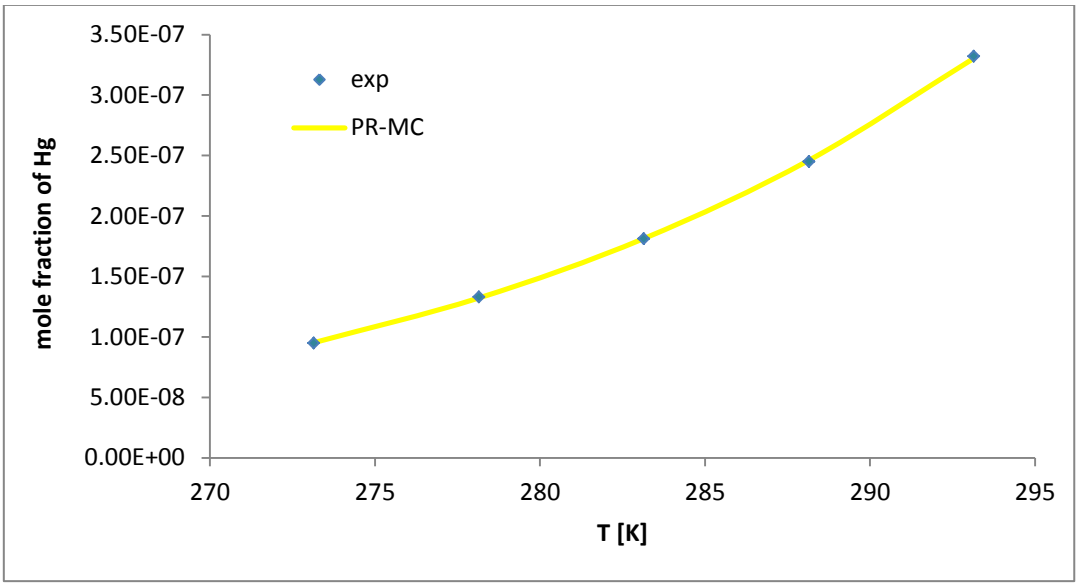

Figure E24: Mole fraction of Hg in propane calculated with PR-MC EOS with k_{ij} parameters in the liquid phase

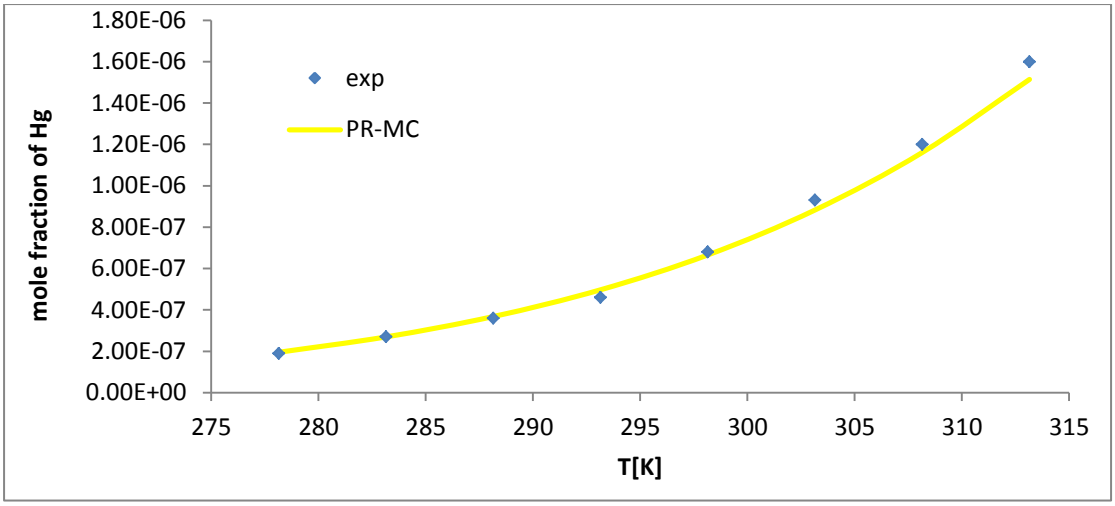

Figure E25: Mole fraction of Hg in n.C_5 calculated with PR-MC EOS with k_{ij} parameters in the liquid phase

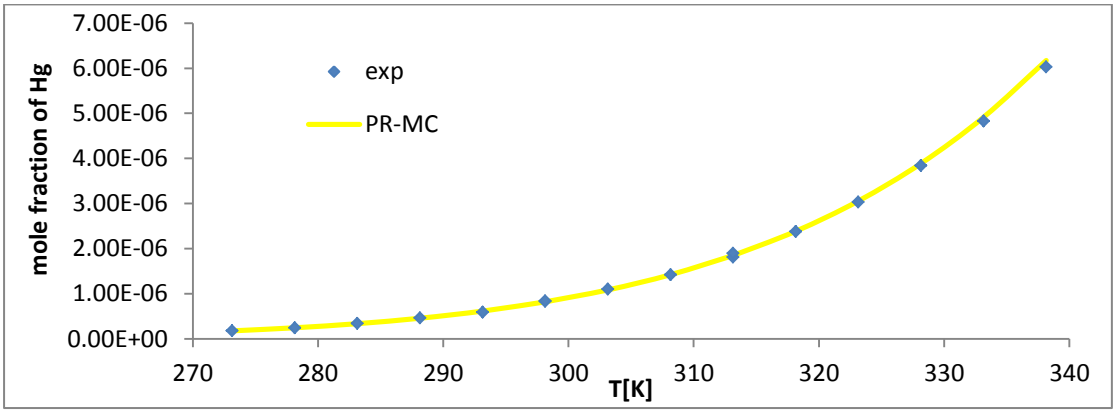

Figure E26: Mole fraction of Hg in n.C_6 calculated with SRK-Twu EOS with k_{ij} parameters in the liquid phase

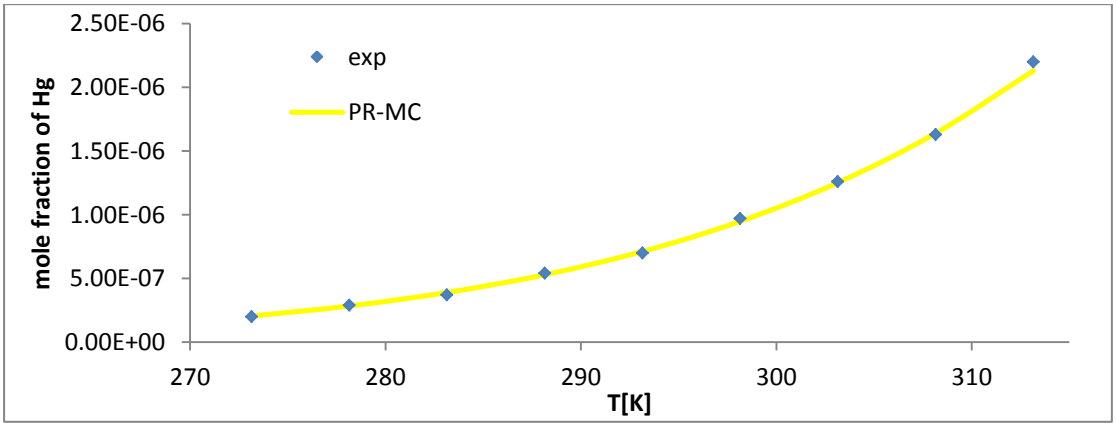

Figure E27: Mole fraction of Hg in n.C_7 calculated with SRK-Twu EOS with k_{ij} parameters in the liquid phase

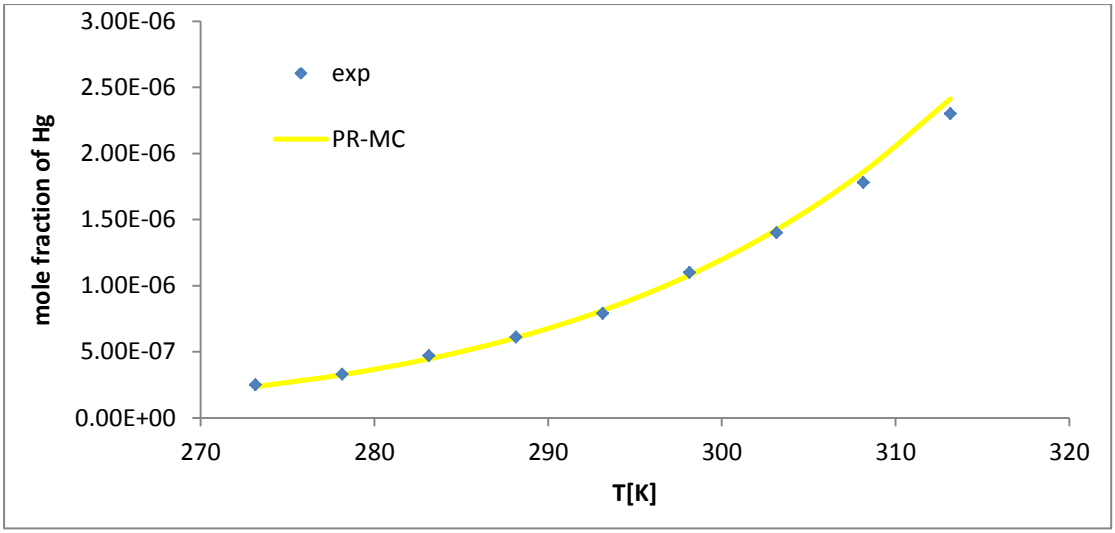

Figure E28: Mole fraction of Hg in n.C_8 calculated with PR-MC EOS with k_{ij} parameters in the liquid phase

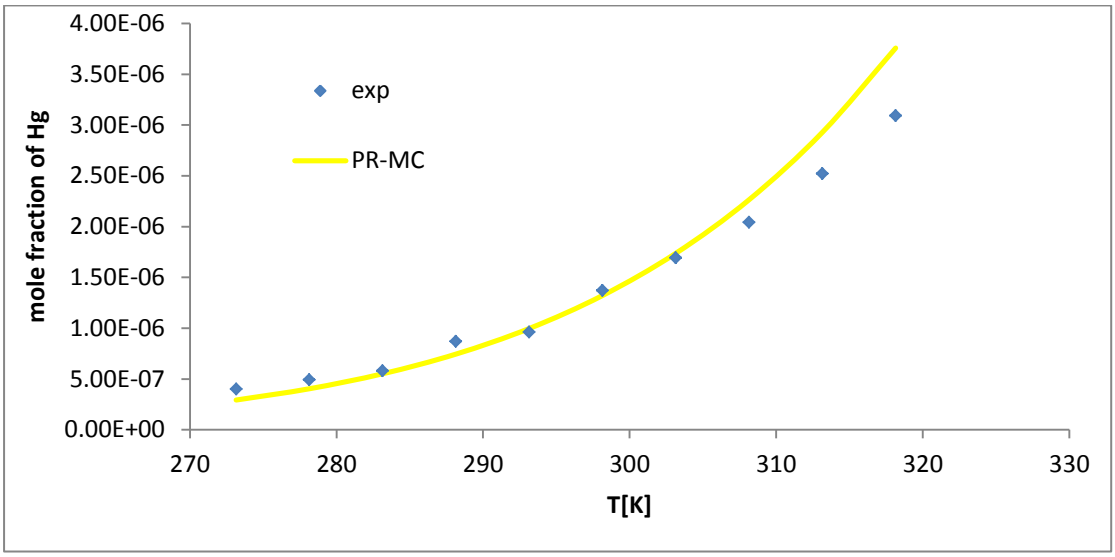

Figure E29: Mole fraction of Hg in n.C_{10} calculated with PR-MC EOS with k_{ij} parameters in the liquid phase

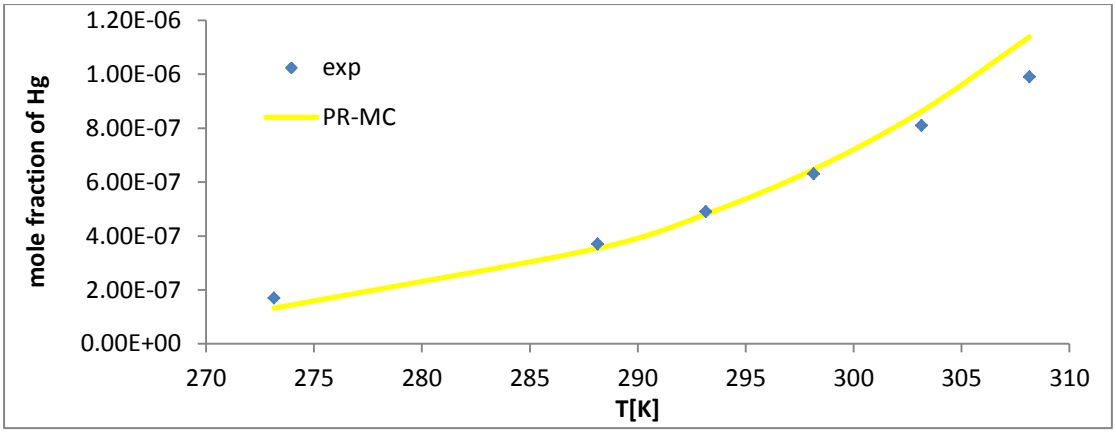

Figure E30: Mole fraction of Hg in 2.2-dm-C_4 calculated with PR-MC EOS with k_{ij} parameters in the liquid phase

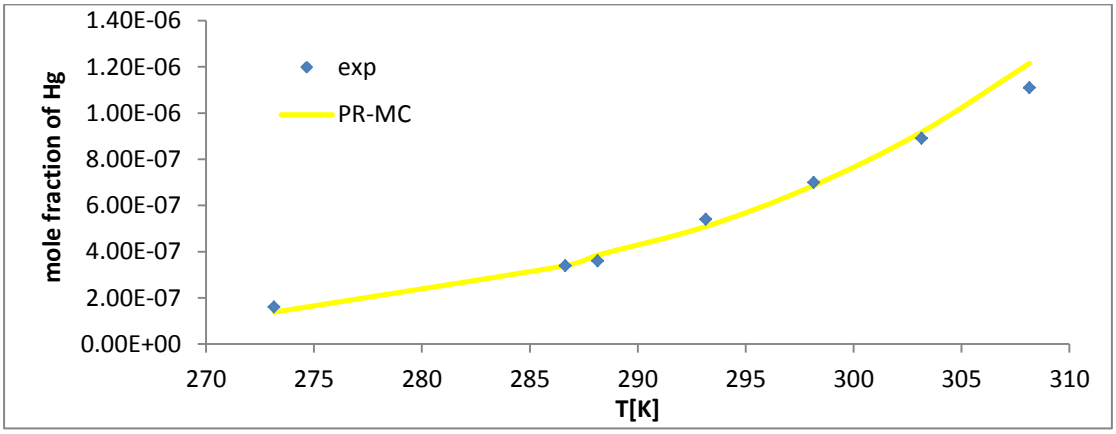

Figure E31: Mole fraction of Hg in 2.2.4-tm-C_5 calculated with PR-MC EOS with k_{ij} parameters in the liquid phase

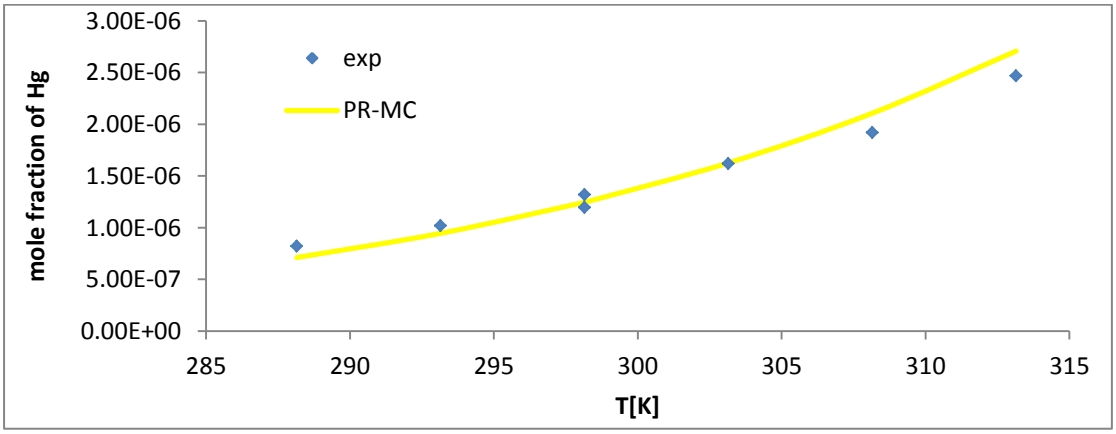

Figure E32: Mole fraction of Hg in cy-C_6 calculated with PR-MC EOS with k_{ij} parameters in the liquid phase

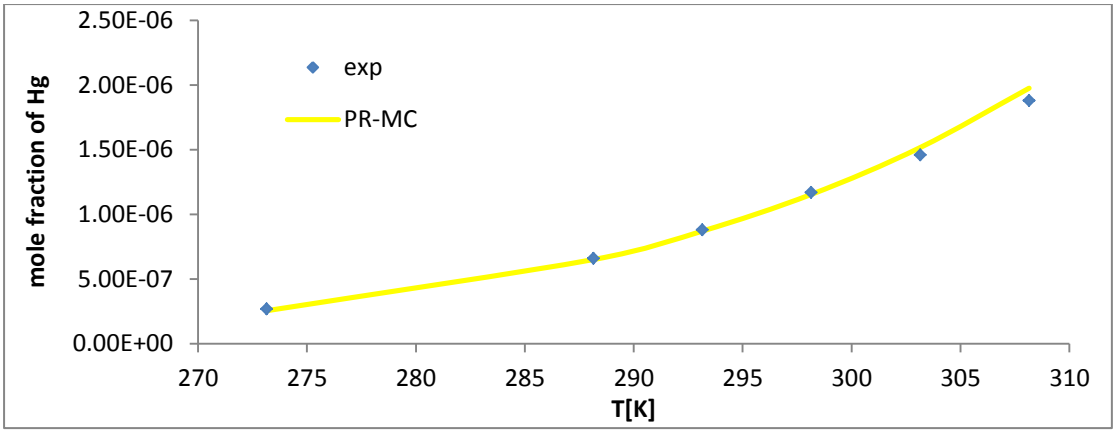

Figure E33: Mole fraction of Hg in m-cy-C_6 calculated with PR-MC EOS with k_{ij} parameters in the liquid phase

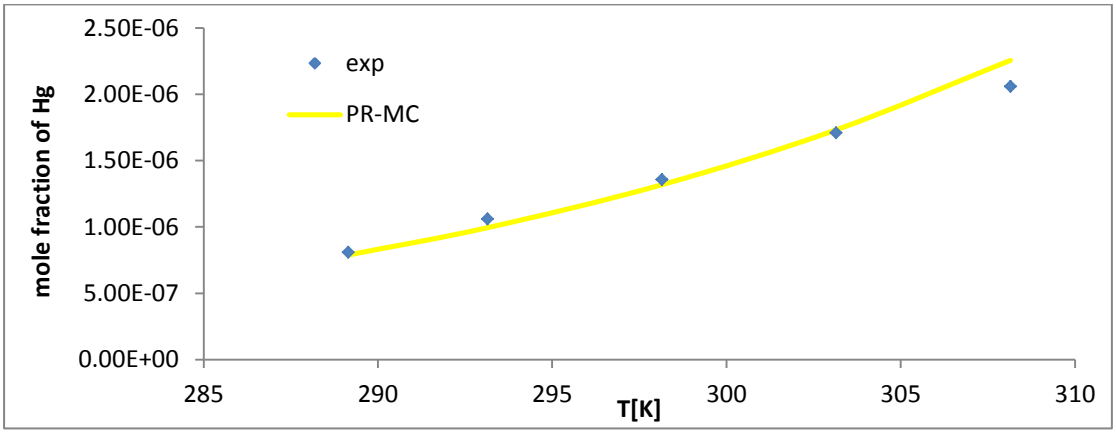

Figure E34: Mole fraction of Hg in cis-1.2-dm-cy-C_6 calculated with PR-MC EOS with k_{ij} parameters in the liquid phase

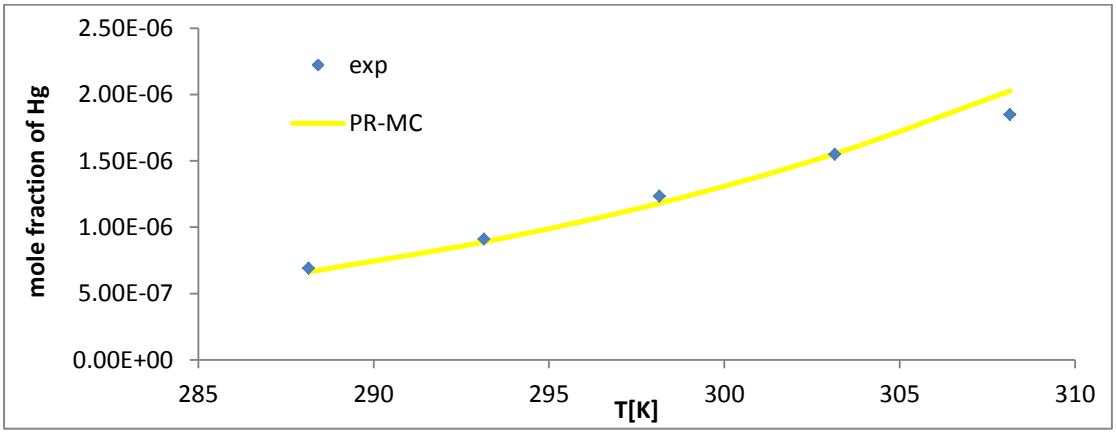

Figure E35: Mole fraction of Hg in trans-1.2-dm-cy-C_6 calculated with PR-MC EOS with k_{ij} parameters in the liquid phase

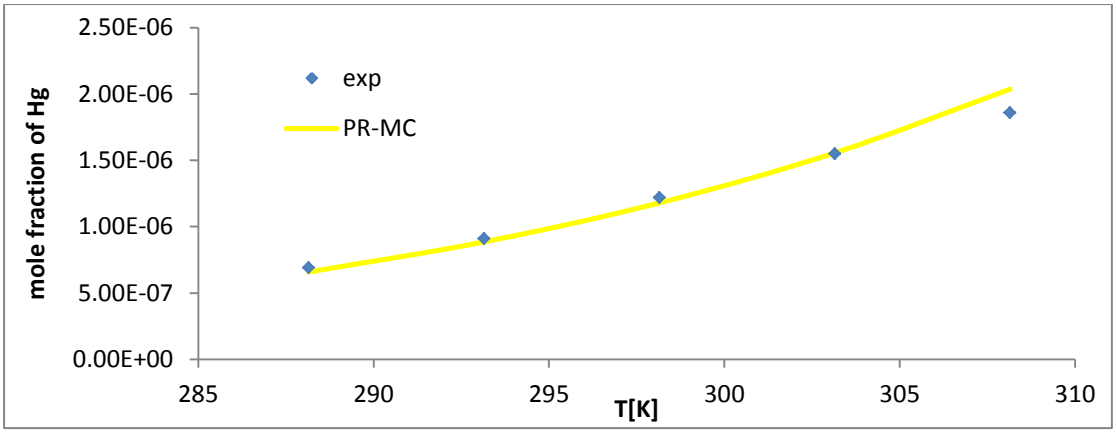

Figure E36: Mole fraction of Hg in trans-1.4-dm-cy-C_6 calculated with PR-MC EOS with k_{ij} parameters in the liquid phase

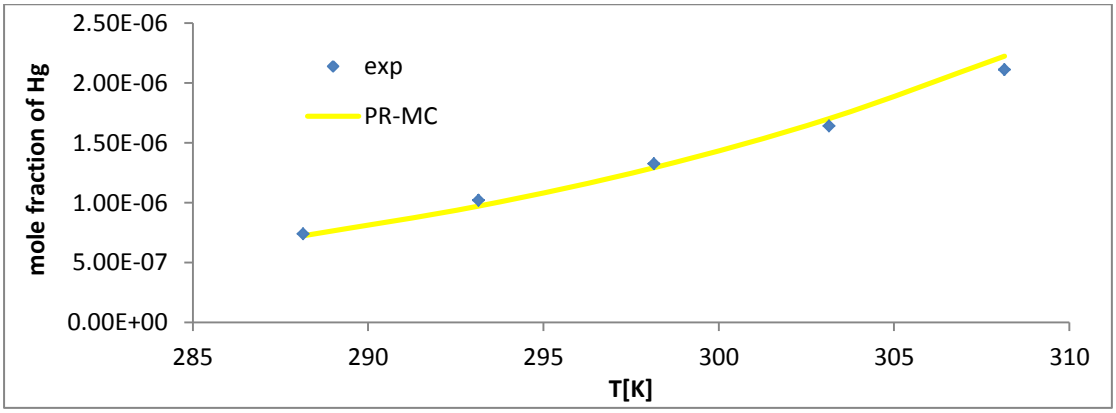

Figure E37: Mole fraction of Hg in cis-1.4-dm-cy-C_6 calculated with PR-MC EOS with k_{ij} parameters in the liquid phase

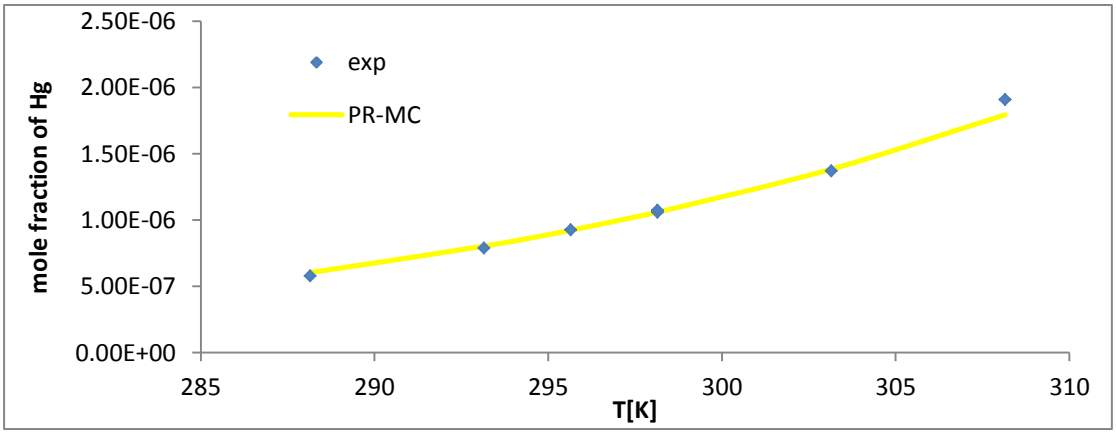

Figure E38: Mole fraction of Hg in benzene calculated with PR-MC EOS with k_{ij} parameters in the liquid phase

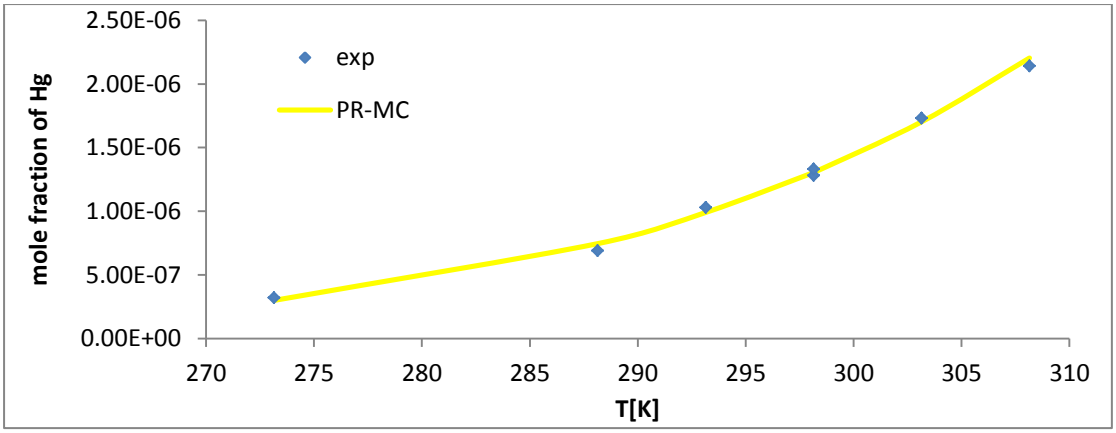

Figure E39: Mole fraction of Hg in toluene calculated with PR-MC EOS with k_{ij} parameters in the liquid phase

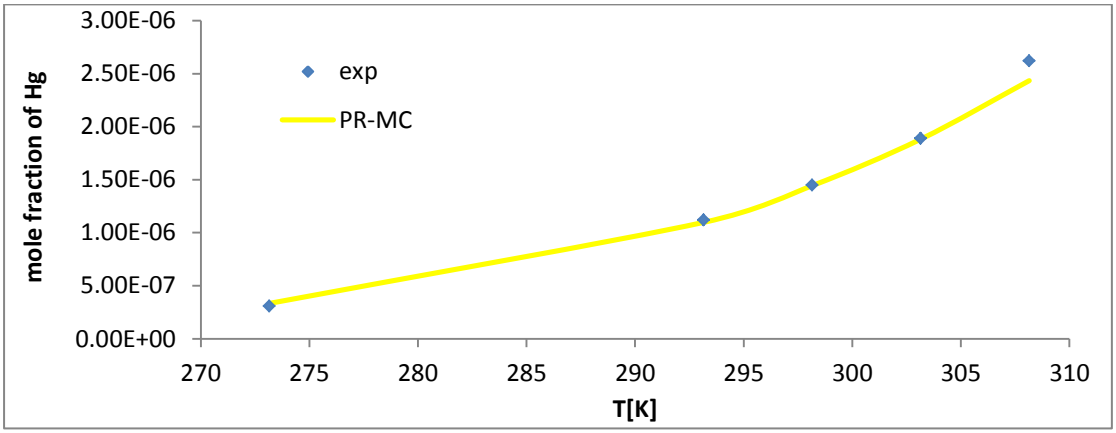

Figure E40: Mole fraction of Hg in o-xylene calculated with PR-MC EOS with k_{ij} parameters in the liquid phase

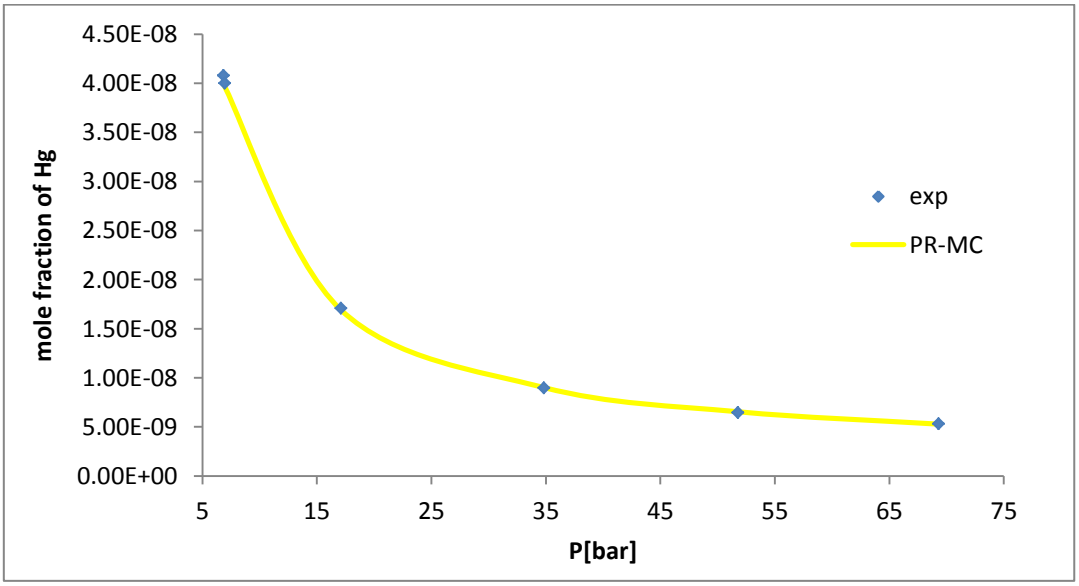

Figure E41: Mole fraction of Hg in N_2 calculated with PR-MC EOS with k_{ij} parameters in the vapor phase

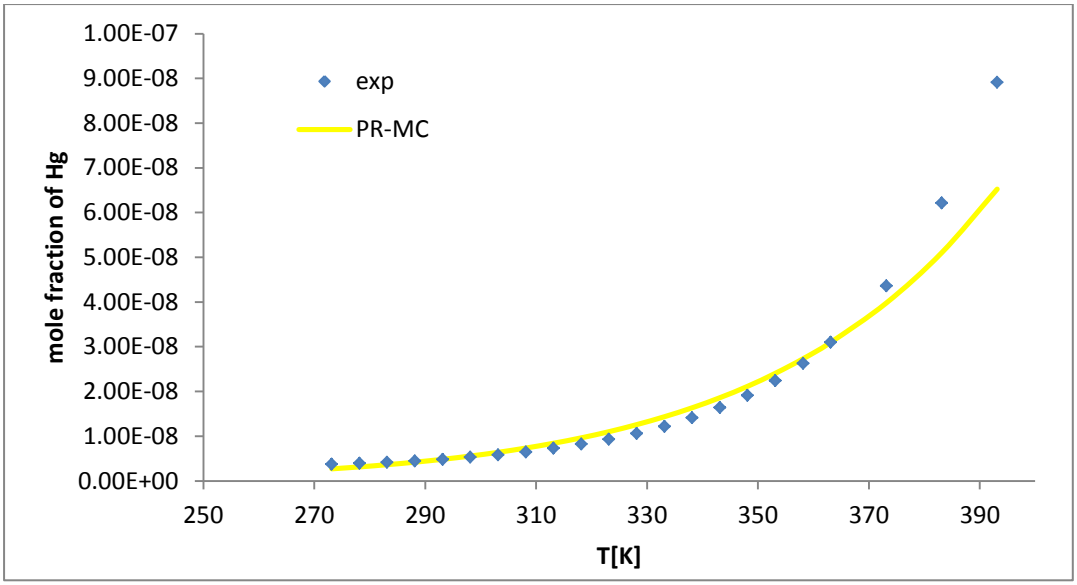

Figure E42: Mole fraction of Hg in water calculated with PR-MC EOS with k_{ij} parameters

Table E1: Analytical results and absolute deviations of the mole fraction of Hg in methane for the SRK-Twu EOS in the vapor phase

Confidential data

Table E2: Analytical results and absolute deviations of the mole fraction of Hg in ethane for the SRK-Twu EOS in the liquid phase

Confidential data

Table E3: Analytical results and absolute deviations of the mole fraction of Hg in propane for the SRK-Twu EOS in the liquid phase

Confidential data

Table E4: Analytical results and absolute deviations of the mole fraction of Hg in n.C_5 for the SRK-Twu EOS in the liquid phase

		k_{ij}=const	
T[K]	**x_{exp}**	**x_{calc}**	**Dx%**
278.15	1.90E-07	1.94E-07	2.00
283.15	2.70E-07	2.68E-07	0.67
288.15	3.60E-07	3.67E-07	1.98
293.15	4.60E-07	4.97E-07	8.12
298.15	6.80E-07	6.67E-07	1.89
303.15	9.30E-07	8.87E-07	4.67
308.15	1.20E-06	1.17E-06	2.68
313.15	1.60E-06	1.53E-06	4.66

Table E5: Analytical results and absolute deviations of the mole fraction of Hg in n.C_6 for the SRK-Twu EOS in the liquid phase

		k_{ij}=const	
T[K]	**x_{exp}**	**x_{calc}**	**Dx%**
273.15	1.80E-07	1.72E-07	4.62
278.15	2.40E-07	2.40E-07	0.16
283.15	3.40E-07	3.31E-07	2.74
288.15	4.60E-07	4.52E-07	1.84
293.15	5.90E-07	6.10E-07	3.45
298.15	8.30E-07	8.17E-07	1.56
298.15	8.41E-07	8.17E-07	2.81
303.15	1.10E-06	1.08E-06	1.46
308.15	1.42E-06	1.43E-06	0.38
313.15	1.81E-06	1.86E-06	2.63
313.15	1.90E-06	1.86E-06	2.16
318.15	2.38E-06	2.41E-06	1.06
323.15	3.03E-06	3.09E-06	1.94
328.15	3.84E-06	3.94E-06	2.56
333.15	4.83E-06	4.99E-06	3.25
338.15	6.03E-06	6.27E-06	4.05

Table E6: Analytical results and absolute deviations of the mole fraction of Hg in n.C_7 for the SRK-Twu EOS in the liquid phase

		k_{ij}=const	
T[K]	**x_{exp}**	**x_{calc}**	**Dx%**
273.15	2.00E-07	2.02E-07	1.10
278.15	2.90E-07	2.81E-07	2.95
283.15	3.70E-07	3.87E-07	4.70
288.15	5.40E-07	5.28E-07	2.28
293.15	7.00E-07	7.12E-07	1.66
298.15	9.70E-07	9.51E-07	1.99
303.15	1.26E-06	1.26E-06	0.11
308.15	1.63E-06	1.65E-06	1.34
313.15	2.20E-06	2.15E-06	2.25

Table E7: Analytical results and absolute deviations of the mole fraction of Hg in n.C_8 for the SRK-Twu EOS in the liquid phase

		k_{ij}=const	
T[K]	**x_{exp}**	**x_{calc}**	**Dx%**
273.15	2.50E-07	2.33E-07	6.76
278.15	3.30E-07	3.24E-07	1.90

Continuation of table E7			
283.15	4.70E-07	4.45E-07	5.39
288.15	6.10E-07	6.04E-07	0.90
293.15	7.90E-07	8.14E-07	2.99
298.15	1.10E-06	1.08E-06	1.38
303.15	1.40E-06	1.43E-06	2.39
308.15	1.78E-06	1.88E-06	5.51
313.15	2.30E-06	2.44E-06	6.12

Table E8: Analytical results and absolute deviations of the mole fraction of Hg in n.C_{10} for the SRK-Twu EOS in the liquid phase

		k_{ij}=const	
T[K]	**x_{exp}**	**x_{calc}**	**Dx%**
273.15	4.00E-07	2.90E-07	27.38
278.15	4.90E-07	4.01E-07	18.10
283.15	5.80E-07	5.48E-07	5.43
288.15	8.70E-07	7.42E-07	14.70
293.15	9.60E-07	9.95E-07	3.60
298.15	1.37E-06	1.32E-06	3.60
303.15	1.69E-06	1.74E-06	2.88
308.15	2.04E-06	2.27E-06	11.27
313.15	2.52E-06	2.94E-06	16.68
318.15	3.09E-06	3.78E-06	22.33

Table E9: Analytical results and absolute deviations of the mole fraction of Hg in 2.2-dm-C_4 for the SRK-Twu EOS in the liquid phase

		k_{ij}=const	
T[K]	**x_{exp}**	**x_{calc}**	**Dx%**
273.15	1.70E-07	1.31E-07	23.15
288.15	3.70E-07	3.53E-07	4.70
293.15	4.90E-07	4.80E-07	1.98
298.15	6.30E-07	6.48E-07	2.81
303.15	8.10E-07	8.65E-07	6.81
308.15	9.90E-07	1.15E-06	15.68

Table E10: Analytical results and absolute deviations of the mole fraction of Hg in 2.2.4-tm-C_5 for the SRK-Twu EOS in the liquid phase

		k_{ij}=const	
T[K]	**x_{exp}**	**x_{calc}**	**Dx%**
273.15	1.60E-07	1.38E-07	13.69

Continuation of table E10			
286.65	3.40E-07	3.40E-07	0.12
288.15	3.60E-07	3.85E-07	7.04
293.15	5.40E-07	5.09E-07	5.74
298.15	7.00E-07	6.87E-07	1.88
303.15	8.90E-07	9.18E-07	3.15
308.15	1.11E-06	1.22E-06	9.56
318.15	3.09E-06	3.78E-06	22.33

Table E11: Analytical results and absolute deviations of the mole fraction of Hg in cy-C_6 for the SRK-Twu EOS in the liquid phase

		k_{ij}=const	
T[K]	**x_{exp}**	**x_{calc}**	**Dx%**
288.15	8.20E-07	7.07E-07	13.79
293.15	1.02E-06	9.42E-07	7.67
298.15	1.32E-06	1.24E-06	5.81
298.15	1.20E-06	1.24E-06	3.83
303.15	1.62E-06	1.63E-06	0.45
308.15	1.92E-06	2.11E-06	10.02
313.15	2.47E-06	2.72E-06	10.15

Table E12: Analytical results and absolute deviations of the mole fraction of Hg in m-cy-C_6 for the SRK-Twu EOS in the liquid phase

		k_{ij}=const	
T[K]	**x_{exp}**	**x_{calc}**	**Dx%**
273.15	2.70E-07	2.54E-07	6.10
288.15	6.60E-07	6.50E-07	1.55
293.15	8.80E-07	8.71E-07	1.00
298.15	1.17E-06	1.16E-06	1.09
303.15	1.46E-06	1.52E-06	4.34
308.15	1.88E-06	1.99E-06	5.77

Table E13: Analytical results and absolute deviations of the mole fraction of Hg in cis-1.2-dm-cy-C_6 for the SRK-Twu EOS in the liquid phase

		k_{ij}=const	
T[K]	**x_{exp}**	**x_{calc}**	**Dx%**
289.15	8.10E-07	7.87E-07	2.79
293.15	1.06E-06	9.94E-07	6.26
298.15	1.36E-06	1.32E-06	2.78
303.15	1.71E-06	1.73E-06	1.38

Continuation of table E13			
308.15	2.06E-06	2.26E-06	9.76

Table E14: Analytical results and absolute deviations of the mole fraction of Hg in cis-1.4-dm-cy-C_6 for the SRK-Twu EOS in the liquid phase

		k_{ij}=const	
T[K]	**x_{exp}**	**x_{calc}**	**Dx%**
288.15	7.40E-07	7.28E-07	1.62
293.15	1.02E-06	9.74E-07	4.48
298.15	1.33E-06	1.29E-06	2.56
303.15	1.64E-06	1.70E-06	3.57
308.15	2.11E-06	2.21E-06	4.96

Table E15: Analytical results and absolute deviations of the mole fraction of Hg in trans-1.2-dm-cy-C_6 for the SRK-Twu EOS in the liquid phase

		k_{ij}=const	
T[K]	**x_{exp}**	**x_{calc}**	**Dx%**
288.15	6.90E-07	6.60E-07	4.32
293.15	9.10E-07	8.87E-07	2.53
298.15	1.23E-06	1.18E-06	4.34
303.15	1.55E-06	1.56E-06	0.46
308.15	1.85E-06	2.04E-06	10.09

Table E16: Analytical results and absolute deviations of the mole fraction of Hg in trans-1.4- dm-cy-C_6 for the SRK-Twu EOS in the liquid phase

		k_{ij}=const	
T[K]	**x_{exp}**	**x_{calc}**	**Dx%**
288.15	6.90E-07	6.60E-07	4.34
293.15	9.10E-07	8.86E-07	2.58
298.15	1.22E-06	1.18E-06	3.24
303.15	1.55E-06	1.56E-06	0.36
308.15	1.86E-06	2.03E-06	9.36

Table E17: Analytical results and absolute deviations of the mole fraction of Hg in benzene for the SRK-Twu EOS in the liquid phase

		k_{ij}=const	
T[K]	**x_{exp}**	**x_{calc}**	**Dx%**
288.15	5.80E-07	6.01E-07	3.68
293.15	7.90E-07	8.02E-07	1.50
295.65	9.27E-07	9.23E-07	0.46
298.15	1.06E-06	1.06E-06	0.05
298.15	1.07E-06	1.06E-06	1.33
303.15	1.37E-06	1.39E-06	1.30
308.15	1.91E-06	1.80E-06	5.62

Table E18: Analytical results and absolute deviations of the mole fraction of Hg in toluene for the SRK-Twu EOS in the liquid phase

		k_{ij}=const	
T[K]	**x_{exp}**	**x_{calc}**	**Dx%**
273.15	3.20E-07	2.95E-07	7.70
288.15	6.90E-07	7.43E-07	7.70
293.15	1.03E-06	9.90E-07	3.84
298.15	1.28E-06	1.31E-06	2.17
298.15	1.33E-06	1.31E-06	1.82
303.15	1.73E-06	1.71E-06	1.07
308.15	2.14E-06	2.22E-06	3.79

Table E19: Analytical results and absolute deviations of the mole fraction of Hg in o-xylene for the SRK-Twu EOS in the liquid phase

		k_{ij}=const	
T[K]	**x_{exp}**	**x_{calc}**	**Dx%**
273.15	3.10E-07	3.29E-07	6.08
293.15	1.12E-06	1.10E-06	1.95
298.15	1.45E-06	1.45E-06	0.08
303.15	1.89E-06	1.89E-06	0.26
308.15	2.62E-06	2.46E-06	6.20

Table E20: Analytical results and absolute deviations of the mole fraction of Hg in N_2 for the SRK-Twu EOS in the vapor phase

Confidential data

Table E21: Analytical results and absolute deviations of the mole fraction of Hg in water for the SRK-Twu EOS

kij	T [K]	P [bar]	Mole fraction of Hg (exp)	Mole fraction of Hg (calc)	abs dev %
0.5804	273.15	1	3.73E-09	2.71E-09	27.36
0.5931	278.15	1	3.91E-09	3.14E-09	19.72
0.6058	283.15	1	4.15E-09	3.63E-09	12.53
0.6185	288.15	1	4.46E-09	4.19E-09	6.04
0.6312	293.15	1	4.83E-09	4.83E-09	0.00
0.6439	298.15	1	5.28E-09	5.56E-09	5.27
0.6566	303.15	1	5.83E-09	6.39E-09	9.56
0.6693	308.15	1	6.48E-09	7.33E-09	13.11
0.6820	313.15	1	7.27E-09	8.40E-09	15.55
0.6947	318.15	1	8.20E-09	9.62E-09	17.26
0.7074	323.15	1	9.31E-09	1.10E-08	18.08
0.7202	328.15	1	1.06E-08	1.25E-08	18.36
0.7329	333.15	1	1.22E-08	1.43E-08	17.21
0.7456	338.15	1	1.41E-08	1.63E-08	15.60
0.7583	343.15	1	1.64E-08	1.86E-08	13.18
0.7710	348.15	1	1.91E-08	2.11E-08	10.57
0.7837	353.15	1	2.24E-08	2.40E-08	7.20
0.7964	358.15	1	2.63E-08	2.73E-08	3.73
0.8091	363.15	1	3.10E-08	3.10E-08	0.00
0.8345	373.15	1	4.36E-08	3.99E-08	8.59
0.8599	383.15	1	6.21E-08	5.12E-08	17.59
0.8853	393.15	1	8.91E-08	6.56E-08	26.36

Table E22: Analytical results and absolute deviations of the mole fraction of Hg in methane for the PR-MC EOS in the vapor phase

Confidential data

Table E23: Analytical results and absolute deviations of the mole fraction of Hg in ethane for the PR-MC EOS in the liquid phase

Confidential data

Table E24: Analytical results and absolute deviations of the mole fraction of Hg in propane for the PR-MC EOS in the liquid phase

Confidential data

Table E25: Analytical results and absolute deviations of the mole fraction of Hg in n.C_5 for the PR-MC EOS in the liquid phase

		k_{ij}=const	
T[K]	**x_{exp}**	**x_{calc}**	**Dx%**
278.15	1.90E-07	1.95E-07	2.76
283.15	2.70E-07	2.69E-07	0.20
288.15	3.60E-07	3.68E-07	2.20
293.15	4.60E-07	4.97E-07	8.11
298.15	6.80E-07	6.66E-07	2.10
303.15	9.30E-07	8.83E-07	5.05
308.15	1.20E-06	1.16E-06	3.23
313.15	1.60E-06	1.51E-06	5.35

Table E26: Analytical results and absolute deviations of the mole fraction of Hg in n.C_6 for the PR-MC EOS in the liquid phase

		k_{ij}=const	
T[K]	**x_{exp}**	**x_{calc}**	**Dx%**
273.15	1.80E-07	1.75E-07	2.68
278.15	2.40E-07	2.44E-07	1.46
283.15	3.40E-07	3.35E-07	1.53
288.15	4.60E-07	4.55E-07	0.98
293.15	5.90E-07	6.14E-07	4.00
298.15	8.30E-07	8.19E-07	1.34
298.15	8.41E-07	8.19E-07	2.59
303.15	1.10E-06	1.08E-06	1.53
308.15	1.42E-06	1.42E-06	0.03
313.15	1.81E-06	1.85E-06	2.02
313.15	1.90E-06	1.85E-06	2.74
318.15	2.38E-06	2.39E-06	0.22
323.15	3.03E-06	3.06E-06	0.87
328.15	3.84E-06	3.89E-06	1.28
333.15	4.83E-06	4.92E-06	1.77
338.15	6.03E-06	6.17E-06	2.37

Table E27: Analytical results and absolute deviations of the mole fraction of Hg in n.C_7 for the PR-MC EOS in the liquid phase

		k_{ij}=const	
T[K]	**x_{exp}**	**x_{calc}**	**Dx%**
273.15	2.00E-07	2.04E-07	1.99
278.15	2.90E-07	2.83E-07	2.32
283.15	3.70E-07	3.89E-07	5.14

Continuation of table E27			
288.15	5.40E-07	5.29E-07	2.10
293.15	7.00E-07	7.11E-07	1.61
298.15	9.70E-07	9.48E-07	2.28
303.15	1.26E-06	1.25E-06	0.63
308.15	1.63E-06	1.64E-06	0.59
313.15	2.20E-06	2.13E-06	3.20

Table E28: Analytical results and absolute deviations of the mole fraction of Hg in n.C_8 for the PR-MC EOS in the liquid phase

		k_{ij}=const	
T[K]	**x_{exp}**	**x_{calc}**	**Dx%**
273.15	2.50E-07	2.36E-07	5.46
278.15	3.30E-07	3.27E-07	0.91
283.15	4.70E-07	4.48E-07	4.78
288.15	6.10E-07	6.06E-07	0.61
293.15	7.90E-07	8.13E-07	2.96
298.15	1.10E-06	1.08E-06	1.72
303.15	1.40E-06	1.42E-06	1.74
308.15	1.78E-06	1.86E-06	4.55
313.15	2.30E-06	2.41E-06	4.88

Table E29: Analytical results and absolute deviations of the mole fraction of Hg in n.C_{10} for the PR-MC EOS in the liquid phase

		k_{ij}=const	
T[K]	**x_{exp}**	**x_{calc}**	**Dx%**
273.15	4.00E-07	2.93E-07	26.86
278.15	4.90E-07	4.04E-07	17.60
283.15	5.80E-07	5.51E-07	4.96
288.15	8.70E-07	7.45E-07	14.38
293.15	9.60E-07	9.97E-07	3.83
298.15	1.37E-06	1.32E-06	3.53
303.15	1.69E-06	1.74E-06	2.79
308.15	2.04E-06	2.26E-06	10.99
313.15	2.52E-06	2.93E-06	16.19
318.15	3.09E-06	3.76E-06	21.60

Table E30: Analytical results and absolute deviations of the mole fraction of Hg in 2.2-dm-C_4 for the PR-MC EOS in the liquid phase

		k_{ij}=const	
T[K]	**x_{exp}**	**x_{calc}**	**Dx%**
273.15	1.70E-07	1.33E-07	22.03
288.15	3.70E-07	3.54E-07	4.26
293.15	4.90E-07	4.81E-07	1.81
298.15	6.30E-07	6.47E-07	2.71
303.15	8.10E-07	8.62E-07	6.44
308.15	9.90E-07	1.14E-06	15.01

Table E31: Analytical results and absolute deviations of the mole fraction of Hg in 2.2.4-tm-C_5 for the PR-MC EOS in the liquid phase

		k_{ij}=const	
T[K]	**x_{exp}**	**x_{calc}**	**Dx%**
273.15	1.60E-07	1.38E-07	13.59
286.65	3.40E-07	3.40E-07	0.10
288.15	3.60E-07	3.85E-07	7.05
293.15	5.40E-07	5.09E-07	5.76
298.15	7.00E-07	6.87E-07	1.91
303.15	8.90E-07	9.18E-07	3.10
308.15	1.11E-06	1.22E-06	9.48

Table E32: Analytical results and absolute deviations of the mole fraction of Hg in cy-C_6 for the PR-MC EOS in the liquid phase

		k_{ij}=const	
T[K]	**x_{exp}**	**x_{calc}**	**Dx%**
288.15	8.20E-07	7.11E-07	13.31
293.15	1.02E-06	9.45E-07	7.35
298.15	1.32E-06	1.25E-06	5.68
298.15	1.20E-06	1.25E-06	3.98
303.15	1.62E-06	1.63E-06	0.39
308.15	1.92E-06	2.11E-06	9.73
313.15	2.47E-06	2.71E-06	9.64

Table E33: Analytical results and absolute deviations of the mole fraction of Hg in m-cy-C_6 for the PR-MC EOS in the liquid phase

		k_{ij}=const	
T[K]	**x_{exp}**	**x_{calc}**	**Dx%**
273.15	2.70E-07	2.56E-07	5.12
288.15	6.60E-07	6.52E-07	1.27
293.15	8.80E-07	8.72E-07	0.95
298.15	1.17E-06	1.16E-06	1.28
303.15	1.46E-06	1.52E-06	3.91
308.15	1.88E-06	1.98E-06	5.10

Table E34: Analytical results and absolute deviations of the mole fraction of Hg in cis-1.2-dm-cy-C_6 for the PR-MC EOS in the liquid phase

		k_{ij}=const	
T[K]	**x_{exp}**	**x_{calc}**	**Dx%**
289.15	8.10E-07	7.89E-07	2.62
293.15	1.06E-06	9.95E-07	6.14
298.15	1.36E-06	1.32E-06	2.75
303.15	1.71E-06	1.73E-06	1.31
308.15	2.06E-06	2.26E-06	9.54

Table E35: Analytical results and absolute deviations of the mole fraction of Hg in cis-1.4-dm-cy-C_6 for the PR-MC EOS in the liquid phase

		k_{ij}=const	
T[K]	**x_{exp}**	**x_{calc}**	**Dx%**
288.15	7.40E-07	7.24E-07	2.13
293.15	1.02E-06	9.72E-07	4.70
298.15	1.33E-06	1.29E-06	2.54
303.15	1.64E-06	1.70E-06	3.80
308.15	2.11E-06	2.22E-06	5.37

Table E36: Analytical results and absolute deviations of the mole fraction of Hg in trans-1.2-dm-cy-C_6 for the PR-MC EOS in the liquid phase

		k_{ij}=const	
T[K]	**x_{exp}**	**x_{calc}**	**Dx%**
288.15	6.90E-07	6.63E-07	3.84
293.15	9.10E-07	8.89E-07	2.27
298.15	1.23E-06	1.18E-06	4.30
303.15	1.55E-06	1.55E-06	0.26

Continuation of table E36			
308.15	1.85E-06	2.03E-06	9.59

Table E37: Analytical results and absolute deviations of the mole fraction of Hg in trans-1.4-dm-cy-C_6 for the PR-MC EOS in the liquid phase

		k_{ij}=const	
T[K]	**x_{exp}**	**x_{calc}**	**Dx%**
288.15	6.90E-07	6.59E-07	4.57
293.15	9.10E-07	8.86E-07	2.68
298.15	1.22E-06	1.18E-06	3.23
303.15	1.55E-06	1.56E-06	0.44
308.15	1.86E-06	2.04E-06	9.52

Table E38: Analytical results and absolute deviations of the mole fraction of Hg in benzene for the PR-MC EOS in the liquid phase

		k_{ij}=const	
T[K]	**x_{exp}**	**x_{calc}**	**Dx%**
288.15	5.80E-07	6.04E-07	4.12
293.15	7.90E-07	8.03E-07	1.69
295.65	9.27E-07	9.23E-07	0.39
298.15	1.06E-06	1.06E-06	0.09
298.15	1.07E-06	1.06E-06	1.38
303.15	1.37E-06	1.38E-06	1.02
308.15	1.91E-06	1.79E-06	6.08

Table E39: Analytical results and absolute deviations of the mole fraction of Hg in toluene for the PR-MC EOS in the liquid phase

		k_{ij}=const	
T[K]	**x_{exp}**	**x_{calc}**	**Dx%**
273.15	3.20E-07	3.00E-07	6.38
288.15	6.90E-07	7.46E-07	8.08
293.15	1.03E-06	9.91E-07	3.80
298.15	1.28E-06	1.30E-06	1.91
298.15	1.33E-06	1.30E-06	2.06
303.15	1.73E-06	1.70E-06	1.58
308.15	2.14E-06	2.20E-06	2.99

Table E40: Analytical results and absolute deviations of the mole fraction of Hg in o-xylene for the PR-MC EOS in the liquid phase

		k_{ij}=const	
T[K]	**x_{exp}**	**x_{calc}**	**Dx%**
273.15	3.10E-07	3.33E-07	7.56
293.15	1.12E-06	1.10E-06	2.02
298.15	1.45E-06	1.44E-06	0.47
303.15	1.89E-06	1.88E-06	0.43
308.15	2.62E-06	2.43E-06	7.11

Table E41: Analytical results and absolute deviations of the mole fraction of Hg in N_2 for the PR-MC EOS in the vapor phase

Confidential data

Table E42: Analytical results and absolute deviations of the mole fraction of Hg in water for the PR-MC EOS

kij	T [K]	P [bar]	Mole fraction of Hg (exp)	Mole fraction of Hg (calc)	abs dev %
0.5736	273.15	1	3.73E-09	2.70E-09	27.68
0.5859	278.15	1	3.91E-09	3.13E-09	20.00
0.5981	283.15	1	4.15E-09	3.63E-09	12.59
0.6104	288.15	1	4.46E-09	4.19E-09	6.06
0.6227	293.15	1	4.83E-09	4.83E-09	0.00
0.6350	298.15	1	5.28E-09	5.56E-09	5.30
0.6473	303.15	1	5.83E-09	6.39E-09	9.60
0.6595	308.15	1	6.48E-09	7.35E-09	13.36
0.6718	313.15	1	7.27E-09	8.42E-09	15.78
0.6841	318.15	1	8.20E-09	9.63E-09	17.47
0.6964	323.15	1	9.31E-09	1.10E-08	18.25
0.7086	328.15	1	1.06E-08	1.26E-08	18.76
0.7209	333.15	1	1.22E-08	1.44E-08	17.66
0.7332	338.15	1	1.41E-08	1.64E-08	15.96
0.7455	343.15	1	1.64E-08	1.86E-08	13.45
0.7578	348.15	1	1.91E-08	2.12E-08	10.75
0.7700	353.15	1	2.24E-08	2.41E-08	7.44
0.7823	358.15	1	2.63E-08	2.73E-08	3.86
0.7946	363.15	1	3.10E-08	3.10E-08	0.00
0.8192	373.15	1	4.36E-08	3.98E-08	8.77
0.8437	383.15	1	6.21E-08	5.10E-08	17.83
0.8683	393.15	1	8.91E-08	6.52E-08	26.78

Appendix F

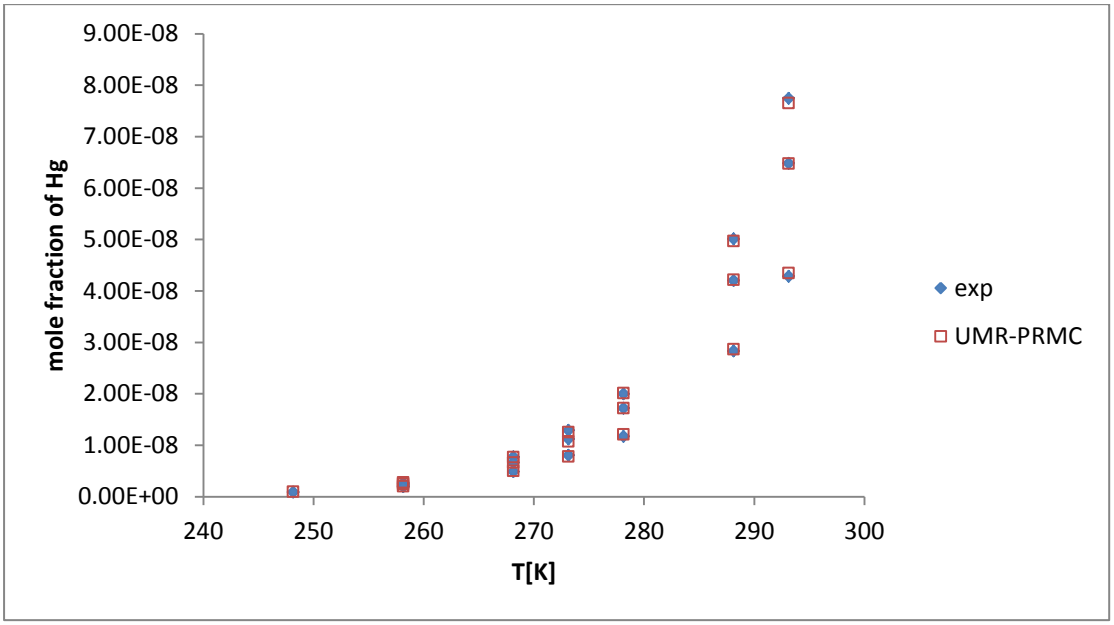

Figure F1: Mole fraction of Hg in methane calculated with the UMR-PRMC model in the vapor phase

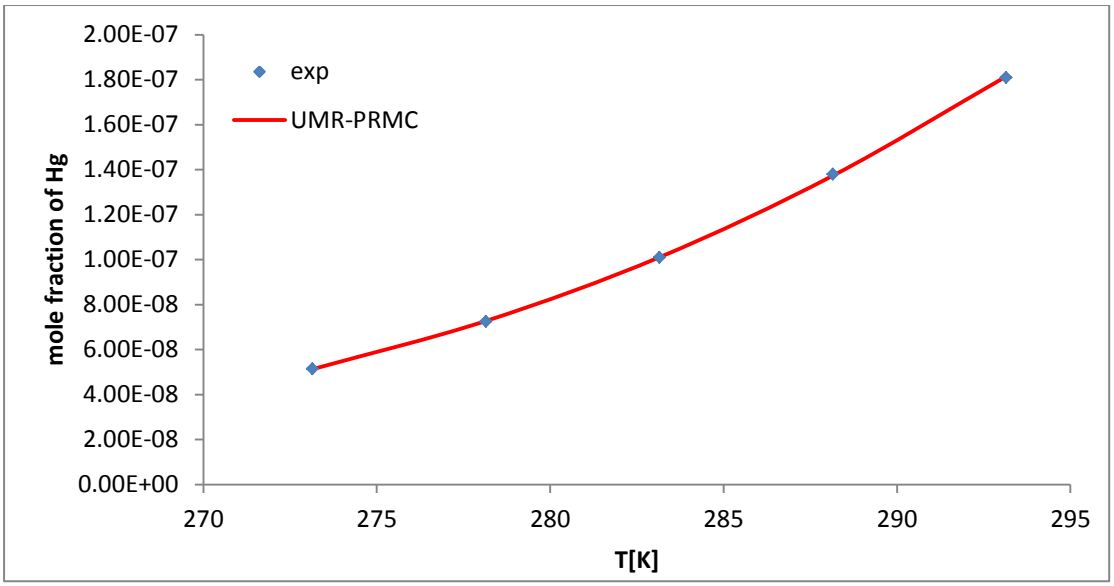

Figure F2: Mole fraction of Hg in ethane calculated with the UMR-PRMC model in the liquid phase

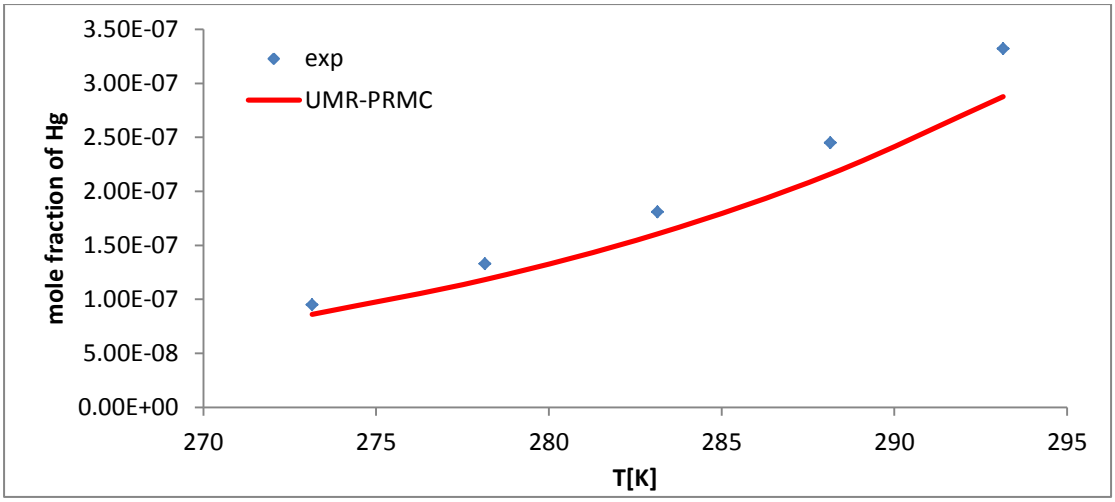

Figure F3: Mole fraction of Hg in propane calculated with the UMR-PRMC model in the liquid phase

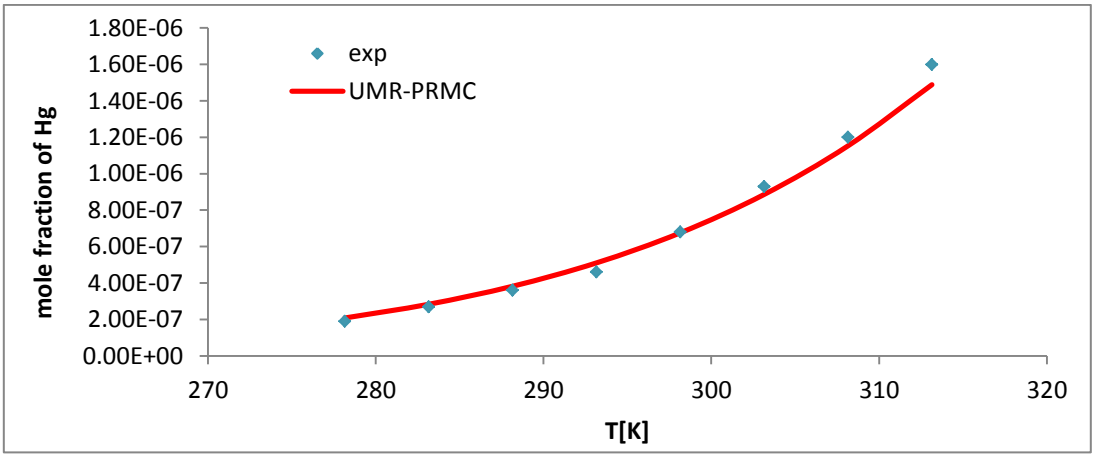

Figure F4: Mole fraction of Hg in n.C_5 calculated with the UMR-PRMC model in the liquid phase

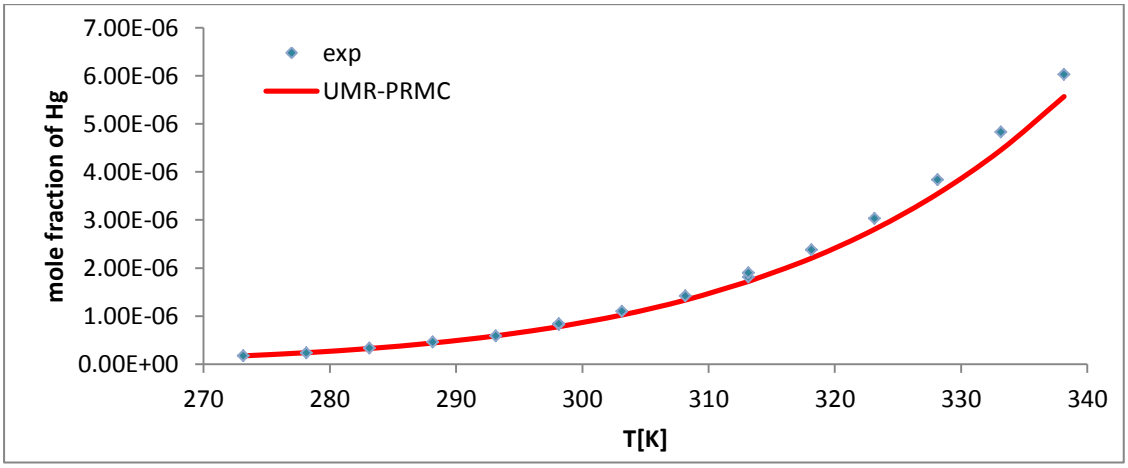

Figure F5: Mole fraction of Hg in n.C_6 calculated with the UMR-PRMC model in the liquid phase

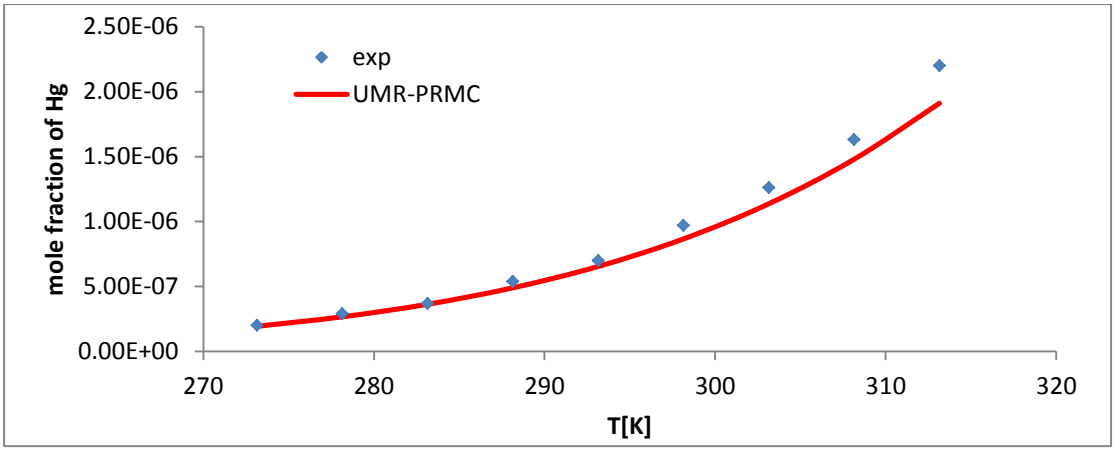

Figure F6: Mole fraction of Hg in n.C_7 calculated with the UMR-PRMC model in the liquid phase

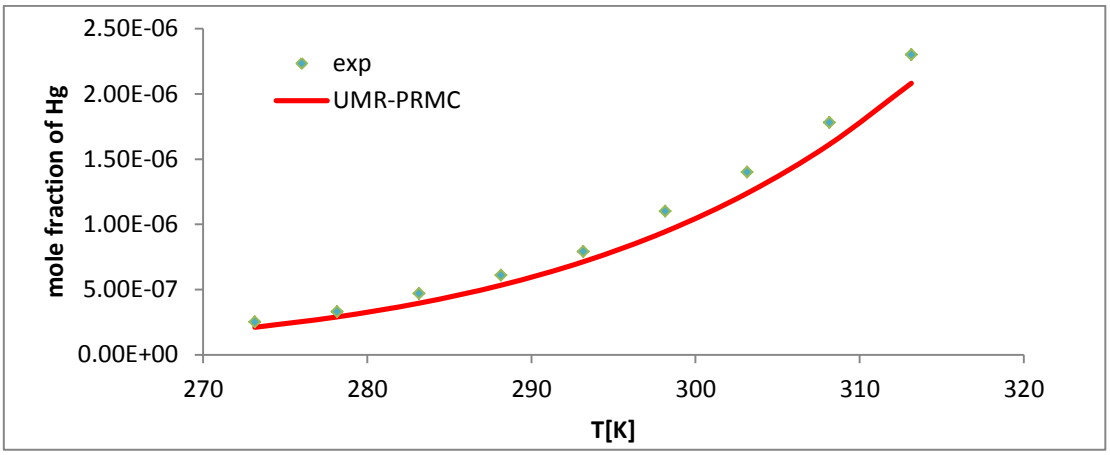

Figure F7: Mole fraction of Hg in n.C_8 calculated with the UMR-PRMC model in the liquid phase

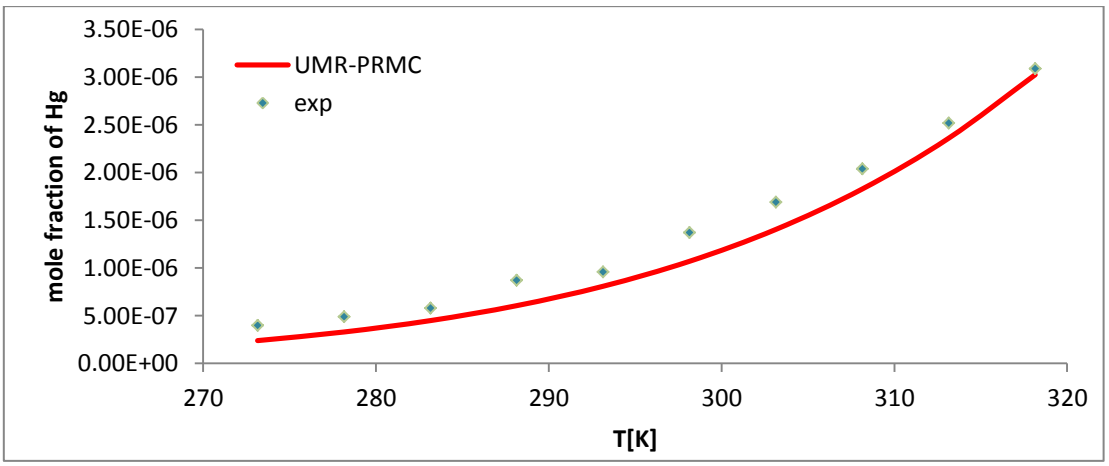

Figure F8: Mole fraction of Hg in n.C_{10} calculated with the UMR-PRMC model in the liquid phase

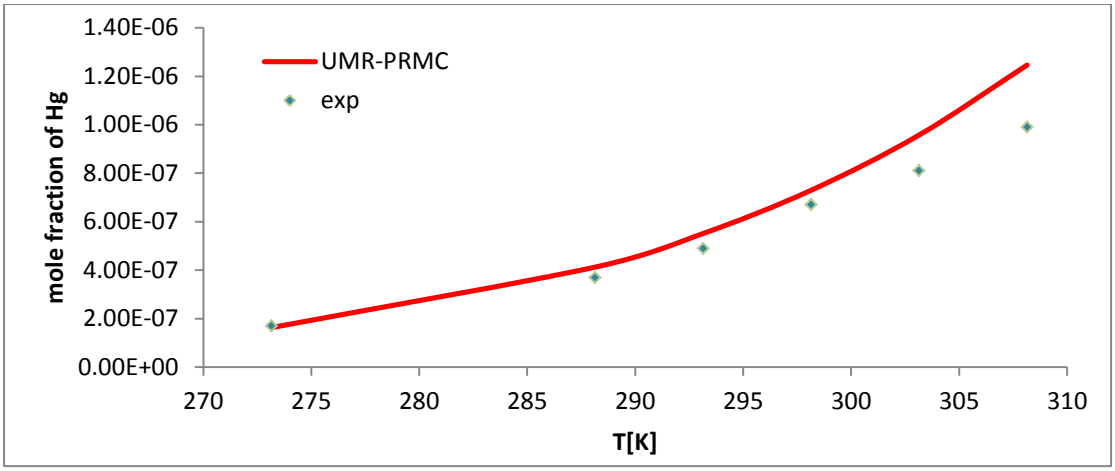

Figure F9: Mole fraction of Hg in 2.2-dm-C_4 calculated with the UMR-PRMC model in the liquid phase

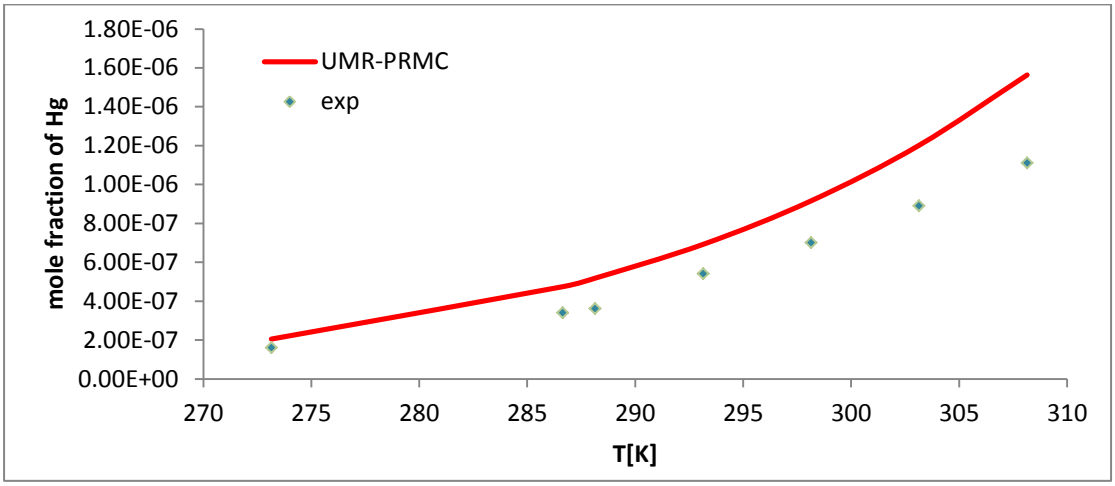

Figure F10: Mole fraction of Hg in 2.2.4-tm-C_5 calculated with the UMR-PRMC model in the liquid phase

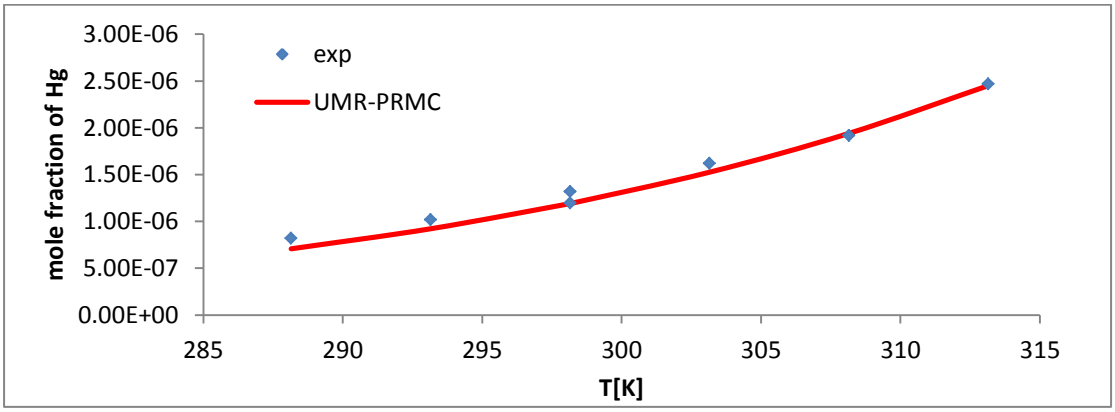

Figure F11: Mole fraction of Hg in cy-C_6 calculated the UMR-PRMC model in the liquid phase

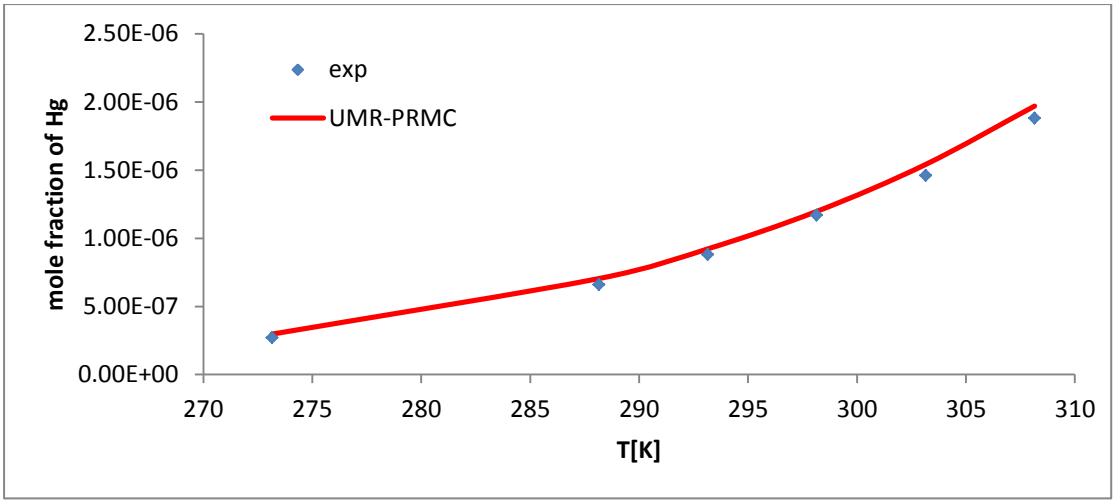

Figure F12: Mole fraction of Hg in m-cy-C_6 calculated with the UMR-PRMC model in the liquid phase

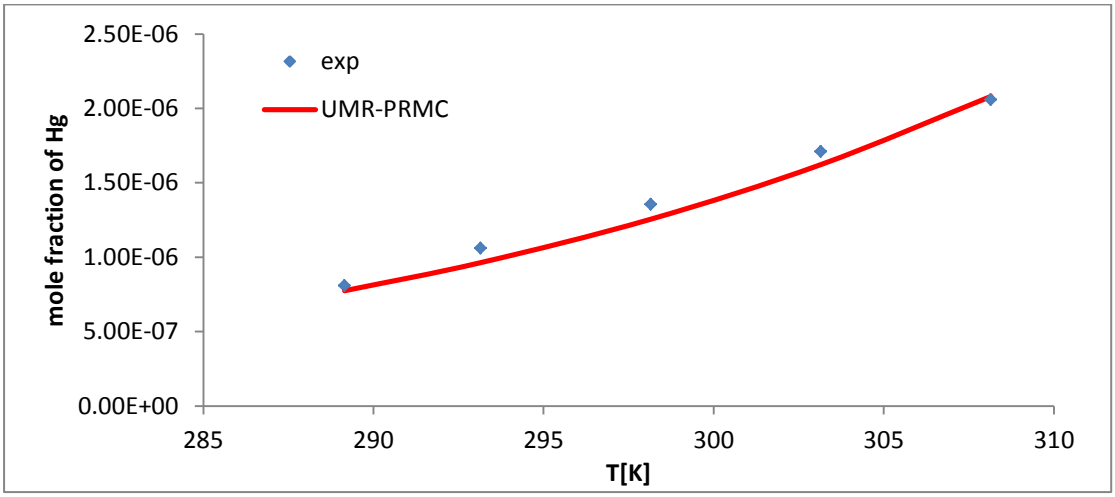

Figure F13: Mole fraction of Hg in cis-1.2-dm-cy-C_6 calculated with the UMR-PRMC model in the liquid phase

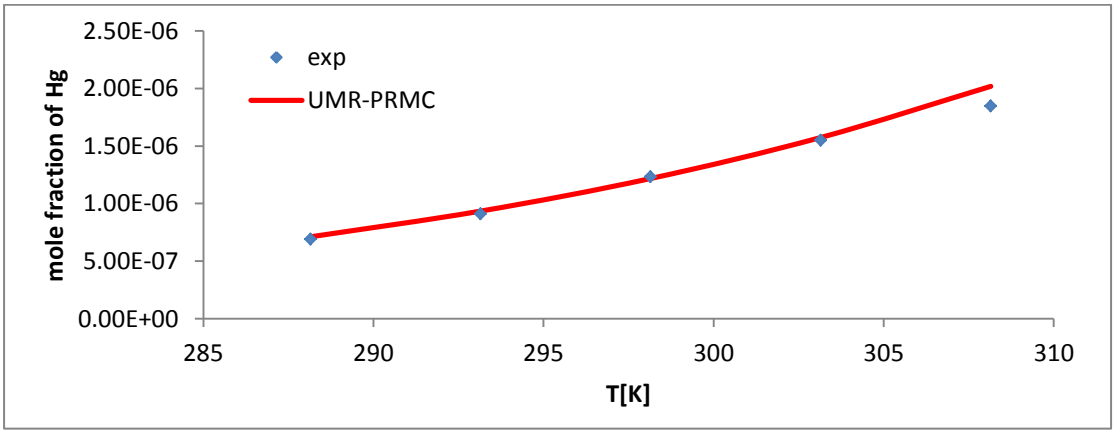

Figure F14: Mole fraction of Hg in trans-1.2-dm-cy-C_6 calculated with the UMR-PRMC model in the liquid phase

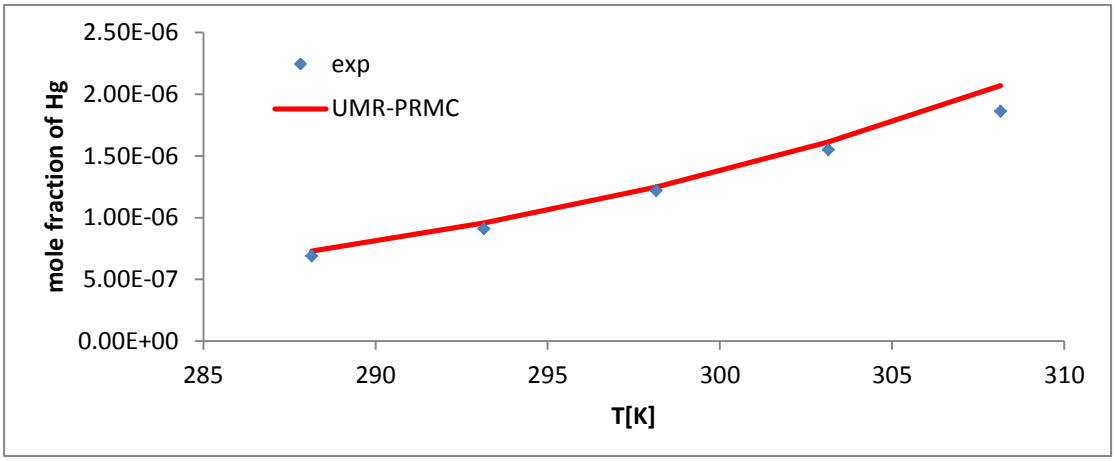

Figure F15: Mole fraction of Hg in trans-1.4-dm-cy-C_6 calculated with the UMR-PRMC model in the liquid phase

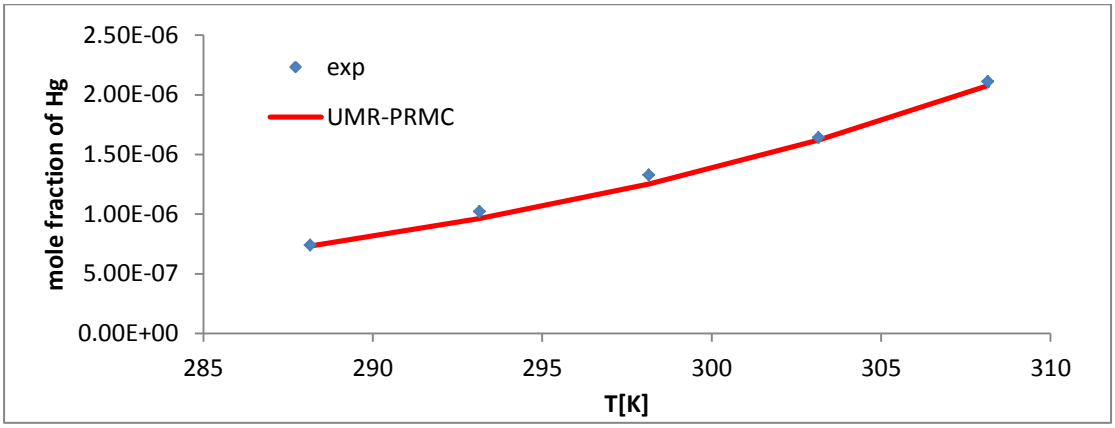

Figure F16: Mole fraction of Hg in cis-1.4-dm-cy-C_6 calculated the UMR-PRMC model in the liquid phase

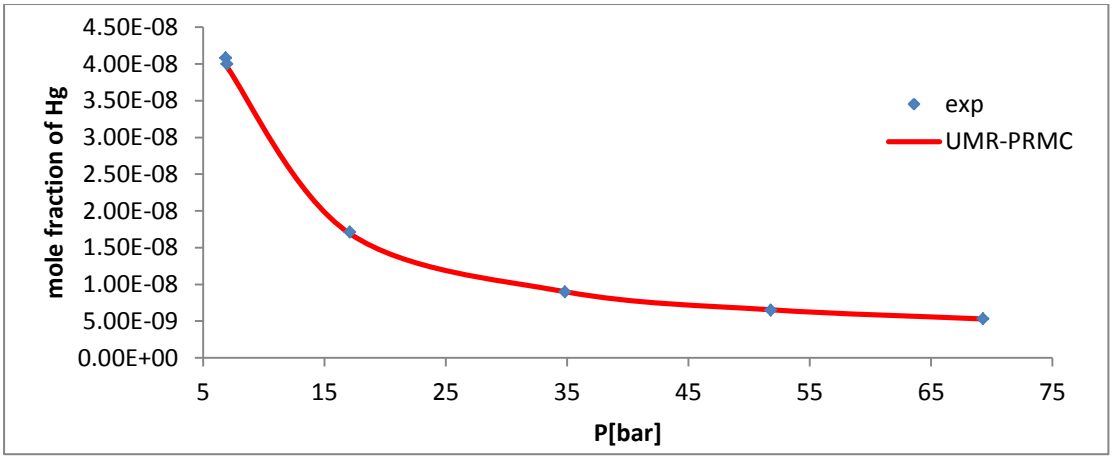

Figure F17: Mole fraction of Hg in N_2 calculated with the UMR-PRMC model in the vapor phase

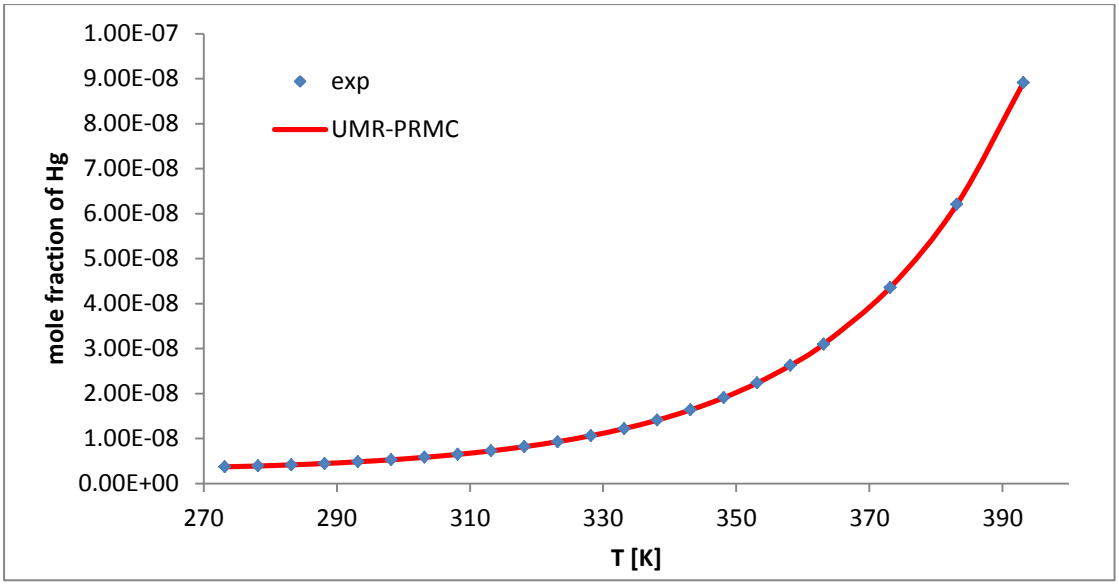

Figure F18: Mole fraction of Hg in water calculated with the UMR-PRMC model

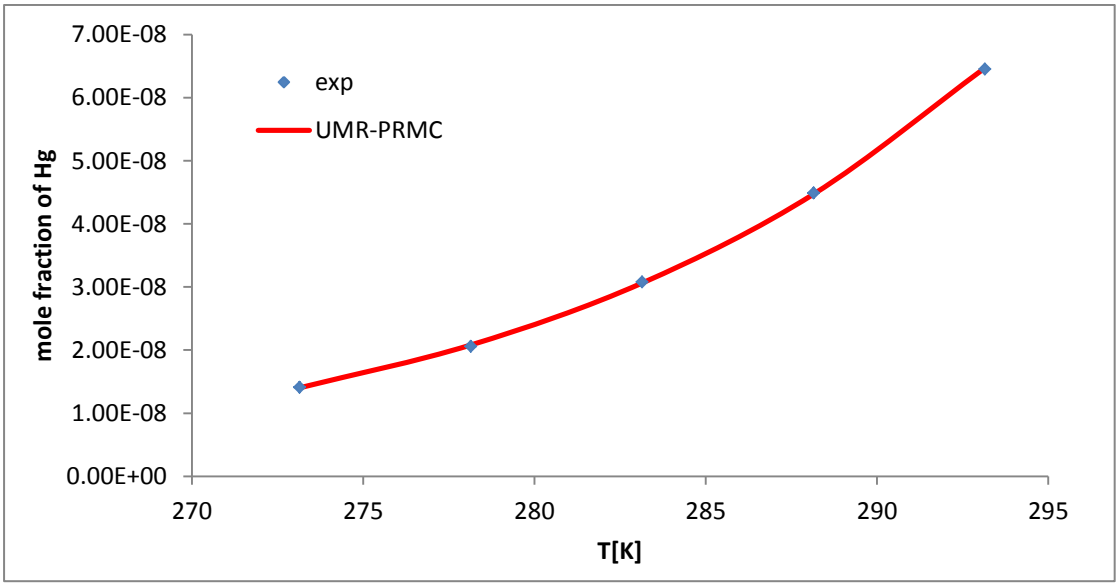

Figure F19: Mole fraction of Hg in CO_2 calculated with the UMR-PRMC model

Table F1: Analytical results and absolute deviations of the mole fraction of Hg in methane for the UMR-PRMC model in the vapor phase

Confidential data

Table F2: Analytical results and absolute deviations of the mole fraction of Hg in ethane for the UMR-PRMC model in the liquid phase

Confidential data

Table F3: Analytical results and absolute deviations of the mole fraction of Hg in propane for the UMR-PRMC model in the liquid phase

Confidential data

Table F4: Analytical results and absolute deviations of the mole fraction of Hg in n.C_5 for the UMR-PRMC model in the liquid phase

T[K]	P[bar]	x_{exp}	x_{calc}	Dx%
278.15	1.00	1.90E-07	2.08E-07	9.52
283.15	1.00	2.70E-07	2.83E-07	4.99
288.15	1.00	3.60E-07	3.82E-07	6.18
293.15	1.00	4.60E-07	5.10E-07	10.97
298.15	1.00	6.80E-07	6.76E-07	0.66
303.15	1.00	9.30E-07	8.86E-07	4.71
308.15	1.00	1.20E-06	1.15E-06	3.91
313.15	1.00	1.60E-06	1.49E-06	6.97

Table F5: Analytical results and absolute deviations of the mole fraction of Hg in n.C_6 for the UMR-PRMC model in the liquid phase

T[K]	P[bar]	x_{exp}	x_{calc}	Dx%
273.15	1.00	1.80E-07	1.74E-07	3.11
278.15	1.00	2.40E-07	2.40E-07	0.10
283.15	1.00	3.40E-07	3.27E-07	3.72
288.15	1.00	4.60E-07	4.42E-07	4.01
293.15	1.00	5.90E-07	5.90E-07	0.03
298.15	1.00	8.30E-07	7.81E-07	5.94
298.15	1.00	8.41E-07	7.81E-07	7.14
303.15	1.00	1.10E-06	1.02E-06	6.88
308.15	1.00	1.42E-06	1.33E-06	6.12
313.15	1.00	1.81E-06	1.72E-06	4.97
313.15	1.00	1.90E-06	1.72E-06	9.41
318.15	1.00	2.38E-06	2.21E-06	7.32
323.15	1.00	3.03E-06	2.81E-06	7.36
328.15	1.00	3.84E-06	3.55E-06	7.61
333.15	1.00	4.83E-06	4.46E-06	7.76
338.15	1.00	6.03E-06	5.57E-06	7.69

Table F6: Analytical results and absolute deviations of the mole fraction of Hg in n.C_7 for the UMR-PRMC model in the liquid phase

T[K]	P[bar]	x_{exp}	x_{calc}	Dx%
273.15	1.00	2.00E-07	1.94E-07	3.19
278.15	1.00	2.90E-07	2.67E-07	8.03
283.15	1.00	3.70E-07	3.63E-07	1.78
288.15	1.00	5.40E-07	4.90E-07	9.22
293.15	1.00	7.00E-07	6.55E-07	6.45
298.15	1.00	9.70E-07	8.67E-07	10.65
303.15	1.00	1.26E-06	1.14E-06	9.74
308.15	1.00	1.63E-06	1.48E-06	9.20
313.15	1.00	2.20E-06	1.91E-06	13.14

Table F7: Analytical results and absolute deviations of the mole fraction of Hg in n.C_8 for the UMR-PRMC model in the liquid phase

T[K]	P[bar]	x_{exp}	x_{calc}	Dx%
273.15	1.00	2.50E-07	2.11E-07	15.76
278.15	1.00	3.30E-07	2.90E-07	12.06
283.15	1.00	4.70E-07	3.96E-07	15.84
288.15	1.00	6.10E-07	5.34E-07	12.51
293.15	1.00	7.90E-07	7.13E-07	9.74
298.15	1.00	1.10E-06	9.44E-07	14.18
303.15	1.00	1.40E-06	1.24E-06	11.51
308.15	1.00	1.78E-06	1.61E-06	9.41
313.15	1.00	2.30E-06	2.08E-06	9.47

Table F8: Analytical results and absolute deviations of the mole fraction of Hg in n.C_{10} for the UMR-PRMC model in the liquid phase

T[K]	P[bar]	x_{exp}	x_{calc}	Dx%
273.15	1.00	4.00E-07	2.39E-07	40.29
278.15	1.00	4.90E-07	3.29E-07	32.84
283.15	1.00	5.80E-07	4.49E-07	22.67
288.15	1.00	8.70E-07	6.05E-07	30.45
293.15	1.00	9.60E-07	8.08E-07	15.78
298.15	1.00	1.37E-06	1.07E-06	21.88
303.15	1.00	1.69E-06	1.40E-06	16.89
308.15	1.00	2.04E-06	1.83E-06	10.39
313.15	1.00	2.52E-06	2.36E-06	6.33
318.15	1.00	3.09E-06	3.03E-06	2.10

Table F9: Analytical results and absolute deviations of the mole fraction of Hg in 2.2-dm-C_4 for the UMR-PRMC model in the liquid phase

T[K]	P[bar]	x_{exp}	x_{calc}	Dx%
273.15	1.00	1.70E-07	1.63E-07	4.01
288.15	1.00	3.70E-07	4.13E-07	11.61
293.15	1.00	4.90E-07	5.52E-07	12.57
298.15	1.00	6.30E-07	7.30E-07	8.96
303.15	1.00	8.10E-07	9.58E-07	18.25
308.15	1.00	9.90E-07	1.25E-06	25.91

Table F10: Analytical results and absolute deviations of the mole fraction of Hg in 2.2.4-tm-C_5 for the UMR-PRMC model in the liquid phase

T[K]	P[bar]	x_{exp}	x_{calc}	Dx%
273.15	1.00	1.60E-07	2.05E-07	28.12
286.65	1.00	3.40E-07	4.74E-07	39.56
288.15	1.00	3.60E-07	5.18E-07	44.02
293.15	1.00	5.40E-07	6.92E-07	28.22
298.15	1.00	7.00E-07	9.16E-07	30.88
303.15	1.00	8.90E-07	1.20E-06	35.03
308.15	1.00	1.11E-06	1.56E-06	40.86
318.15	1.00	3.09E-06	2.05E-07	28.12

Table F11: Analytical results and absolute deviations of the mole fraction of Hg in cy-C_6 for the UMR-PRMC model in the liquid phase

T[K]	P[bar]	x_{exp}	x_{calc}	Dx%
288.15	1.00	8.20E-07	7.08E-07	13.68
293.15	1.00	1.02E-06	9.22E-07	9.62
298.15	1.00	1.32E-06	1.19E-06	9.79
298.15	1.00	1.20E-06	1.19E-06	0.56
303.15	1.00	1.62E-06	1.53E-06	5.81
308.15	1.00	1.92E-06	1.94E-06	1.08
313.15	1.00	2.47E-06	2.45E-06	0.77

Table F12: Analytical results and absolute deviations of the mole fraction of Hg in m-cy-C_6 for the UMR-PRMC model in the liquid phase

T[K]	P[bar]	x_{exp}	x_{calc}	Dx%
273.15	1.00	2.70E-07	2.97E-07	9.95

Continuation of table F12				
288.15	1.00	6.60E-07	7.04E-07	6.72
293.15	1.00	8.80E-07	9.22E-07	4.79
298.15	1.00	1.17E-06	1.20E-06	2.31
303.15	1.00	1.46E-06	1.54E-06	5.58
308.15	1.00	1.88E-06	1.97E-06	4.78

Table F13: Analytical results and absolute deviations of the mole fraction of Hg in cis-1.2-dm-cy-C_6 for the UMR-PRMC model in the liquid phase

T[K]	P[bar]	x_{exp}	x_{calc}	Dx%
289.15	1.00	8.10E-07	7.74E-07	4.38
293.15	1.00	1.06E-06	9.63E-07	9.14
298.15	1.00	1.36E-06	1.26E-06	7.44
303.15	1.00	1.71E-06	1.62E-06	5.14
308.15	1.00	2.06E-06	2.08E-06	0.99

Table F14: Analytical results and absolute deviations of the mole fraction of Hg in cis-1.4-dm-cy-C_6 for the UMR-PRMC model in the liquid phase

T[K]	P[bar]	x_{exp}	x_{calc}	Dx%
288.15	1.00	7.40E-07	7.32E-07	1.02
293.15	1.00	1.02E-06	9.62E-07	5.65
298.15	1.00	1.33E-06	1.25E-06	5.45
303.15	1.00	1.64E-06	1.62E-06	1.23
308.15	1.00	2.11E-06	2.08E-06	1.58

Table F15: Analytical results and absolute deviations of the mole fraction of Hg in trans-1.2-dm-cy-C_6 for the UMR-PRMC model in the liquid phase

T[K]	P[bar]	x_{exp}	x_{calc}	Dx%
288.15	1.00	6.90E-07	7.11E-07	3.08
293.15	1.00	9.10E-07	9.35E-07	2.73
298.15	1.00	1.23E-06	1.22E-06	1.28
303.15	1.00	1.55E-06	1.57E-06	1.59
308.15	1.00	1.85E-06	2.02E-06	9.16

Table F16: Analytical results and absolute deviations of the mole fraction of Hg in trans-1.4- dm-cy-C_6 for the UMR-PRMC model in the liquid phase

T[K]	P[bar]	x_{exp}	x_{calc}	Dx%
288.15	1.00	6.90E-07	7.29E-07	5.72

Continuation of table F16				
293.15	1.00	9.10E-07	9.59E-07	5.34
298.15	1.00	1.22E-06	1.25E-06	2.45
303.15	1.00	1.55E-06	1.61E-06	4.11
308.15	1.00	1.86E-06	2.07E-06	11.23

Table F17: Analytical results and absolute deviations of the mole fraction of Hg in benzene for the UMR-PRMC model in the liquid phase (separate fit)

T[K]	**P[bar]**	**x_{exp}**	**x_{calc}**	**Dx%**
288.15	1.00	5.80E-07	5.79E-07	0.11
293.15	1.00	7.90E-07	7.88E-07	0.24
295.65	1.00	9.27E-07	8.89E-07	4.12
298.15	1.00	1.06E-06	1.06E-06	0.12
298.15	1.00	1.07E-06	1.06E-06	1.17
303.15	1.00	1.37E-06	1.42E-06	3.32
308.15	1.00	1.91E-06	1.87E-06	2.06

Table F18: Analytical results and absolute deviations of the mole fraction of Hg in toluene for the UMR-PRMC model in the liquid phase (separate fit)

T[K]	**P[bar]**	**x_{exp}**	**x_{calc}**	**Dx%**
273.15	1.00	3.20E-07	2.89E-07	9.65
288.15	1.00	6.90E-07	7.35E-07	6.56
293.15	1.00	1.03E-06	9.83E-07	4.54
298.15	1.00	1.28E-06	1.30E-06	1.76
298.15	1.00	1.33E-06	1.30E-06	2.21
303.15	1.00	1.73E-06	1.71E-06	1.15
308.15	1.00	2.14E-06	2.23E-06	4.04

Table F19: Analytical results and absolute deviations of the mole fraction of Hg in o-xylene for the UMR-PRMC model in the liquid phase (separate fit)

T[K]	**P[bar]**	**x_{exp}**	**x_{calc}**	**Dx%**
273.15	1.00	3.10E-07	3.22E-07	3.92
293.15	1.00	1.12E-06	1.10E-06	1.40
298.15	1.00	1.45E-06	1.47E-06	1.09
303.15	1.00	1.89E-06	1.93E-06	2.01
308.15	1.00	2.62E-06	2.51E-06	4.02

Table F20: Analytical results and absolute deviations of the mole fraction of Hg in benzene for the UMR-PRMC model in the liquid phase (simultaneous fit)

T[K]	P[bar]	x_{exp}	x_{calc}	Dx%
288.15	1.00	5.80E-07	6.03E-07	3.90
293.15	1.00	7.90E-07	8.04E-07	1.74
295.65	1.00	9.27E-07	9.00E-07	2.96
298.15	1.00	1.06E-06	1.06E-06	0.20
298.15	1.00	1.07E-06	1.06E-06	1.09
303.15	1.00	1.37E-06	1.39E-06	1.54
308.15	1.00	1.91E-06	1.81E-06	5.40

Table F21: Analytical results and absolute deviations of the mole fraction of Hg in toluene for the UMR-PRMC model in the liquid phase (simultaneous fit)

T[K]	P[bar]	x_{exp}	x_{calc}	Dx%
273.15	1.00	3.20E-07	2.80E-07	12.54
288.15	1.00	6.90E-07	7.26E-07	5.27
293.15	1.00	1.03E-06	9.77E-07	5.10
298.15	1.00	1.28E-06	1.30E-06	1.77
298.15	1.00	1.33E-06	1.30E-06	2.20
303.15	1.00	1.73E-06	1.72E-06	0.56
308.15	1.00	2.14E-06	2.25E-06	5.25

Table F22: Analytical results and absolute deviations of the mole fraction of Hg in o-xylene for the UMR-PRMC model in the liquid phase (simultaneous fit)

T[K]	P[bar]	x_{exp}	x_{calc}	Dx%
273.15	1.00	3.10E-07	3.27E-07	5.57
293.15	1.00	1.12E-06	1.11E-06	1.11
298.15	1.00	1.45E-06	1.47E-06	1.09
303.15	1.00	1.89E-06	1.92E-06	1.75
308.15	1.00	2.62E-06	2.50E-06	4.51

Table F23: Analytical results and absolute deviations of the mole fraction of Hg in N_2 for the UMR-PRMC model in the vapor phase

Confidential data

Table F24: Analytical results and absolute deviations of the mole fraction of Hg in water for the UMR-PRMC model

T [K]	P [bar]	Mole fraction of Hg (exp)	Mole fraction of Hg (calc)	abs dev %
273.15	1	3.73E-09	3.72E-09	0.17
278.15	1	3.91E-09	3.91E-09	0.04
283.15	1	4.15E-09	4.15E-09	0.11
288.15	1	4.46E-09	4.46E-09	0.02
293.15	1	4.83E-09	4.83E-09	0.05
298.15	1	5.28E-09	5.29E-09	0.10
303.15	1	5.83E-09	5.83E-09	0.00
308.15	1	6.48E-09	6.48E-09	0.04
313.15	1	7.27E-09	7.26E-09	0.10
318.15	1	8.20E-09	8.19E-09	0.08
323.15	1	9.31E-09	9.30E-09	0.07
328.15	1	1.06E-08	1.06E-08	0.27
333.15	1	1.22E-08	1.22E-08	0.10
338.15	1	1.41E-08	1.41E-08	0.04
343.15	1	1.64E-08	1.64E-08	0.16
348.15	1	1.91E-08	1.91E-08	0.04
353.15	1	2.24E-08	2.24E-08	0.18
358.15	1	2.63E-08	2.63E-08	0.04
363.15	1	3.10E-08	3.10E-08	0.07
373.15	1	4.36E-08	4.36E-08	0.06
383.15	1	6.21E-08	6.21E-08	0.05
393.15	1	8.91E-08	8.92E-08	0.09

Table F25: Analytical results and absolute deviations of the mole fraction of Hg in CO_2 for the UMR-PRMC model in the liquid phase

Confidential data

Appendix G

Table G1: B.P.P calculation with the UMR-PRMC model for the estimation of the mole fraction of Hg in ethane in the vapor phase

Confidential data

Table G2: B.P.P calculation with the PR-MC model for the estimation of the mole fraction of Hg in ethane in the vapor phase

Confidential data

Table G3: B.P.P calculation with the SRK-Twu model for the estimation of the mole fraction of Hg in ethane in the vapor phase

Confidential data

Table G4: B.P.P calculation with the UMR-PRMC model for the estimation of the mole fraction of Hg in propane in the vapor phase

Confidential data

Table G5: B.P.P calculation with the PR-MC model for the estimation of the mole fraction of Hg in propane in the vapor phase

Confidential data

Table G6: B.P.P calculation with the SRK-Twu model for the estimation of the mole fraction of Hg in propane in the vapor phase

Confidential data

Table G7: B.P.P calculation with the UMR-PRMC model for the estimation of the mole fraction of Hg in CO_2 in the vapor phase

Confidential data

Table G8: B.P.P calculation with the PR-MC model for the estimation of the mole fraction of Hg in CO_2 in the vapor phase

Confidential data

Table G9: B.P.P calculation with the SRK-Twu model for the estimation of the mole fraction of Hg in CO_2 in the vapor phase

Confidential data

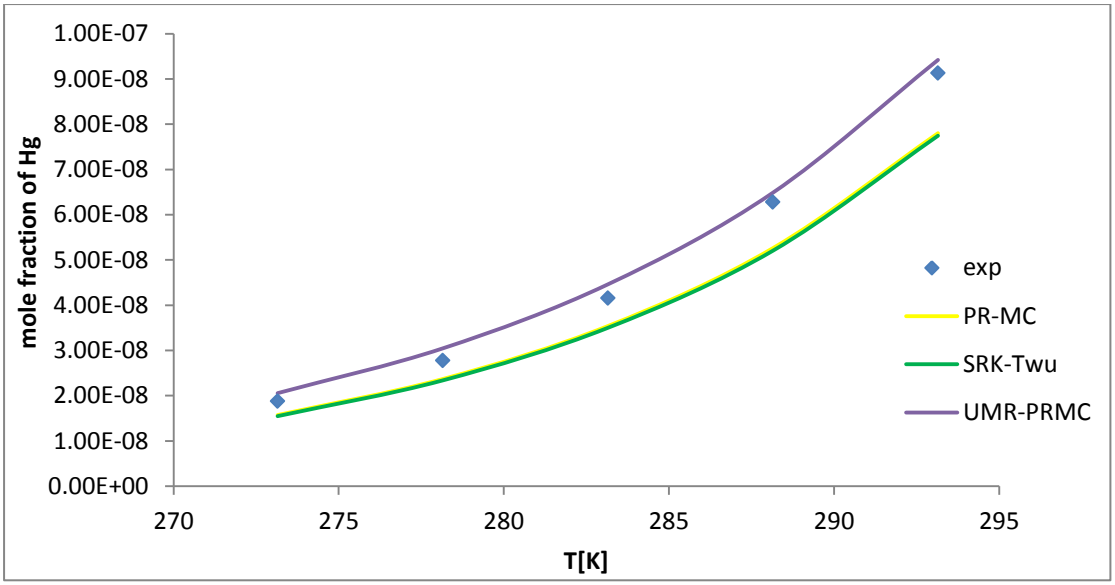

Figure G1: Mole fractions of Hg with ethane in the vapor phase estimated by all models by B.P.P calculation

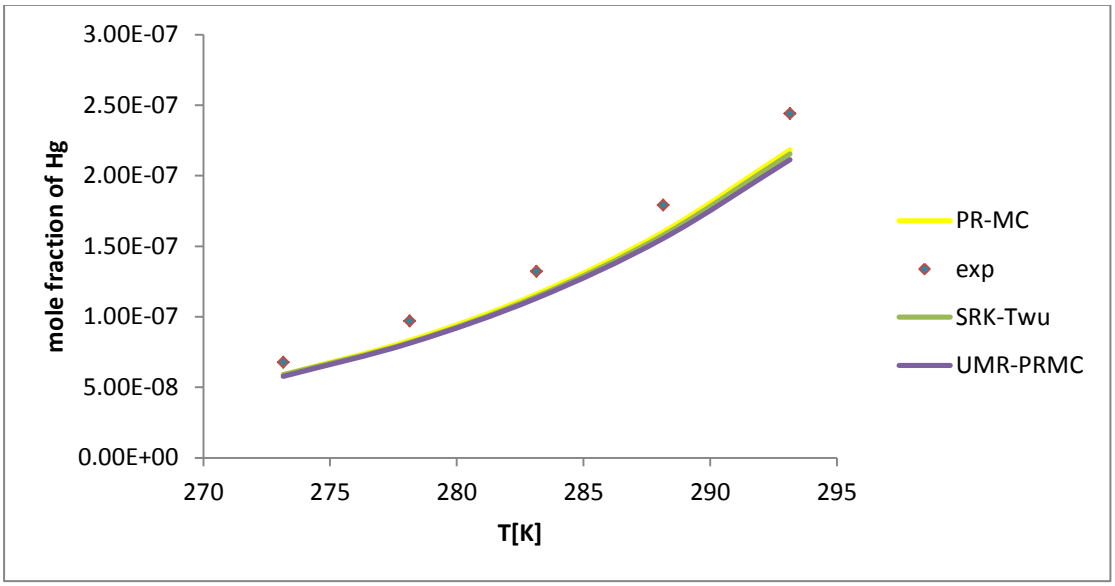

Figure G2: Mole fractions of Hg with propane in the vapor phase estimated by all models by B.P.P calculation

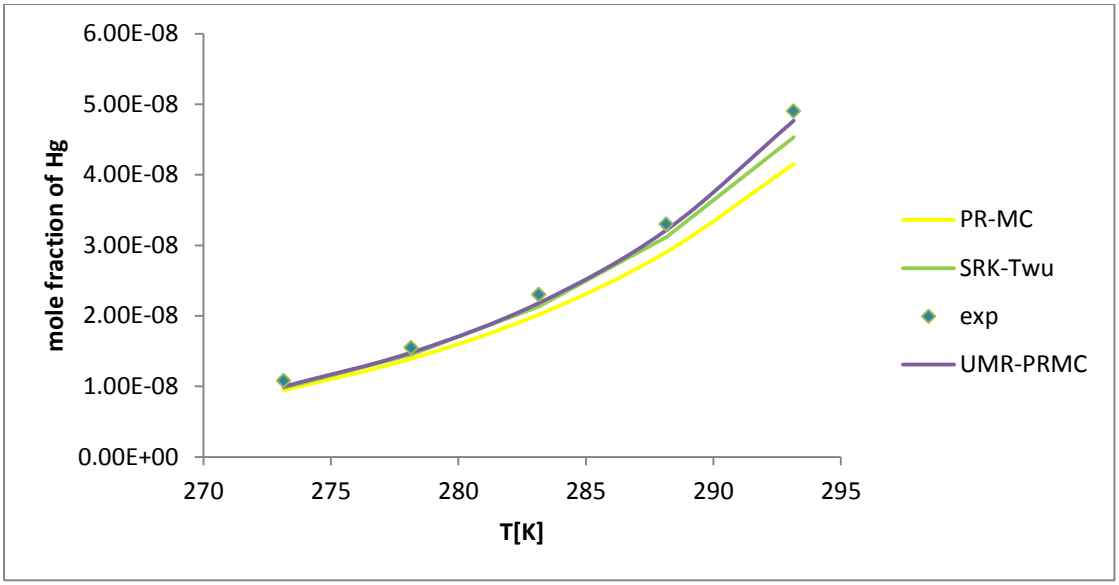

Figure G3: Mole fractions of Hg with CO_2 in the vapor phase estimated by all models by B.P.P calculation

Appendix H

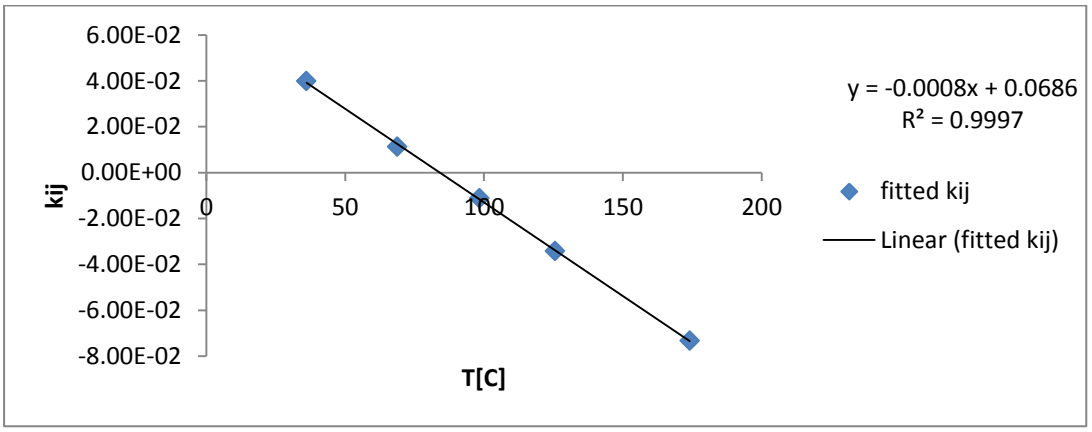

Figure H1: Generalized correlations for the PR-MC's k_{ij} parameters of paraffinic HCs based on their T_b property

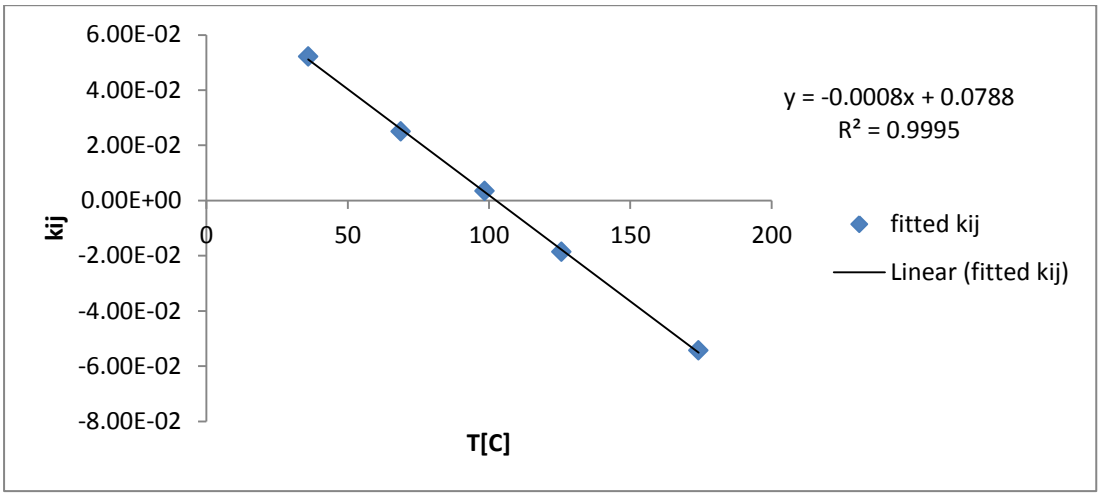

Figure H2: Generalized correlations for the SRK-Twu's k_{ij} parameters of paraffinic HCs based on their T_b property

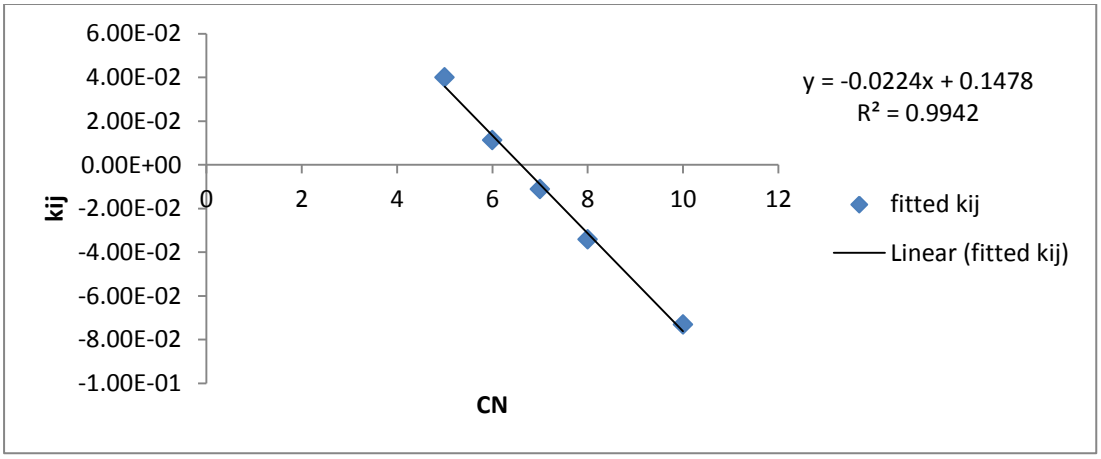

Figure H3: Generalized correlations for the PR-MC's k_{ij} parameters of paraffinic HCs based on their CN

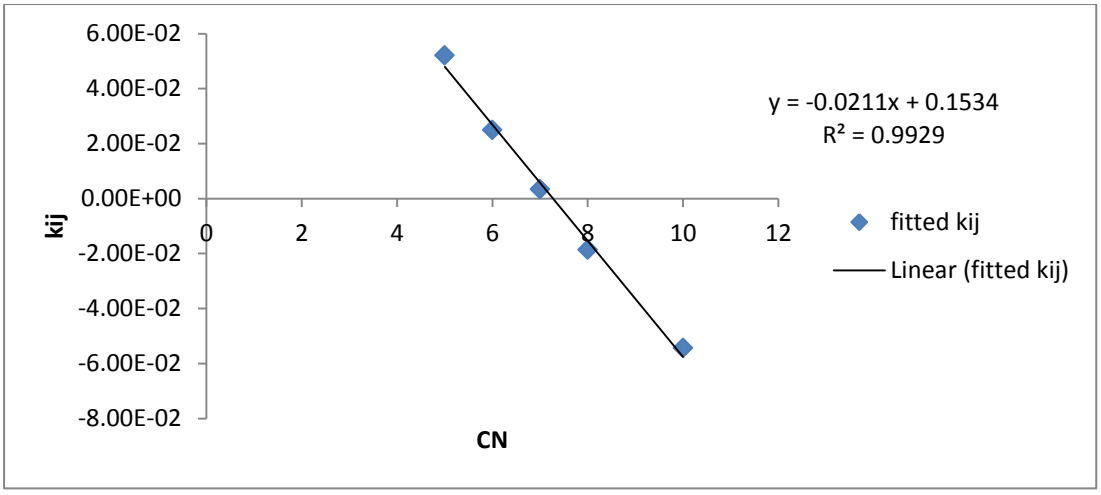

Figure H4: Generalized correlations for the SRK-Twu's k_{ij} parameters of paraffinic HCs based on their CN

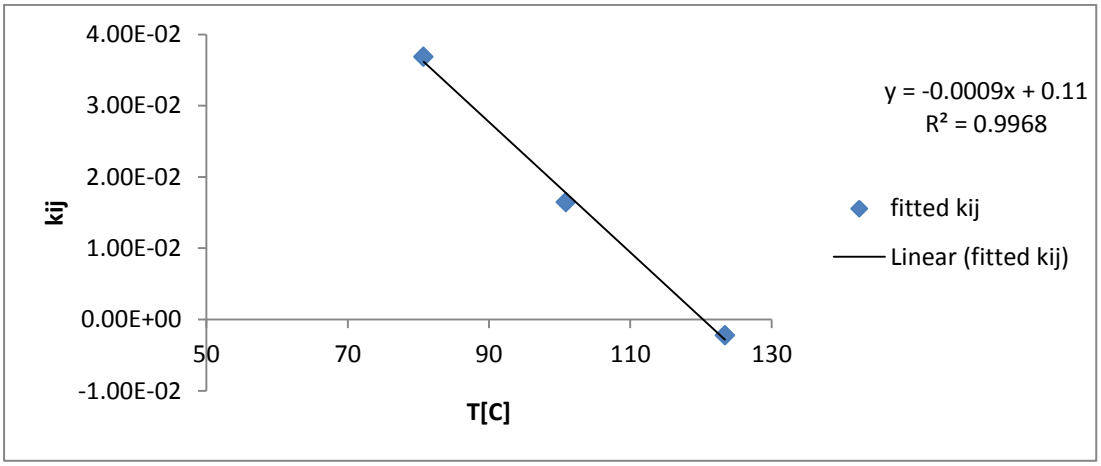

Figure H5: Generalized correlations for the PR-MC's k_{ij} parameters of naphthenic HCs based on their T_b property

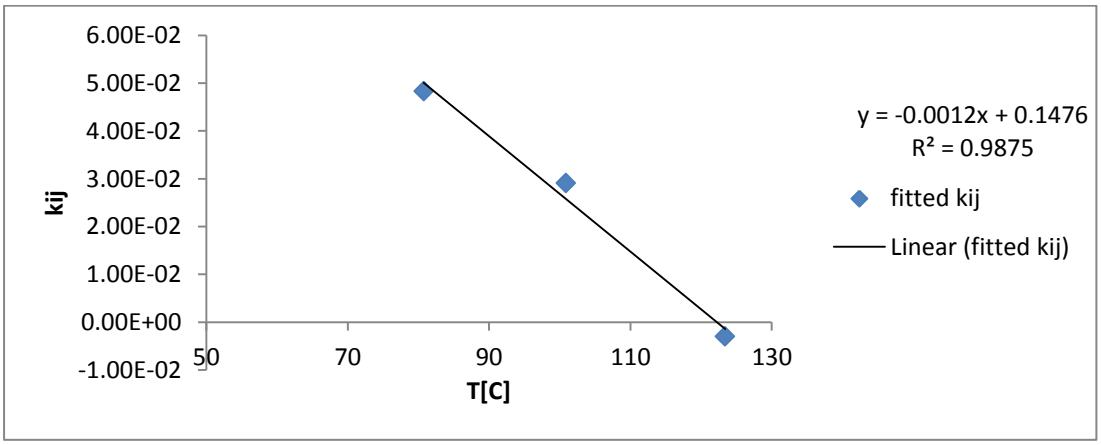

Figure H6: Generalized correlations for the SRK-Twu's k_{ij} parameters of naphthenic HCs based on their T_b property

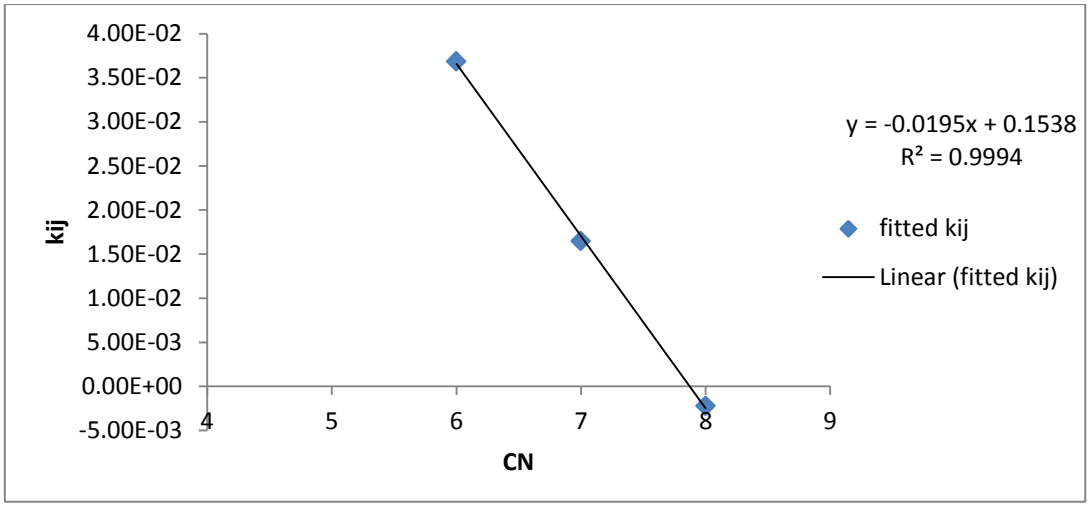

Figure H7: Generalized correlations for the PR-MC's k_{ij} parameters of naphthenic HCs based on their CN

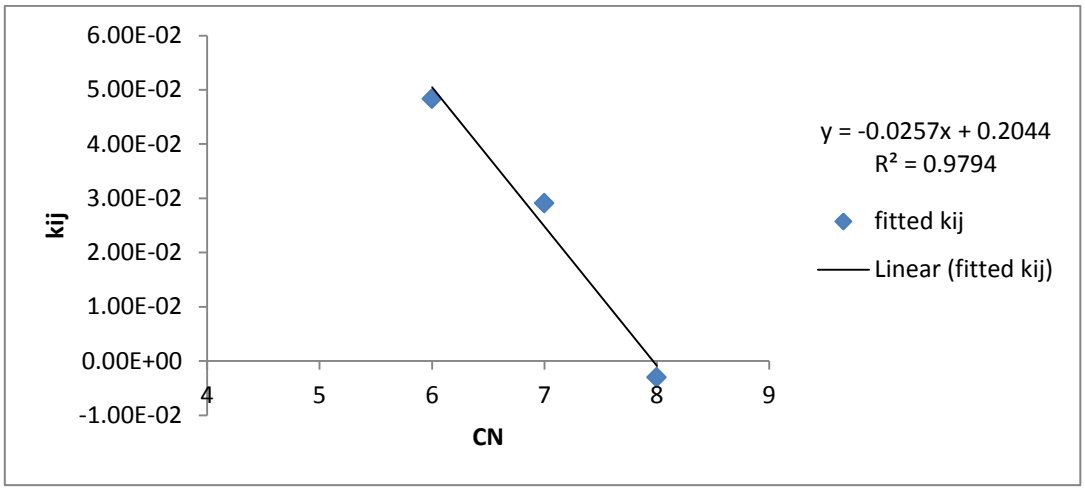

Figure H8: Generalized correlations for the PR-MC's k_{ij} parameters of naphthenic HCs based on their CN

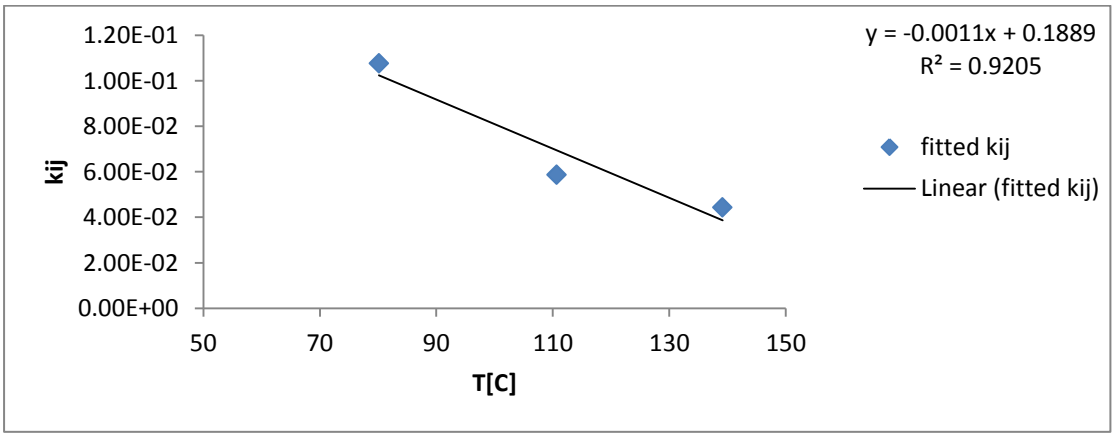

Figure H9: Generalized correlations for the PR-MC's k_{ij} parameters of aromatic HCs based on their T_b property

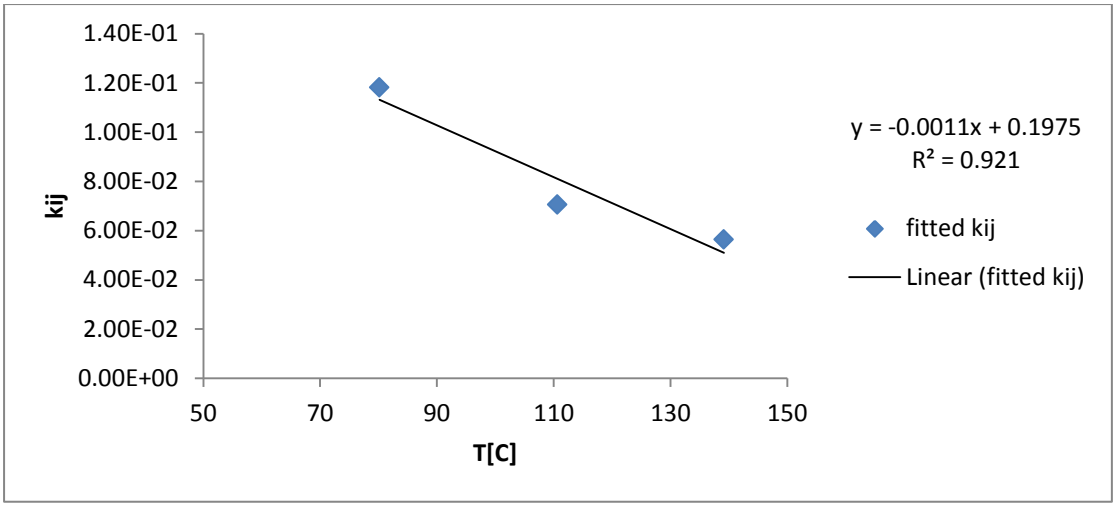

Figure H10: Generalized correlations for the SRK-Twu's k_{ij} parameters of aromatic HCs based on their T_b property

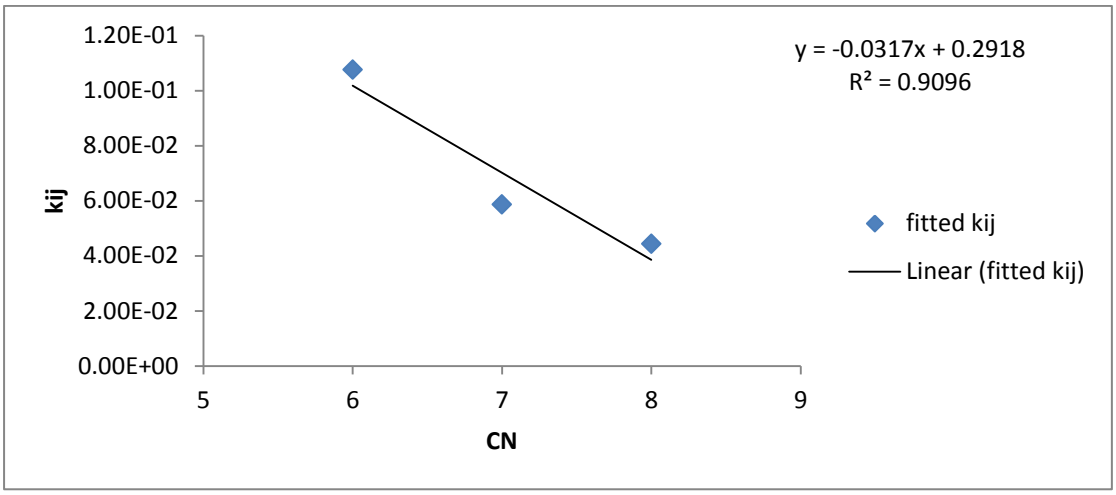

Figure H11: Generalized correlations for the PR-MC's k_{ij} parameters of aromatic HCs based on their CN

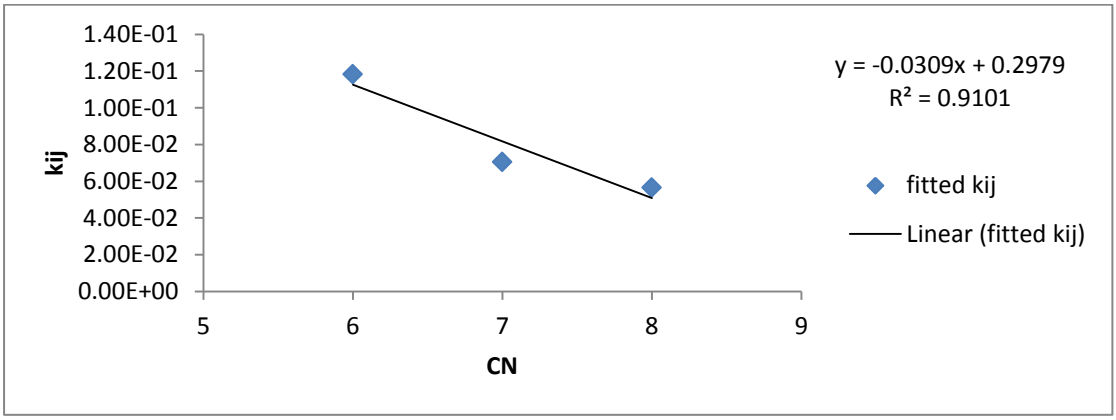

Figure H12: Generalized correlations for the SRK-Twu's k_{ij} parameters of aromatic HCs based on their CN

Appendix I

Table I1: Analytical results for Hg in iso-butane with the UMR-PRMC model for both liquid and vapor phase and their respective absolute deviations

Confidential data

Table I2: Analytical results for Hg in iso-butane with the PR-MC model using the T_b based generalized correlations for both liquid and vapor phase and their respective absolute deviations

Confidential data

Table I3: Analytical results for Hg in iso-butane with the PR-MC model using the CN based generalized correlations for both liquid and vapor phase and their respective absolute deviations

Confidential data

Table I4: Analytical results for Hg in iso-butane with the SRK-Twu model using the T_b based generalized correlations for both liquid and vapor phase and their respective absolute deviations

Confidential data

Table I5: Analytical results for Hg in iso-butane with the SRK-Twu model using the CN based generalized correlations for both liquid and vapor phase and their respective absolute deviations

Confidential data

Appendix J

Table J1: Analytical results for Hg in iso-butane and propane with the UMR-PRMC model in the liquid phase and their respective absolute deviations

Confidential data

Table J2: Analytical results for Hg in iso-butane and propane with the PR-MC model using the T_b based generalized correlations in the liquid phase and their respective absolute deviations

Confidential data

Table J3: Analytical results for Hg in iso-butane and propane with the PR-MC model using the CN based generalized correlations in the liquid phase and their respective absolute deviations

Confidential data

Table J4: Analytical results for Hg in iso-butane and propane with the SRK-Twu model using the T_b based generalized correlations in the liquid phase and their respective absolute deviations

Confidential data

Table J5: Analytical results for Hg in iso-butane and propane with the SRK-Twu model using the CN based generalized correlations in the liquid phase and their respective absolute deviations

Confidential data

Table J6: Analytical results for Hg in n.C_4, n.C_5 and n.C_6 with the UMR-PRMC model in the liquid phase and their respective absolute deviations

Confidential data

Table J7: Analytical results for Hg in n.C_4, n.C_5 and n.C_6 with the PR-MC model using the T_b based generalized correlations in the liquid phase and their respective absolute deviations

Confidential data

Table J8: Analytical results for Hg in n.C_4, n.C_5 and n.C_6 with the PR-MC model using the CN based generalized correlations in the liquid phase and their respective absolute deviations

Confidential data

Table J9: Analytical results for Hg in $n.C_4$, $n.C_5$ and $n.C_6$ with the SRK-Twu model using the T_b based generalized correlations in the liquid phase and their respective absolute deviations

Confidential data

Table J10: Analytical results for Hg in $n.C_4$, $n.C_5$ and $n.C_6$ with the SRK-Twu model using the CN based generalized correlations in the liquid phase and their respective absolute deviations

Confidential data